N70-21426
NASA CR-109092

NATIONAL AERONAUTICS AND SPACE ADMINISTRATION

Technical Memorandum 33-425

Proceedings of the 4th Aerospace Mechanisms Symposium

Held at the University of Santa Clara
Santa Clara, California
May 22-23, 1969

Edited by
George G. Herzl
and
Mary Fran Buehler

JET PROPULSION LABORATORY
CALIFORNIA INSTITUTE OF TECHNOLOGY
PASADENA, CALIFORNIA
January 15, 1970

NATIONAL AERONAUTICS AND SPACE ADMINISTRATION

Technical Memorandum 33-425

Proceedings of the 4th Aerospace Mechanisms Symposium

Held at the University of Santa Clara
Santa Clara, California
May 22-23, 1969

Edited by
George G. Herzl
and
Mary Fran Buehler

JET PROPULSION LABORATORY
CALIFORNIA INSTITUTE OF TECHNOLOGY
PASADENA, CALIFORNIA
January 15, 1970

Prepared Under Contract No. NAS 7-100
National Aeronautics and Space Administration

Preface

The 4th Aerospace Mechanisms Symposium, held at the University of Santa Clara, Santa Clara, California, on May 22–23, 1969, was sponsored by the University of Santa Clara, the Jet Propulsion Laboratory, and Lockheed Missiles & Space Company. The symposium brought together more than 200 representatives from almost 60 organizations concerned with the use of mechanisms in space.

The 21 papers presented were divided into four sessions with the following chairmen:

Session I	Robert E. Fischell, Chairman Johns Hopkins University
	James P. O'Neill, Co-chairman TRW Systems Group
Session II	Bruce E. Tinling, Chairman NASA Ames Research Center
	Edgar J. Buerger, Co-Chairman General Electric Company
Session III	Henry Frankel, Chairman NASA Goddard Space Flight Center
	Douglas Dwyre, Co-chairman Philco-Ford Corporation
Session IV	Fred Forbes, Chairman Wright-Patterson Air Force Base
	Alfred Rinaldo, Co-chairman Lockheed Missiles & Space Company

In Session II, a panel discussion on spacecraft booms was presented by Charles Staugaitis, NASA Goddard Space Flight Center; John MacNaughton, Spar Aerospace Products, Ltd.; James M. Talcott, Fairchild Hiller Corporation; and the panel moderator, George G. Herzl, Lockheed Missiles & Space Company. Another feature of the session was the showing of two films on the thermal flutter of booms. Films were shown and discussed by Bruce E. Tinling, NASA Ames Research Center, and H. P. Frisch, NASA Goddard Space Flight Center.

Prior Symposia in This Series

First Aerospace Mechanisms Symposium
May 19–20, 1966
University of Santa Clara
Santa Clara, California

Proceedings, AD 638 916, are available from:
The Clearinghouse for Federal Scientific and Technical Information
Department of Commerce
Washington, D.C.

2nd Aerospace Mechanisms Symposium
May 4–5, 1967
University of Santa Clara
Santa Clara, California

Proceedings, TM 33-355, are available from:
Jet Propulsion Laboratory
California Institute of Technology
Pasadena, California

3rd Aerospace Mechanisms Symposium
May 23–24, 1968
Jet Propulsion Laboratory
Pasadena, California

Proceedings, TM 33-382, are available from:
Jet Propulsion Laboratory
California Institute of Technology
Pasadena, California

Contents

Session I

Session II

Session III

Contents (contd)

Session III (contd)

Session IV

Opening Remarks

George G. Herzl
Lockheed Missiles & Space Company

In the name of the symposium's organizing committee, I wish to welcome you to the 4th Aerospace Mechanisms Symposium. This symposium is sponsored by the University of Santa Clara, the Jet Propulsion Laboratory of the California Institute of Technology, and Lockheed Missiles & Space Company.

Mechanisms are the very backbone of modern spacecraft, and there is every indication that future spacecraft will contain even more sophisticated mechanisms. Tremendous strides have been made in the short history of aerospace mechanisms, and a great deal of design and flight experience has been accumulated. Aerospace designers have invented mechanisms that do not have terrestrial counterparts by taking advantage of the unique characteristics of the space environment. They have also significantly extended the state of the art of many conventional mechanisms for their use in space over extended periods of time. As a result, the scope of the design principles, details, and applications with which the aerospace mechanism designer must be familiar has grown in variety, complexity, and volume.

The purpose of this symposium is to provide an opportunity for the aerospace mechanisms designer to compare and correlate the specific knowledge gained from a wide variety of important mechanism design efforts. We hope to achieve a great deal of cross-pollination of ideas among the various projects and among the participants of the symposium. This year, we have extended the program to include a panel discussion on spacecraft booms, with a question-and-answer period. We have also allotted more time for discussion after each paper and have added informal gathering sessions at the end of the day. We urged each author to discuss the blind alleys, and especially the failures, he encountered in the course of his work. He learned his lesson from them, and we want to learn ours. If this symposium achieves nothing else but the prevention of one failure—in flight or in development—it will have performed a valuable service to the overall United States space effort.

This volume presents the papers offered at the symposium in order to provide the aerospace mechanisms designer with a useful source of ideas and information and to serve as a stimulant to the continuance of a periodic professional interchange in the field of aerospace mechanisms.

The chairman is especially appreciative of the preparation effort and cooperation of the symposium participants whose papers are presented in this volume. In addition, special thanks for making the symposium possible are due to the Very Reverend Thomas Terry, S. J., President, University of Santa Clara; Dr. W. H. Pickering, Director, Jet Propulsion Laboratory, California Institute of Technology; and Dr. W. C. Griffith, Vice-President, Lockheed Missiles & Space Company. The contribution of all phases of the symposium organization and planning by R. K. Pefley, S. Weissenberger, and E. J. Fisher of the University of Santa Clara; P. Bomke and P. T. Lyman of the Jet Propulsion Laboratory; J. L. Adams of Stanford University; and A. L. Rinaldo of Lockheed Missiles & Space Company is greatly appreciated as are the efforts of Mrs. Mary Fran Buehler of the Jet Propulsion Laboratory in the editorial preparation of this publication.

Organizations Represented at the 4th Aerospace Mechanisms Symposium

Aeroflex Labs, Inc.

Aerojet General Corporation

Aerospace Corporation

Aerotherm Corporation

Altair

Amerace Esna Corporation
Stimsonite Division

Ametek, Inc.

Applied Research Laboratories

Atomics International

Ball Brothers Research Corporation

Beckman Instruments, Inc.

The Bendix Corporation

The Boeing Company

British Embassy, Washington, D.C.

California State College at San Jose

Dalmo Victor Company

Douglas Aircraft Company

ESL, Inc.

ESSA-NESC

Fairchild Hiller Company

General Dynamics Corporation
Convair Division

General Electric Company

Goodyear Aerospace Corporation

Grumman Aircraft Engineering Corporation

Hughes Aircraft Company

International Business Machines Corporation

ITT Aerospace–Optical Division

Jet Propulsion Laboratory

Johns Hopkins University

Lockheed-California Company

Lockheed Missiles & Space Company

Martin Marietta Corporation

McDonnell Douglas Corporation

NASA Ames Research Center

NASA Goddard Space Flight Center

NASA Headquarters

NASA Marshall Space Flight Center

North American Rockwell Corporation

Philco-Ford Corporation

Physics Research & Development, Inc.

Quantic Industries, Inc.

Radiation Incorporated

RCA, Astro-Electronics Division

Santa Barbara Research Center

Seattle University

Sherman Fairchild Technology Center

Singer–General Precision, Inc.

Spar Aerospace Products, Ltd.

Stanford University

Sylvania Electric Products, Inc.

TRW Systems Group

United States Air Force Aero Propulsion Laboratory

United States Air Force Office of Aerospace Research

United States Naval Research Laboratory

United Technology Center

University of California at Berkeley

University of Michigan

University of Santa Clara

Westinghouse Electric Corporation

Session I

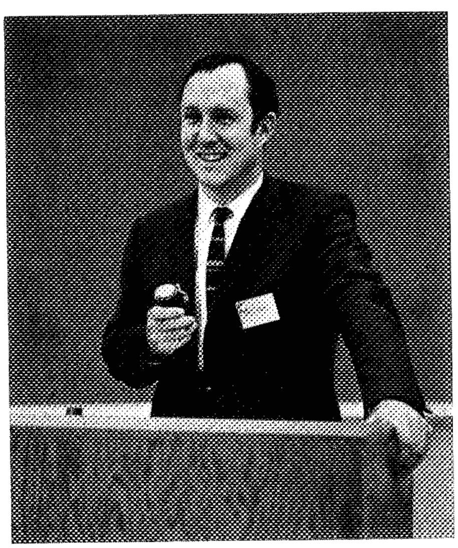

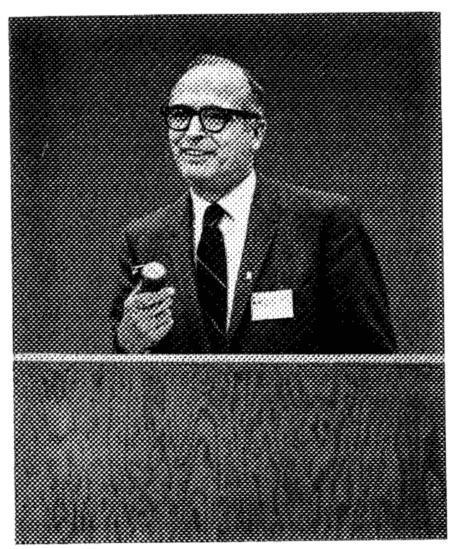

OVERLEAF: *Fred Mobley, Johns Hopkins University (left), substituting for Session Chairman Robert E. Fischell, also of Johns Hopkins University, who could not attend the symposium; and James P. O'Neill, TRW Systems Group (right), Session Co-chairman*

70N21427

Soil Sampler Development for Unmanned Probes*

W. H. Bachle
Philco-Ford Corporation
Space and Re-entry Systems Division
Newport Beach, California

Two prototype soil samplers for unmanned space probes are described. One is deployed vertically and uses an abrading cone for sample acquisition. The other is deployed by a telescoping boom and uses a rotating wire brush for sample acquisition. These samplers were designed primarily to collect a soil sample for biological investigation. Extensive testing of these prototype samplers indicates that the wire brush is the better sample acquisition device, although the boom deployment system is mechanically more complex than the vertical deployment system, which uses canted rollers running in a tube to feed the sampler into the surface.

I. Introduction

Unmanned space probes can be landed on the surface of a planet to acquire specific information about the physical characteristics of the surface and to search for the existence of life. Such a landed probe will contain instruments to acquire samples of the planet's environment and to perform their analyses. The samples may be taken *in situ* by placing the instrument on the planetary surface. More complex instruments, such as the gas chromatograph, mass spectrometer, and some life detection instruments, will require that a soil sample be collected from the surface and delivered to them. This identifies the soil sampler mechanism as a component of an unmanned planetary surface probe.

After the project definition study phase of the Automated Biological Laboratory, two prototype soil sampling mechanisms were fabricated and tested. These mechanisms were to collect soil samples for use in biological rather than geological investigations.

II. Design Criteria

The design criteria defined for these sampling mechanisms were concerned with the sampler deployment mode and the sample requirements. The sampler was to use

*The work reported in this paper was conducted at Philco-Ford Corporation, Newport Beach, Calif., under Contract No. NASw-1065 for the Bioscience Programs Office, National Aeronautics and Space Administration Headquarters, and Contract No. 951935 for the Space Sciences Division, Jet Propulsion Laboratory.

vertical deployment to the surface in one case and horizontal deployment away from the probe in the other case. The sample requirements are as follows:

(1) The sample should be collected from the planetary surface to a depth of several millimeters. No capability for penetrating solid rock is required.

(2) The amount of collected sample per sampling attempt should be 1 to 10 g.

(3) Repeated sampling ability at different locations is desirable.

(4) The soil sample should contain particles less than one millimeter in diameter.

(5) The sampler design should prevent heating or chemical contamination of the sample and should not reduce the content of biological material in the sample by selective sorting.

III. Sampler Design Descriptions

The design of these soil sampling mechanisms was evolved by generating 32 concepts in sketch form. These were submitted to the Jet Propulsion Laboratory for review by a panel who selected eight of these concepts for more detailed engineering layout and design. These eight designs were again reviewed, and the two final designs to be fabricated were chosen.

A. Vertically Deployed Soil Sampler

This soil sampler is shown in Fig. 1, partially disassembled in order to expose the mechanical features. The concept uses a large-diameter, conical, abrading sample-acquisition head mounted at the end of a long drive shaft. The drive shaft is attached to a canted roller feed assembly through a small over-running clutch. The feed assembly, in turn, is connected to the output gearbox of the drive motor assembly. This overall assembly is the portion of the sampler mechanism that is free to move inside a cylindrical support tube. At the base of the support tube is mounted an annular soil-sample collection chamber to which the sample is ultimately transferred by means of centrifugal action in a high-speed spin.

A unique feature of this mechanism is the set of canted feed rollers that cause the sampler to deploy itself axially along the support tube. Three rollers on this feed assembly are mounted at the end of small torsion bar shafts in such a way that the rollers are preloaded against the inside wall of the support tube. These rollers are canted at an angle with respect to the axis of the support tube so that as the assembly is rotated, the rollers follow a helical path along the inner surface of the tube. In this manner, the sampler mechanism can be advanced or retracted, depending on the direction of rotation of the feed assembly. The drive motor is mounted in a carriage supported by eight rollers that are also spring-loaded against the inner surface of the support tube. These rollers are aligned so they are free to roll axially along the tube, while at the same time reacting the torque from the motor through the high frictional resistance offered by the rollers in a circumferential direction. Power is supplied to the drive motor through two beryllium/copper tapes that unwind from small drums mounted at the top of the support tube. The tape drums are connected to two small negator spring motors that are wound up as the tape is deployed and later provide the power necessary to rewind the tapes onto their drums during sampler retraction.

The operational sequence for this sampler is shown in Fig. 2 and Table 1. In the sampling mode, the sampler advances along the support tube until it contacts the soil surface. The conical head abrades the surface by means of two carbide cutting blades. Soil passes to the inside of the abrading head through slits located ahead of each blade. As this occurs, the canted feed rollers continue to attempt to advance the sampler into the surface. The resistance to further advance produces reactions at the canted feed rollers, causing the torsion bars to wind up. This action reduces the cant angle until an angle is reached that produces a feed rate compatible with the penetration rate of the sampling head, while at the same time maintaining an axial thrust of about 15 lb to ensure active abrasion of the surface.

After a programmed time interval, the power to the drive motor is reversed, causing the feed assembly to carry the sampler back up the support tube to its stowed position where the drive motor carriage encounters a stop. The feed assembly continues to advance since it is connected to the driving gearbox through a spring-loaded slip joint. This, in turn, causes a small disk clutch mounted on the end of the sampling head drive shaft to engage its counterpart mounted on a high-speed output shaft of the coaxial gearbox.

The clutch action causes the sampling head drive shaft to spin up and deliver the soil sample, by means of centrifugal action, to the annular soil collection chamber.

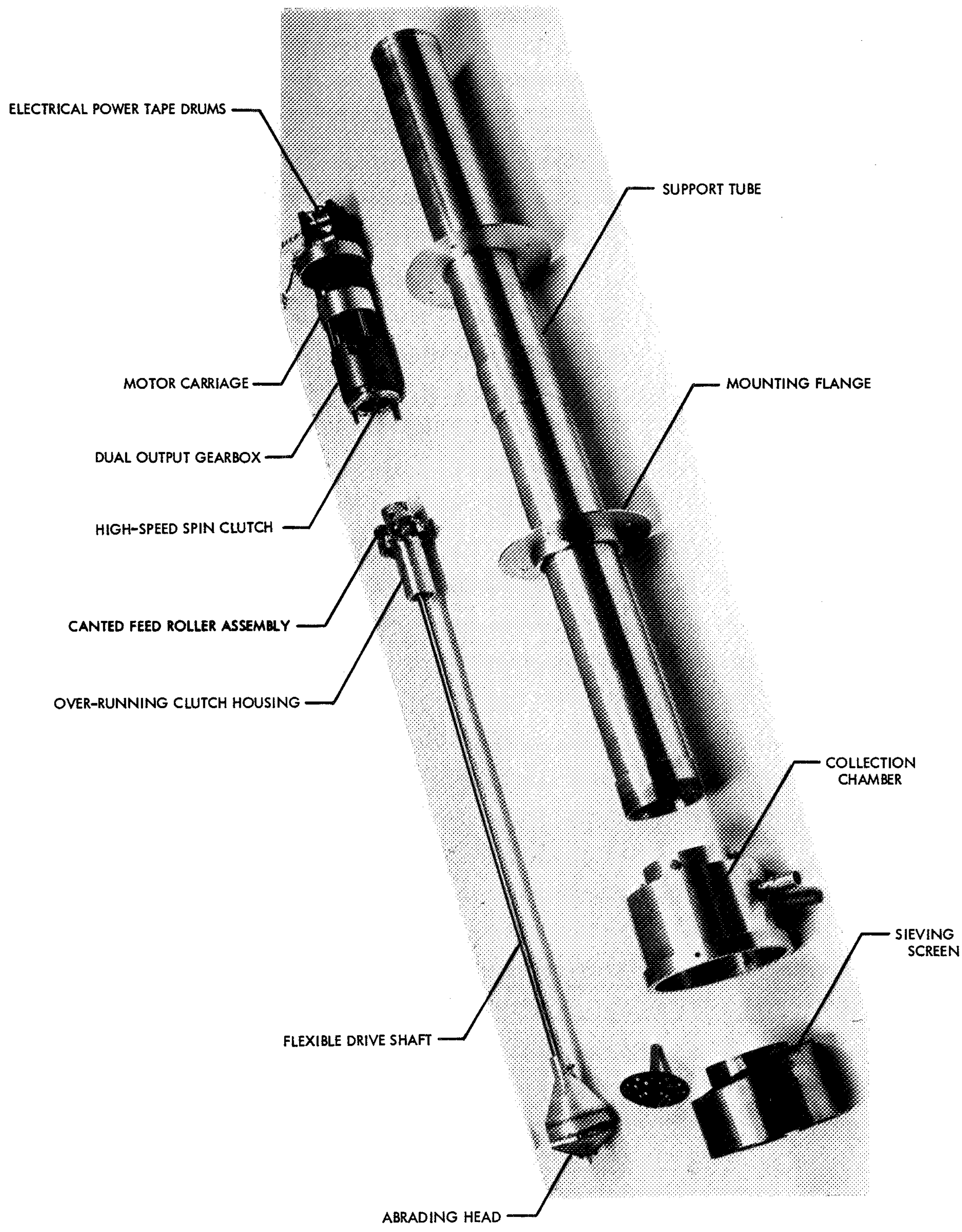

Fig. 1. Vertically deployed soil sampler

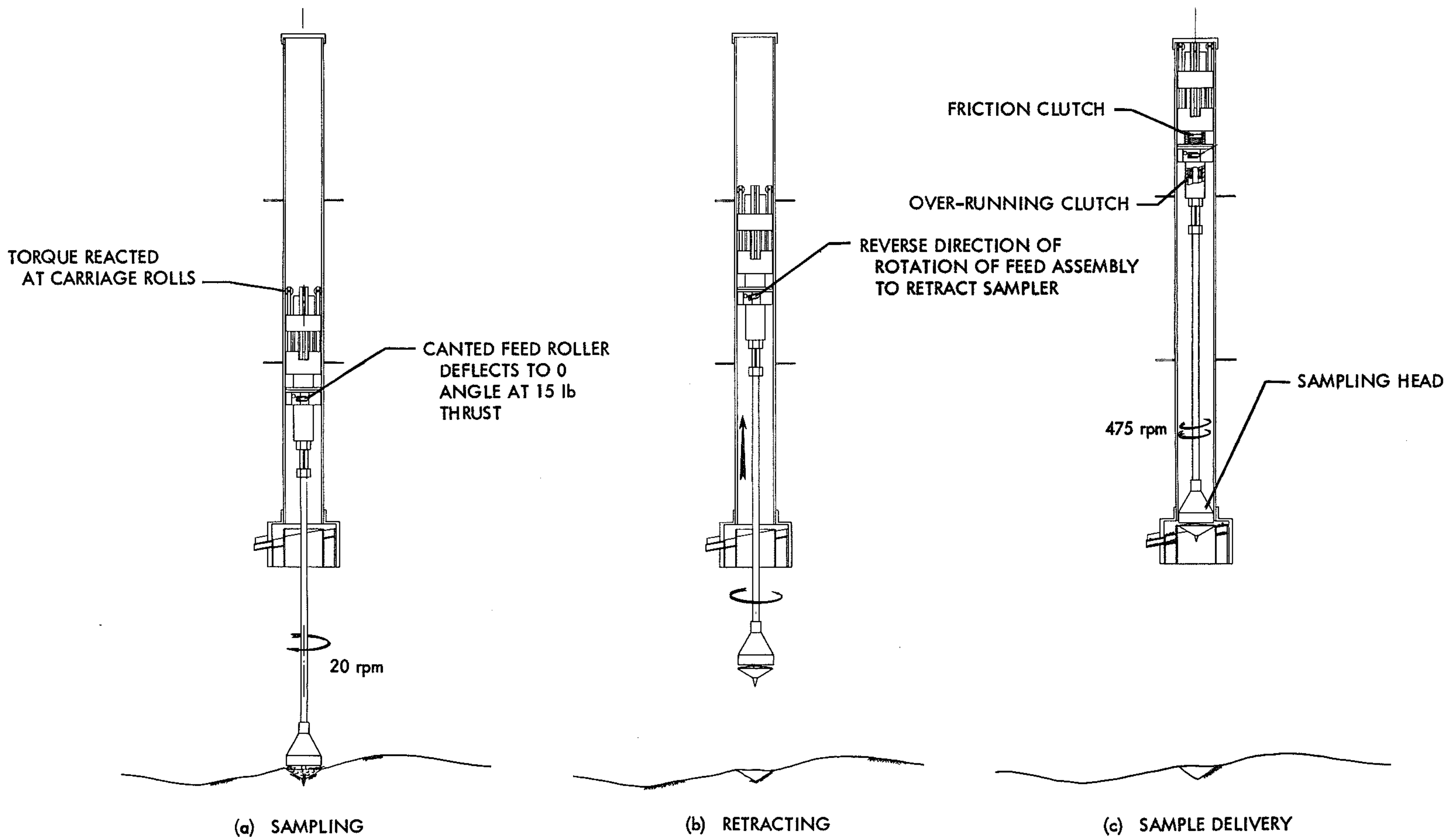

Fig. 2. Operational sequence, vertically deployed sampler

Table 1. Operation of vertically deployed sampler

Step No.	Step
	Sampling (Fig. 2a)
1	Motor is started to drive sampler down tube by action of canted feed roller assembly.
2	Maximum axial thrust is maintained on abrading head as it rotates.
	Retracting (Fig. 2b)
3	Drive motor is reversed to cause feed assembly to carry sampler assembly up the support tube.
	Sample delivery (Fig. 2c)
4	Drive motor reaches end of support tube and continued feed causes friction clutch to engage, transferring soil by centrifugal action of high-speed spin.
5	Vibrating action of sampling head on tube wall shakes soil through sieving screen.

The drive shaft is free to spin rapidly by virtue of the over-running clutch coupling it to the slowly turning feed assembly. The soil sample is delivered onto a 1-mm mesh sieving screen by this action. It is shaken through the screen with vibration caused by the action of the unbalanced sampling head striking the walls of the support tube.

The weight of this prototype sampler is 7.4 lb. Several of the components do not represent optimum designs from a weight standpoint: for example, the soil collector assembly (1.7 lb), the support tube (1.8 lb), and the motor carriage assembly (2.0 lb). It is estimated that design optimization with some miniaturization could reduce this weight by a factor of 2.

The average power consumed by this sampling mechanism is approximately 15 W.

B. Horizontally Deployed Soil Sampler

This soil sampler is mounted on the end of a 10-ft telescoping boom as shown in Fig. 3. The inset in Fig. 3 shows a closeup view of the sampling head, which consists of a thin circular wire brush that rotates inside a close-fitting shroud. The brush projects past the shroud a small amount in the area that makes contact with the surface during sampling. The wire brush is driven through a spur gear drive train incorporated in the shroud. This configuration of the sampling head was chosen to provide a geometry that would most easily pass between rocks and reach down into narrow fissures.

The telescoping boom is used with this sampler to deploy it to the surface, traverse the sampler over the surface, and provide a sample transport path to the probe. Boom extension is achieved by closing a valve at each end and pressurizing the interior. Two beryllium/copper tapes located inside the boom and attached to the tip segment are deployed from motor-driven drums to control the extension rate as well as to provide a means of retracting the boom. The tapes also serve as electrical conductors to provide power to the wire brush sampler drive motor.

The gearbox located at the base of the telescoping boom houses the extension and the elevation drive gear trains. One motor is used to drive these gear trains simultaneously. An over-running clutch is used in the elevation drive gear train to release the elevation drive when the sampler is traversing the surface.

Two methods of soil transport are incorporated in this sampler mechanism. A blower mounted on a cyclone collector located at the support structure is used to induce a flow of air through the sampling head and the telescoping boom. This flow was intended to carry small particles to the cyclone collector continuously as sampling proceeded. The other method is mechanical. A small cavity built into the sampling head shroud receives material carried into the shroud by the wire brush. This sample is delivered by elevating the boom to a vertical position, allowing the sample to fall down through the boom.

The schematic diagram in Fig. 4 illustrates the sequence of events in a sampling cycle (also see Table 2). Aside from a start and stop command, the control of these events is incorporated in the mechanism. Both drive motors are driven simultaneously at all times in the sampling cycle. The valves located at each end of the boom are actuated through slip clutches connected to the gear trains in the sampling head and the extension/elevation gearbox. A double-pole double-throw switch is actuated at full extension or full retraction through a geared drive to reverse the polarity of the electrical power to each drive motor. Thus, once the cycle is initiated, the sampler mechanism will automatically step through these events until commanded to stop. The arrival of the boom at the vertical position is used to actuate a pin release so that a spring mounted in the base structure can step the sampler to a new azimuth position for the subsequent run.

The weight of this prototype sampler is 11.5 lb. The sampling head and its drive motor weigh 1.4 lb. The bulk of the weight is associated with the boom deployment

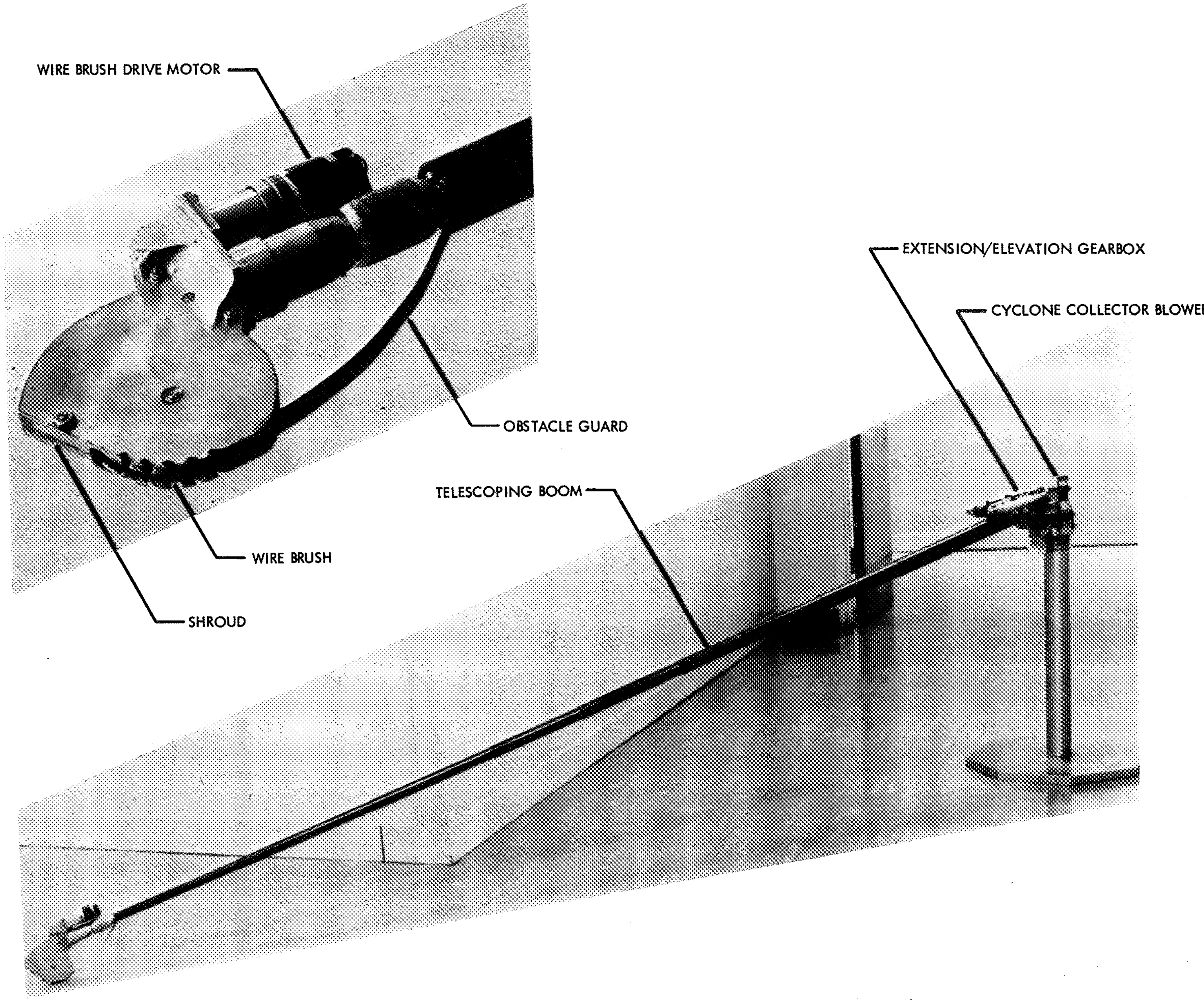

Fig. 3. Horizontally deployed soil sampler

mechanism. Components that are not optimized from a weight standpoint are the telescoping boom (3.2 lb), the extension/elevation gearbox (1.9 lb), and the support structure (3.3 lb).

The average power required to operate this sampler is 40 to 50 W.

IV. Sampler Testing

Tests were conducted to evaluate the mechanical performance and sample acquisition capability of each of these sampler mechanisms. Most of the testing was performed in the laboratory, using artificially prepared soil models. Some limited testing was accomplished in the field on the Kelso (California) sand dunes and at five test sites at Pisgah crater near Barstow, California. The sampling test runs made with each mechanism are summarized in Table 3. Many more runs were made with the vertically deployed sampler because it was simpler to operate and easier to clean, and because it suffered fewer mechanical malfunctions.

A. Sample Acquisition

The vertically deployed sampler always collected a sample if it was attacking a soil model it could penetrate. The amount of sample collected was a function of soil strength and operation time. In loose material, such as sand and silt, 1 min was sufficiently long to acquire 30 to 40 g of sample. On hardpan or vesicular pumice, a run of this duration would result in a sample quantity of approximately 1 g. On soil models such as lichen-covered rock, this sampler mechanism always failed to collect because the tip would not penetrate enough to allow the blades to abrade the surface. This sampler will not collect unless a sufficient amount of loose material is available to pile up ahead of the cutting blades and force its way through the slots in the cone. Operation of this sampler with its axis off vertical demonstrated that it can collect and retrieve a sample of a material that it is capable of penetrating at angles as high as 30 deg.

Although far fewer test runs were made with the wire brush, it was possible to operate it on enough different soil models to evaluate its sample acquisition performance. The sample collection cavity in the shroud is sized to hold about 30 g of material. On loose materials, this cavity generally filled in the first 10 to 20 s of operation. On more cohesive material such as hardpan or vesicular pumice, this sampler collects from 0.2 to 5 g of material in a complete traverse. The actual amount collected depends on such variables as the strength of the soil and the surface irregularity that determines the percentage of time that the wire brush remains in contact with the surface. Successful sampling is achieved on surfaces such as the lichen-covered rock, indicating that the wire brush is a more universal sampler than the abrading cone. When this sampler was operated in a rubble mixture containing pebbles roughly 5 mm in diameter, the brush would invariably stall because pebbles of this particular size would become wedged between the brush and the shroud. Even though this occurred in some cases as soon as the brush contacted the surface, some sample was always acquired that could be retrieved by elevating the boom to the vertical position.

The pneumatic mode of sample transport proved to be unsatisfactory in its present form. The flow velocities were so low inside the boom that only those very fine particles which obey the Stokes law were transported. Samples collected in this manner never exceeded fractions of a gram of very fine soil particles.

B. Mechanical Performance

The vertically deployed sampler operated with very few malfunctions, as is demonstrated by the large number of test runs that were completed. Early in the laboratory testing it was found necessary to incorporate a light knurl on the canted feed rollers to prevent axial slippage. In operation, this caused the inner wall of the support tube to be embossed and eventually caused material to flake off the wall. The support tube was replaced three times during the test phases. The canted-roller torsion bars are highly stressed and a few failures of these occurred during the testing.

The malfunctions associated with the horizontally deployed wire brush were mostly concerned with the telescoping boom extension and elevation control mechanisms. Because the leakage rate out of the boom was high, the pneumatic extension proved to be unreliable and extremely wasteful of pressurizing gas. As a result, the pneumatic deployment was not used in most of the tests with this sampler mechanism.

The only mechanical failure suffered by the wire brush sampling head occurred during the field tests. Abrasion from the rotating wire brush finally wore through a thin section of the magnesium shroud in the area where the brush leaves and enters the shroud. This occurred after approximately 20 complete runs.

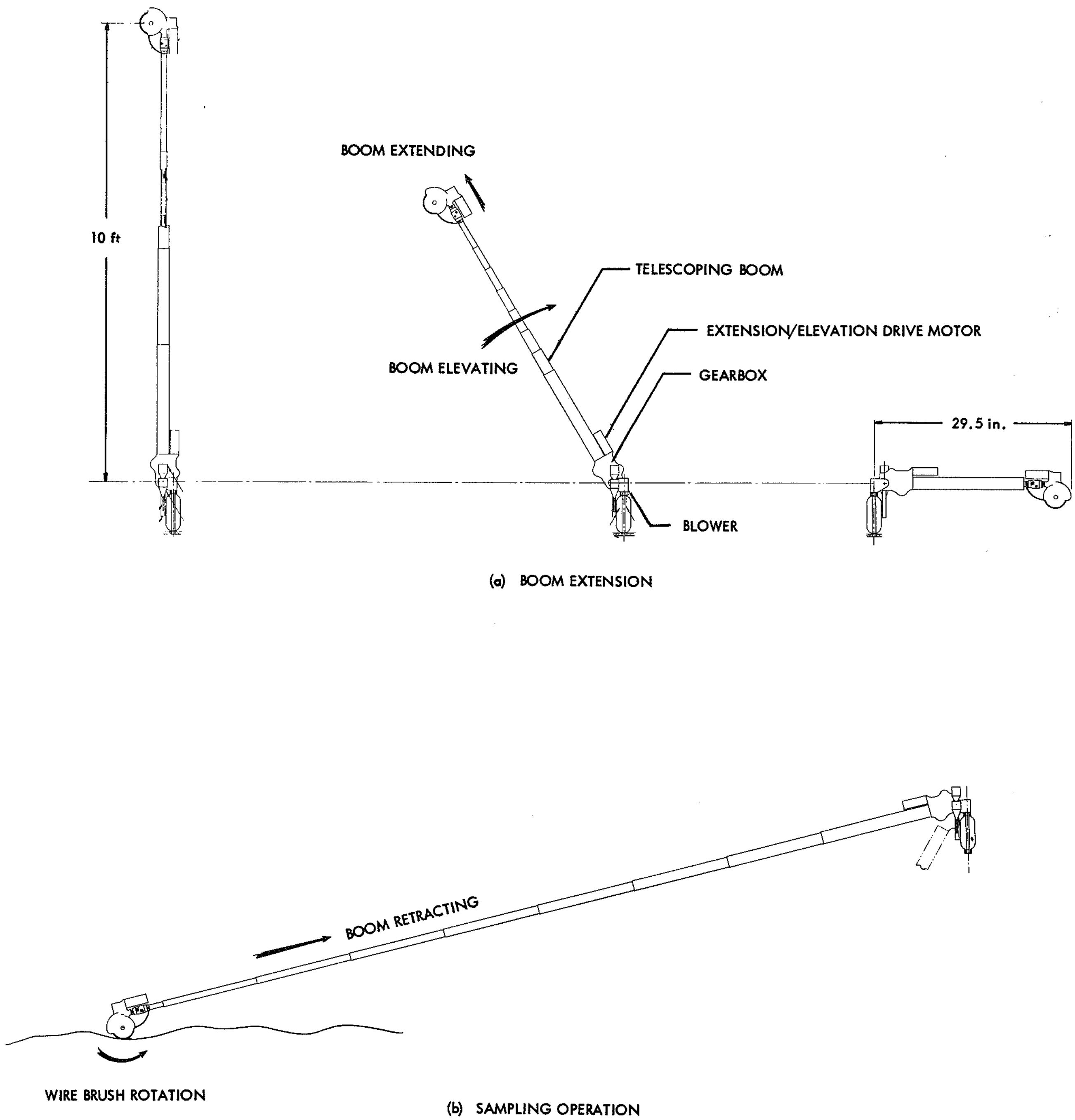

Fig. 4. Operational sequence, horizontally deployed sampler

Table 2. Operation of horizontally deployed sampler

Step No.	Step
	Start position
1	Boom deployment is initiated by activating both drive motors, closing the valves to the boom.
2	Boom is pressurized to provide extension force.
	Initial extension (Fig. 4a)
3	Extension rate of boom is controlled by two tapes fed from drums inside the gearbox.
4	Elevation to vertical position occurs simultaneously with boom extension.
	Extension completed
5	At full extension, both drive motors are reversed, starting boom retraction and lowering of boom to the surface. Boom valves open at this time.
6	When sampler contacts the surface, over-running clutch releases boom from the elevation drive.
	Sampling operation (Fig. 4b)
7	Sampling begins when the sampler reaches the surface. Continued retraction of boom causes sampler to traverse the surface.
8	Soil is collected mechanically in the chamber located inside the shroud. Soil particles entrained in the airflow up the boom are carried continuously to the cyclone collector.
9	When retraction of boom is complete, both drive motors are reversed, repeating extension and elevation.
10	When the drive motors are again reversed, the boom valves open, allowing the mechanically collected soil sample to drop down the boom and be delivered to the spacecraft.

C. Biological Assay

As part of the field test program, an attempt was made to compare the collected sample with a control sample taken by hand to determine whether there were any changes in the biological material contained in the soil. Several assay procedures were used; however, the most successful results were obtained by dilution plate counts to detect viable organisms. In most cases, the collected sample showed no detectable differences from the control. The vertically deployed sampler mechanism did appear to have degraded the viable count for some of the runs in the Kelso dune sand. This could have been the result of destruction of organisms by the sampler, or it may have been due to local variations in the population of organisms in the sand. Test runs were made in the laboratory on sand inoculated with *Bacillus subtilis* spores. These runs indicated no detectable reduction of viable organisms by the sampler.

Table 3. Summary of sampler testing

Type of test	Vertically deployed sampler		Horizontally deployed sampler	
	Total runs	Run time, h	Total runs	Run time, h
Initial laboratory tests	38	3.1	45[a]	3.7[a]
Final laboratory tests	103	2.0	19	1.3
Field tests	29	0.8	14	1.0
Total testing	170	5.9	33	2.3

[a]Tests performed with an early breadboard version to optimize configuration.

V. Conclusions

Of the two mechanisms described, the vertically deployed soil sampler is simpler and mechanically more reliable, but with limitations in its sampling ability. The horizontally deployed soil sampler has an improved sampling ability with a reduced mechanical reliability. Since most of the malfunctions occurred in the boom deployment system, care should be taken not to condemn the sample acquisition mechanization associated with it as unreliable. Refinements in the boom design can be made to improve reliability, or alternate deployment schemes can be considered. This points up the strong interaction that exists between sample acquisition, sampler deployment, and sample transport. Ultimately, these must be related to and be compatible with the landed spacecraft on which the soil sampler mechanism is to be mounted.

Page intentionally left blank

70N21428

Evolution of a Spacecraft Antenna System*

A. Kampinsky
Goddard Space Flight Center
Greenbelt, Maryland

The mechanically despun antenna for spin-stabilized spacecraft has evolved from a simple, rotatable planar reflector to a more sophisticated multifrequency, attitude-sensing, high-gain antenna for deep space probes, tactical communications, and community broadcast applications. The design goal is a lifetime of 2 to 5 yr in space environment with simple mechanical mechanisms, low power consumption, high communications gain, and low noise and magnetic "spillage." The design concepts are proved by the actual flight experiences of (1) the ATS III mechanical antenna system, which, since November 1967, has performed as predicted, (2) the Intelsat III antenna system derived from the predecessor reflective antenna design, and (3) the extension to a military high-capacity despun antenna platform system.

I. Introduction

The early communications spacecraft (*Courier*, *Relay*, *Telstar* and *Syncom*) represent a particularly simple spin-stabilization technique; concurrently, these carried simple antennas that made figures of revolution about the spin axis and thus provided low-gain earth coverage. The first of the subsequent NASA *Applications Technology Satellites* (ATS I) was equipped with a unidirectional, electronically collimated antenna radiation envelope, which was counterrotated against the spacecraft spin; however, electrical dissipative losses and circuit degradations resulted in operational performance 45% below specification levels. Later spacecraft in the spin-stabilized series—ATS III and *Intelsat III A* and *B*[1]—feature a mechanically counterrotating antenna system whose unidirectional earth-coverage radiation provides the highest effective gain figures for communications. The ATS III has been in continuous operation for 15 mo (since November 1967), with a projected lifetime of 5 yr of operation.

The most significant criterion of reliability—simplicity—is inherent in the mechanically despun antenna and in the minimum number of collimation elements and beam-pointing controls. Electronic antenna systems require about 5,000 parts, compared with about 1,800 for the

*The author holds U.S. Patent 3,341,151, granted September 1967, for *Apparatus Providing for a Directive Field Pattern and Attitude Sensing of a Spin Stabilized Satellite*. This concept and patent form the basis of the mechanically despun antennas of the NASA ATS and the Comsat *Intelsat*, as well as the extension to tactical communications spacecraft.

[1]Part of the *International Telecommunications Satellite* (*Intelsat*) series of the Communications Satellite Corporation (Comsat).

ATS III mechanical antenna. Additional features are (1) multiple spaced-frequency operation for uplink and downlink simultaneous receiving and transmitting capabilities, (2) communications bandwidths of hundreds of megahertz, (3) elimination of electrical rotary joints to minimize noise, and (4) an inherent capacity to automatically point a high-gain radiation beam at the earth or to be steered by ground command. Finally, the mechanical antenna system was designed to operate in a fail-safe mode if electrical or mechanical components should fail. The antenna system described herein can revert to the inherent, primary, low-gain omnidirectional antenna system (5 dB) compared with the unidirectional gain of 17.5 dB. The mechanical antenna designs have been applied to space probes, steerable broadcast satellites, and tactical military communications satellites.

II. Antenna System Requirements

The ATS III mechanically despun antenna system (Fig. 1) directly replaces the electronic phased array originally designed for ATS spacecraft. Existent phased-array control electronics not only synchronizes the mechanical antenna rotation with sun line/spacecraft pulses, but continues to control spacecraft spin rates and attitude control jets. Telemetry inputs from ground commands are accepted to direct the radiation envelope on the earth's surface, to direct the antenna toward another region of space (and during eclipse periods), and to control the fail-safe operations.

The vibration spectrum of the launch environment boost phase, of random and peak gravitational forces

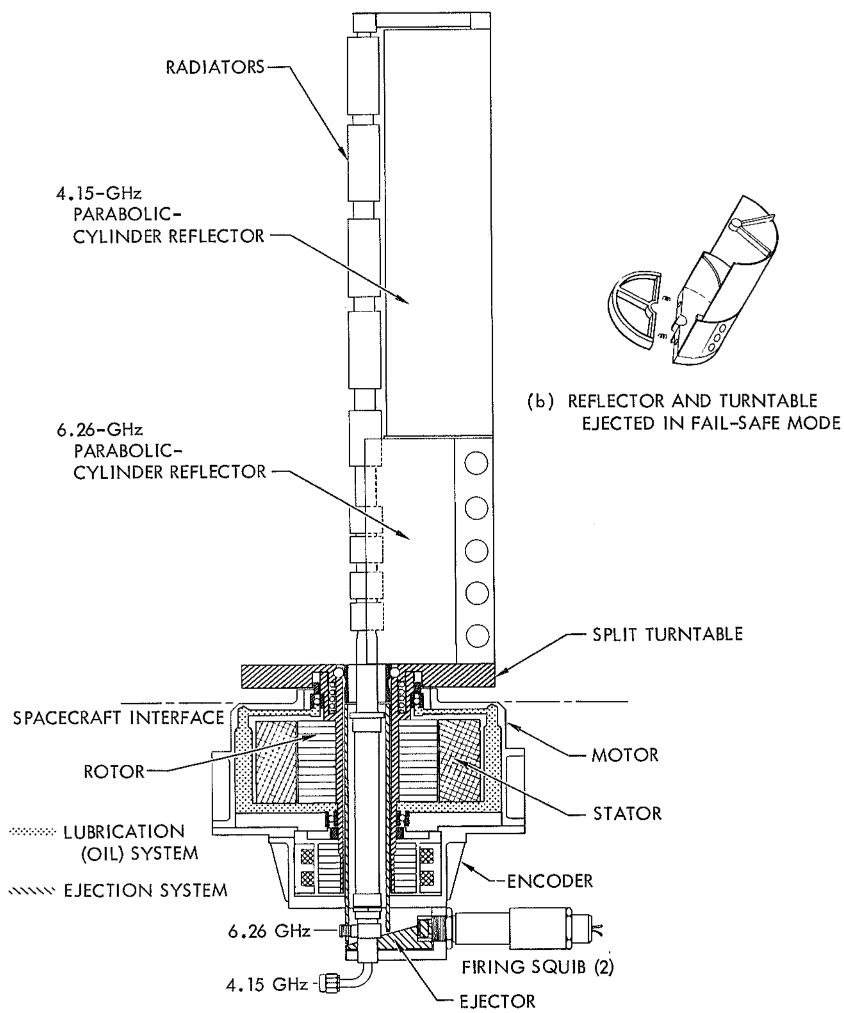

(a) CROSS SECTION OF ANTENNA SYSTEM

Fig. 1. Antenna system for the ATS III

(8.0–15 g, maximum) is supplanted by hard-vacuum operations (10^{-10} torr), ultraviolet and particle bombardments, and thermal differentials of 200°F. The latter problem particularly precluded the use of cement-bonded metal-sandwich construction materials and exposed dielectrics.

The electrical specifications require unidirectional radiation patterns for both 6-GHz uplink and 4-GHz downlink frequencies, with boresighting within 0.1 deg for the 17.5-dB gain envelope (56 times power) and rotational modulation levels within 0.5 dB. No rotary joints or electrical discontinuities were permitted, in order to avoid dispersion, attenuation, or noise generation within the 150-MHz communications bandwidths within a 0.5-dB level above inherent system noise.

Mechanical bearings, lubrication, and drive motor systems were to be qualified on an 8,000-h life test under space vacuum and temperature conditions. Dual reliability analyses of virtually every component were set, with a level-of-success goal of 0.97 for 1 yr of operation and 0.95 for 5 yr.

III. Development

A. Radio Frequency Performance

Spin-stabilized communication spacecraft with the spin axis perpendicular to the earth's equatorial plane require the antenna radiation envelope axis to be perpendicular to the spacecraft spin axis, as shown in Fig. 2a. In this

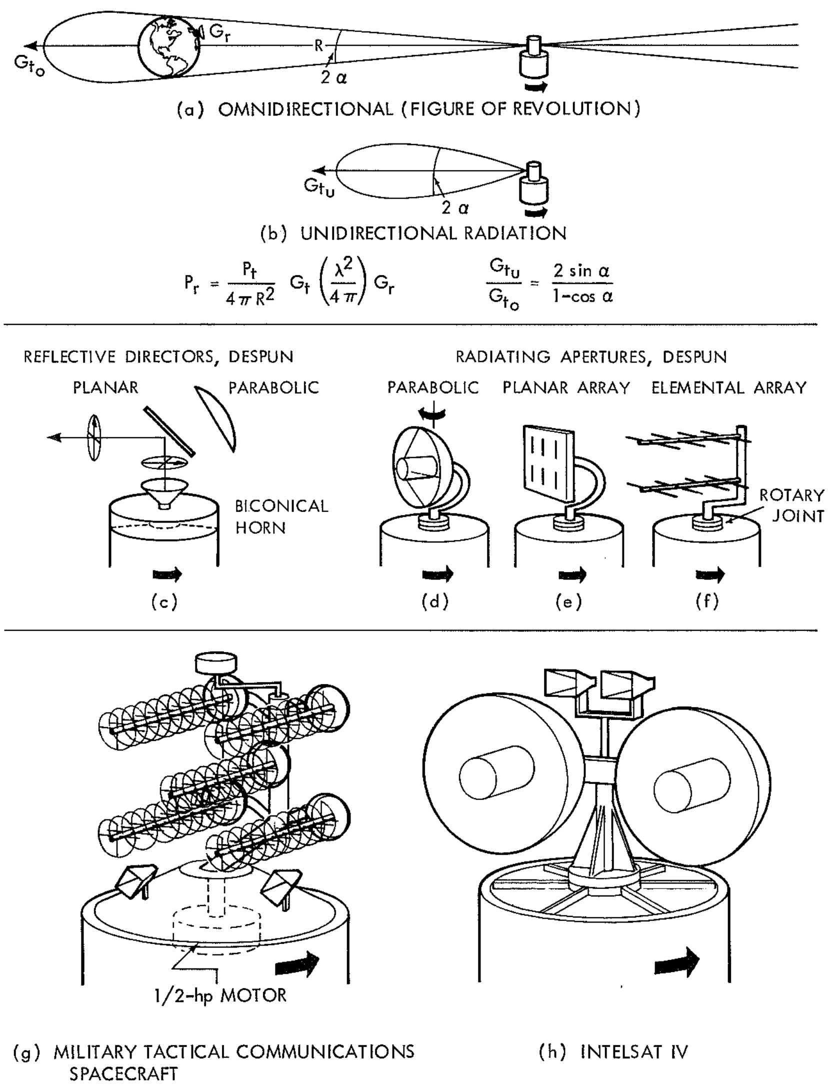

Fig. 2. Evolution of antennas for spinning aircraft

figure, α = half angle of radiated beam, R = range, G_r = gain of receiving antenna, C_{t_o} = gain of transmitting omnidirectional antenna, G_{t_u} = gain of transmitting unidirectional antenna, P_r = receiver power, P_t = transmitter power, and λ = wavelength. In the earliest designs, a primary horn radiator, with circularly symmetric E and H fields about the horn axis, was utilized with planar or parabolic inclined reflectors. This mode was discarded because only circularly polarized radiation was permissible and radiation patterns were asymmetrical about the principal earth-pointing axis. In the current design, a collinear primary radiator, rigidly locked to the spacecraft (Fig. 1a), is coupled with a rotating cylindrical parabolic reflector and requires no radio frequency rotary joints. Linear polarization is inherent and is utilized, during operations, to determine spacecraft attitude and to deduce ionospheric electron density values by Faraday rotation measurements at ground stations. A cylindrical polarization grating was also developed for use if circular polarization were required.

The cylindrical parabolic antenna system provides a 20-deg beamwidth in the plane containing the spin axis by disposition of two sets of radiators (3 wavelengths) for each frequency, and in the orthogonal plane by the aperture dimensions of the two-section parabolic cylinder. The resultant gain figure is 17.5 dB, referred to a linearly polarized radiator. For highest gain figures, antenna reflector sizes can be increased, and the resultant narrow beamwidths can be directed in the plane perpendicular to the spin axis by positioning the reflector and in the orthogonal plane by phase steering of the beam. If the beam is switched above and below the normal to the spin axis, an error signal is generated with respect to an incident signal from ground station directed toward the spacecraft (this concept is part of the basic patent for the mechanically despun antennas). The error signal may be utilized as an indicator of the spacecraft attitude and may be fed to the attitude control system to correct the spacecraft attitude with respect to an earth-line reference. The increasing size of spacecraft would require despinning a section of the spacecraft, and hence a platform is provided upon which large, complete antenna systems are affixed (Fig. 2). A recently launched military tactical communications spacecraft and a large-capacity Comsat spacecraft, *Intelsat IV*, are based upon this concept as extensions of the original designs.

B. Electromechanical Aspects

The elements of the radiating dipoles are essentially all metal-to-metal with no dielectric materials directly exposed to ultraviolet radiation to avoid degradations. The cylindrical reflector is of electron-beam-welded aluminum construction for stiffness. Electroformed nickel-honeycomb was considered; however, all efforts were made to avoid magnetic materials, which could, in space probe applications, provide magnetic fluctuations.

The antenna drive system consists of a 32-pole, permanent magnet, synchronous, pulse-actuated stepper motor[2] driven by a train of pulses (2^7) which are phase-locked to a train of 2^9 pulses triggered by a sun-line spacecraft sensor. Ground command inputs may also provide position control, synchronization, and beam steering via telemetry channel inputs.

The angular position of the motor shaft and the attached reflector is known and is controlled within 0.7 $\pm$0.35 deg from a shaft-mounted encoder. In orbit, the motor is started in rotation by pulse trains of low frequency, and the motor follows the input pulses at the rate of one quarter tooth displacement per pulse—128 pulses per revolution. At operational spin rates of 100 $\pm$50 rpm, the motor runs continuously in a slew mode and is locked to the sun pulse through a phase-locked loop and pulse generator as part of the spacecraft jet control system. Power to the motor is supplied by solid-state series/parallel-driven circuits which energize four stator windings in sequence. An electrical damper circuit to limit load oscillation is included.

C. Bearing System

The bearing system, shown in Fig. 1, consists of two sets of high-precision instrument-type angular contact bearings in stainless steel races.[3] The balls are separated by a cotton-fibre-reinforced phenolic retainer.[4] Under gravity-free loading, ball skidding was anticipated; hence, a spring-loaded washer was added to provide a 12-lb axial thrust load, which is translated into a radial thrust load to ensure a constant torque and bearing load even under thermal excursions of 100°F. The increased friction torque was 0.0025 in.-lb out of the total friction torque for the bearing system of 0.0165 in.-lb (0.020 nominal to 0.040 in.-lb maximum). The motor torque capability of 0.2 in.-lb provides a safety factor of 5 for temperature environment of −20°F storage, starting temperature of

[2]General Precision Systems Inc., Kearfott Products Division, Little Falls, N.J.

[3]MPB-3-TAR 25-32 size and type, Miniature Precision Bearings, Inc., 10 Precision Park, Keene, N.H.

[4]MIL P 79 FBE phenolic retainer.

20°F, and a maximum of 120°F for starting and operational levels. For the 12-lb preload, the bearing life is computed at 1.93×10^5 h or 22 yr.

D. Lubrication System

The 5-yr design goal for successful operation was directly related to the choice of the lubrication system for the spatial hard vacuum (10^{-10} torr) and a total radiation dosage per year of approximately 5×10^6 ergs/g. Lubrication systems fall into three general categories:

(1) Solid film coatings. Solid films would not evaporate; however, life in hard vacuum is severely limited. Molybdenum disulfide burnished in inert (argon) atmosphere, gold, silver, and Teflon coatings are utilized in terrestrial and spacecraft services. Since the lubricant film cannot be replenished, the limited-wear characteristics and ensuing debris can cause erratic torque behavior wherever the solid film wears off. Film penetration failure contributes to premature bearing failure when the cohesive characteristics are exceeded.

(2) Solid lubricant in bearing retainer structure. This method provides a replenishing supply of lubricant to the bearing; however, this design is unproved in reliability and life characteristics.

(3) Oils and greases. These have long been satisfactorily used in rolling-contact bearings under normal environmental conditions. Evaporation at low pressure (especially for mineral oils) removes light fractions, leaves a viscous residual, and imposes a variable torque on the bearing system. Oils of a single molecular species give fairly constant rates of evaporation, and residual oils have the same characteristic as the original lubricant. Liquid lubricants have been used in *Tiros II* and *Orbiting Solar Observatory* spacecraft for 2 yr of operation.

An oil system, therefore, was chosen as the most reliable type of lubricant. An annular reservoir, filled with a nylon fiber matrix (25% porosity), stores 25 g of Apiezon-C oil with a long-chain, polar molecule additive for superior adhesion to races and balls. The oil flows, in parallel, to the upper and lower bearings and exits to space through upper and lower annular (0.004-in.) molecular seal apertures. The evaporation of the lubricant can be calculated from kinetic gas theory at equilibrium. The lubricant loss is computed as 0.0691 g/cm^2-yr. The reservoir volume required for 5 yr is 1.565 cm^3/cm^2 for an operating temperature range between 20 and 120°F at the motor. Based on measurements, the evaporation rate is extrapolated to 0.1 g/yr, and the reservoir capacity is 22 cm^3 (24 g); hence the expected life based on complete evaporation of all the lubricants is 240 yr at a motor operating temperature of 120°F.

Two sets of bearings and motors were run in cold-wall vacuum chambers at 10^{-8} torr for 8,000 h, and the bearings were then disassembled and examined for wear. Maximum frictional torque at 20°F was 0.05 in.-lb; the oil evaporation rate at 120°F was less than 1.0 g/yr for bearings where races were fully exposed to space and 0.1 g/yr for the controlled-aperture molecular seal. The bearing wear condition was termed "unused" in the bearing retainer pockets (usually a maximum-wear area), which had no indications of surface wear and no evidence of pits, surface scratches, or cold welds. The test results of 8,000 h, under space-equivalent conditions, were deemed sufficiently conclusive to be extrapolated to the longer 3- to 5-yr operational goal.

IV. Reliability Assessment

Extremely high reliability assurance levels placed a critical dependence upon the motor-bearing-lubrication system. Dual, completely independent electronics subsystems represent the selectable, switched, parallel-standby antenna positioning and control system. Each of the symmetrical circuits conveys sun reference timing pulses and telemetry control signals to the motor-driving circuits. This latter subsystem utilizes series-redundant and switched, parallel-standby techniques to actuate the motor.

Failure rate analysis was made for every integrated circuit over operational temperatures between −20 and +120°F, for an acceleration factor no greater than 64 and a 100% screening basis for all semiconductor components.

The cost of this reliability series–parallel redundancy protection is:

(1) A fourfold increase in parts and costs.

(2) Less than a fourfold increase in weight and volume.

(3) A reduction in motor driver efficiency (the motor power of 4.6 W required 1.232 W in the redundant mode control circuitry against 0.308 W in the nonredundant control circuit).

(4) Increased difficulty of circuit inspection and failure detection.

The motor-bearing-drive system reliability was analyzed by two techniques—the AVCO-RAD[5] and the RCA-Montreal[6]—for mechanical and electromechanical parts. The AVCO-RAD analysis neglects wearing, assuming that wear life is greatly in excess of a random failure (constant), and is primarily concerned with a random defect in bearings or motor windings. The RCA-Montreal method assumes that wear is the principal consideration and therefore that failure rate is a function of time. The former arrives at a constant failure rate of 0.020%/1,000 h, and the latter at a variable failure rate of 0.0025%/1,000 h for the first year to 0.028%/1,000 h for the first 5 yr; however, the mean wear life of 10^6 h (11.4 yr) is obtained for the motor-bearing-drive system, and a specific calculation yields a mean wear life of 28 yr. The random failure therefore is considered as the determinant of success rather than the wear function. Accordingly, a reliability summary based upon the random failure analysis indicates that the system reliability figures are 0.99578, 0.98297, and 0.96521 for operating times of 1, 3, and 5 yr, respectively.

[5]*Failure Rates,* IDEP 347.40.00-B8-01. AVCO Corporation, RAD Division, Wilmington, Mass., Apr. 1962 (now out of print).

[6]*Proposed Procedures for Reliability Assessment of Mechanical and Electromechanical Parts,* IDEP 347.25.00.00-F8-01. RCA Victor Company, Ltd., 1001 Lenoir St., Montreal, Quebec, Can., Jan. 1963.

V. Fail-Safe Mode of Operation

The high probability of success of the mechanical system is nevertheless backed by a fail-safe mode of operation. When a determination is made that the mechanical system has somehow failed, ground command initiates an order to fire the dual squibs. This action elevates a cylindrical concentric tube to unlock the split turntable from the rotating shaft. The split turntable, under compressed springs, allows separation of the two major parts away from the collinear radiator stack with a velocity of 5 ft/s, as shown in Fig. 1b. The antenna system continues to operate as a lower-gain omnidirectional radiator symmetrically disposed about the original spacecraft spin axis.

VI. Conclusion

The mechanically despun antenna concept is now demonstrated on an operational quality basis on spacecraft in orbit—ATS III and *Intelsat III A* and *B*—and has received major consideration for galactic space probes and broadcast satellite applications. A logical extension has been to despin a major portion of a spacecraft and to mount antennas as single or multiple apertures to achieve high gain figures (30–40 dB) for communications.

This has been possible because bearing, motor, and lubrication technologies have been judiciously applied and tested to assure 5-yr lifetime probabilities greater than 0.965 for the system.

70N 21429

Spacecraft Mechanism Testing in the Molsink Facility*

J. B. Stephens
Jet Propulsion Laboratory
Pasadena, California

The 10-ft Space Molecular Sink Simulator Facility (Molsink), which simulates the "permissive" extreme-high-vacuum environment of outer space, is described. In the Molsink, for every 10,000 molecules that leave a test item, only a few return. Test results are discussed for the following components of the Mariner Mars 1969 spacecraft: the prototype infrared spectrometer motor and gear train mechanism and both the wide-angle and narrow-angle camera shutters.

I. Introduction

This paper describes the 10-ft Space Molecular Sink Simulator Facility, now operational at the Jet Propulsion Laboratory, and its uses. The triple-wall construction combines an extreme-high-vacuum capability (10^{-12} torr) with an anechoic configuration. The inner wall is cooled to 14°K and coated with evaporated titanium to effect a very high capture coefficient for all gas molecules. Even helium may be captured by this wedge fin molecular trap.

To date, three *Mariner Mars 1969* mechanisms have been tested, and the first phase of a cooperative JPL, TRW,[1] and U.S. Air Force study of friction phenomena has been completed. Some experiments have been performed for the study of microbial death in the space environment. A program has also been started to define the density profile of rocket plumes at high vacuums. Within the next year, it is planned to complete the experiments above and to perform calibration tests on various lunar atmosphere mass spectrometers and development tests of several *Mariner Mars 1971* mechanisms.

A Molsink calibration and evaluation program, which was started several months ago but deferred because of the press of flight project tests, is now planned to be completed by July 1969. This program is primarily to make an experimental verification of the Molsink Factor (see Section III) by allowing various gases to leave the center of the chamber under controlled conditions and measuring the amount that returns.

II. The Facility

The Molsink facility, illustrated in Fig. 1, is a 10-ft-diam, triple-walled, extreme-high-vacuum chamber with walls that cryogenically and chemically pump gases produced by the test item. The cryopumping is accomplished by a spherical molecular trap (Moltrap) wedge fin array (Figs. 2

*This paper presents the results of one phase of research carried out at the Jet Propulsion Laboratory, California Institute of Technology, under Contract No. NAS 7-100, sponsored by the National Aeronautics and Space Administration.

[1]TRW Systems Group, One Space Park, Redondo Beach, Calif.

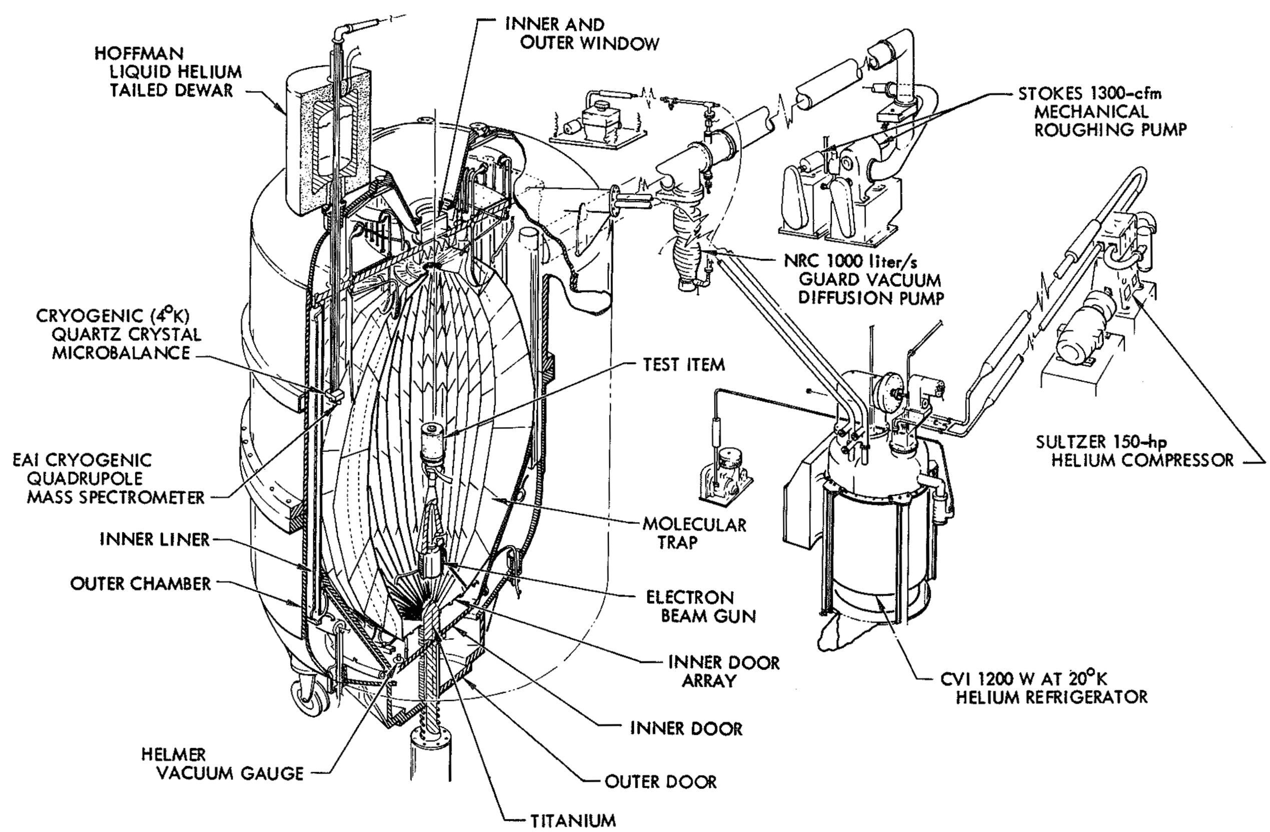

Fig. 1. Schematic drawing of the Molsink chamber. The outer carbon steel pressure vessel is sealed with O-rings, rough-pumped with a mechanical pump, and sustained with an oil-diffusion pump. The LN_2-cooled vacuum-tight inner liner is rough-pumped through the inner door, which is closed during sustained operation

and 3) with a 96-in. effective diameter. The Moltrap is constructed of 0.016-in.-thick aluminum sheets that are spot-welded to aluminum tubes; the tubes are cooled to 14°K by a 1200-W helium refrigerator. The angles of the fins are such that projections of their surface planes are tangent to a 10-in. sphere at the center of the Moltrap, a configuration that provides an order-of-magnitude capture improvement, compared with a smooth spherical wall, when the test item gas load is from within the same 10-in. spherical volume. The chemical pumping is accomplished by an electron-beam titanium sublimator mounted on the inner door of the chamber. Titanium is deposited upon the inside surface of the Moltrap array.

III. The Environment

The simulation of the molecular sink of space for the testing of spacecraft mechanisms can be confusing because it refers to a passive rather than an active property of space. The fact that space has no walls nor many objects in it creates the condition where molecules that leave a spacecraft do not return (mean free path of molecules is 10^8 km). Since the important environmental parameter for surface-effect phenomena is the net molecular flux on the surface, and since the test item is the major source of gas in a well designed facility, the significant measure of facility performance is the Molsink Factor (the ratio of the number of molecules that leave the test item to the number that return).

In this chamber, for every 10,000 molecules that leave the test item, only a few will return to it. This value is based upon a hypothetical spherical test item 10 in. in diameter operating at 300°K and emitting gases such as oxygen and nitrogen (see Fig. 4). The number returning

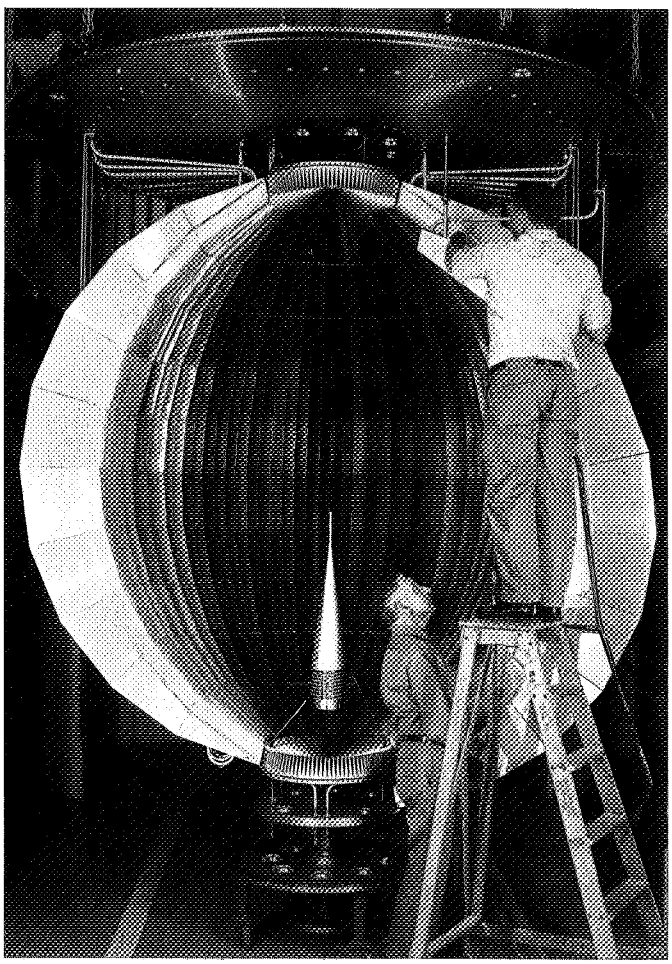

Fig. 2. The molecular trap elements being installed in the bulkhead plate of the inner liner

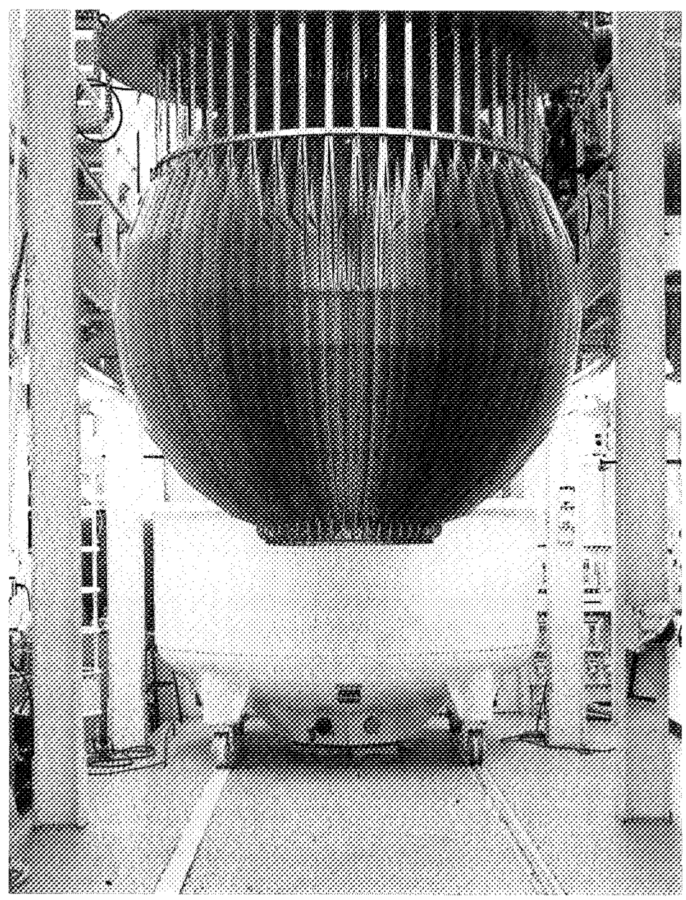

Fig. 3. The completed Moltrap, which is an anechoic chamber for gases because of the 2000-ft² area of 14°K surface exposed to the test item

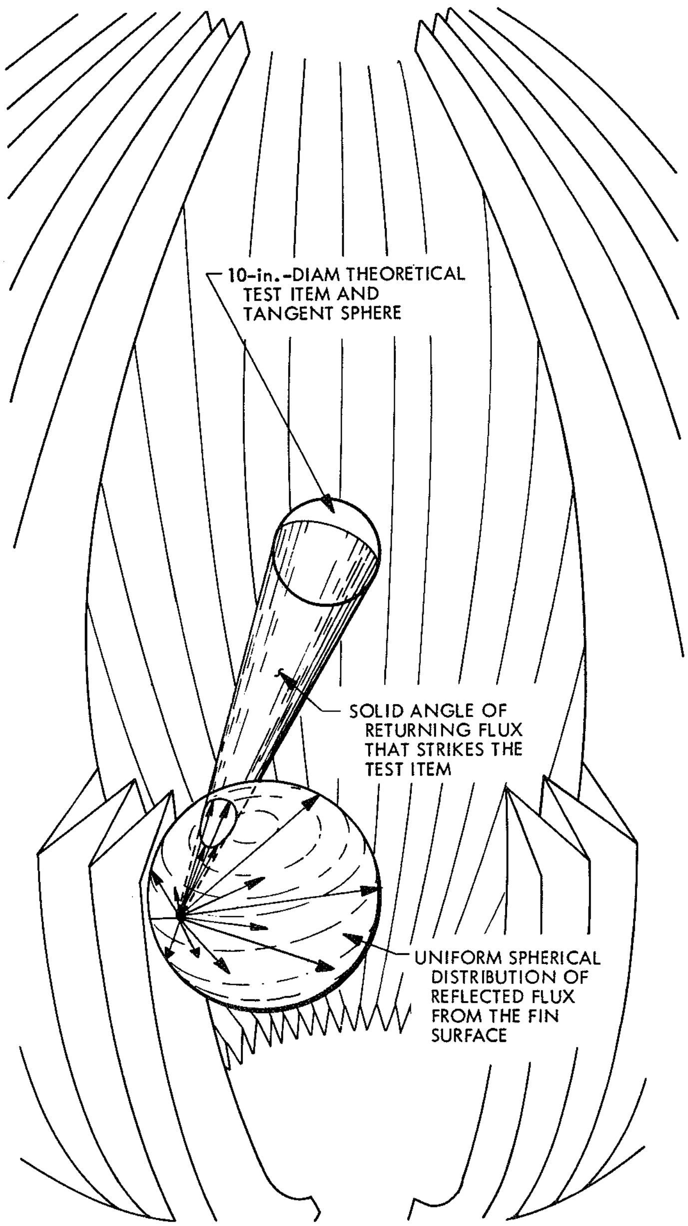

Fig. 4. The relation of Knudsen's law to the molecular trap configuration. Most of the rebounding molecules restrike the adjacent fin surface, where a larger fraction is captured because of the molecules' initial accommodation at the first encounter

would be much less for more easily condensed gases such as water and most hydrocarbons; this number is much larger for helium and hydrogen. The titanium chemisorbs hydrogen at a pumping rate of 7 million liters/s, and it also apparently physisorbs helium at a small but significant rate.

IV. Infrared Spectrometer Tests

Three tests were performed on one prototype *Mariner Mars 1969* infrared spectrometer motor and gear train mechanism (Fig. 5) built by the Space Sciences Laboratory at the University of California, Berkeley. The gears and bearings were coated with a 2×10^{-5}-in. thin film of tungsten disulfide.[2] In each case, the mechanism was outgassed to simulate the trip to Mars. The gear drive bearings "seized" after run periods in the vacuum of 135 h, 28 h, and 4.7 h, respectively. The gear drive was completely refurbished between the first and second tests. The third test was made after a partial disassembly and reassembly, but without refurbishing the bearings with thin-film lubricant.

As a result of these tests, glass-filled Teflon bushings were installed to replace the thin-film lubricated journal bearings.

V. Wide-Angle Camera Shutter Tests

A number of development tests were performed on the *Mariner Mars 1969* wide-angle camera shutter mechanism (Fig. 6), a combination shutter and filter-changing mechanism operated by a linear solenoid.[3] During the first of these tests, the voltage pulse required for reliable operation increased to an unacceptable level, indicating an increase in friction in the mechanism. The solenoid was then made more powerful. Two shutters with the improved solenoids were operated some 122,000 and 46,000 cycles respectively in the Molsink chamber without failure.

Figure 7 presents photomicrographs showing the scoring resulting from the local failure of the thin-film lubricant. However, this problem was overcome by the additional power of the improved solenoid.

VI. Narrow-Angle Camera Shutter Tests

One *Mariner Mars 1969* narrow-angle camera shutter was life-tested in the Molsink chamber; 31,000 cycles were run prior to operating in the Molsink for 100,000 cycles, and 68,000 cycles were accumulated after the test without failure.

[2]MPB Corporation, Dicronite Lubricants Division, Mountain View, Calif.

[3]See "A Combination Shutter and Filter-Changing Mechanism," by Allen G. Ford and James A. Cutts, in these *Proceedings*.

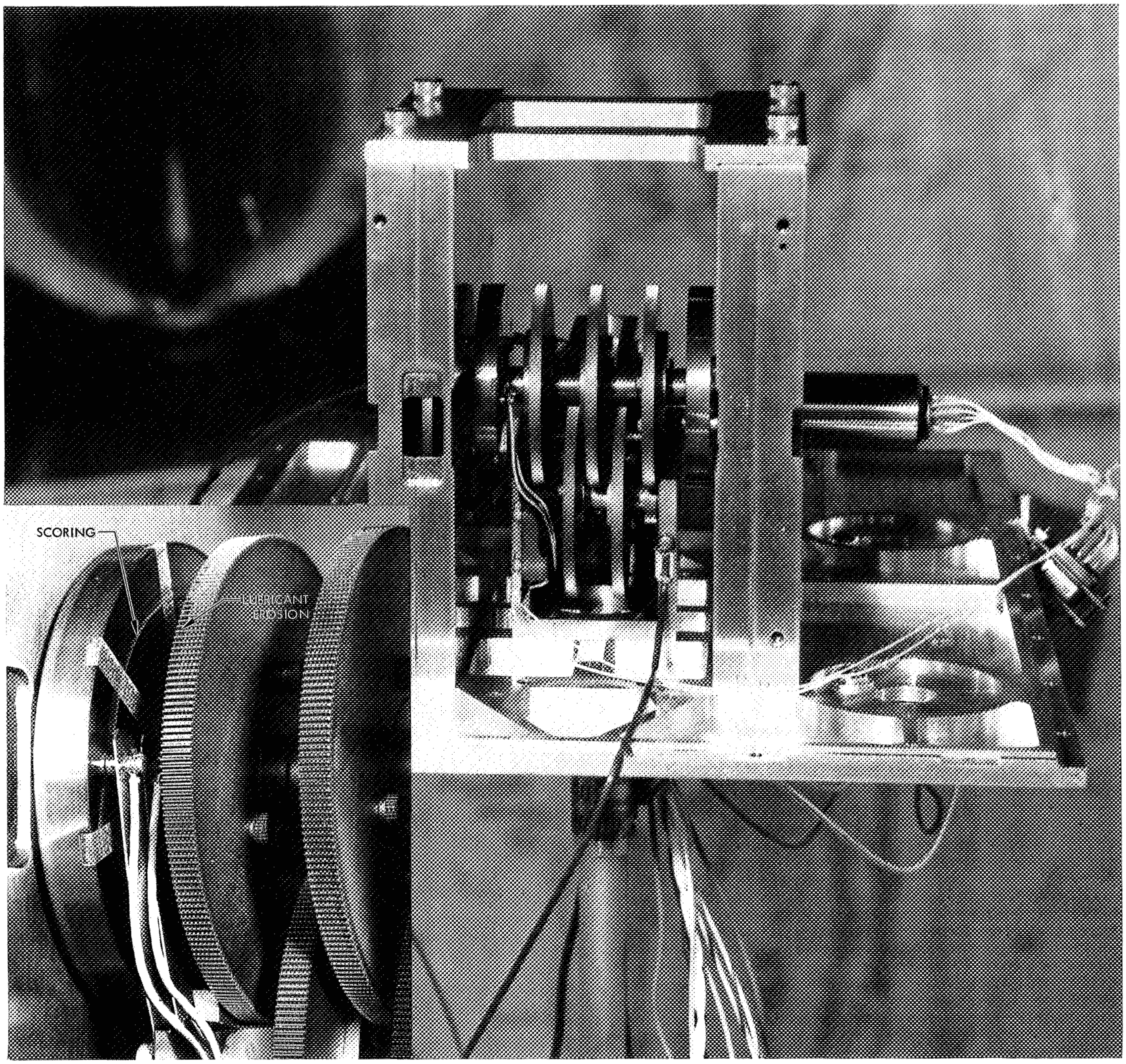

Fig. 5. The *Mariner Mars 1969* infrared spectrometer drive mechanism. Note loss of lubricant on gear teeth and scoring of simulated slip ring. Failure of mechanism was in journal bearing thin-film lubricant

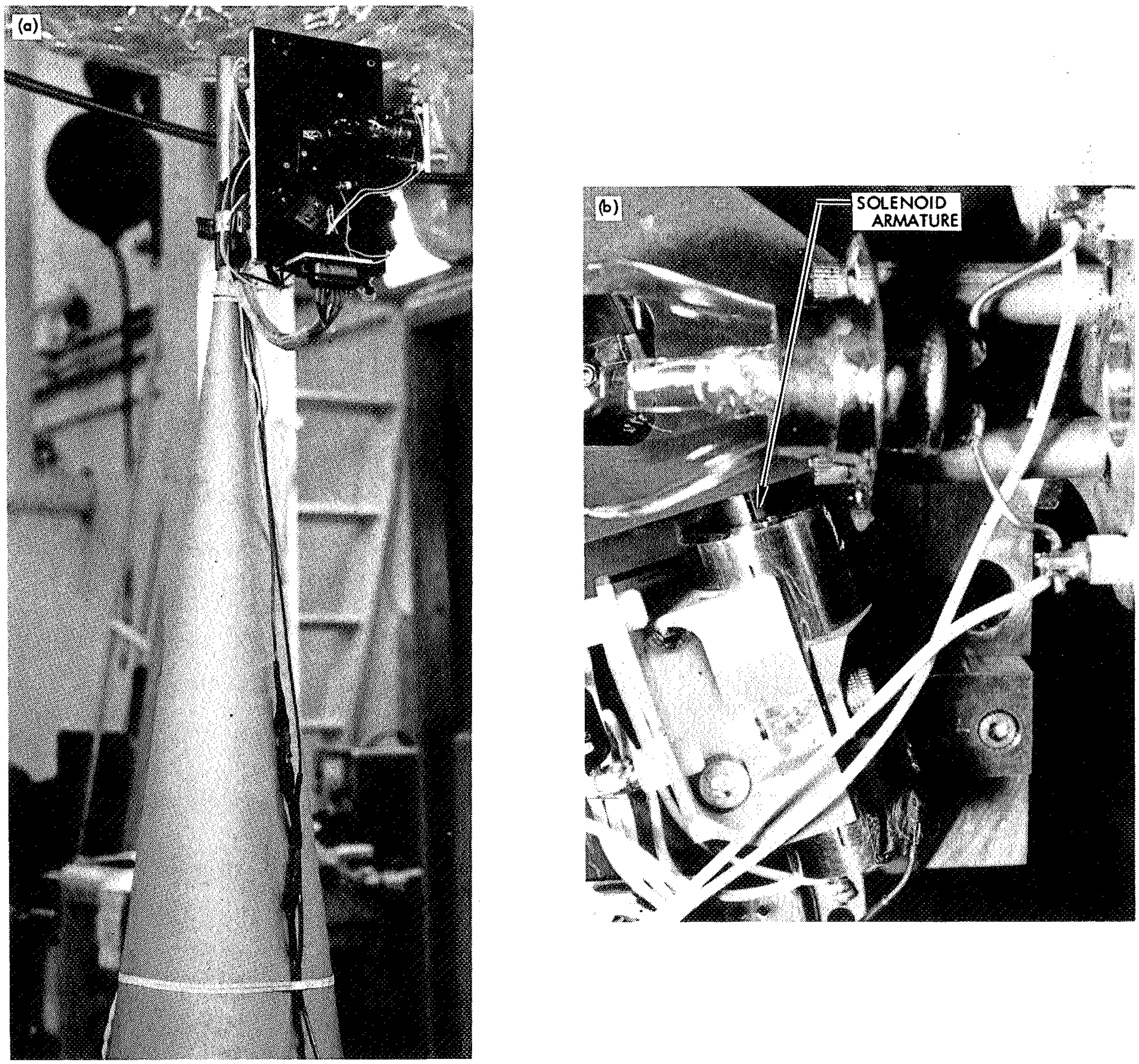

Fig. 6. The *Mariner Mars 1969* wide-angle camera shutter mechanism: (a) on Molsink test fixture, (b) closeup view. Unbalanced loading of solenoid caused thin-film lubricant to be removed from armature shaft

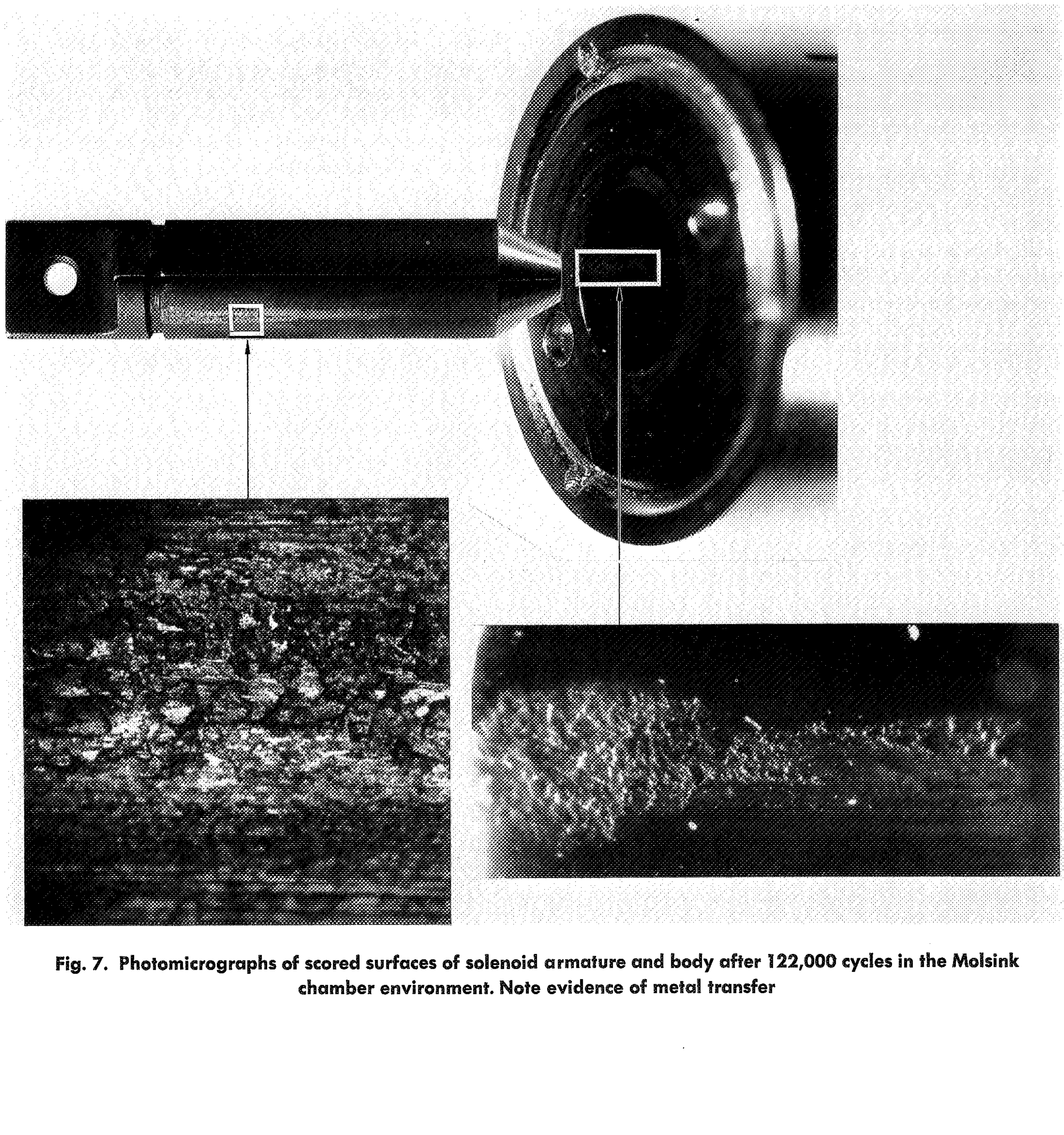

Fig. 7. Photomicrographs of scored surfaces of solenoid armature and body after 122,000 cycles in the Molsink chamber environment. Note evidence of metal transfer

VII. Summary

Our goal has been to develop a facility and techniques that permit the investigation of those surface-effect phenomena that are important to spacecraft performance and to do this by using spacecraft hardware under conditions closely approximating those in space. The most important aspect of space in this regard is the molecular sink, by which is meant the passive environment that allows molecules ejected from a spacecraft to leave and not interact with the spacecraft again.

In the past, surface-effect phenomena (cold welding of mechanisms, degradation of thermal control coatings, viability of microorganisms) have been investigated in small, tightly sealed, and cleanly evacuated chambers using idealized test objects with low outgassing rates. While such facilities are very successful in minimizing the indigenous and facility-induced molecular flux, they do not provide an effective molecular sink and, therefore, cannot be used to realistically test actual spacecraft hardware, which typically have high outgassing rates.

Because of the space limitations of this paper, no attempt has been made to cover this subject completely.[4] Rather, it is hoped that an introduction to this new kind of facility and the tests conducted in it will stimulate consideration of experimental explorations which heretofore have not been possible.

[4]A detailed description and analysis of the Molsink facility will be presented in *Space Molecular Sink Simulator Facility*, Technical Report 32-1110, Jet Propulsion Laboratory, Pasadena, Calif., to be published.

70N21430

Dynamics of Human Self-Rotation*

Thomas R. Kane
Stanford University
Stanford, California

Self-rotation of astronauts by moving various parts of the body is discussed in reference to results obtained from dynamical analyses dealing with yaw, pitch, and roll motions. A pitch maneuver and two yaw maneuvers are considered in detail. One of the latter is similar to the righting movements of a falling cat, whereas the other involves conical motions of arms or legs.

I. Introduction

The fact that animals (e.g., falling cats) and humans (e.g., gymnasts, trapeze performers, and divers) can perform well-controlled self-rotation maneuvers leads one to surmise that an astronaut in a state of free fall may be able to control his orientation in space by performing appropriate relative motions of parts of his body. With this idea in mind, the author and his students have attacked a number of problems of dynamics whose solution may be expected to facilitate the development of effective self-rotation techniques. It is the purpose of this paper to present a brief review of some of this work.

II. The Falling Cat

Figure 1 shows a cat falling after being released from rest. It appears from the photographs that the torso of the cat bends, but does not twist appreciably; that the spine is bent, successively, forward, to one side, backward, to the other side, and then forward again; and that backward bending is considerably less pronounced than forward bending. A mechanical system capable of moving in such a way as to reflect these features of the motion of a falling cat is shown in Fig. 2, where A and B designate identical, rigid, right-circular cylinders connected to each other at a point 0 on their axes; A^* and B^* are the axes of the cylinders; K is a line fixed in A and making an angle α with A^*; and N is the normal to the plane determined by A^* and B^*. This system can move in the manner stipulated if

(1) B^* remains on the surface of a right-circular cone with axis K and semivertex angle β.

(2) ${}^R\omega^A$ and ${}^R\omega^B$, the angular velocities of A and B in a reference frame R in which N and the bisector of the angle between A^* and B^* are fixed, satisfy the equation

$$ {}^R\omega^A \cdot \mathbf{c} = {}^R\omega^B \cdot \mathbf{c} \tag{1}$$

where $\mathbf{c}$ is a vector parallel to the bisector of the angle between A^* and B^*.

(3) The inertial orientation of $\mathbf{c}$ remains fixed.

*This work was supported, in part, by the National Aeronautics and Space Administration under NGR-05-202-209.

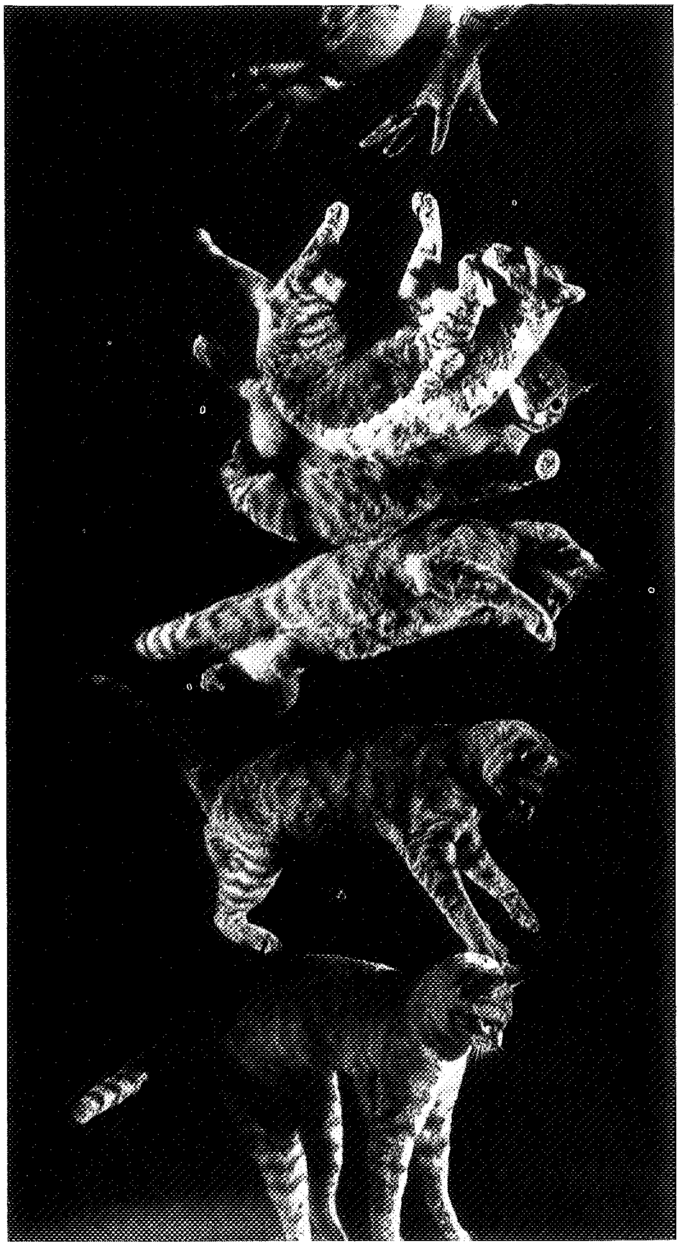

Fig. 1. Righting movements of a falling cat (Ralph Crane—LIFE Magazine)

The results obtained (Ref. 1) by solving the equations of motion of the system subject to these requirements can be presented in the form of plots showing the cylinders A and B at discrete instants of time, as in Fig. 3, and a check on the validity of the theory may be obtained by superimposing these plots on the corresponding photographs, as in Fig. 4.

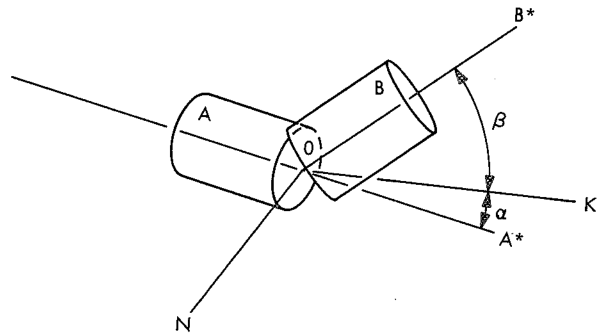

Fig. 2. A mechanical system capable of simulating the motions of the falling cat

III. Human Self-Rotation

A human being can perform motions similar to those just described. However, he may find it excessively arduous or even impossible to do so when he is wearing a pressure suit. Furthermore, the "cat maneuver" can, at best, produce only a yaw rotation, i.e., a rotation about an axis that is approximately parallel to the spine of a man standing straight. Hence it is necessary to explore alternative self-rotation techniques for yaw, as well as methods for generating pitch and roll motions.

A two-phase maneuver that produces yaw motion and that may be performed either with the arms or with the legs is illustrated in Fig. 5. When the legs are used, the motion proceeds as follows: In Phase 1, the legs are placed as when taking a step in walking, and each leg is then moved on the surface of a cone whose axis is parallel to the spine. In Phase 2, the forward leg is brought to the rear and vice versa, each leg moving in a plane parallel to the plane of symmetry of the torso, until the initial configuration has been recovered. To analyze this maneuver, the human body was modeled (Ref. 2) as a system of three rigid bodies, one representing the torso, head, and arms (or legs), and the remaining two each representing one leg (or arm). A condition similar to that expressed by Eq. (1) was imposed in order to exclude motions involving twisting of arms or legs, and the equations of motion were then solved analytically, the solution yielding a relationship between the yaw per cycle and semi-angle of limb (arm or leg) spread. In Fig. 6, quantitative results are shown for a man having typical inertia properties and performing the maneuver (1) with the legs, (2) with the arms unencumbered, and (3) with the arms while holding a 5-lb weight in each hand. It can be seen that use of the legs is considerably more effective than that of the arms,

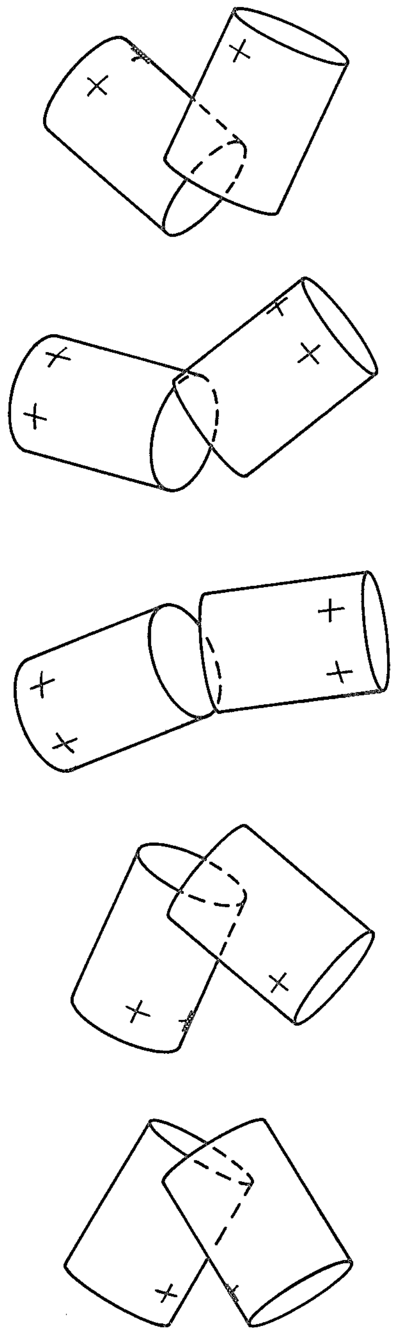

Fig. 3. Computer plots showing the motion of the mechanical system of Fig. 2

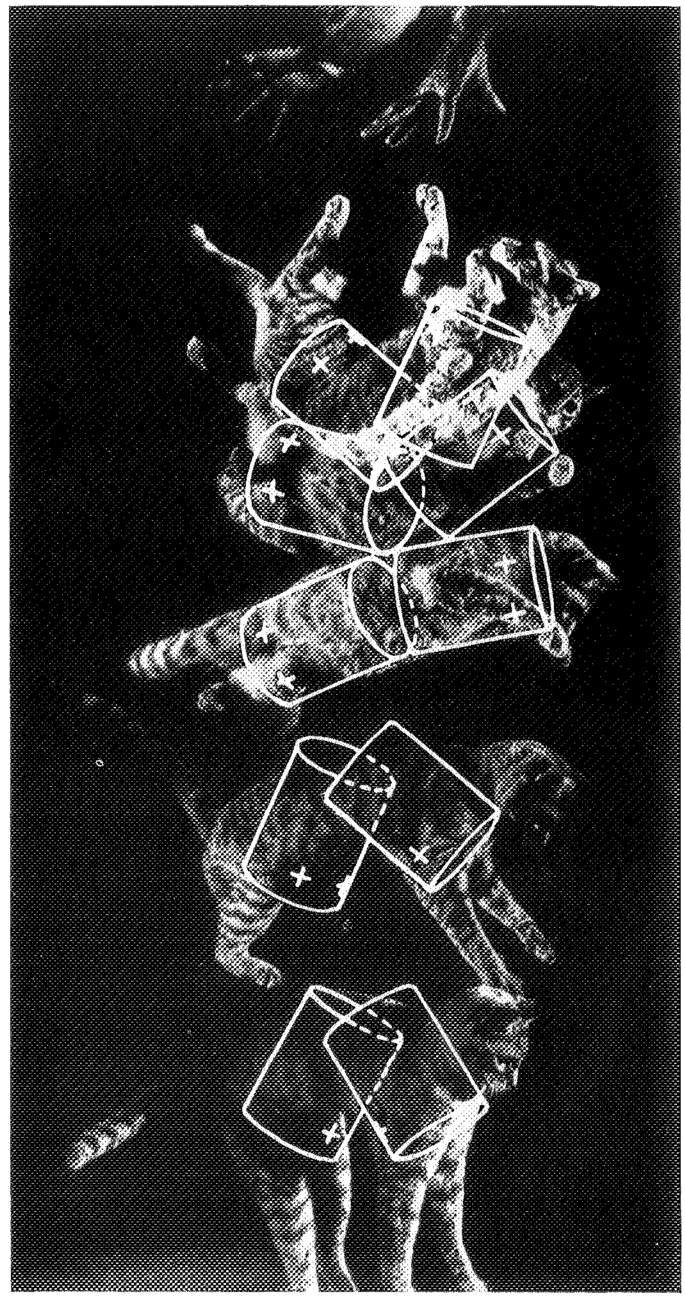

Fig. 4. Superposition of computer plots and photograph

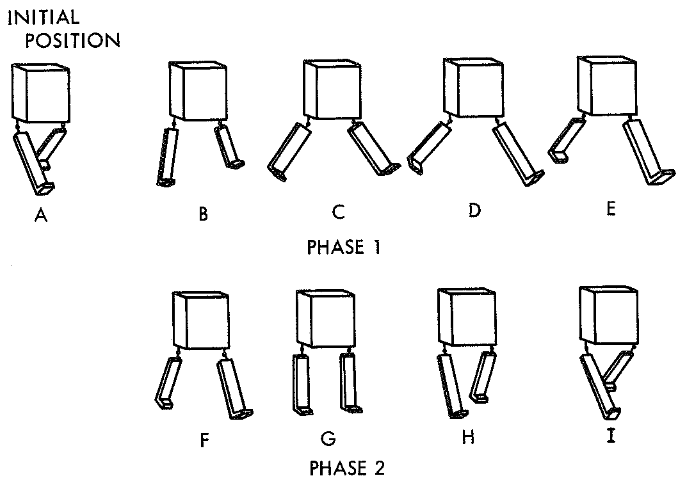

Fig. 5. A two-phase maneuver for producing yaw motion

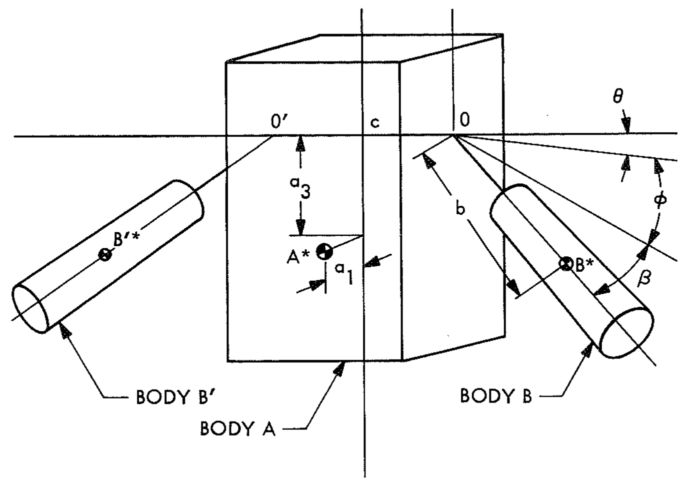

Fig. 7. A mathematical model for a pitch-motion analysis

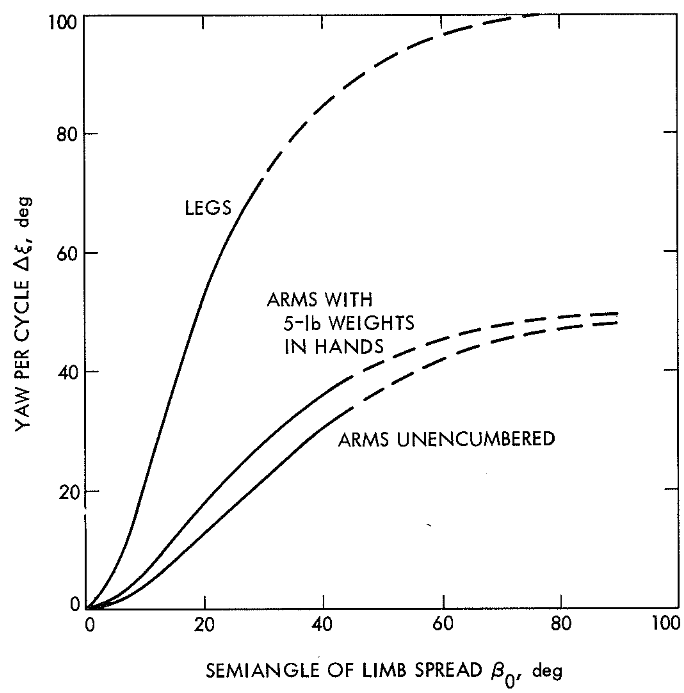

Fig. 6. Yaw reorientation as a function of semiangle of limb spread

and that holding weights in the hands does not help substantially.

Pitch motion, i.e., rotation about an axis that is perpendicular to the plane of symmetry of the torso, can be produced most easily by revolving the arms symmetrically, each arm moving on the surface of a cone. Three angles are required to specify this arm motion: the semivertex angle of the conical surface on which each arm moves and two angles that locate the axis of one cone. In Fig. 7, which shows the mathematical model used for this investigation (Ref. 2), the first of these angles is designated β and the remaining two are called θ and ϕ. Numerical evaluation of a definite integral is required to determine the relationship between these angles and $\Delta\xi$, the pitch rotation produced during one cycle of the maneuver. Results obtained by performing such integrations are shown in Figs. 8 and 9, the first of which permits one to assess the effectiveness of holding the legs in a tucked position, rather than straight, or of holding weights in the hands. Figure 9 brings a practically significant fact to light: As the slope of each curve is rather small so long as the angle ϕ remains below, say, 30 deg, little is lost, and something may even be gained, by using values of ϕ other than zero; i.e., by lowering the arms. This fact is of interest because the human shoulder is so constructed that a person can perform the motions under consideration much more easily with $\phi > 0$ than with $\phi = 0$.

The yaw and pitch maneuvers discussed so far are "pure" in the sense that each cycle of these maneuvers produces rotation about a single space-fixed axis. This fact greatly simplifies the associated analyses. By the same token, roll maneuvers are difficult to analyze because they are inherently "impure." A computer program that can be employed to study reorientations resulting from arm motions intended to produce nearly pure roll has been developed (Ref. 3), but the program has not been used to date to generate extensive data, partly because it is always possible to obtain a desired roll reorientation by performing, successively, a 90-deg yaw, a pitch equal in magnitude to the desired roll, and a second 90-deg yaw.

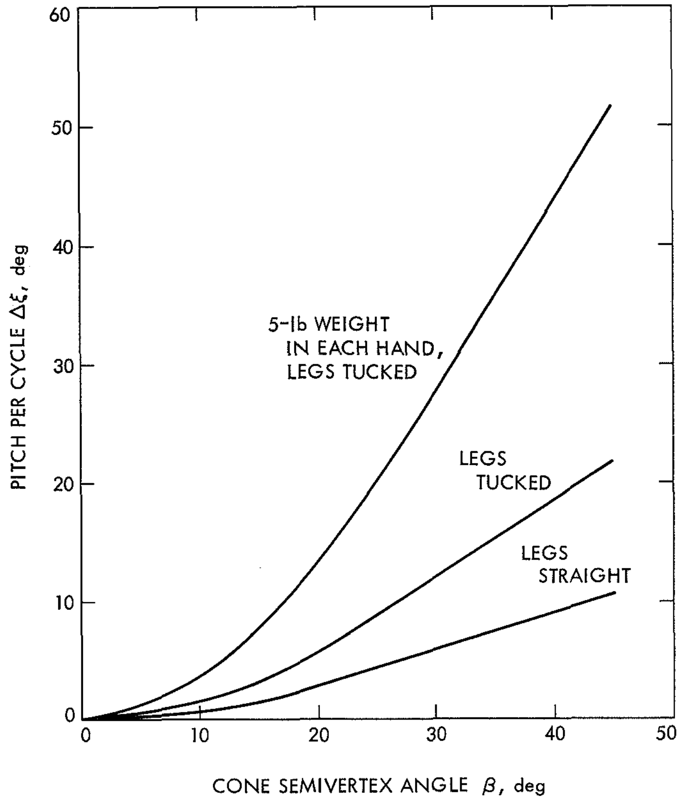

Fig. 8. Pitch reorientation as a function of cone semivertex angle (cone axes parallel to pitch axis, $\theta = \phi = 0$)

In principle, limb movements can serve not only to alter the orientation of a man initially at rest but also to transform one state of *rotational* motion into another. For example, if a man is in a position of "attention" while moving with an angular velocity that is parallel to the yaw axis, he can, by raising and lowering one arm, convert this motion into a rotation during which the angular velocity is parallel to the roll axis when the man is again in a position of "attention." A rationale for selecting arm motions that accomplish this objective is described in Ref. 4. However, the fact that maneuvers of this kind must be performed with considerable precision suggests that the knowledge gained in the investigations concerned with this topic is more readily applicable to satellite attitude control than to human self-rotation.

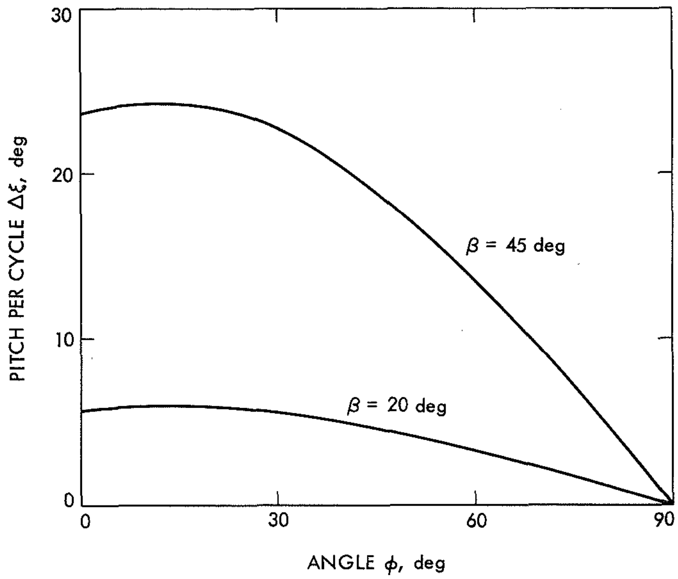

Fig. 9. Pitch reorientation as a function of ϕ ($\theta = 0$ deg, legs tucked)

Finally, limb motions can be employed in conjunction with external forces, such as those furnished by gas jets, to control the orientation of a man in space. Problems in this class are currently being studied.

IV. Conclusion

Some movements of bodies in free fall have been analyzed. The results of such analyses may help in assessing different methods of self-rotation that can be used by astronauts.

References

1. Kane, T. R., and Scher, M. P., "A Dynamical Explanation of the Falling Cat Phenomenon," accepted for publication in *Int. J. Solids Structures.*
2. Scher, M. P., and Kane, T. R., *Pitch and Yaw Motions of a Human Being in Free Fall,* Technical Report 190. Department of Applied Mechanics, Stanford University, Stanford, Calif., 1968.

References (contd)

3. Riddle, B. C., and Kane, T. R., *Reorientation of a Human Being in Free Fall*, Technical Report 182. Department of Applied Mechanics, Stanford University, Stanford, Calif., 1968.

4. Kane, T. R., and Scher, M. P., "A Method of Active Attitude Control Based on Energy Consideration," submitted to *J. Spacecraft Rockets.*

70N 21431

A Hard-Wire Rotating Coupling

E. H. Wrench
Convair Division of General Dynamics Corporation
San Diego, California
L. Veillette
Goddard Space Flight Center
Greenbelt, Maryland

This paper describes the hard-wire rotating coupling, a device for making continuous soldered-wire connections between a spacecraft and an oriented solar array. Test data on a laboratory model indicating a life of more than 200,000 cycles are included, together with the design for a hermetically sealed, two-degrees-of-freedom rotating coupling.*

I. Introduction

Operation of sun-pointing energy collectors from earth-pointing spacecraft may require continuous relative rotation between the spacecraft and the array. Although some success has been obtained in the operation of bearings, gears, motors, and slip rings in the space environment, such installations are potential failure sources and are only reluctantly proposed for long-term space missions.

An alternative approach, called the hard-wire rotating coupling, permits use of a continuous multiple-soldered-wire connection between two bodies that have unlimited angular freedom, without the use of slip rings, rotary transformers, or interruptions in the circuits. When the coupling is used for solar pointing arrays, all moving parts, including the drive motor, the paddle-support bearings, gears, etc., can be hermetically enclosed in a pressurized container without the use of penetration seals.

*Wrench, E. H., *Coupling*, U.S. Patent 3,358,072. Dec. 12, 1967.

II. Operating Principle

Operation of the coupling can be understood by visualizing a flexible conducting member such as a hose (Fig. 1a). Obviously the two ends of such a conductor can be rotated continuously at the same rate. Furthermore, if the conductor is bent around a 90-deg corner, the ends can still be rotated continuously (Fig. 1b). If one end of the conductor is pointed at the sun and rotated about the line of sight, the other end will rotate about an axis normal to the line of sight.

The axis of the solar collector (Fig. 1c) can be made coincident with that of the flexible conductor at one end, while the earth-pointing axis of the spacecraft is affixed normal to the axis of the conductor at the opposite end. Rotation of both ends of the conductor will now cause the angle between the two lines of sight to progress through successive circles of arc. Any angle and any continuous sequence of angles can be maintained without twist in the conductor as long as one end is free to rotate about the line of sight.

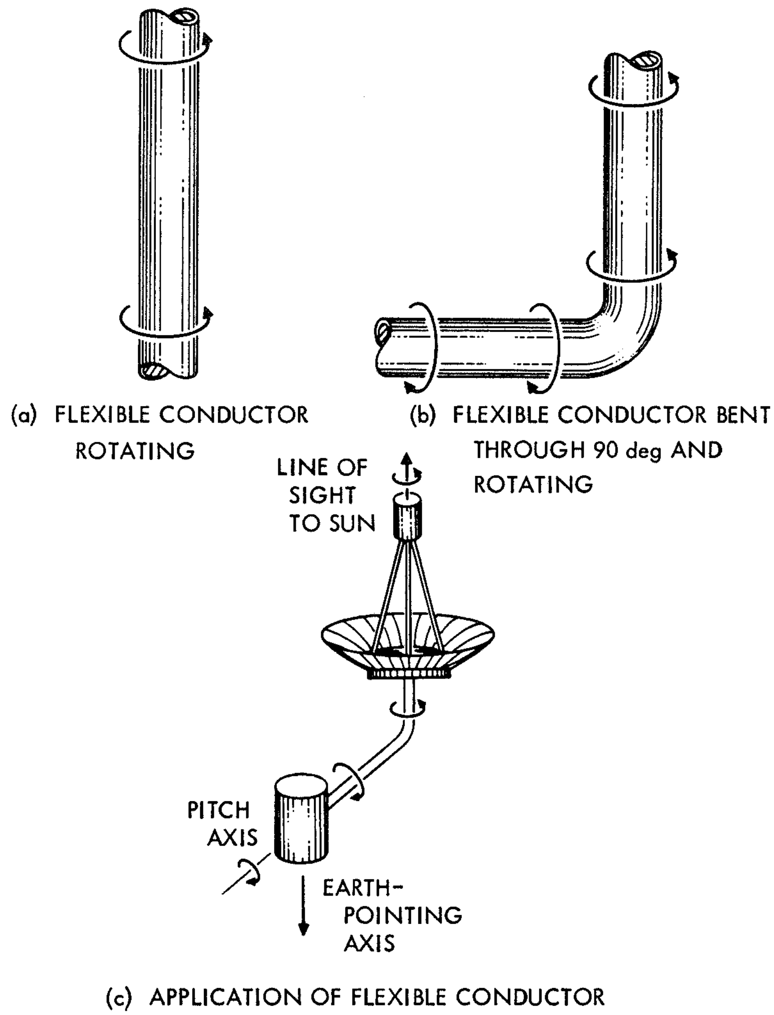

Fig. 1. Operating principle

III. Bevel Gear Joint

In the original design of the joint, it was realized that the power and signal connections should be as flexible as possible to maximize life and that the conductors themselves should therefore not be utilized to transmit torque. Identical kinematic operation can be obtained with a pair of rigid hollow shafts coupled by bevel gears. These components are employed as a protective structure to enclose the flexible conducting cable. This configuration (Fig. 2a) has been employed in all the units built to date.

A typical bevel gear coupling (Fig. 2b) was fabricated and tested by the Space Power Technology Branch at the Goddard Space Flight Center. The coupling employed 2-in.-diam bevel gears and a helical flexible conductor consisting of two No. 12 stranded power leads and 10 No. 30 signal leads, enclosed within a heat-shrink tube. Incandescent lamps drawing 1.3 A of current at 40 Vdc were mounted on the sun-pointing side of the coupling and the joint was rotated at 20 rpm; the current I was constant. The IR voltage drop of the conducting cable was monitored by the signal circuit to determine the onset of resistance changes resulting from cable deterioration. The test continued until complete failure occurred. In tests completed to date, the cable survived a minimum of 200,000 revolutions before deterioration (Fig. 3). After 200,000 revolutions, individual wires of the stranded cable began to separate, and complete failure occurred between 350,000 and 500,000 revolutions. Since the joint is intended for solar-array application requiring only one revolution per orbit, the 200,000 revolutions represent a life of more than 20 years.

(a) SCHEMATIC DIAGRAM

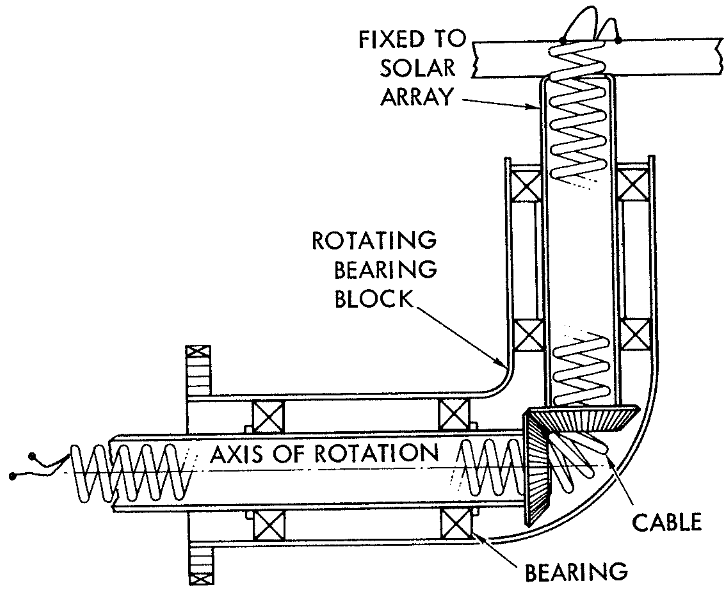

(b) TEST CONFIGURATION

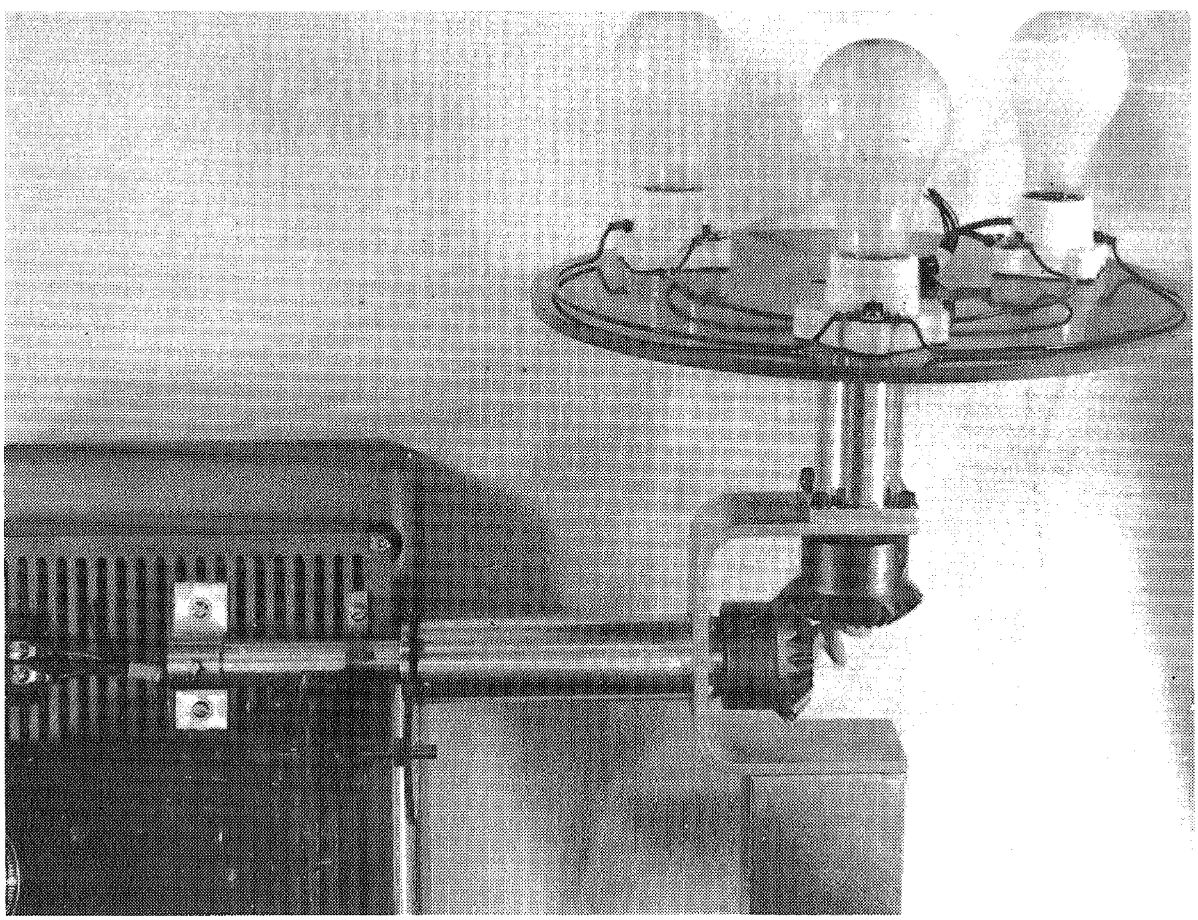

Fig. 2. Bevel gear joint

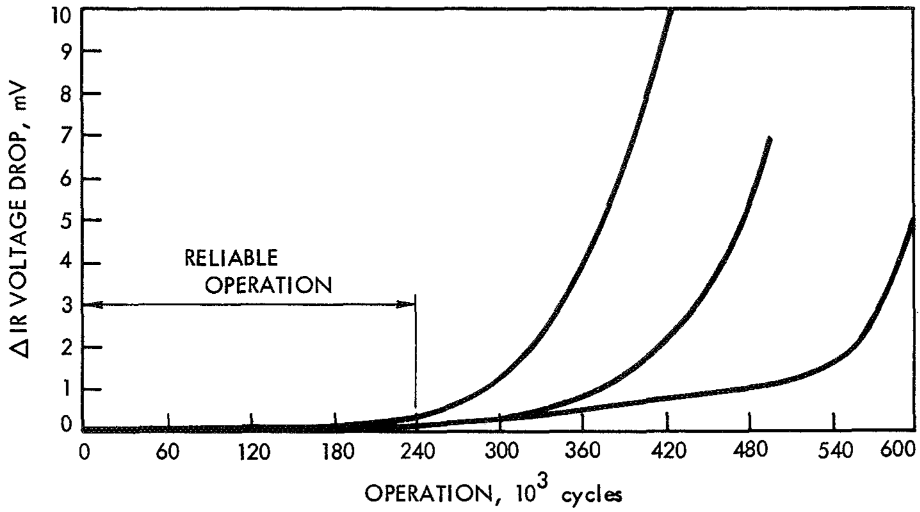

Fig. 3. Power cable life tests. Data are shown for three tests under identical conditions, using the cable described in Sec. III

IV. Hermetic Sealing

The tests at Goddard Space Flight Center were performed on an unsealed coupling operated in an earth ambient environment. A principal advantage of the hard-wire joint is the ability to seal the joint hermetically for space application. Again referring to the hose analogy, we can visualize a pair of flexible coaxial tubes (Fig. 4a). The inner tube represents the electrical cable, while the outer tube, a bellows, completely encloses the joint. Since one end of both the cable and the bellows is fixed with respect to the spacecraft, while the other ends are fixed with respect to the solar array, the two ends of the bellows can be capped off and the cable brought out through glass-to-metal feedthroughs. Figure 4b shows the concept of a completely hermetically sealed panel support arm. While other systems require that at least the paddle-support bearings be outside the sealed cavity, a unique feature of the hard-wire joint is that all components, including the support bearings, are hermetically sealed.

In actual practice, a sealed hard-wire coupling would probably not utilize a single pair of bevel gears. As Fig. 4b indicates, the required flexible electrical cable will have some finite allowable bend radius for the desired life. The bevel gears required to enclose the cable will have a diameter of twice the bend radius. To enclose such a configuration would require a bellows having a bend radius only a fraction of the diameter of the bellows, a difficult if not impossible configuration. A more practical technique is to effect the 90-deg bend in two or more steps. Figure 4c shows a joint employing two pairs of 22.5-deg bevels (to effect a total angle of 90 deg). The gear diameter is reduced from twice to only 0.67 of the bend radius. Obviously this technique can be carried beyond the two-pair arrangement; however, the two-pair joint is suitable for sealing.

V. Two-Axis Pointing

So far we have been concerned only with rotating the line of sight about a single axis of the spacecraft. For some applications it may be desirable to position the line of sight simultaneously about two axes. A practical solution to two-axis control is to employ two joints in series. The first coupling would provide rotation about the pitch axis of the spacecraft, while the second joint would permit adjustment of the angle between the line of sight and the pitch axis. Such an arrangement would allow conical scan with cone angles from 0 to 180 deg.

It is necessary to provide independent drives for each of the two degrees of freedom available in the series coupling. While we would normally locate drive motors within the spacecraft, this is not the most convenient location in the case of the two-axis joint. We must remember that the center flexible cable and the enclosing torque tubes and gears are effectively part of the spacecraft. Any component attached to this tube can be directly electrically wired to either the spacecraft or solar array and can be sealed within the captive atmosphere.

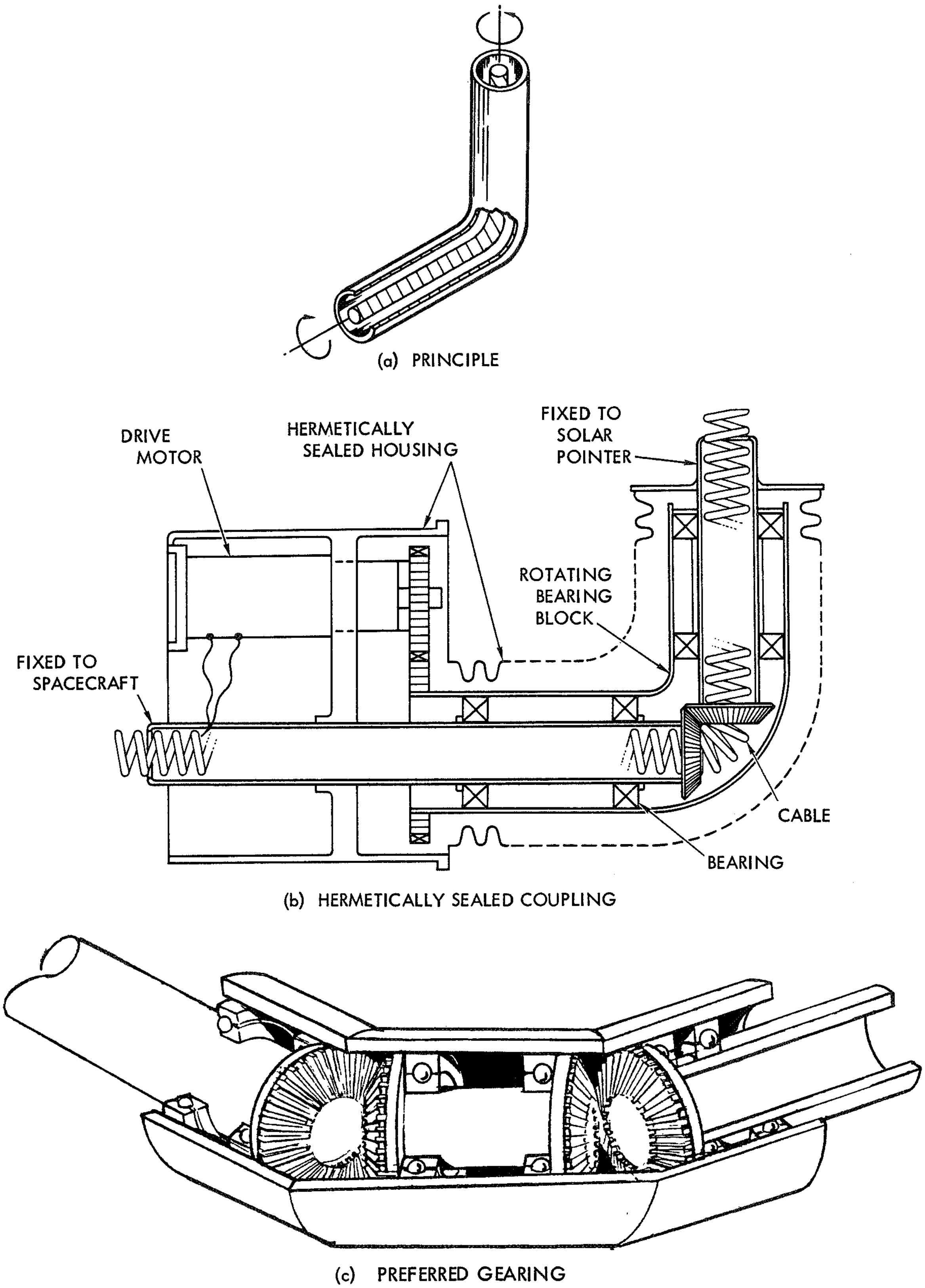

Fig. 4. Hermetically sealed couplings

Through the use of the pitch-axis torque tube as a frame of reference, the rotation in pitch is effected by torquing the pitch bearing block relative to the reference torque tube. Similarly, the second degree of freedom is obtained by torquing the yaw bearing block with respect to the pitch block. Both motions can be obtained independently by a pair of motors and a differential anchored to the center torque tube and located between the couplings. In a proposed configuration (shown in Fig. 5), the base of the motors is attached to the central torque tube, where it is electrically common to the spacecraft body.

VI. Spacecraft Interface

We have thus far arrived at a hermetically sealed, two-axis joint with continuous electrical connectors between the array, the spacecraft, and the pointing control motors. We should next examine the requirement that use of this joint would impose upon the spacecraft.

The hard-wire joint, as described above, imposes a unique requirement on the solar array since it is necessary for the array to rotate about the line of sight to the sun. The most efficient shape, of course, is a circle. Further, since a symmetrical configuration will generally impose fewer demands on the attitude control system, a pair of panels is preferred. A suitable configuration employing two circular panels has been designed by Convair, and a model (Fig. 6) has been fabricated. The circular configuration lends itself to stowage within the circular cross section of the booster heat shields. Two panels, each equal in diameter to the available envelope, can be accommodated. For a booster the size of an *Atlas*, 150 ft^2 of solar array can be provided without folding the panel. If even more area is required, each panel can be configured as a hexagon and provided with hinged petals. The hinged petals permit a total area of 260 ft^2 to be accommodated in the 10-ft-diam envelope.

VII. Conclusions

The hard-wire rotating coupling has some important advantages in that it:

(1) Permits direct electrical connection of power and sensor leads between solar array and spacecraft in systems undergoing continuous rotation.

(2) Eliminates sliding electrical contacts and friction torque present in slip ring assemblies.

(3) Does not require power-conversion circuitry as does the rotary transformer.

(4) Generates no radio frequency interference.

(5) Is simple in concept; the system assembly is not critical, and close tolerances are not required.

(6) Can be constructed inexpensively.

(7) Can be hermetically sealed without the use of shaft penetration seals and with all parts of the orientation mechanism in the sealed environment.

The hard-wire rotating coupling is the only method presently known in which a direct electrical connection can be made between the solar array and the spacecraft in the presence of continuous rotational motion between the array and spacecraft.

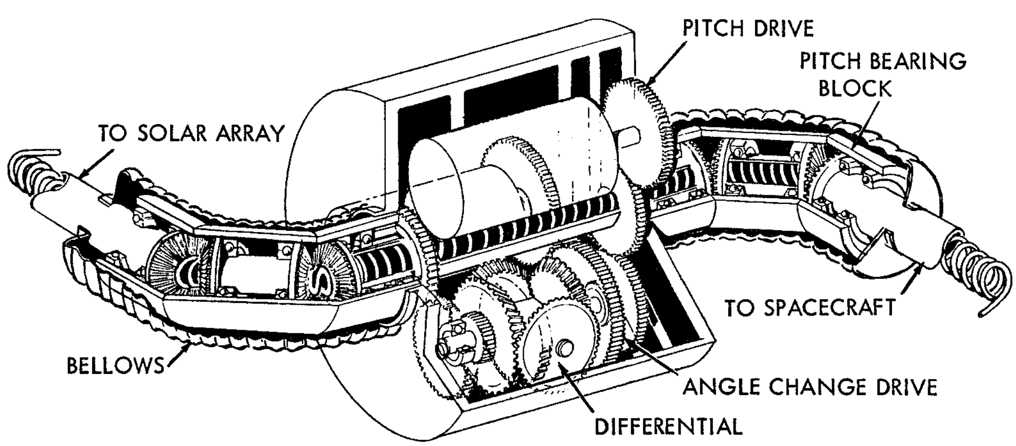

Fig. 5. Hermetic coupling for two-axis pointing

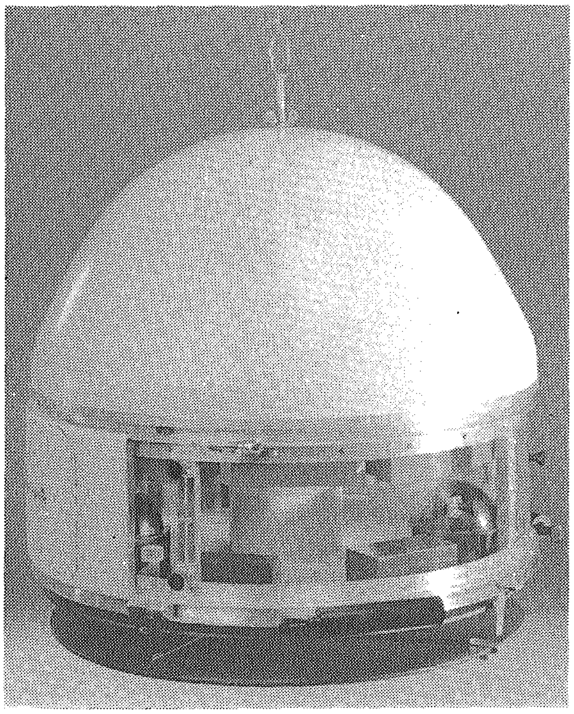

(a) STOWED

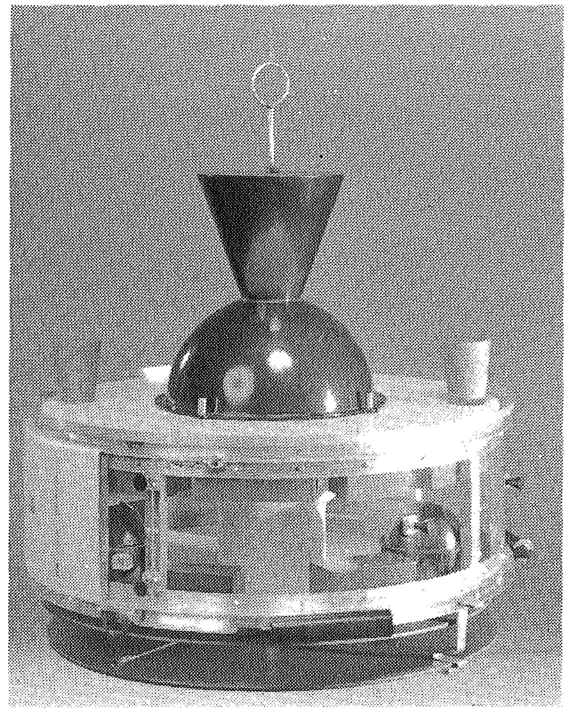

(b) HEAT SHIELD JETTISONED

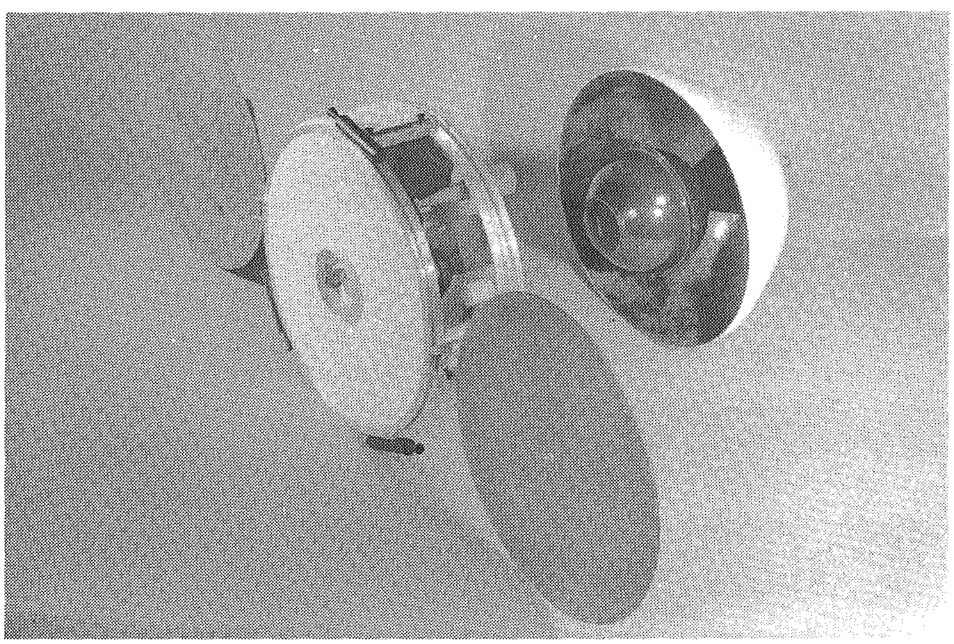

(c) SOLAR ARRAY DEPLOYED

Fig. 6. Spacecraft model incorporating coupling. In (a) and (b), the circular solar panels are folded under the model

Page intentionally left blank

Session II

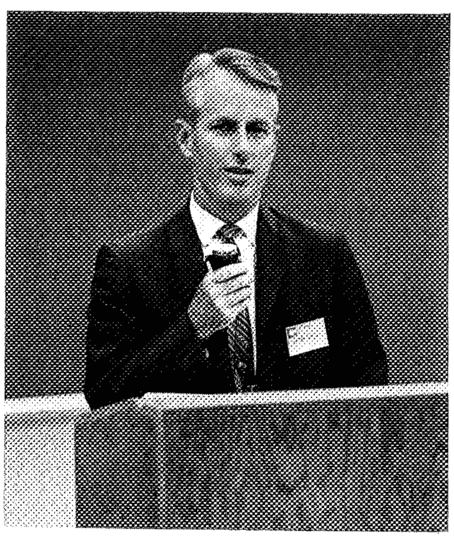

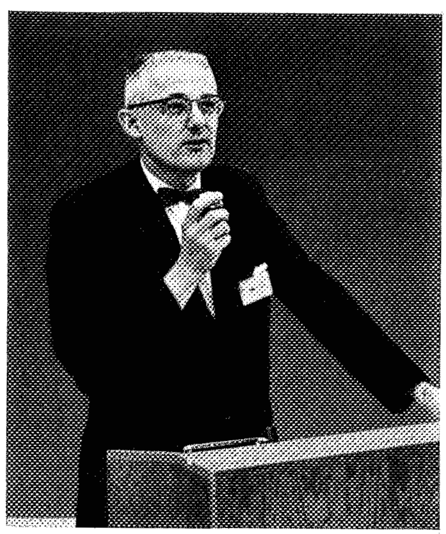

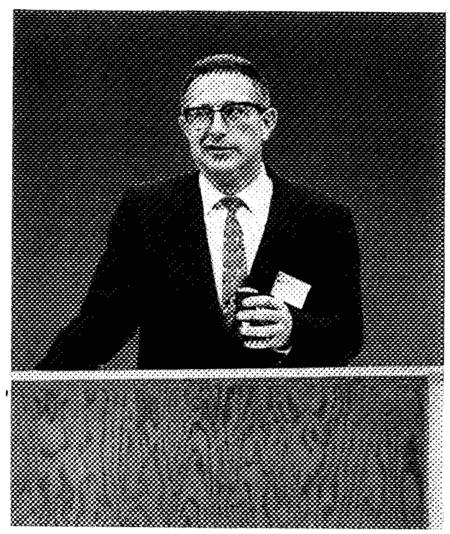

OVERLEAF: *Bruce E. Tinling, NASA Ames Research Center (left), Session Chairman; Edgar J. Buerger, General Electric Company (center), Co-chairman; and George G. Herzl, Lockheed Missiles & Space Company (right), moderator of panel discussion on spacecraft booms*

70N21432

State-of-the-Art Materials and Design for Spacecraft Booms

Charles Staugaitis
Goddard Space Flight Center
Greenbelt, Maryland

Five spacecraft boom concepts were developed in response to a comprehensive investigation of spacecraft materials and design conducted by the Goddard Space Flight Center. The boom designs and the materials used for each are discussed and evaluated.

I. Introduction

In the first quarter of 1965, the Materials Research and Development Branch, Goddard Space Flight Center, initiated a comprehensive boom materials and design investigation to develop boom configurations superior to the DeHavilland[1] Storable Tubular Extendible Member (STEM), the only available concept at the time for gravity-gradient and antenna applications. The adequacy of the overlapped STEM, in lengths substantially less than 100 ft, had been amply demonstrated. However, far greater length requirements were anticipated—lengths up to 1000 ft, in which the STEM's performance was questioned from both structural and thermal viewpoints. Specifically, the STEM's negligible torsional stiffness and marginal thermal bend properties could, as a result of transverse loading and consequent torsional coupling, perilously degrade its performance in service.

[1]Now Spar Products, Ltd., Malton, Ontario, Canada.

Since the beginning of this program, a variety of promising designs have been developed, each of which exhibits a memory; that is, the originally flattened tape, upon leaving the deployment mechanism, will form into a tubular configuration by elastic response when relieved of all restraint.

II. Design Concepts Studied

In the search for new ideas both in materials and in design, the five concepts described below were selected for study and development. These boom designs represent all the basic concepts either currently in production or in the latter stages of development, with one exception, the Spar Bi-STEM. The primary purpose of the study was to investigate the thermal and mechanical properties of these promising boom configurations. To obtain data on thermal behavior, the test booms were evaluated experimentally in a unique 14-ft-high vacuum chamber designed specifically for this purpose. The basic configurations of the designs studied, along with that of the Bi-STEM, are shown in Fig. 1. The contractors and their boom concepts are as follows:

(1) General Electric Company—a 0.50-in.-diam overlapped tubular configuration similar to the STEM design but fabricated from molybdenum, a non-heat-treatable refractory metal. This metal was selected because it exhibits desirable physical properties (better conductivity, lower thermal expansion coefficient and elastic modulus, etc.) but it does not require a precise precipitation heat treatment to stabilize the tape as a permanently overlapped boom. The boom seam can be digitated by the use of an electrical discharge machining process to promote torsional rigidity.

(2) General Dynamics Corporation, Convair Division—a 0.75-in.-diam overlapped woven mesh comprising two dissimilar metallic wires, the circumferential part being a copper–beryllium alloy 25, and the longitudinal wire Elgiloy (a cobalt base alloy).

The bimetal approach was taken because thermal conductivity is very important in the circumferential directions but not so important in the longitudinal. In contrast, thermal expansion is a critical parameter in the longitudinal direction but has very little radial effect. Therefore, BeCu, with its good thermal conductivity, was selected for the circumferential wire, while Elgiloy, because of its relatively low expansion coefficient and high strength properties, was chosen for the longitudinal wire. This rigidized mesh boom is currently produced with an open area of approximately 76%. Any marginal section can be removed and the ends can be easily joined by a unique splicing technique.

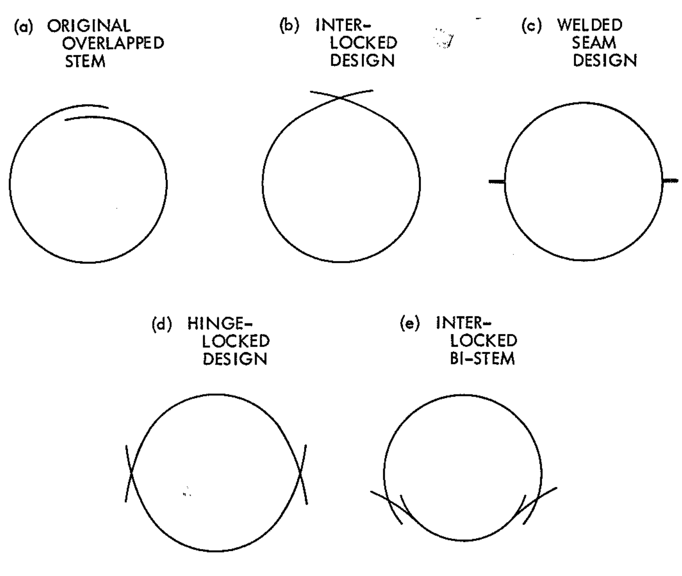

Fig. 1. Current boom design concepts

(3) Westinghouse Electric Corporation—a 0.50-in.-diam interlocking perforated BeCu boom, exhibiting a torsional rigidity several orders of magnitude over that of the overlapped STEM, with a perforated surface of sufficient transparency and reflectance to solar illumination to markedly reduce thermal bending. The unique helical hole pattern essentially averages the thermal radiation impinging on both the internal and external surfaces, resulting in a constant ratio of outside to inside absorptivity that is maintained independent of boom orientation or position along the boom's length. In addition, to enhance straightness (a most important requirement for gravity-gradient applications), a controlled spiral is introduced during the joining operation; the spiral has a period of about one revolution in 16 ft.

To provide the necessary surface reflectance and internal absorptance, the boom is plated with aluminum and coated with Ebanol C (copper oxide) respectively. This particular boom is intended for the ATS-E satellite scheduled for launch some time in August 1969. Future work will involve implementation of a splicing concept for boom repair and antenna application.

(4) The Marquardt Corporation—a tubular element fabricated by welding two strips of BeCu along their edge. While this concept is the poorest from the thermal bend viewpoint, four other vendors are in various steps of development and production of this configuration. Structurally, the concept is far superior to the DeHavilland STEM, both in bend stiffness and in torsional rigidity.

(5) American Machine & Foundry Company—a concept identical with the DeHavilland STEM, except that the boom is formed from a flat BeCu strip of a different temper and its silver surface is produced by electroplating rather than by the brush method (Dalic process), thus ensuring a uniform thickness not achieved by the brush method. Because of funding limitations, both the Marquardt and American Machine & Foundry programs have been terminated.

III. Other Current Boom Designs

The boom design program described above, plus the recognition of the need for advancing the performance of booms, both thermally and structurally, stimulated others, including the Fairchild-Hiller Corporation and Spar Products, Ltd., to develop configurations to meet these requirements. As a consequence, the Radio Astronomy Explorer Satellite (RAE) incorporates Ag-plated BeCu interlocked and perforated boom elements ⅝ in. in diameter that are capable of reaching lengths of 1000 ft. This satellite has already demonstrated remarkable stability and performance in orbit. Despite this success, a new double-interlock (hingelock) concept is under current development at Fairchild-Hiller and is intended for subsequent application on RAE-B.

On the other hand, Spar, still representing the leader in overall boom production and experience, is matching the achievements of its competition by developing several varieties of boom configuration that represent marked advances over their initial STEM design. Essentially, the concept consists of a boom within a boom and is referred to as a Bi-STEM. These double-walled, interlocked Bi-STEMs are produced in a variety of sizes and represent different degrees of torsional constraint.

IV. Conclusion

The investigation of boom materials and design discussed above was undertaken because of the dearth of information then available on the many boom concepts in production or in the process of development. Ultimately, this investigation may serve to characterize more rigorously the variety of concepts presently available, allow a more critical selection of the particular configurations needed for a given application (gravity-gradient stabilization antennas, remote probes, etc.), and, above all, ensure the attainment of a high reliability level, so obviously important to the success of a spacecraft mission.

Page intentionally left blank

70N21433

Some Thoughts on Gearhead Electric Motors for Spacecraft Boom Deployment Mechanisms

by John MacNaughton
Spar Aerospace Products, Ltd.
Malton, Ontario, Canada

To aid in the selection of a gearhead electric motor, the advantages and disadvantages of dc and ac motors and of wet and dry lubricants are discussed. Some general advice is given on choices that can be made for specific spacecraft applications, depending on the length of time the motor must operate and on whether the operation will be intermittent or continuous.

I. Introduction

Many deployable spacecraft booms employ a gearhead electric motor as the prime mover for accomplishing the extension and retraction functions. This component, therefore, constitutes one of the most important machine elements in the boom deployment mechanism. The selection of a motor suitable for a particular mission is at best difficult, and is often the result of considerable debate, where personal opinion plays a larger role than would normally be considered desirable.

This paper is intended to record one writer's feelings on the subject.

II. Direct Current or Alternating Current?

Direct current brush-type motors exhibit many desirable characteristics:

(1) High power-to-weight ratio.

(2) High starting-torque-to-weight ratio.

(3) High efficiency.

(4) Low cost.

In addition, since a spacecraft's basic supply of electrical power is direct current, there is considerable merit in specifying a dc motor. There are many problems, however, with this simple approach. To mention a few:

(1) Conventional brush materials, even high-altitude ones, do not like the hard vacuum of space.

(2) The simplest form of direct current motor employs a permanent magnet field, with attendant high residual magnetic field strength.

(3) Brushes are a source of radio frequency interference.

(4) Brushes are prone to wear.

There are solutions to these problems, but unfortunately they create additional problems; i.e.,

(1) If a hermetically sealed motor is selected, additional cost, size, and weight result.

(2) If a dc brushless or stepper motor is selected, additional cost, size, and weight result.

(3) If a motor with a wound field instead of a permanent magnet field is selected, to reduce magnetic field strength, boom deployment speed is made more difficult to control.

Brushless dc motors require electronic or optical switching and generally operate in one direction only, unless the added complication of a double commutator is employed. Stepper motors require electronic switching to make them operate and are generally comparatively massive due to their extremely low efficiency.

The considerations above tend to indicate that a brushless ac motor could be a final solution, despite its low starting torque, large size, low efficiency, and the need for a special inverter.

A ray of sunshine on the horizon is a vacuum brush material developed by the Boeing Aircraft Company. It shows promise of removing one of the main restrictions to the use of dc brush-type motors in space—that of long life in a hard vacuum. This material will be tested in orbit in a boom deployment mechanism this year. It has already passed the applicable qualification tests.

III. Lubrication

How should the bearings and gears be lubricated? There seems to be no clear-cut answer to this question either. Some say that dry lubrication is mandatory, others prefer the Ball Brothers[1] wet lubrication process (Vac Kote). Wet lubricants are often criticized, since their vapours are prone to recondense on adjacent spacecraft surfaces.

Being simple minded, I prefer to start with a simple wet lubricant such as F-50/G-300, and then be convinced that it can't be used before specifying more exotic systems.

IV. Past Experience

My company has had experience with most of the aforementioned motor and lubrication systems, but we have *not* conducted exhaustive motor/gearhead testing in simulated space environments.

Unfortunately, no hard rules are forthcoming from this experience. For example:

(1) An unsealed dc motor with permanent magnet field and high-altitude brushes, lubricated with F-50/G-300 low-vapour-pressure grease, has performed extension and retraction of a gravity-gradient boom 9 months after insertion into low earth orbit.

(2) Motors of the same configuration as (1) above operated all *Gemini* high frequency antennas and magnetometer booms and the target *Agena's* rendezvous antenna boom after missions of up to 2 weeks duration in low earth orbit.

(3) Hermetically sealed dc wound field motors, with high-altitude brushes and lubricated with diesters, performed extension and retraction functions for up to six months on ATS A and D. All motors functioned normally up to the time both spacecraft ceased to function.

(4) Synchronous 28-V ac motors, with dry lubricated armature bearings and F-50/G-300–MOS_2 loaded grease in the gearhead, have been operating the *DODGE* gravity gradient booms for almost 2 yr at the time of writing.

(5) Direct current stepper motors, Vac Kote-lubricated, operated three sun shield actuators successfully on ATS D.

(6) Semihermetically sealed (O-ring shaft seal) dc permanent magnet field motors, with high-altitude brushes and lubricated with diesters, were used successfully to deploy the *ISIS 1* sounder antennas.

V. Recommended Practice

Although no hard and fast rules emerge from this experience, some rough guidelines do. These are presented below, and express a personal opinion only.

(1) Motor operations to be complete within one month of launch. Ideal for sounder rockets:

   (a) Open dc brush-type motor.

   (b) Permanent magnet or wound field, depending on magnetic specifications.

   (c) F-50/G-300 lubrication.

[1]See "Lubrication of DC Motors, Slip Rings, Bearings, and Gears for Long-Life Space Applications," by B. J. Perrin and R. W. Mayer, *Proceedings of the 3rd Aerospace Mechanisms Symposium*, TM 33-382. Jet Propulsion Laboratory, Pasadena, California, Oct. 1, 1969.

(2) Motor operations to start up to 1 yr after launch and to be complete 1 month thereafter:

    (a) Semihermetically sealed brush-type dc motor.

    (b) Permanent magnet or wound field, depending on magnetic specifications.

    (c) Diester lubrication.

(3) Intermittent motor operation covering a period of up to 1 yr after launch:

    (a) Open dc brush-type motor (Boeing brushes).

    (b) Permanent magnet or wound field, depending on magnetic specifications.

    (c) Dry lubrication system.

(4) Intermittent motor operation, covering a period of up to 3 yr after launch:

    (a) Hermetically sealed brush-type dc motor.

    (b) Permanent magnet or wound field, depending on magnetic specifications.

    (c) Diester lubrication.

(5) Frequent operation, covering periods up to 5 yr after launch:

    (a) Alternating current synchronous or dc stepper, based on availability of suitable electric power.

    (b) Dry or Ball Brothers lubrication.

(6) Customer preference may dictate the final approach, as motor selection is still a highly personalized activity.

VI. Conclusions

There have been few recorded spacecraft failures attributed directly to gearhead electric motors. This record should not lull us into a false sense of security, as it is probably due to intensive development of a previously selected motor configuration, rather than selecting the motor on the basis of widely disseminated and recognised test results.

Many prime spacecraft contractors have performed limited testing of certain motor concepts intended for use in space; however, their results are not generally available throughout the industry and seldom find their way to the motor manufacturer. This anomalous situation exists because, in general, only the large prime contractors can afford the costs of this type of development work, and, for proprietary reasons, they do not disseminate the information obtained.

I feel that significant research and development funds should be made available directly to motor manufacturers for advancing the industry's knowledge of this important component. I further feel that a single government agency should be given jurisdiction over such a program.

Page intentionally left blank

70N 21434

Checklist for Boom Selection

James M. Talcott
Fairchild Hiller Corporation
Germantown, Maryland

With the increase in types of booms and in boom applications, the potential user is faced with more and more complex choices. A brief review of typical boom applications is given, along with a checklist of available parameters, including length, diameter, thickness, general configuration, coatings, deployment/extension rates, telemetry, and electrical considerations.

I. Introduction

The development of a long rod which may be stored in a package with small dimensions was started around 1960. In the few years that have passed since that first flight it has been estimated that over one thousand booms have been flown with varying degrees of success. The configuration of the booms flown has varied considerably and evolution towards the mechanical properties of a closed tube is reflected in these booms and in those being developed for future use.

Along with this evolution has come a sophistication of analytical techniques used to predict boom/spacecraft interactions, an extensive backlog of "off the shelf" mechanisms and, of significant import, considerable knowledge of the factors influencing and the limitations of these booms. Correlation between flight data and the predicted dynamics of several recently flown vehicles is very impressive as is the complex "double dead beat" gravity-gradient capture technique used on the RAE–*Explorer* 38 (Ref. 1). The source of unpredicted anomalous dynamic behavior of several spacecraft using booms has been identified, and several boom configurations have been developed to preclude recurrences (Ref. 2).

With this background it is now feasible to determine, with a high degree of confidence, the boom configuration required to adequately perform a specified mission and to accurately size a "new" deployment mechanism. The factors entering into the selection of a boom/mechanism combination are:

(1) The intended use of the boom.

(2) The environment to which the boom is subjected.

(3) The boom's effect on the spacecraft.

These factors and their impact on boom choice are discussed in general terms to provide a checklist for the user.

II. Intended Use

An early aerospace use of the extendible boom was as an antenna for a topside sounding experiment flown on an *Alouette*. The boom system used was made up of four units deployed to form a crossed dipole in the satellite's spin plane. This same general configuration has been used since and is planned on future flights for additional topside sounding, electric field measurements, and other experiments concerned with low-frequency wave propagation including both communications and natural phenomena.

An application making somewhat greater use of the extendible boom is gravity-gradient stabilization. Initially, two-axis stabilization was accomplished with a single boom and tip mass (Ref. 3). Later versions, made up of three booms configured in a swept back Y, have passively accomplished three-axis stabilization. A number of systems have recently been proposed which make use of the basic gravity-gradient concept but are implemented to improve the satellite's pointing accuracy. Several of these proposed systems are enhanced by a damper mounted at the boom tip rather than an inactive tip mass. Considerable effort has gone into the study of a gimballed deployment mechanism by which a tip mass could be oriented by command. Another interesting concept is the use of the deployment mechanism as the tip mass, thereby eliminating dead weight. Power and telemetry leads must, of course, be run from the spacecraft to the mechanism.

Electrical leads are also a requirement for the extension of experiment packages away from the spacecraft and, as such, they have been given considerable attention. The extension of magnetometers and other experiments away from the influence of the parent spacecraft has, in the past, been limited to relatively short distances. This has primarily been due to an experiment orientation requirement which the original open section booms could not provide. Several of the various interlocked concepts, however, do provide considerable bending and torsional stiffness and will undoubtedly be used for experiment extension in the near future.

Electric field measurements using one dipole antenna have been made on several spacecraft and many sounding rockets. The previously mentioned *Explorer 38* uses its 750-ft booms both for gravity-gradient stabilization and as the receiving antennas for low-frequency emissions from space. A similar concept using 2000-ft dipoles for transmitting and receiving has been proposed for subsurface electromagnetic soundings of the moon. Navigational aids, using the interferometer concepts and the long base line provided by extendible booms, have been proposed for aircraft, ships, and weather balloon tracking. In a somewhat more structural vein, these elements are presently being designed and fabricated for the extension of flexible solar arrays.

From this outline of the versatility of the extendible boom and the confidence generated by its many successful applications, one may conclude that its use will continue to grow in the aerospace field. Like any useful tool, the extendible boom will be recognized as a convenient, if not necessary, device for many applications. However, its limitations, like those of the useful tool, must also be realized.

III. The Effect of a Hostile Environment

The limitations of the extendible boom are associated with its ability to adequately perform in a hostile environment. As with any structural element, performance may be degraded by either stress or deflection or both. However, unlike most structural elements, long booms are subject to large deflections at low stress levels, these deflections being caused by loads normally considered negligible for the typical beam (Ref. 5).

As mentioned previously, several spacecraft containing extendible booms have exhibited unpredicted (and catastrophic) motions. This problem has received considerable attention and its cause has been identified as feedback from "thermal flutter" of the booms. The mechanism of this phenomenon is characterized by the shear center—mass center separation and extremely low torsional rigidity of the open section boom. Even without the dynamic effects of solar heating, the deflections of long antennas due to a thermal gradient may make them unsuitable for certain missions. Fortunately, both the steady state and dynamic deflections of these elements can be made small by the use of an interlocked edge, coatings, and perforations, as evidenced by the RAE.

Orbit-induced loads due to eccentricity are periodic and can result in deflections amplified far above those predicted by steady state calculations. For example, aerodynamic drag forces have a shifted cosine appearance centered about perigee, and each pass through perigee may result in deflections that are either attenuated or amplified. Further, coupling between boom natural frequency and orbital rate can cause additional amplification from this and the forces due to gravity gradient and solar pressure.

The effects of an active attitude control system (ACS) may also be significant. The motions of the relatively rigid satellite hub are, essentially, time-dependent boundary conditions on the boom. Frequency coupling between the ACS logic and the boom's natural bending frequency can result in a limit cycle mode of operation of the ACS with subsequent large expenditure of power or fuel and greatly reduced mission life.

Booms mounted on spinning vehicles have several additional load sources. For booms nominally located in the spin plane, Coriolis and despin accelerations must be considered during deployment and retraction. The lateral loads associated with these accelerations are linearly dependent on deployment rate and can, therefore, be controlled. Tensile forces due to centripetal accelerations have two effects on the boom. The first of these is the tendency for the boom to be pulled from the mechanism. Failure to control the back winding of the mechanism may result in unacceptably high deployment rates and subsequent boom failure. The second effect is the apparent increased stiffness of the axially loaded element. This effect is felt as an increase in bending natural frequency for bending out of the spin plane and may largely account for the fact that no evidence of thermal flutter has been reported on spin-stabilized vehicles.

For booms located out of the spin plane, resonance conditions leading to unstable dynamics may be set up at frequencies well below the critical spin speed of the boom (Ref. 6).

A complete investigation of the performance of these booms, in particular the dynamic interaction of the booms and spacecraft, is a complex, computer-oriented task for lengths greater than about 50 ft. However, for many applications, a checklist, based on past analytical efforts and flight data, is useful to acquaint the potential user with the number and range of parameters available to him and their interaction with each other.

V. User's Checklist

Thus, in a qualitative way, this summary contains many of the options now available in the general class of tubular deployable booms. The boom itself is a thin-walled cylindrical section characterized by:

(1) Length. Typically, length is the choice of the experimenter to yield inertial, electrical, or spatial characteristics. To date, these units have been flown in lengths ranging from 6 to 750 ft.

(2) Diameter. Choice of diameter is mainly influenced by the stiffness desired. By far the most popular diameter at present is ½ in.; however, for sounding rocket applications, ¼-in. antennas are widely used. Two-in.-diam elements have been fabricated and may be considered "state of the art" at this time.

(3) Thickness. Boom wall thickness choice is somewhat limited by storage stress and is generally around 1/250 of the diameter for beryllium–copper. There is, of course, some leeway in this dimension, and ultimate bending moment, thermal gradient, and weight may be traded off to optimize the thickness.

(4) General configuration. Overlap angle, type of interlock, and number of nested elements are also options. Overlap angles around 100 deg have been extensively used, with 180 deg as a practical upper limit. Interlocked elements of both one- and two-piece units are presently being fabricated and tested. To date, the only interlocked antenna flown is a one-piece tape with serrated edges (Ref. 7). The torsional rigidity provided by an interlock precludes the thermal flutter phenomenon and is required for the orientation of experiment packages.

(5) Coatings. Several coatings are available for thermal control and for electrical insulation. Silver-plated booms have exhibited an absorptance of less than 12%. Optically black coatings on the inner surfaces and a hole pattern in conjunction with a silver-plated outer surface have greatly decreased thermal gradients and theoretically can eliminate thermal bending completely. Electrical insulation increases thermal gradient but has been used extensively on electric field measurement experiments.

Some of the options available on the deployment mechanisms are:

(1) Deployment/extension rates. These rates are extremely important on a spinning vehicle. They also can play an important role in gravity-gradient capture and the motion of the spacecraft. Column

loading (inertial) and time over ground stations are also considerations in some applications. Typical rates are from 1 to 10 in./s. Nonmotorized units, which are deployed by the spring energy in the stored tape, are considerably faster and less predictable.

(2) Telemetry. Switches to indicate uncaging, start of deployment, and full deployment, and/or potentiometers to continuously monitor deployed length are commonly used and are recommended. The switches may also be used to automatically stop extension and/or retraction.

(3) Electrical considerations. There is considerable variation in the power required to deploy the various configurations, with the larger booms and faster rates demanding larger power. Redundant RF pickups, various power connectors, control of base capacitance, and isolation of the complete boom or parts thereof from the mechanism or spacecraft have been provided in the past and are, of course, available options now.

We are confident that the evolution of this unique machine element will continue. A generalization of the analytical routines already developed for specific missions will enable optimization of the available boom parameters for future missions. Efforts in materials, both for the booms and ancillary equipment, and improvements in boom manufacturing processes will also play important roles. This technological advancement will be accelerated now that there is a general understanding of the capabilities of existing hardware and an awareness of the factors which influence boom performance.

References

1. Blanchard, D. L., Davis, R. M., Lawlor, E. A., and Beltracchi, L., *Design, Simulation and Flight Performance of the Radio Astronomy Explorer-A Satellite*, x-723-68-463. NASA Goddard Space Flight Center, Nov. 1968.

2. Frisch, H. P., *Thermal Bending Plus Twist of a Thin Walled Cylinder of Open Section With Application to Gravity-Gradient Booms*, NASA TN D-4069. National Aeronautics and Space Administration, Washington, Aug. 1967.

3. Fischell, R. E., and Mobley, F. F., "A System for Passive Gravity-Gradient Stabilization of Earth Satellites," Paper 63-326, presented at the AIAA Guidance and Control Conference, Cambridge, Mass., Aug. 12–14, 1963.

4. Raymond, F. W., Wilhelm, P. G., and Beal, R. T., "Gravity Gradient Flight Experience Acquired With the Naval Research Laboratory Satellites," paper presented at the Symposium on Gravity Gradient Attitude Stabilization, U.S. Air Force Systems Command and Aerospace Corporation, El Segundo, Calif., Dec. 3–5, 1968.

5. Herzl, G. G., "Bending of Unfurlable Tubular Structures in Space," in *Transactions of the 2nd Aerospace Expandable Structures Conference*, held at Minnetonka Beach, Minn., 25–27. AFAPL TR 65-108, Air Force Aero Propulsion Laboratory, Wright-Patterson Air Force Base, 1966.

6. Talcott, J. M., "On the Spin-Stability of a Flexible Body," paper presented at the ASME/AIAA Tenth Structures, Structural Dynamics, and Materials Conference, New Orleans, La., Apr. 14–16, 1969.

7. Angulo, E. D., and Kamachaitis, W. P., "The Radio Astronomy Explorer 1500-ft-Long Antenna Array," in *Proceedings of the 3rd Aerospace Mechanisms Symposium*, TM 33-382. Jet Propulsion Laboratory, Pasadena, Calif., Oct. 1, 1968.

N70-21835

Spacecraft Booms: Present and Future

G. G. Herzl
Lockheed Missiles & Space Company
Palo Alto, California

The present performance of booms is summarized, and some current applications of booms on spacecraft are illustrated by a series of photographs of Russian spacecraft using booms in various ways. Future trends considered include better performance, better manufacturing techniques, longer active operational lifetimes, and the need for very long spacecraft booms.

I. Introduction

Virtually every spacecraft contains a boom, which is the largest object in the satellite. There is no accurate count of the total number of booms that have been flown to date, but it is estimated on the basis of a NASA-sponsored study (Ref. 1), conducted by the author, that more than 1,000 booms have been flown on United States spacecraft alone. Booms have been used to position instruments, to provide gravity-gradient stabilization, to serve as spacecraft antennas, to actuate spacecraft structures, and to perform many other tasks.

II. The State of the Art of Spacecraft Booms

One cannot help being impressed by the overall performance of spacecraft booms to date, considering that booms cannot be adequately tested in the earth environment. There were relatively few failures of booms, although those that occurred did cause failures or severe degradation of the spacecraft mission. There were several instances of boom extension failures caused by malfunctioning of either the motor or the extension mechanisms, while the performance of several spacecraft was severely degraded by the interaction of the boom with the space environment. Much has been learned from these experiences, and considerable improvement in performance and reliability has been achieved.

Spacecraft booms are truly space structures, since they can be fully erected without external support only in the weightless environment of space and would collapse of their own weight on the earth. Spacecraft booms operate under most adverse conditions in space, since they are completely exposed to the thermal vacuum and radiation environment of space, in addition to micrometeorites, and they do not enjoy even the minimal protection that the skin of the spacecraft provides to other subsystems located within the spacecraft. The thermal environment has caused most problems to date, including:

(1) Steady-state bending, due to differential thermal expansion of the parts of the boom facing toward, and away from, the sun, and the following dynamic disturbances:

(2) Thermal shock, which triggers boom oscillation when the spacecraft goes through the boundary of sunlight and shadow of the earth.

(3) Thermally induced self-excited oscillations, resulting from a coupling between the flexural and torsional deflections of the boom.

The hard vacuum in space dictates the design of the electric motor and the extension mechanism and has, in at least one instance, caused cold welding of adjacent layers of the stowed boom. Radiation and micrometeorites tend to degrade the surface characteristics of the boom and thus indirectly aggravate the thermal problems.

Every aspect of boom design is governed by the requirement for extreme length-to-weight ratio. The details of various boom design principles that have been implemented for use in United States spacecraft are described in Refs. 2–6, which were presented at the past Aerospace Mechanisms Symposiums. The implementation of booms in spacecraft is illustrated by their uses in Russian spacecraft (Figs. 1–15 from Refs. 7–9). In the past, the Russians have had an estimated average of 3.5 booms per spacecraft vs 2.5 for the United States. However, the present trend in the United States is toward the use of more booms in each spacecraft.

III. Trends for the United States

The trend for the future in boom design points toward improvements in the following ways:

(1) Better performance to further improve boom straightness under all operating conditions. This will require better thermal control and compensation and improved damping techniques. Three-axis gravity-gradient-stabilized satellites and precision spacecraft instrumentation will also require booms with increased torsional rigidity.

(2) Better manufacturing techniques to further improve the straightness of the boom element itself and to minimize straightness degradation due to repeated boom extensions.

(3) Longer active operational lifetimes, on the order of 2 to 5 yr and more. Such an increased life will become a standard boom operational requirement. This will require further improvements in the boom component design, manufacturing, testing, and overall reliability.

(4) A need for very long spacecraft booms, on the order of 10,000 ft. Booms of this length are technically feasible, but they will require a careful reexamination of many dynamic problems due to extension of the boom that to date have not posed serious difficulties.

Finally, the various trade-off studies in spacecraft involving booms will have to keep pace with the future advances. The availability of longer and straighter booms will significantly improve the performance of various spacecraft systems and instrumentation.

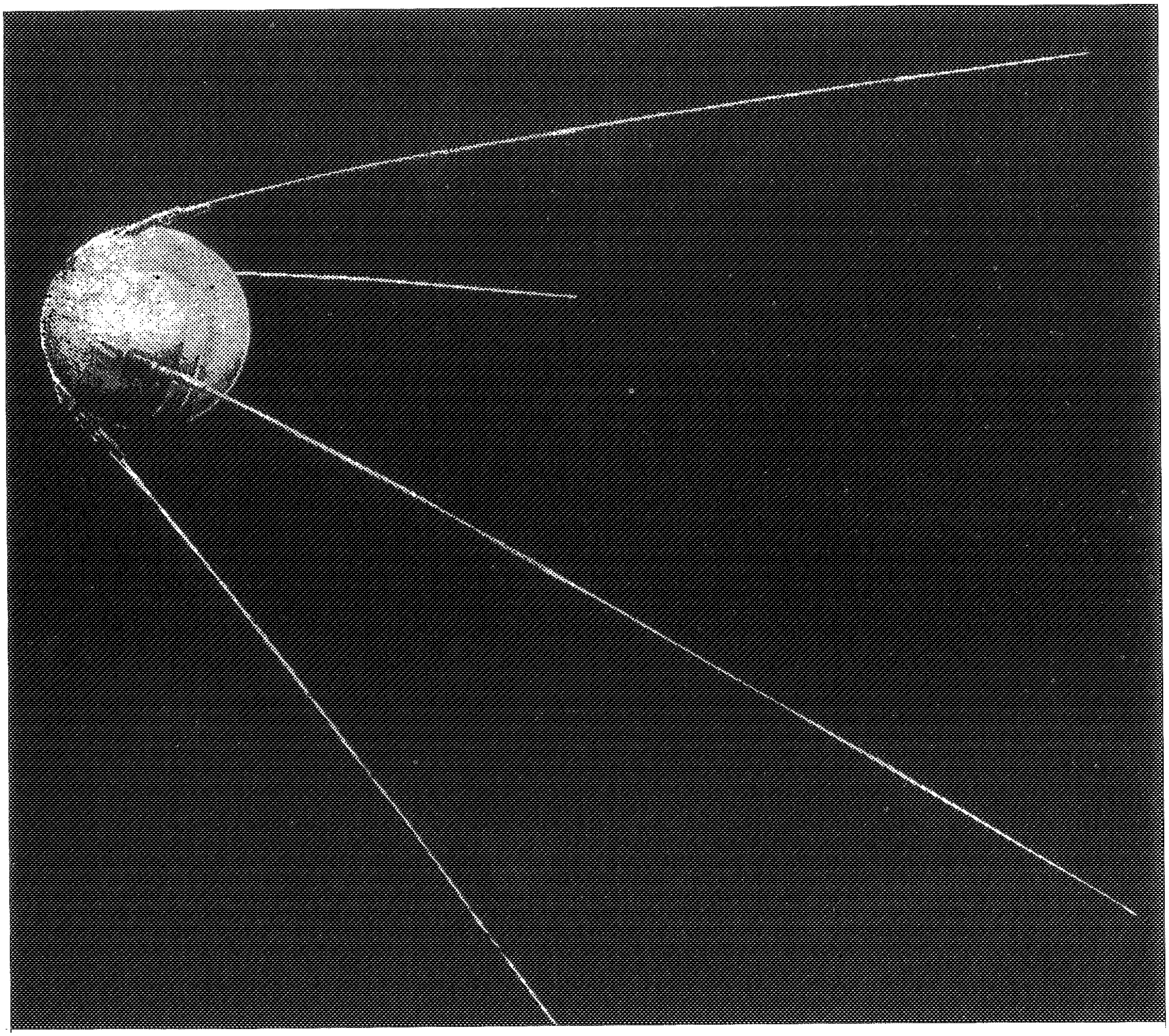

Fig. 1. *Sputnik 1*, first artificial earth satellite

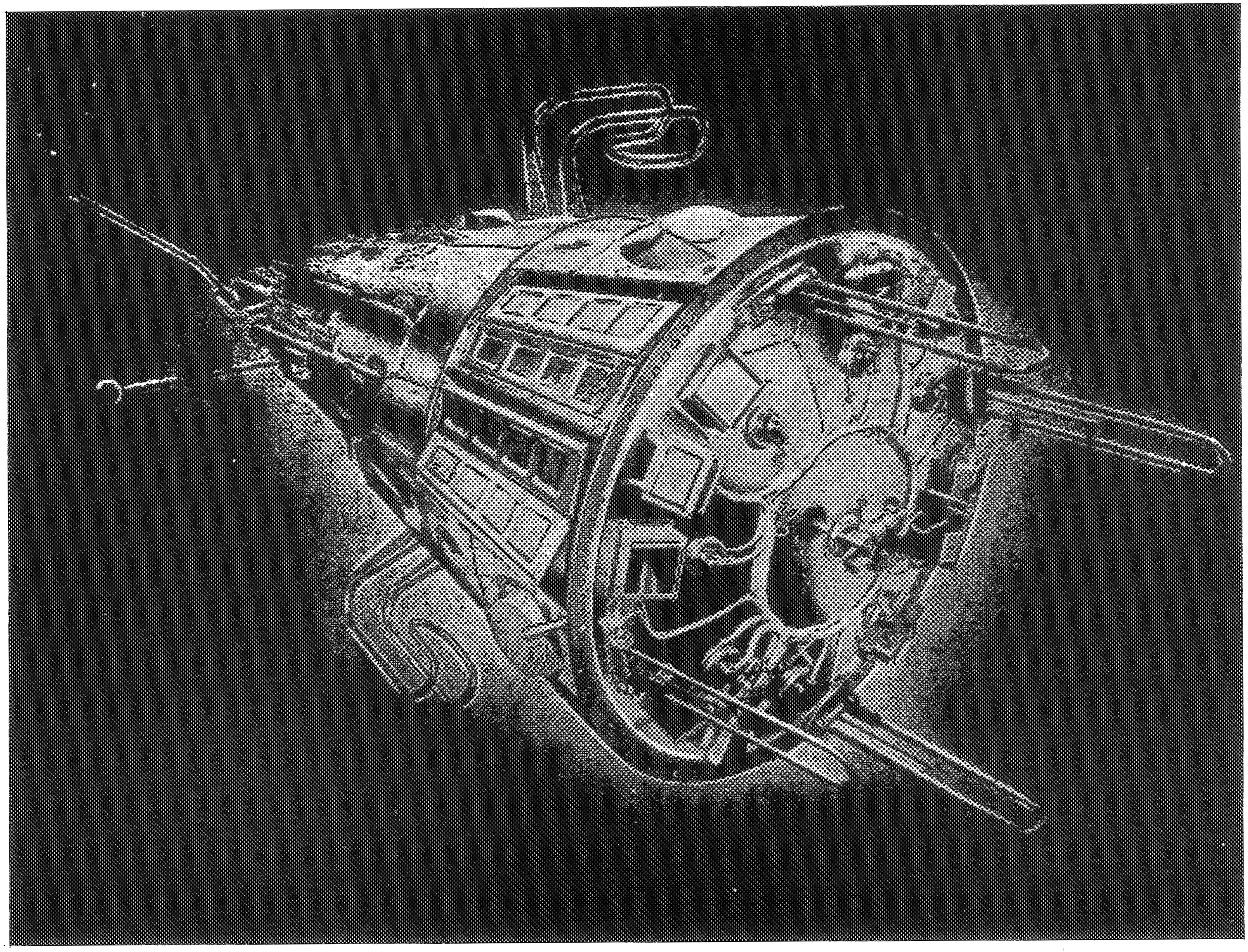

Fig. 2. *Sputnik 3*, which measured ion stream cosmic radiation. This satellite followed the second *Sputnik*, which weighed 1/2 ton and had a dog on board. In *Sputnik 3*, the four front booms are hinged at the periphery and are held with a common pyrotechnic device in the center

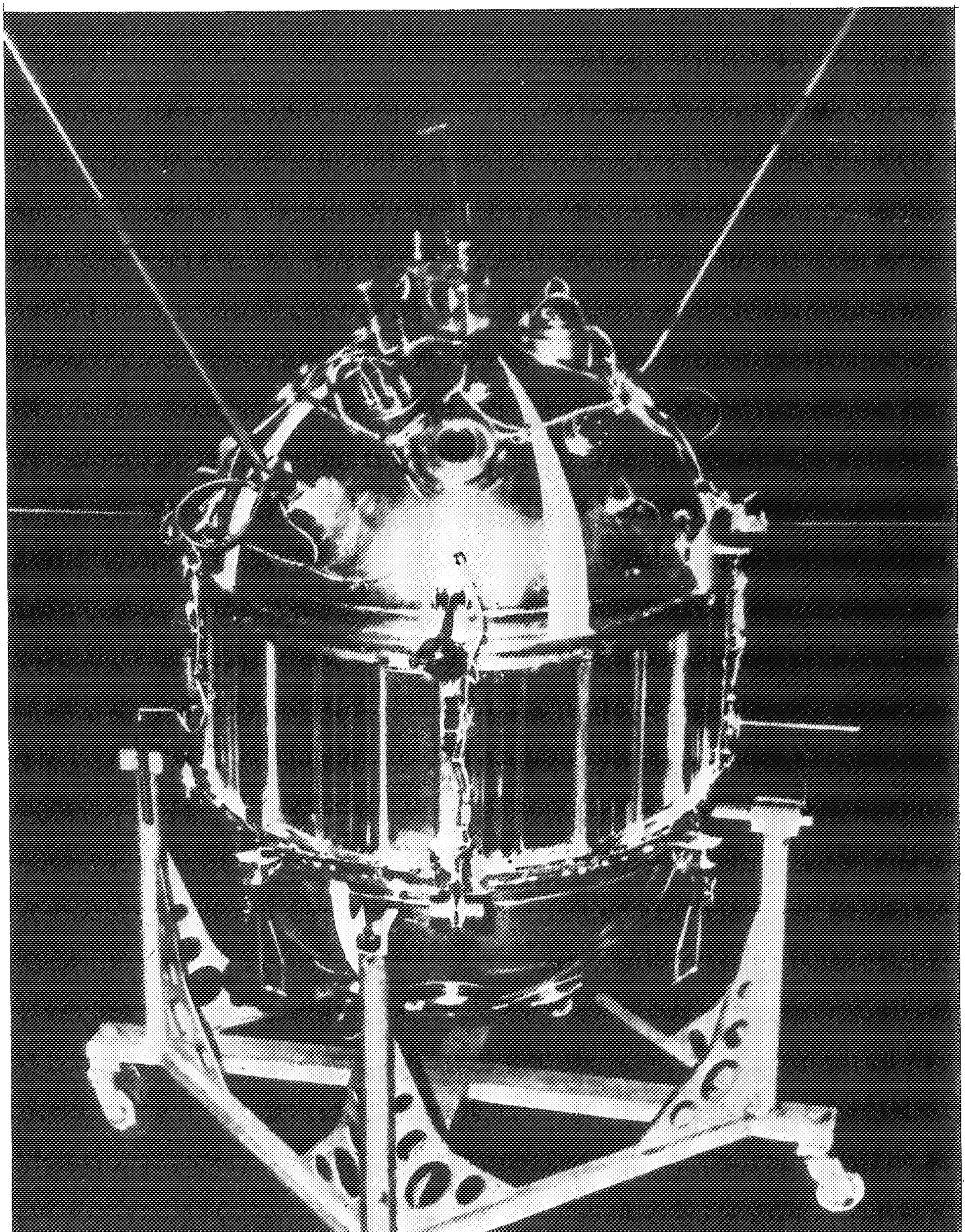

Fig. 3. *Cosmos 2*, the first *Cosmos*-series satellite for ionosphere investigation. There were 173 satellites in the *Cosmos* series between 1962 and 1967, with many booms

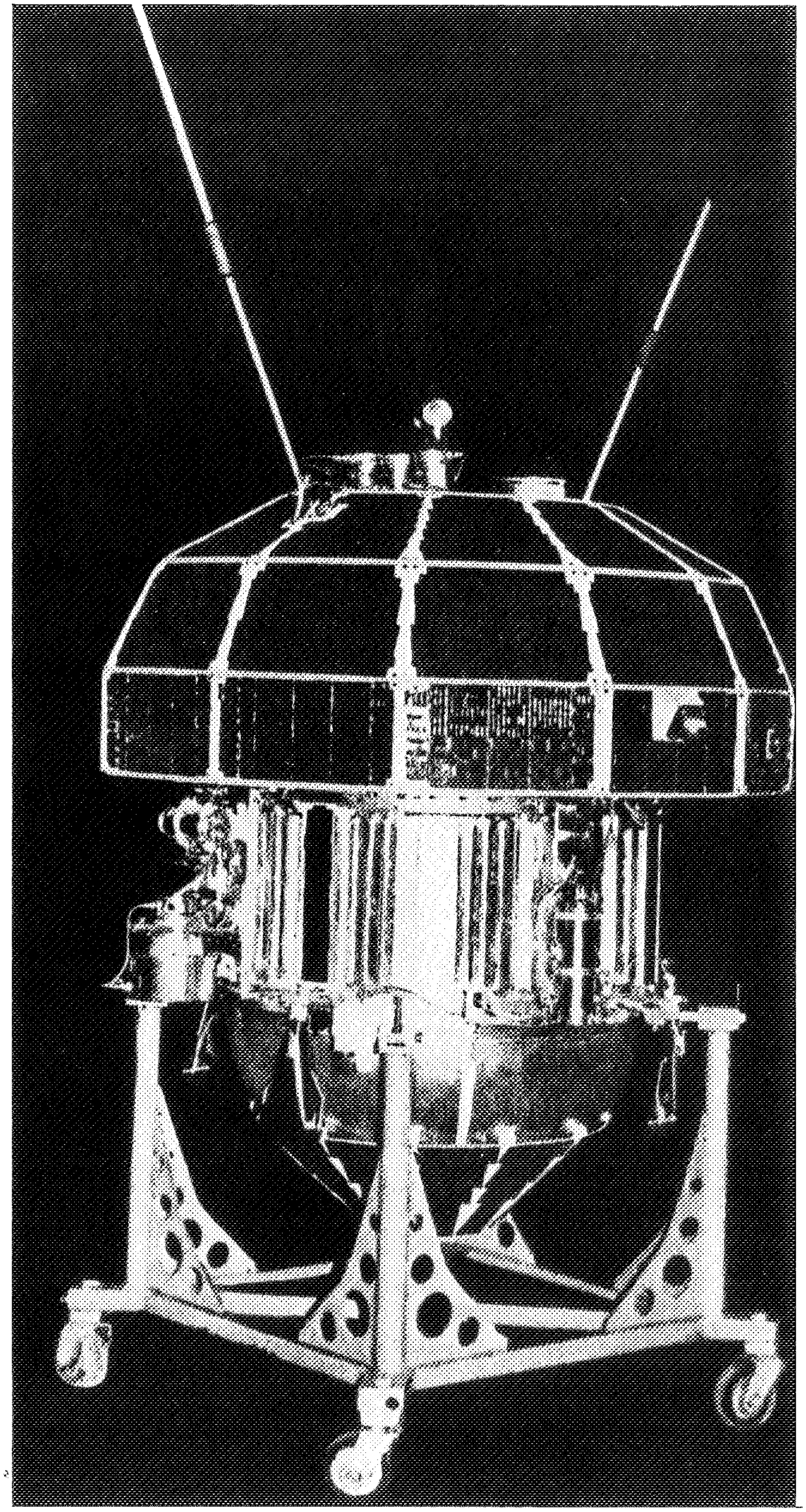

Fig. 4. *Cosmos 5*, for the investigation of low-energy particles

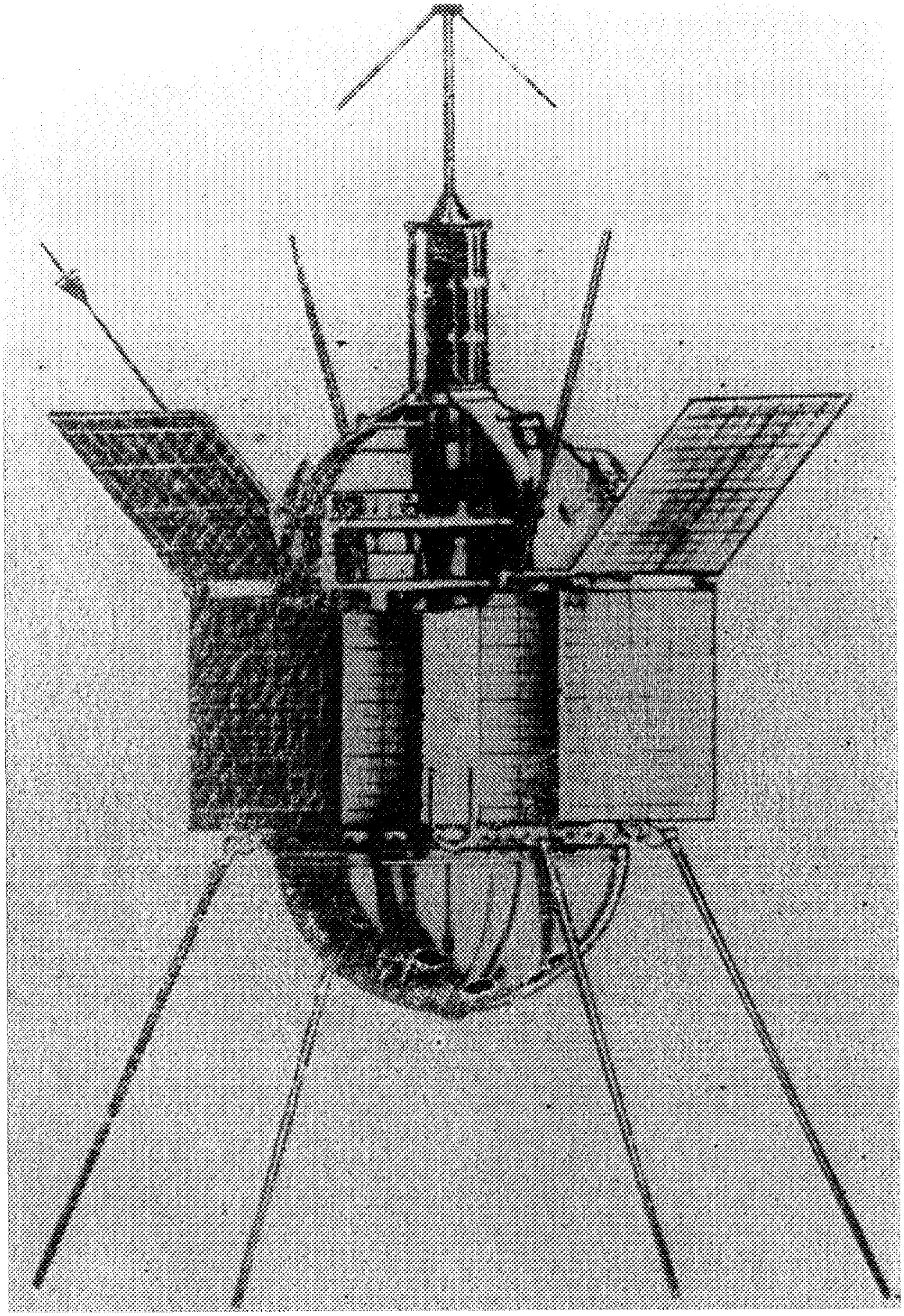

Fig. 5. Cosmos-series satellite with molecular generator on board

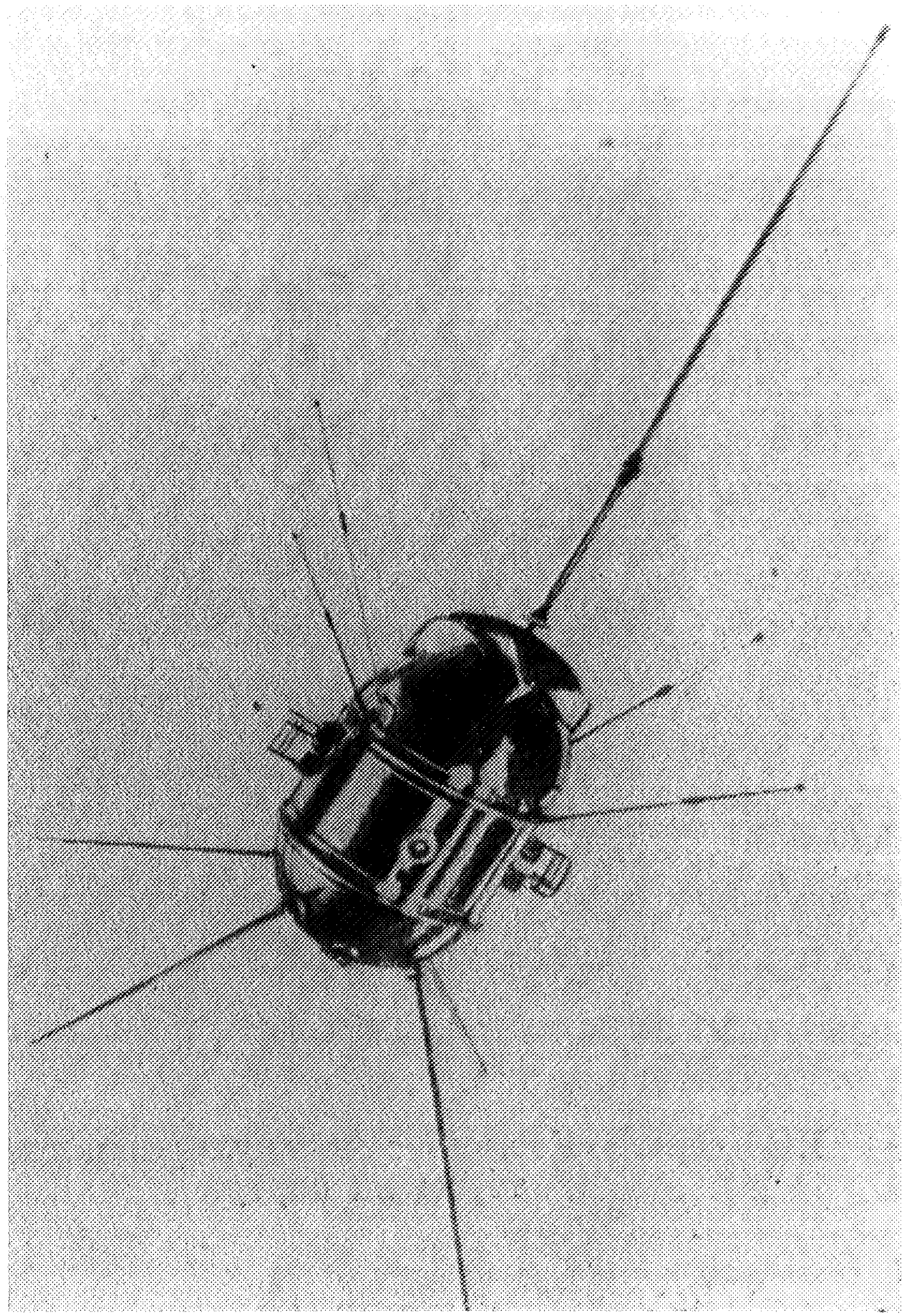

Fig. 6. *Cosmos-series* satellite for magnetic survey of the earth

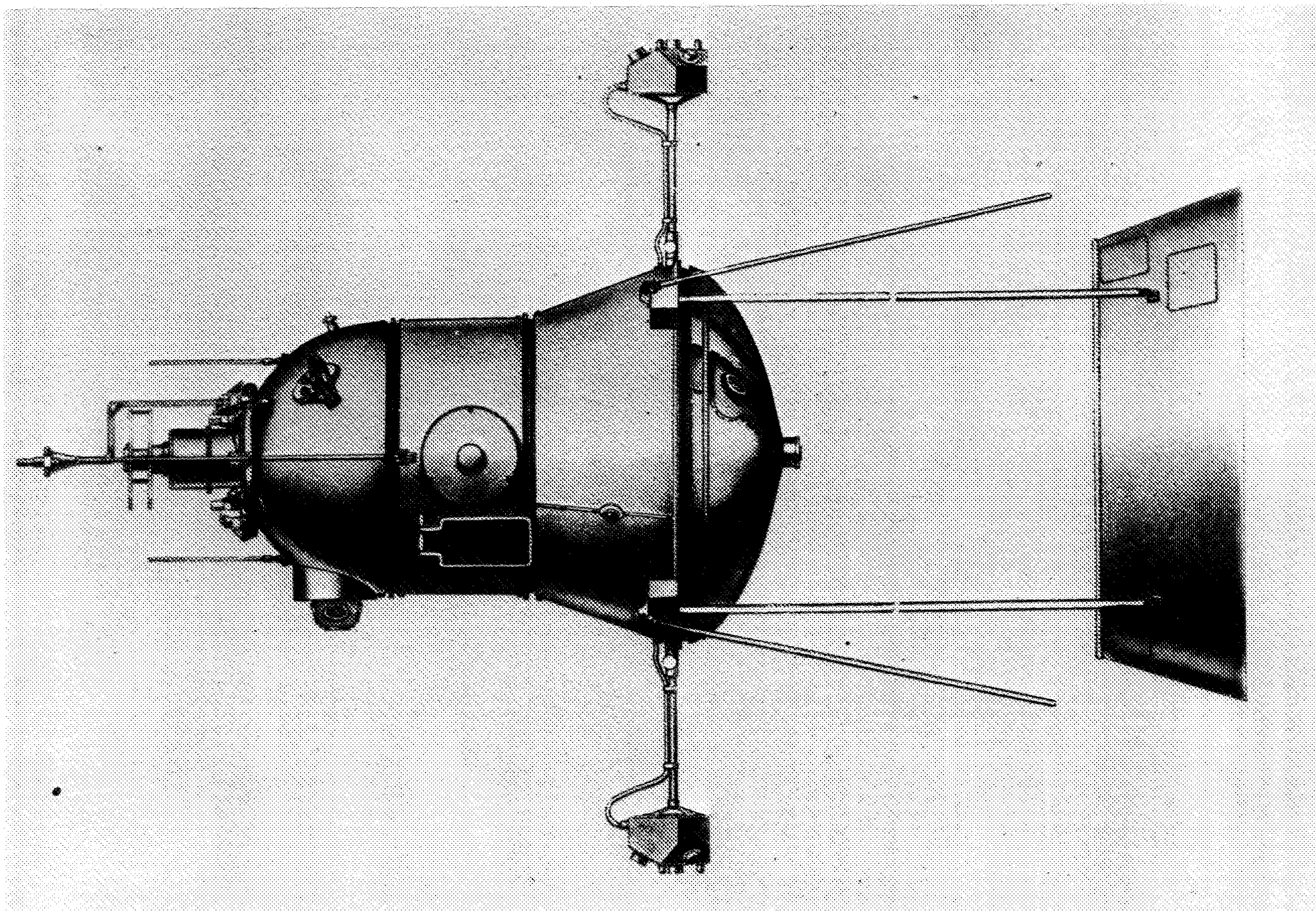

Fig. 7. *Cosmos*-series optical satellite

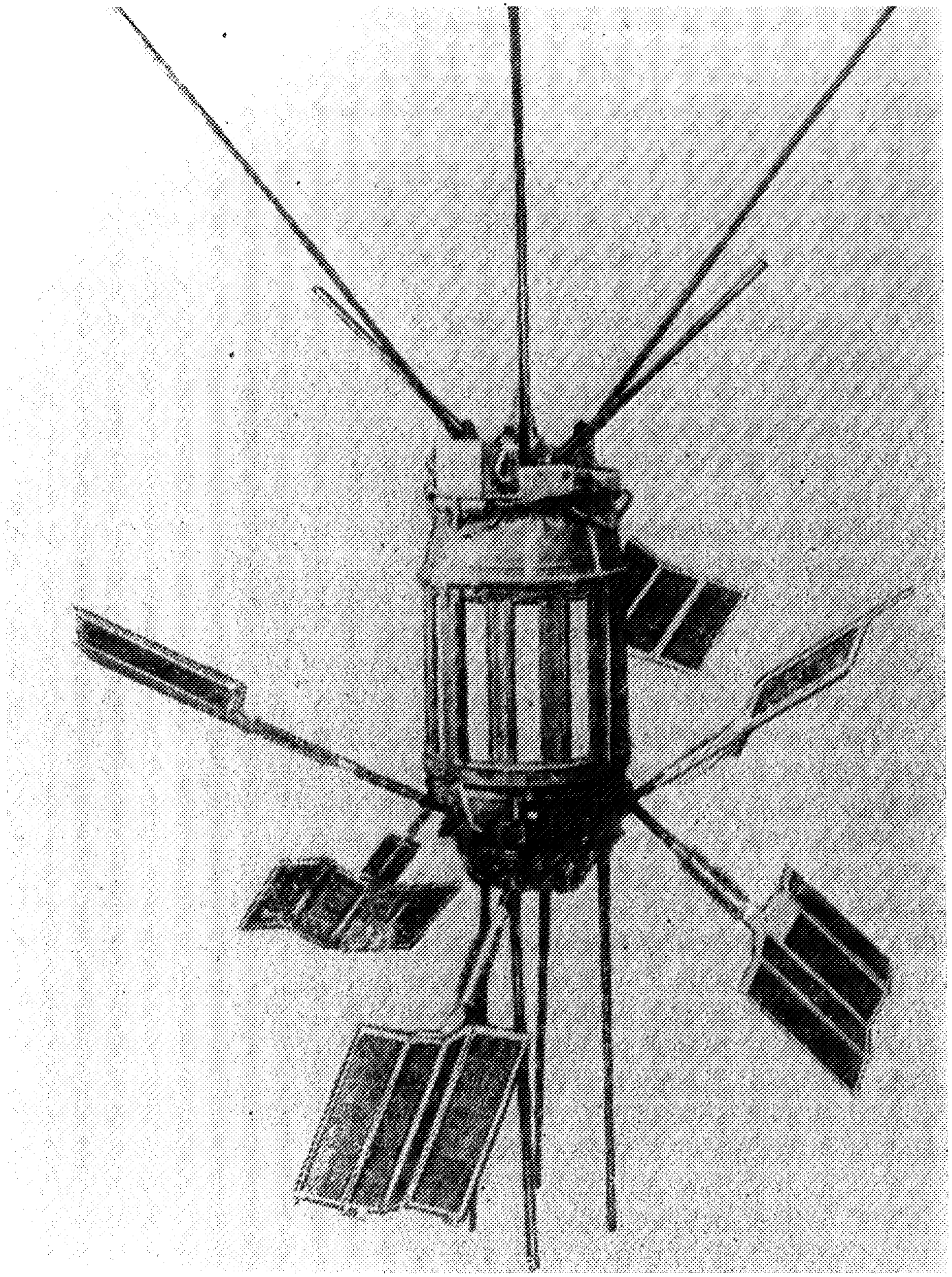

Fig. 8. ***Electron 1*****, launched with** ***Electron 2*** **on the same carrier rocket. Both satellites were launched in highly elliptical orbits; the initial perigees were 406 and 460 km respectively. Booms in this region are exposed to atmospheric bending**

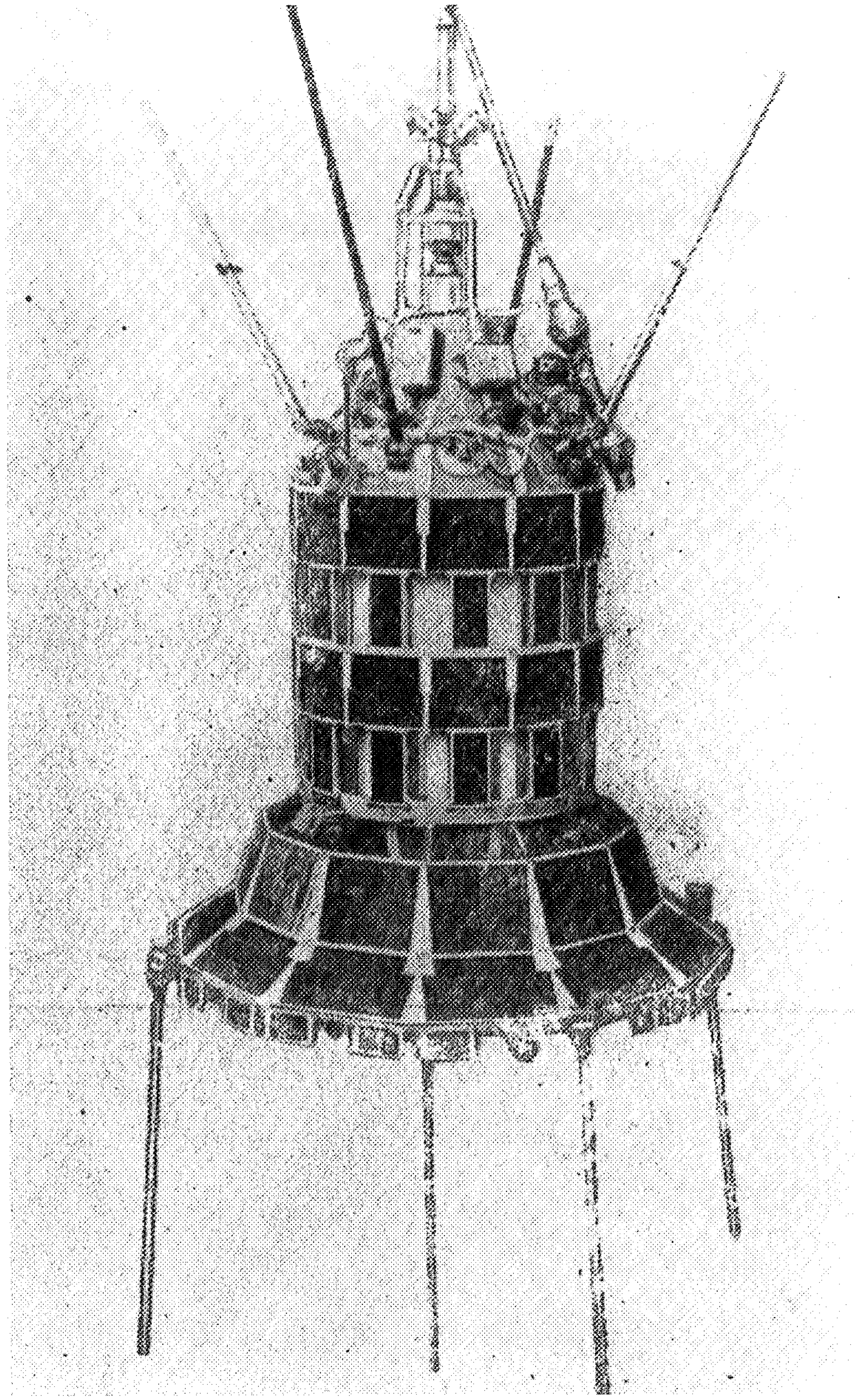

Fig. 9. *Electron 2* satellite

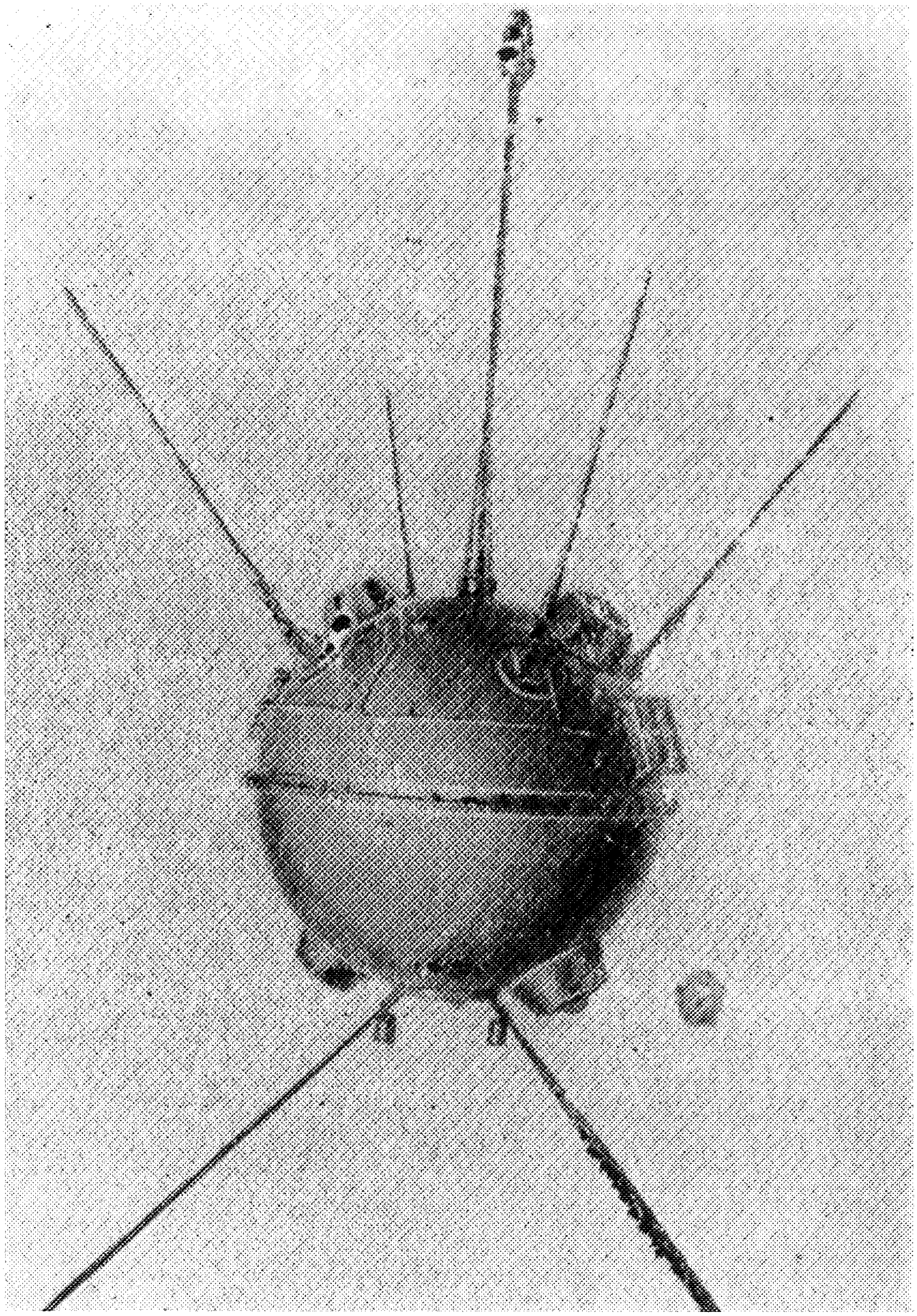

Fig. 10. *Luna 1*, which passed 7.5 km from the surface of the moon

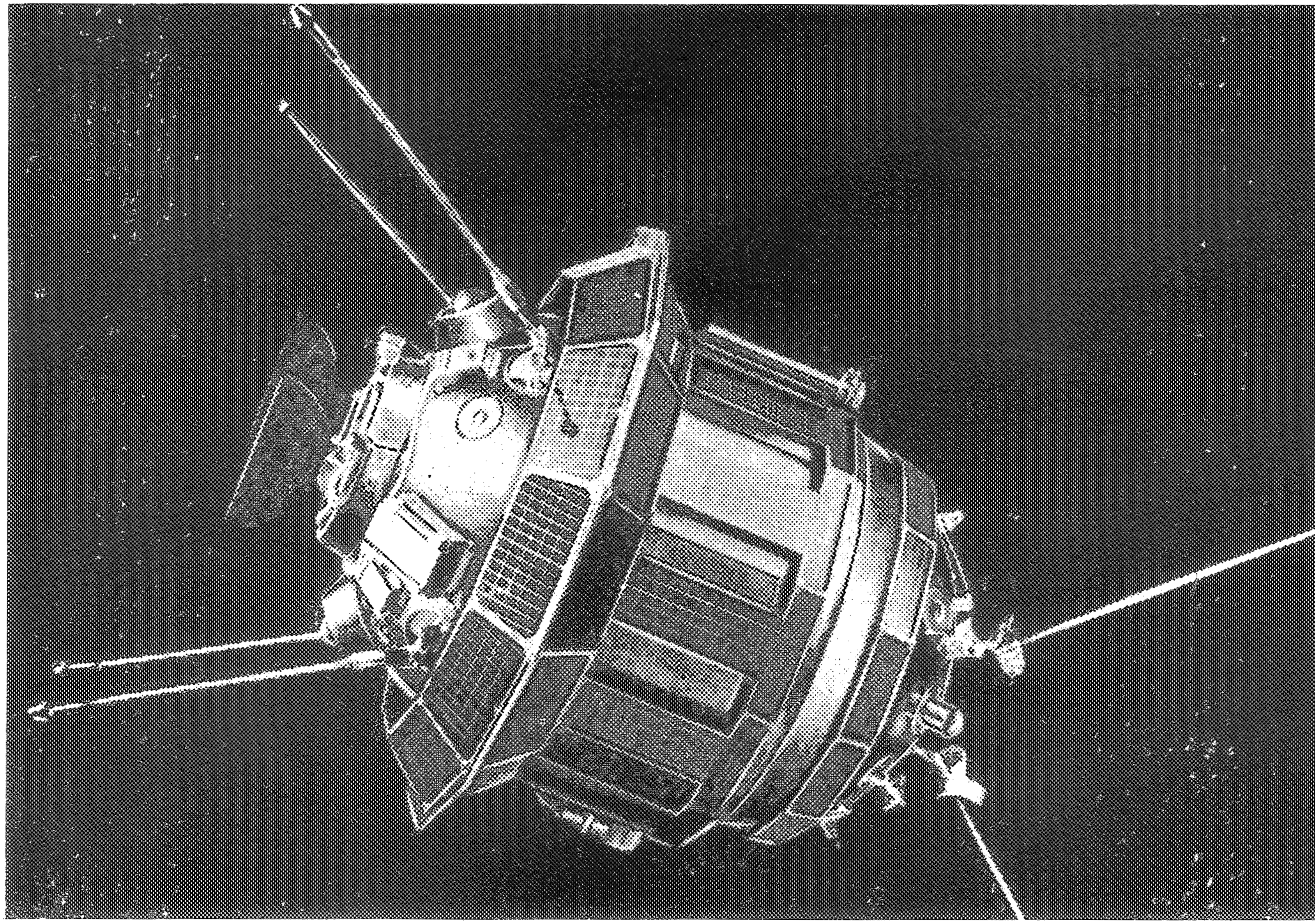

Fig. 11. *Luna 3*, which photographed the lunar surface, automatically processing the pictures in the spacecraft and transmitting them to the earth

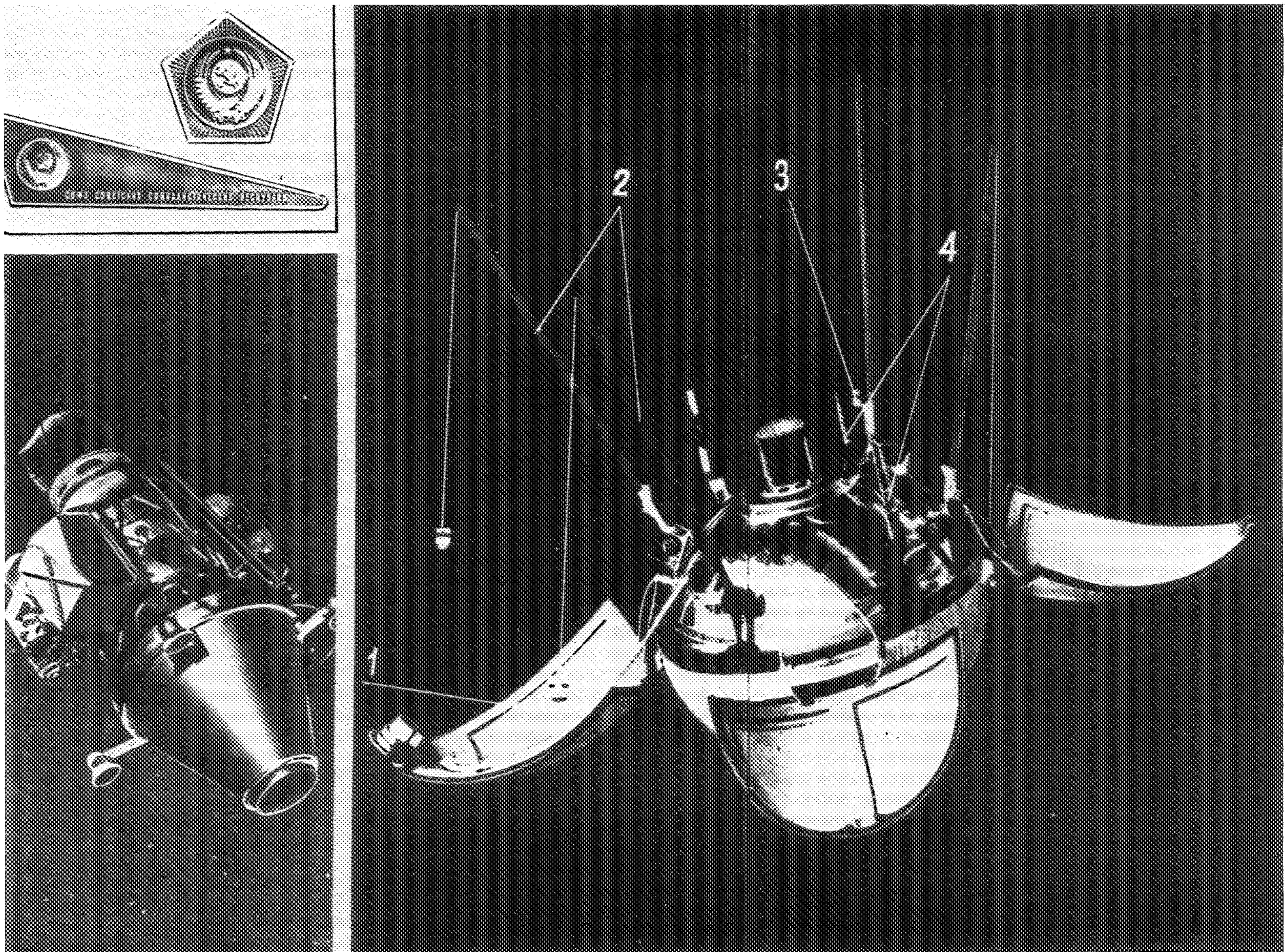

Fig. 12. *Luna 9*, which soft-landed in the Ocean of Storms in February 1966 and transmitted photographs of the lunar surface; (1) petal antennas, (2) stub antennas, (3) brightness standards, and (4) dihedral mirrors

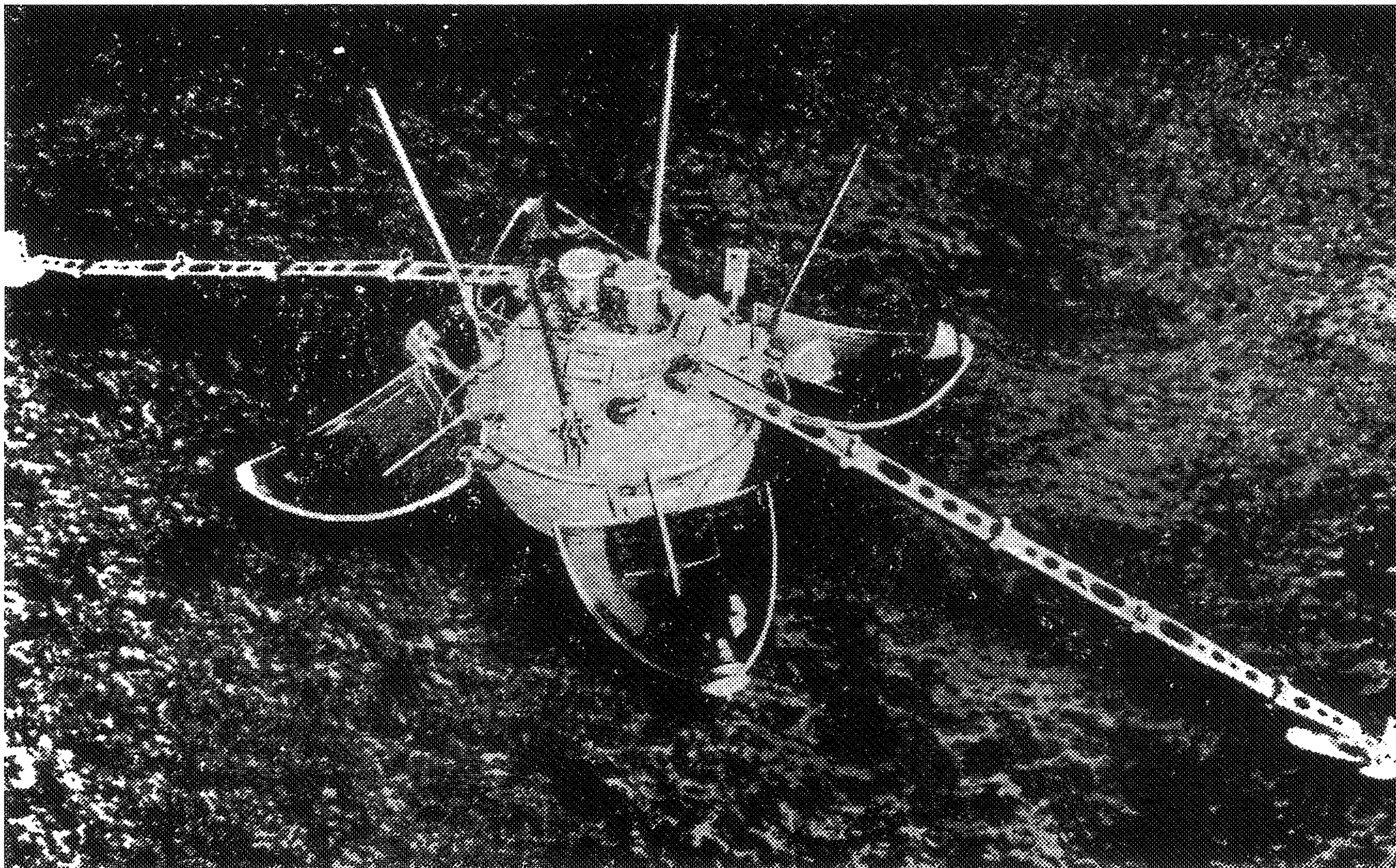

Fig. 13. *Luna 13* moon probe after unfolding of petal antennas. Left, "extendible mechanism" with soil density meter—penetrometer; right, with radiation densitometer transducer

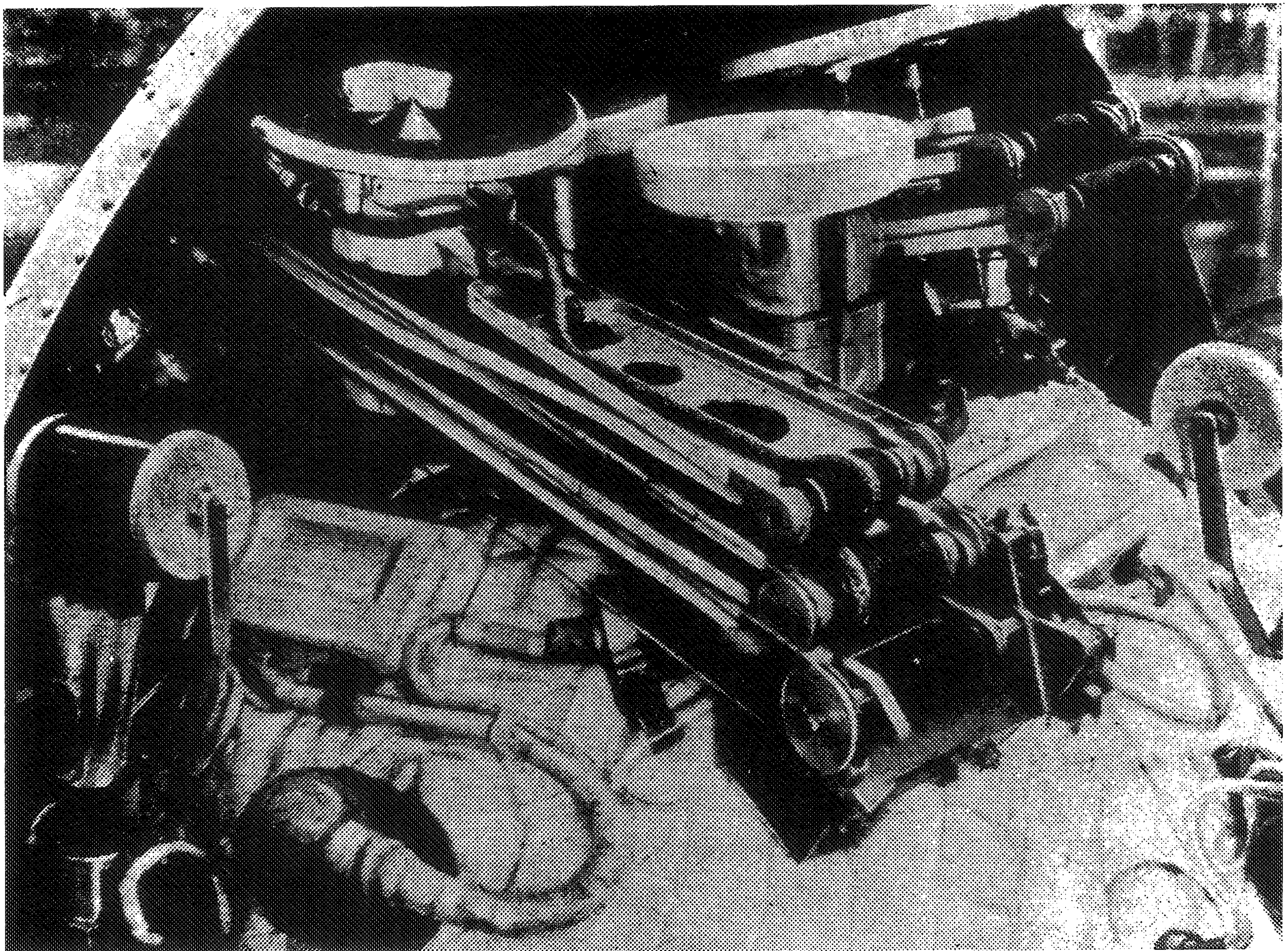

Fig. 14. Interior of *Luna 13*, showing the mounting of instruments and "extendible mechanism"

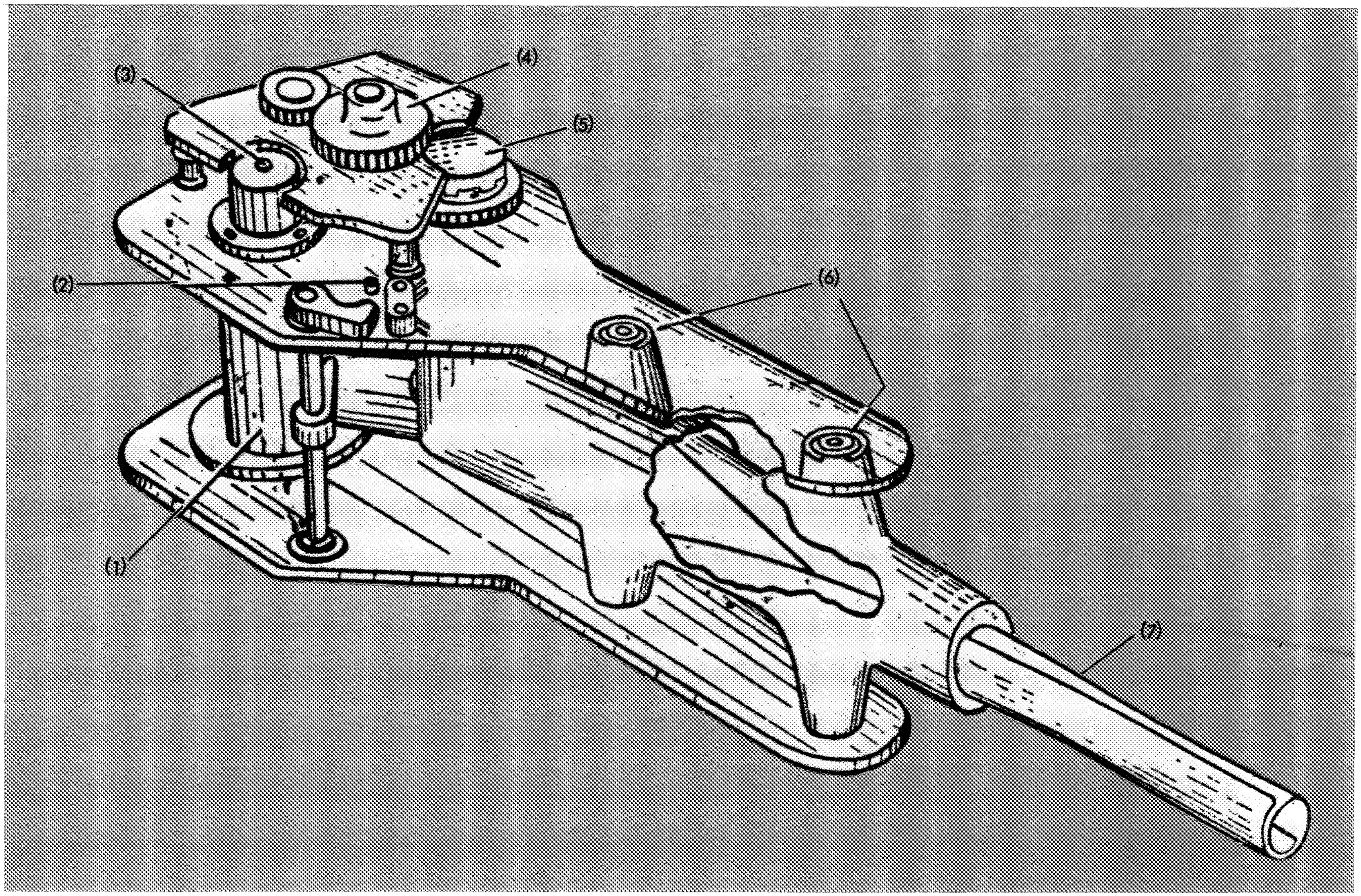

Fig. 15. Illustration from a Soviet book on antennas; (1) drum for winding the antenna, (2) catch (lock), (3) high-frequency connector, (4) reducer, (5) drum for winding Mylar tape, (6) places for fastening mechanisms, and (7) antenna

References

1. Herzl, G. G., *Spacecraft Booms.* To be distributed by Stacey's, a subsidiary of Bro-Dart Industries, 2575 Hanover St., Palo Alto, Calif.

2. Gamble, W. C., "Extendible Boom Device," in *Proceedings of the First Aerospace Mechanisms Symposium,* held at the University of Santa Clara, Santa Clara, Calif., May 19–20, 1966. Edited by G. G. Herzl. AD 638916, U.S. Department of Commerce.

3. MacNaughton, J. D., Weyman, H. N., and Groskopfs, E., "The Bi-STEM—A New Technique in Unfurlable Structures," in *Proceedings of the 2nd Aerospace Mechanisms Symposium,* held at the University of Santa Clara, Santa Clara, Calif., May 4–5, 1967, TM 33-355. Edited by G. G. Herzl. Jet Propulsion Laboratory, Pasadena, Calif., Aug. 15, 1967.

4. Rennie, R. R., "New Closed Tubular Extendible Boom," in *Proceedings of the 2nd Aerospace Mechanisms Symposium,* held at the University of Santa Clara, Santa Clara, Calif., May 4–5, 1967, TM 33-355. Edited by G. G. Herzl. Jet Propulsion Laboratory, Pasadena, Calif., Aug. 15, 1967.

5. Angulo, E. D., and Kamachaitis, W. P., "The Radio Astronomy Explorer 1500-ft-Long Antenna Array," in *Proceedings of the 3rd Aerospace Mechanisms Symposium,* held at the Jet Propulsion Laboratory, Pasadena, Calif., May 23–24, 1968, TM 33-382. Edited by G. G. Herzl. Jet Propulsion Laboratory, Pasadena, Calif., Oct. 1, 1968.

6. Rushing, F. C., Simon, A. B., and Denton, C. I., "Torsionally Rigid and Thermally Stable Boom," in *Proceedings of the 3rd Aerospace Mechanisms Symposium,* held at the Jet Propulsion Laboratory, Pasadena, Calif., May 23–24, 1968, TM 33-382. Edited by G. G. Herzl. Jet Propulsion Laboratory, Pasadena, Calif., Oct. 1, 1968.

7. Tikhonravov, M. K., et al., *Ten Years of Space Research in the USSR,* Academy of Sciences, USSR, Vol. V, No. 5, Sept.–Oct. 1967 (in Russian).

8. *Lunar Research in the USSR,* Novosti Press Agency. Edited by V. Polykov, no date (in Russian).

9. Reznikov, G. B., "Antennae for Flying Apparatuses," *Soviet Radio,* 1967 (in Russian).

Session III

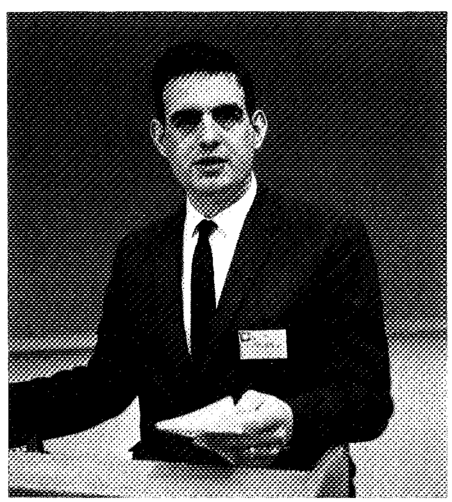

OVERLEAF: *Douglas Dwyre, Philco-Ford Corporation, Session Co-chairman, who served for the entire session. (Henry Frankel, NASA Goddard Space Flight Center, the Session Chairman, was unable to attend the symposium)*

70N21436

A Combination Shutter and Filter-Changing Mechanism*

Allen G. Ford and James A. Cutts
Jet Propulsion Laboratory
Pasadena, California

This paper describes a shutter mechanism that utilizes a disk with equally spaced apertures to alternately transmit and obscure light focused on the image surface of a vidicon camera. The disk is indexed by a ratchet mechanism actuated by a linear solenoid powered by direct current pulses spaced to provide the desired exposure time. Filters in the apertures provide a filter color change with each successive exposure. The shutter is in operation on the Mariner Mars 1969 spacecraft now on the way to Mars, and a modified version is expected to be used on the Mariner Mars 1971 spacecraft. The paper reviews both the design and the performance test results.

I. Introduction

Two cameras are used on the *Mariner Mars 1969* spacecraft: a narrow-angle camera for "closeup" pictures and a wide-angle camera for broader coverage. The cameras are mounted on a platform that is deployed to orient the cameras (as well as various other instruments) toward the planet during encounter. On this mission, the spacecraft will pass Mars at a distance of 3000 km from the surface, during which time 16 pictures will be taken by each camera at 84-s intervals, in addition to eight or nine pre-encounter pictures at over 300,000 km from Mars.

The wide-angle camera, for which this shutter was developed, requires a minimum exposure time of 60 ms and a change of interference filter at each exposure. A sequence of red–green–blue–green is used to determine the chromatic characteristics of the planet by superimposing overlapping portions of adjacent frames. The space between the lens and vidicon face allows a maximum shutter depth of 0.90 in., and a rectangular area of 4 by 5 in., symmetrical about the axis, was allotted. An aperture of 0.50 by 0.60 in. is required at the plane of the shutter.

Opening and closing pulses, spaced to obtain the desired exposure time, are produced by a 770-mF capacitor, which is initially charged at 50 V.

A rotating filter wheel was chosen over a sliding rack because of the inherent saving of friction by pivoting rather than sliding, and because the wheel lent itself to combining the filter-changing and shuttering functions, thus simplifying the mechanism.

*This paper presents the results of one phase of research carried out at the Jet Propulsion Laboratory, California Institute of Technology, under Contract No. NAS 7-100, sponsored by the National Aeronautics and Space Administration.

The design of this shutter was based on the successful *Mariner IV*[1] shutter, which utilized a similar filter wheel but was driven by a rotary solenoid. Since the height limitation did not permit a concentric drive, a latching mechanism utilizing a crank driven by a linear solenoid appeared to be the most straightforward approach.

II. Requirements

In addition to the operational constraints indicated above, the following requirements had to be met:

(1) Weight. The weight was limited to 0.50 lb.

(2) Lubrication. Dry lubricants were most suitable, since the shutter was not to be hermetically sealed and the optical surfaces were consequently exposed to any outgassing from the shutter.

(3) Life. A service life of 20,000 cycles in high vacuum is required, because the shutter will be cycled several hours before encounter.

(4) Exposure time variation. The exposure time must not vary more than 10 percent over all points within the aperture, and the difference between exposure time and pulse spacing must not be greater than 10%.

(5) Storage life. The shutter should be operable after being exposed to hard vacuum for a period of 270 days.

(6) Thermal environment. The shutter must be capable of normal operation at temperatures between −50 and +50°C.

(7) Mechanical environment. The shutter must survive the following tests, on three axes:

(a) Shock, two 200-g, 0.5-ms terminal peak sawtooth pulses.

(b) Static acceleration, ±9 g, 5 min.

(c) Random vibration, shaped spectra, 18 g rms, 60 s.

(d) Sinusoidal vibration (1 octave/min)

Hz	g rms
5–30	1
30–400	15
400–750	50
750–2000	9

[1]The *Mariner IV* spacecraft carried out a flyby mission to Mars in 1965.

III. Description

The shutter is shown in Figs. 1 and 2. As shown in Fig. 2, the filter wheel (1) has four openings with radial edges 45 deg apart, of sufficient size to clear the light

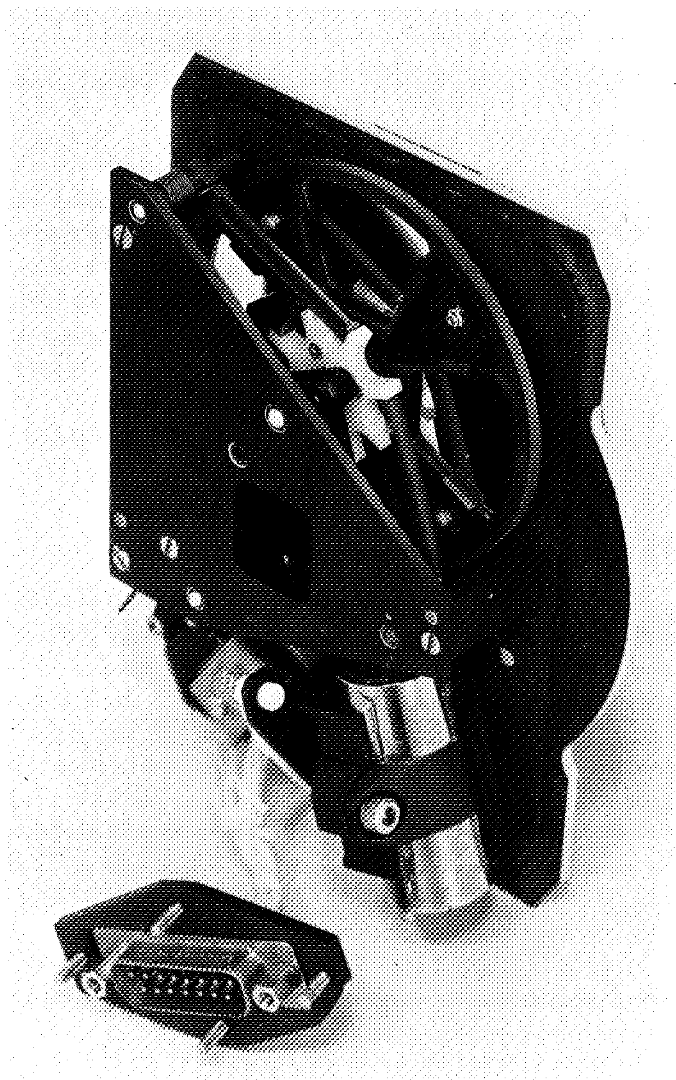

Fig. 1. The shutter mechanism

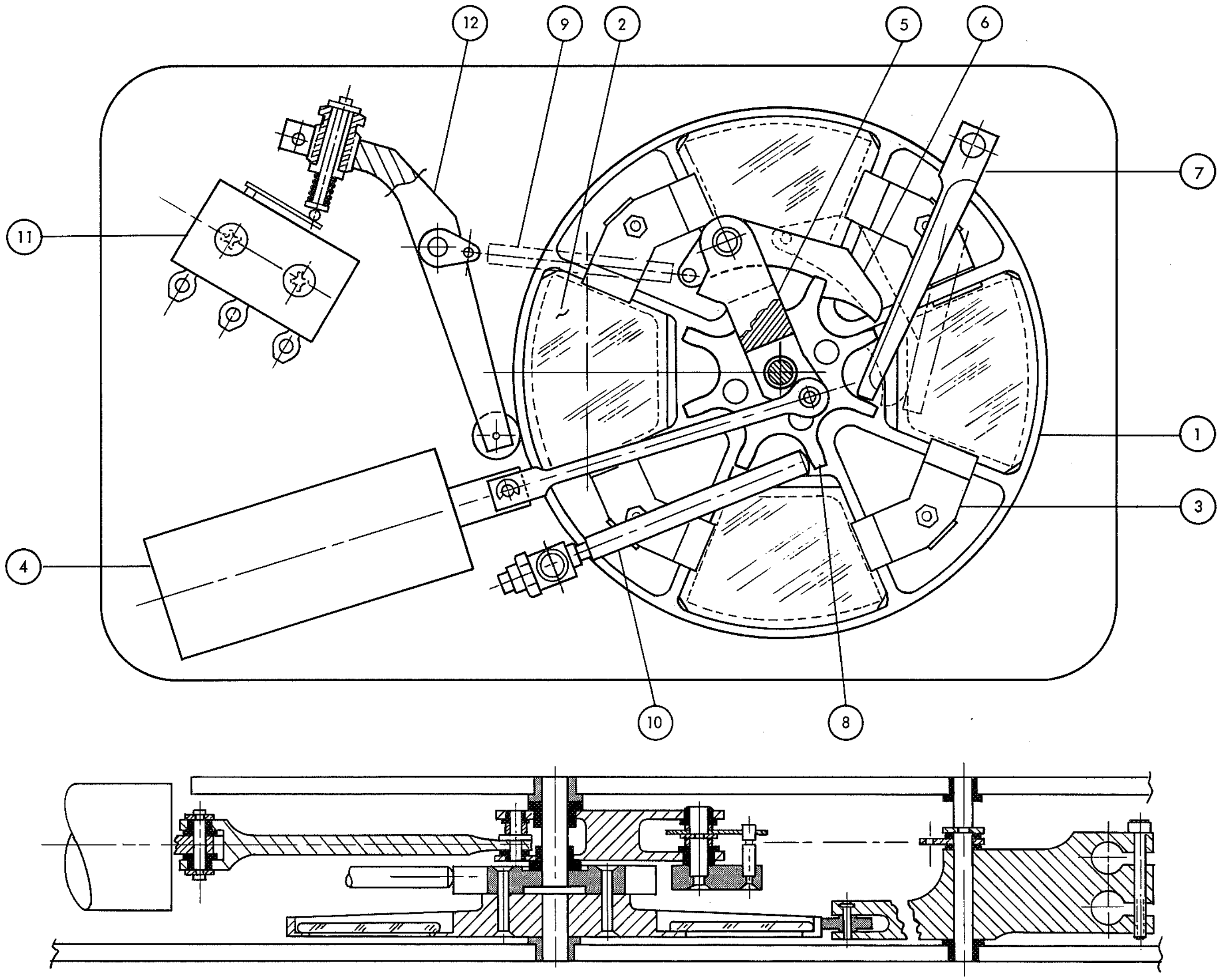

Fig. 2. Schematic diagram of the shutter

path from the lens to the vidicon. Each opening is covered by a glass filter (2) retained by spring clips (3). The filter wheel can be indexed in 45-deg steps. Each such indexing cycle is started by an electrical pulse.

Except during an exposure, the filter wheel is in the closed position, with the opaque web between filters obscuring the aperture. When the wheel is rotated 45 deg into the open position (shown in Fig. 2), light can pass through to the vidicon, but a further 45-deg rotation again obscures the aperture. The time for which the vidicon is exposed to light is controlled by the time between the two indexing cycles, which is, in turn, governed by the separation of the input pulses.

The pulse initiating an indexing cycle energizes the linear solenoid (4), thereby rotating the rocker arm (5) by means of the connector rod. The pawl (6), pivoted on the rocker arm, is consequently driven to the position shown in phantom. In reaching this position, the pawl releases latch A (7), extends the drive spring (9), and then engages with the next cog on wheel (8). The shutter is now said to be cocked. When the solenoid is de-energized, the linkage is returned to its original position by the drive spring, advancing the filter wheel 45 deg. During this travel, the latch follows the pawl inward and is in position to stop the filter wheel at the end of the stroke. The back latch B (10) ratchets over the cogs, preventing back motion of the wheel. Latch B can be adjusted to provide the optimum backlash of the system.

Two microswitches (11) are used to indicate the position of the filter wheel. They are actuated by the spring-loaded follower arm (12), which rides on the rim of the filter wheel. The rim is contoured to actuate one switch at each closed position and to actuate the other switch at one of the closed positions. Thus it can be verified that the shutter closes after each exposure and the filter colors can be correlated with the pictures received.

The major components are made from 6061-T6 aluminum alloy, with a dull black anodized finish. Shafts are stainless steel and bushings are machined from fluorocarbon.

IV. Development and Test

Evaluation of the performance of the prototype shutter was accomplished by two techniques. High-speed movies taken of the shutter operation facilitated greater understanding of the dynamic behavior and the recognition of failure modes and instabilities. However, this method did not provide real-time observation, could not be used to observe intermittent failures, and did not provide a measurement of exposure time values. This information was provided by the second technique, which utilized an optical position sensor to locate the position of the filter wheel at any time. By displaying the output from this position sensor on an oscilloscope, together with the current pulses supplied to the shutter, it was possible to measure the cocking time, the solenoid release time, the wheel rotation (transit) time, and, the most significant parameter of all, the shutter exposure time. In addition, some of the failure modes could be identified.

The following critical design areas were discovered in the course of the extensive development tests:

(1) Wear and dimensional instability.

- (a) Wear and cold flow in the Teflon bushings caused the shutter to fail to cock and the actuating points of the telemetry microswitches to shift.
- (b) Fracture of the anodized surfaces of pawl and latch, due to repeated impact, caused an increase in friction.

(2) Insufficient speed.

- (a) Magnetic sticking of the solenoid delayed the start of filter stepping.
- (b) The high inertia of the thick color filters caused the filter stepping to take longer.

(3) Loss of image quality.

- (a) Contamination of the optical path by solid film lubricant debris caused a loss of image quality.
- (b) Lateral shifting of the image due to the filter tilting as it exposed caused a loss of resolution.

(4) Instabilities in cocking and latching. Intermittent failures occurred because of failure of the latch bars to engage.

These difficulties were met by introducing a number of design improvements as follows:

(1) To provide greater dimensional stability, Teflon was replaced with Delrin AF[2] as the bushing material.

[2]E. I. duPont de Nemours & Co., Inc., Plastics Department, Wilmington, Del.

(2) To avoid the necessity for solid film lubricant, the pawl was fabricated from Delrin AF also and was braced with an aluminum plate. The mechanical adjustment of latch A was abandoned to permit the use of a T-section titanium latch permitting a line contact instead of a point contact with the pawl.

(3) To reduce the weight and increase the stability of latch B, it was fabricated from a hollow cylinder of aluminum.

(4) To reduce magnetic sticking, the solenoid was redesigned to break up the eddy currents that contributed to this.

(5) To reduce inertia and to improve picture resolution, the conventional color filters were replaced with thin (1-mm) glass substrates with interference film coatings.

V. Optimization

A. Determination of Minimum Exposure Time T_{min}

The shuttering operation consists of two essentially identical cycles. The duration of each cycle is set by the width of the pulse required by the cocking cycle and the times required for the solenoid to release, the wheel to rotate, and the latches to engage. For reliable and authentic exposures, the first cycle must be completed before the second is initiated. Therefore, the duration of an indexing cycle sets the minimum command exposure time T_{min} and will be considered synonymous with it.

In Fig. 3, this relationship is illustrated by measurements made on a shutter. Along the horizontal axis, the separation of the pulses supplied to the shutter (exposure time command) is indicated. Along the vertical axis, the corresponding actual exposure times are plotted. As the pulse separation is decreased below the minimum exposure time defined above, the exposure time variation is found to increase until a failure occurs in which the shutter fails to close on the second cycle, and the shutter sticks open.

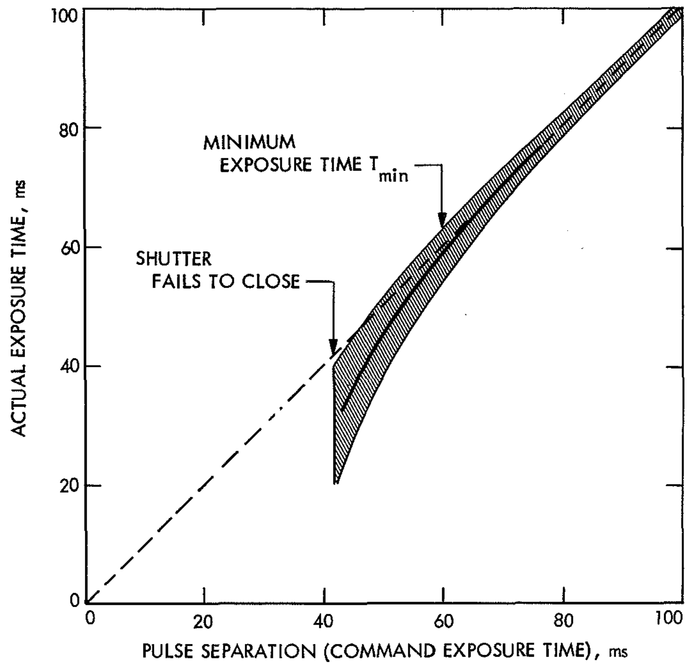

Fig. 3. The relation of command exposure time and actual exposure time

B. Selection of Pulse Width and Drive Spring

The power available in a solenoid pulse was limited by the 770-mF capacitor and the charge of 50 V. The pulse width, however, was under the control of the designers. In order to reduce the minimum exposure time to a low value, it is important to keep this pulse width as short as possible. For the same reason, the strongest possible drive spring should be used consistent with the limitations on solenoid power.

In Fig. 4, each curve shows the minimum combination of pulse voltage and pulse width required to operate the shutter for a particular drive spring. Each curve is labeled with the value of T_{min} measured using a 14-ms pulse width.

By the selection of a 50-V, 14-ms drive pulse and the number 3 drive spring, T_{min} is 60 ms. This comprises the pulse width of 14 ms, the solenoid release time of 10 ms, the wheel rotation time of 26 ms, and the latch stabilization time of 10 ms. Since the shutter will still operate if the voltage drops below 40 V (crosshatched), adequate power margin exists against power supply variations as well as increased friction and high temperature. Table 1, derived from Fig. 4, indicates that it is not possible to equal this performance with either spring 2 or 4.

C. Selection of Latch Springs

The loads on each latch spring must be sufficient to provide positive reliable latching with an adequate safety margin. However, increasing the load on latch A causes an additional load on the solenoid and reduces the voltage margin. Similarly, increasing the load on latch B

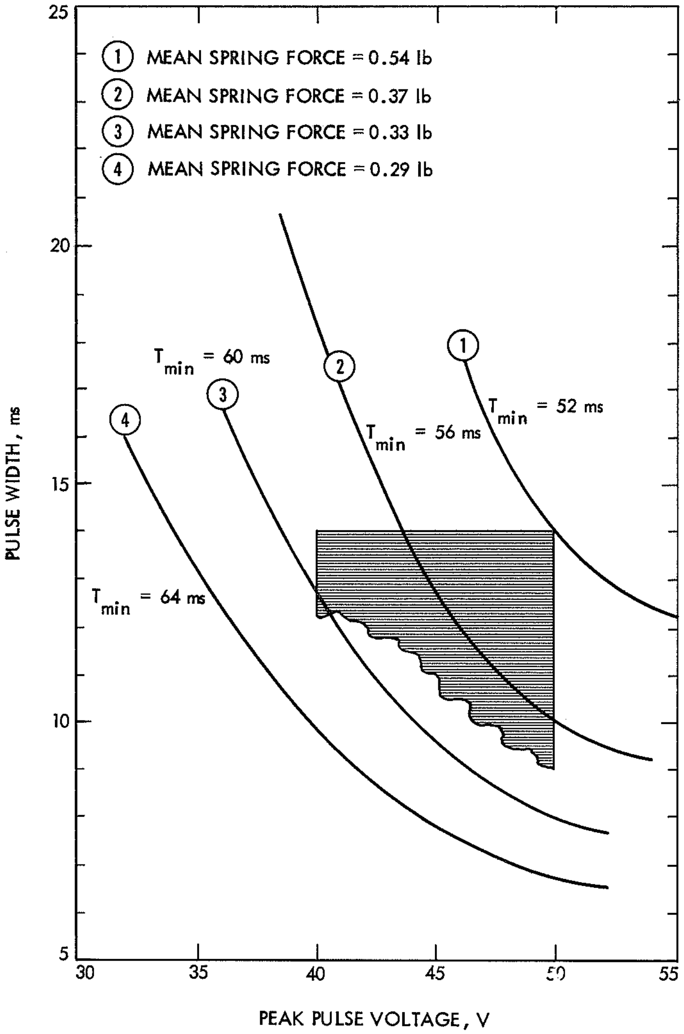

Fig. 4. Voltages and pulse widths required for different drive springs

retards the filter wheel rotation and causes the minimum exposure time to increase.

In Fig. 5, the effect of varying the latch loads about the final optimized design points is illustrated. A large safety margin was utilized, since the optimization of latch loads was performed on only one unit.

VI. Tests

The test program was intended to confirm the suitability of the shutter design for prolonged ground test and further operation in the vacuum environment of space. The basic test sequence consisted of the following:

(1) Simulation of prelaunch subsystem and spacecraft operation. A period of 72 h accelerated operation (26,000 cycles) under ambient temperature and pressure, simulating 600 h spacecraft operation.

(2) Simulation of "space soak." A period of 50 h in the Molecular Sink Space Simulator (Molsink)[3] at 50°C and 10^{-10} torr.

(3) Simulation of space operation. A period of 250 h operation (90,000 cycles) in the Molsink chamber at 0°C and 10^{-12} torr, simulating 2000 h space operation.

Table 1. Shutter operation data

Spring	Desired minimum pulse, V	Corresponding pulse width, ms	Corresponding T_{min}, ms
1	(a)	(a)	(a)
2	38.5	20.5	62.5
3	38.5	14.0	60
4	38.5	11.0	61

[a]The solenoid would not cock the shutter at 38.5 V when this spring was used.

Monitoring techniques permitted the separate verification of reliability and exposure time repeatability and the performance of margin tests.

Voltage margin testing was the most important test, since it gave an indication of whether friction was increasing in the molecular sink environment.

The basic test plan was modified slightly so that, of the two units tested, the first was operated for 122,000 cycles and the second for 46,000 cycles in the Molsink chamber; both performed without any failures. Although changes in the voltage margin were observed, none were attributable to the molecular sink environment.

VII. Conclusion

The mechanism described proved to be a simple, reliable, and rugged device for accomplishing the functions of shuttering and filter changing. It has proved useful for general photosensor evaluation with slow- and medium-speed optical systems as well as in the *Mariner Mars 1969* camera application. It is intended to use a modified form of the mechanism on the *Mariner Mars 1971* spacecraft.

[3]See "Spacecraft Mechanism Testing in the Molsink Facility," by J. B. Stephens, in these *Proceedings*.

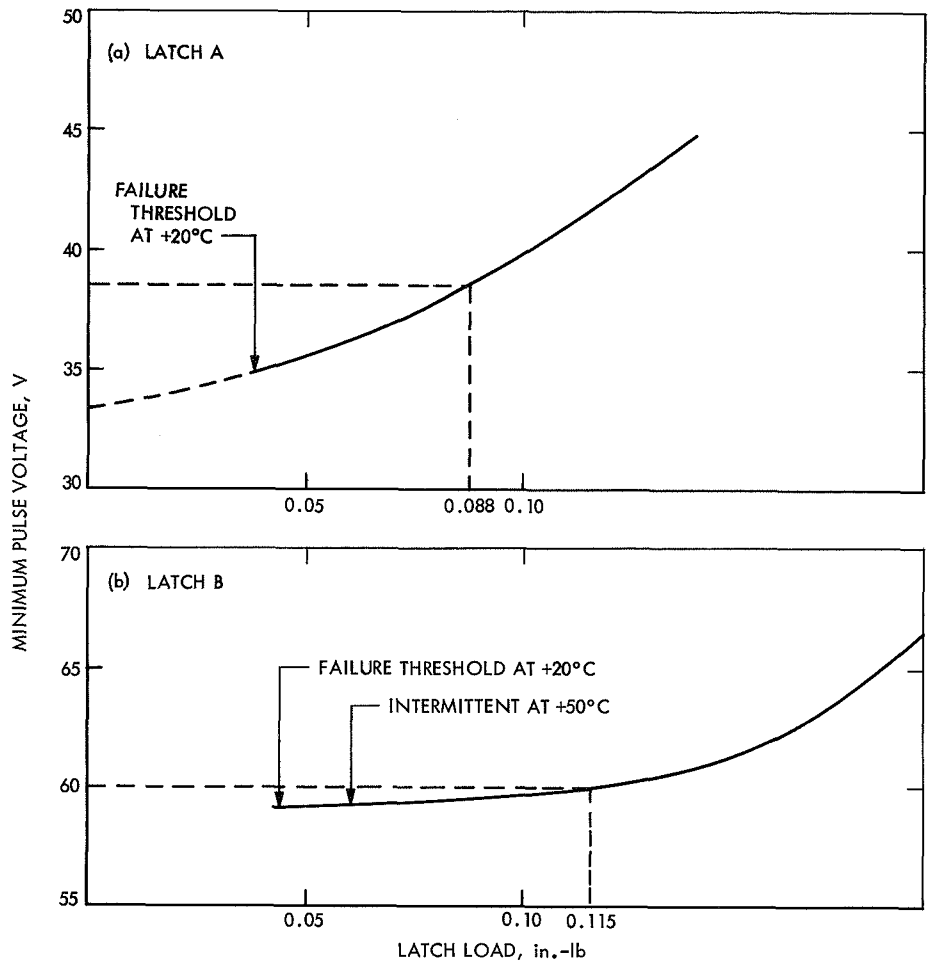

Fig. 5. Selection of latch loads

Acknowledgments

The authors acknowledge the contribution of the following Jet Propulsion Laboratory personnel, who were immediately connected with this project: L. Adams, H. Rosenberg, A. Dunk, C. Kurzweil, J. Kent, D. Norris, J. S. Griffith, and G. Coyle.

Page intentionally left blank

70N21437

A Deployment Fixture for the Simulated Zero-Gravity Testing of a Large-Area Solar Array*

James A. Lackey
The Boeing Company
Seattle, Washington

A large, lightweight, folding modular solar panel assembly requires ground deployment testing to simulate behavior in a space flight environment. This paper describes the design and development of a fixture that provides a simulated zero-gravity deployment system utilizing a carriage suspended on air bearings to support the subpanels during deployment.

I. Introduction

Deployment testing of very large, lightweight, space-deployable structures requires precision ground support equipment for testing on the surface of the earth. Such structures, to meet the requirements of future spacecraft, may involve materials such as beryllium and may be relatively fragile compared with existing structures such as the *Lunar Orbiter* solar panels.

The lightweight, low-powered mechanisms used to deploy these future structures must provide a slow rate of deployment to avoid structural damage. Because very small forces may influence intended deployment behavior, the ground deployment equipment for testing this type of mechanical system must reduce to a near-zero level both (1) structural loads due to gravity and (2) any extraneous forces either aiding or retarding deployment.

*This work was performed for the Jet Propulsion Laboratory, California Institute of Technology, sponsored by the National Aeronautics and Space Administration under Contract No. NAS 7-100.

II. Ground Deployment Test Approach

The solar panel assembly, or quarter array, for which the fixture was designed, consists of 13 large subpanels of beryllium structure connected by aluminum hinges. Five center or "main" subpanels are deployed by a winch, cable, and quadrant system. The "auxiliary" subpanels, appended in pairs to each of the four outboard main subpanels, are deployed by torsion springs. The total deployed size is approximately 65 by 24 ft, and the total weight is about 500 lb. (For an artist's conception of the deployed array, see Fig. 1.)

In considering the ground deployment testing of this assembly, two primary objectives were established:

(1) The test equipment must permit deployment of the panel assembly using the power available for deployment in space as the only significant source of energy. It is considered essential to verify that the lightweight, limited-power mechanisms are, in fact, capable of deploying the panel assembly. This means that if any power-assisted device is used to

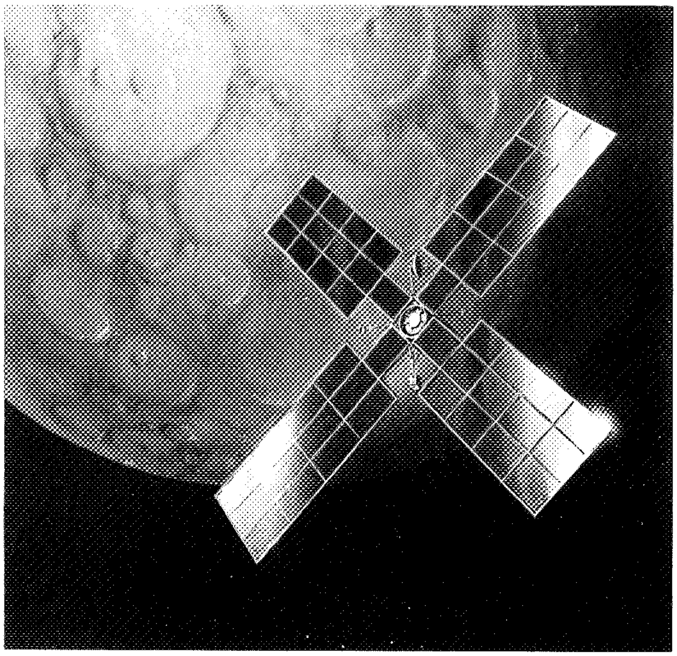

Fig. 1. Artist's conception of the deployed modular solar panel array on an ion-powered Mars flyby spacecraft

overcome frictions and moments due to gravity, such a device must be precisely controlled to avoid either leading or retarding deployment.

(2) The deployment testing of this developmental panel assembly must provide useful data in support of the analysis and design of a final flight-configuration assembly.

The deployment of the five main subpanels is performed separately from the deployment of auxiliary subpanels about their parent main subpanels. This approach allows deployment about vertical hinge lines in all cases and eliminates the large gravity moments which, with any hinge line horizontal, could have been as great as 1,000 times the moment available for deployment in space. The approach resulted in a test plan involving three separate types of tests:

(1) Auxiliary subpanel deployment testing, involving only the single 180-deg motion of each of the two subpanels, permits a straightforward solution. The deploying subpanels are supported by counter-weighted overhead arms pivoting on conventional bearings as shown in Fig. 2.

(2) Main subpanel deployment testing, involving the five sequential and interrelated motions of the main subpanel units, but with pairs of auxiliary subpanels restrained to the main subpanels, presents the most severe technical problems. The design of equipment for this testing is the subject of the remainder of this paper.

(3) A full-sized, sequential deployment demonstration, using a simulated panel assembly of aluminum structure but with prototype mechanisms, was planned to demonstrate the interrelated main and auxiliary subpanel motions and mechanical interactions. In this type of test, since no deployment dynamic data are required, outside power is used as a source of deployment energy and rates are only approximated.

III. Main Subpanel Deployment Concepts

A. Possible Approaches

A great number of approaches to the ground deployment of this panel assembly, or any similar lightweight, low-powered, deployable structure, can be conceived. Analysis and evaluation are simplified by classifying the various approaches as follows:

(1) Support function.
   (a) Overhead suspension.
   (b) Undercarriage support.

(2) Carriage function.
   (a) Articulated arms (duplicating test article geometry).
   (b) Wheeled cars and tracks.
   (c) Free-sliding devices (including air bearings).
   (d) More exotic solutions, such as immersion of a neutral-buoyancy test article in a fluid tank.

(3) Tracking or follower function.
   (a) Fully passive operation; no outside energy source is used.
   (b) Powered operation, either with preprogrammed rates or with a feedback control system.

B. Approaches Studied

Some candidate concepts that were studied are discussed below.

1. Passive overhead arm concept. This concept involves an overhead cantilever folding arm system that

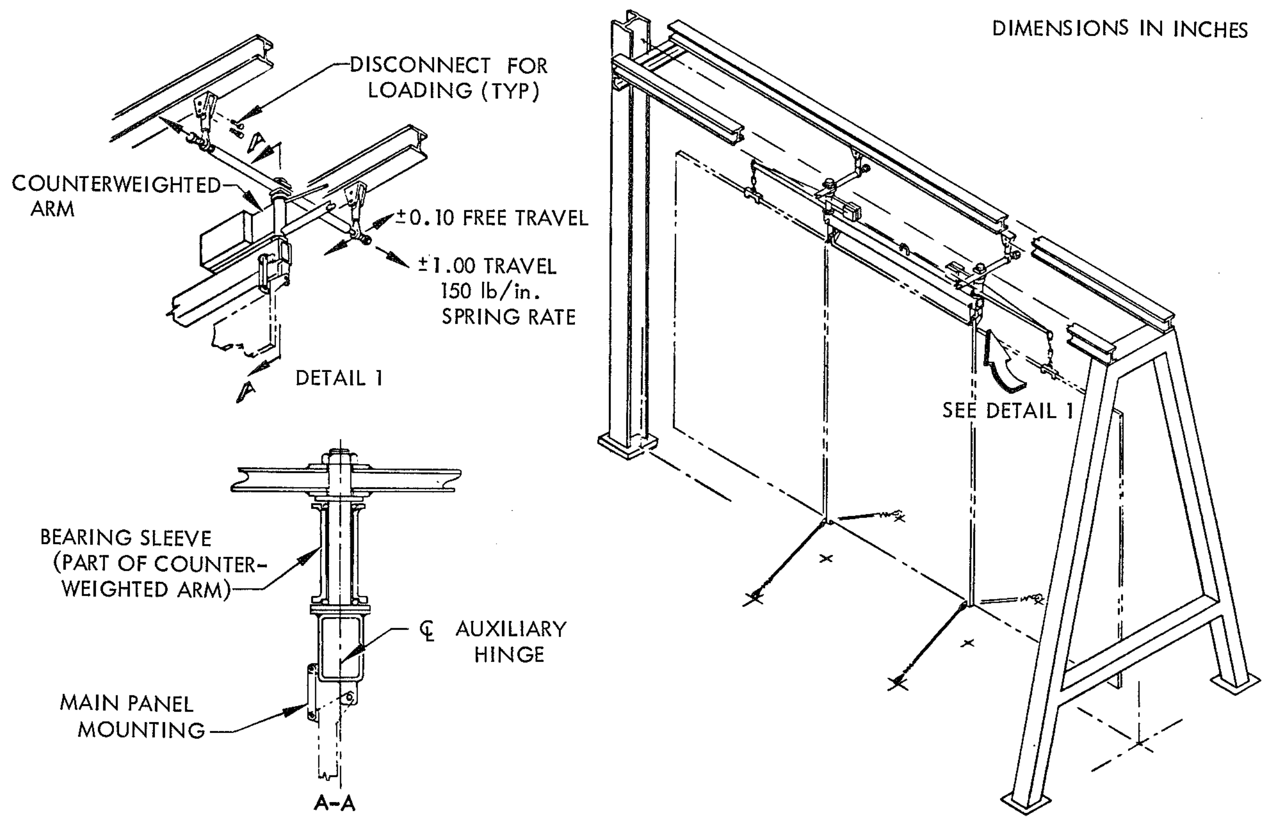

Fig. 2. Auxiliary subpanel deployment equipment

deploys on the same radii as the main subpanels. Major problems in this system include:

(1) Large friction moments in the bearings of the cantilever.

(2) Large inertia of the cantilever arm.

(3) Excessive torsional deflections of such an arm.

2. Powered carriages and overhead tracks. A powered overhead system appears to be one of the most straightforward approaches to deployment, but it is made unattractive by detail design problems such as shifting centers of gravity and complex track and carriage systems. For example, one of the most serious problems involves controlling the lead or lag of the overhead carriage in relation to the test article (in this case, a maximum 0.03-in. lead or lag is permissible). The following difficulties are encountered:

(1) Gravity must be used as a tracking reference, since it is the horizontal vector from the nonvertical suspension line that leads or retards deployment.

(2) Any system based on a plumb-bob approach is subject to false indications because of pendulum-like oscillations.

(3) Optical methods, such as the use of a tracking theodolite, are ruled out because change of position of target points is too rapid and too extreme.

(4) A gyrostabilized light source projecting an optical pattern onto a target mounted on the test article might be workable. Such a system could be used either to record deviations, as in the preprogrammed approach, or to provide feedback information. In either case, carriage inertia is severely increased, space envelope limitations are encountered, and a complex electrical system is required. In such a system, cost is high, reliability is poor, and no performance advantage is gained over a passive system.

3. Air bearing undercarriage concept. This concept involves the deployment of each set of subpanels on a rigidly attached air bearing device. This system most nearly duplicates space ambient deployment conditions.

The precision track surface on which the air bearings ride limits deflections of the panel assembly and minimizes friction and gravity effects on deployment. The flatness and levelness of the track surfaces are critical.

IV. Deployment Equipment Configuration

A deployment fixture, as shown in Fig. 3, was designed and constructed for this program. This fixture was used to test a full-sized, mass-simulated aluminum model of a panel assembly. These tests were performed to qualify the fixture for future use with a beryllium panel assembly and to obtain developmental data for the design and analysis of this flight prototype panel assembly.

The operation of the functional elements of this fixture is shown in Fig. 4. The simulated spacecraft (1) provides a mechanical interface with the first subpanel. A deployment motor winch (2), working through a system of cables and quadrants on the panel assembly, provides the energy for deployment. The air sled (3) supports each deploying set of subpanels and provides a minimum-friction carriage. The air bearing track (4) is a precision-leveled surface on which the air sled travels.

Deployment is stopped near the conclusion of each sequence, and the trailing subpanel of the deploying set is transferred to the overhead suspension lines (5), which are supported by the limited-travel overhead air bearings (6). A crossbeam (7) is removed from the air sled to allow the automatic continuation of the succeeding sequence when the system is restarted. This fixture is fully passive in operation, the flight prototype deployment motor winch being the only significant energy source. An intermittent test operation is employed in which each

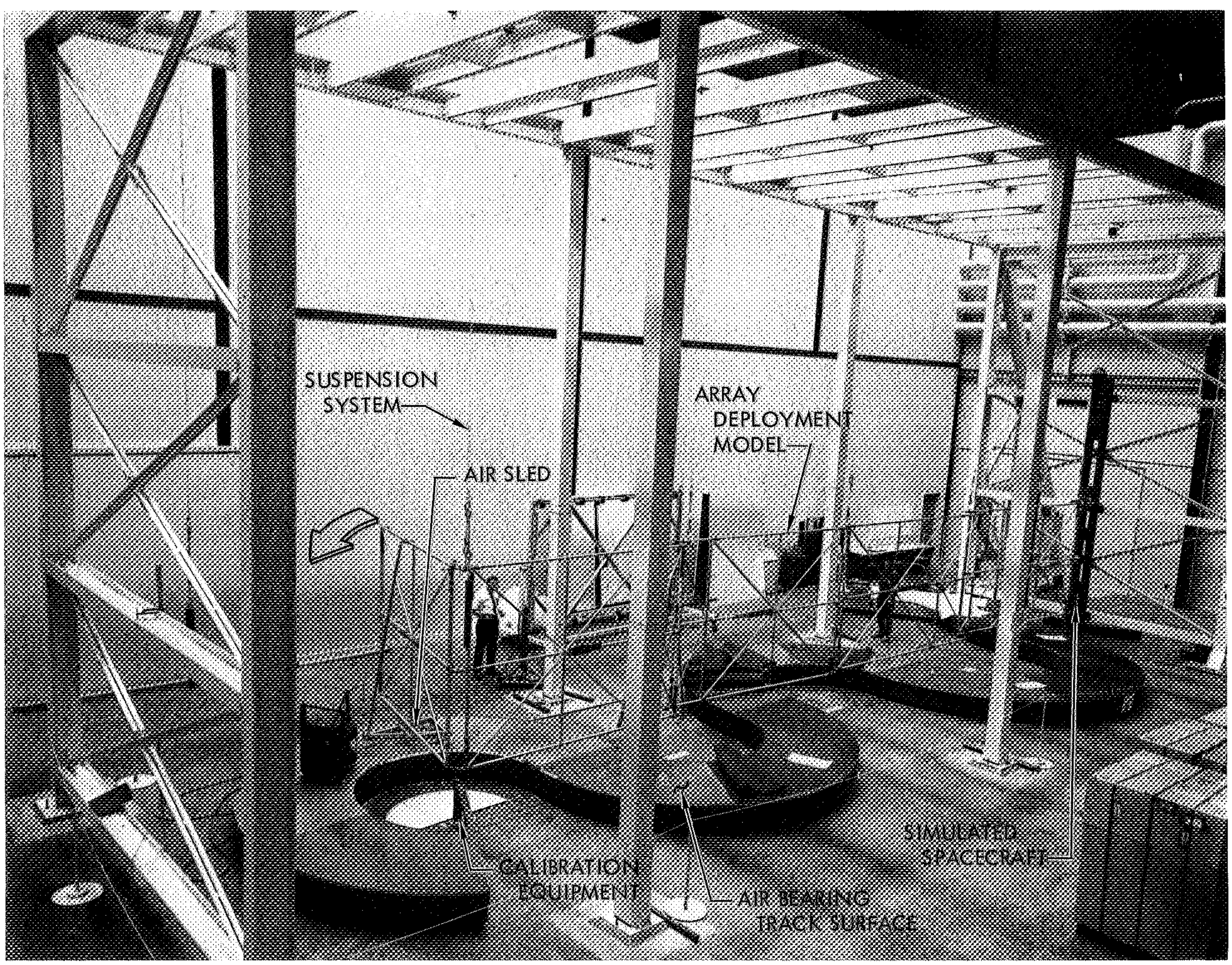

Fig. 3. Deployment fixture and aluminum deployment model

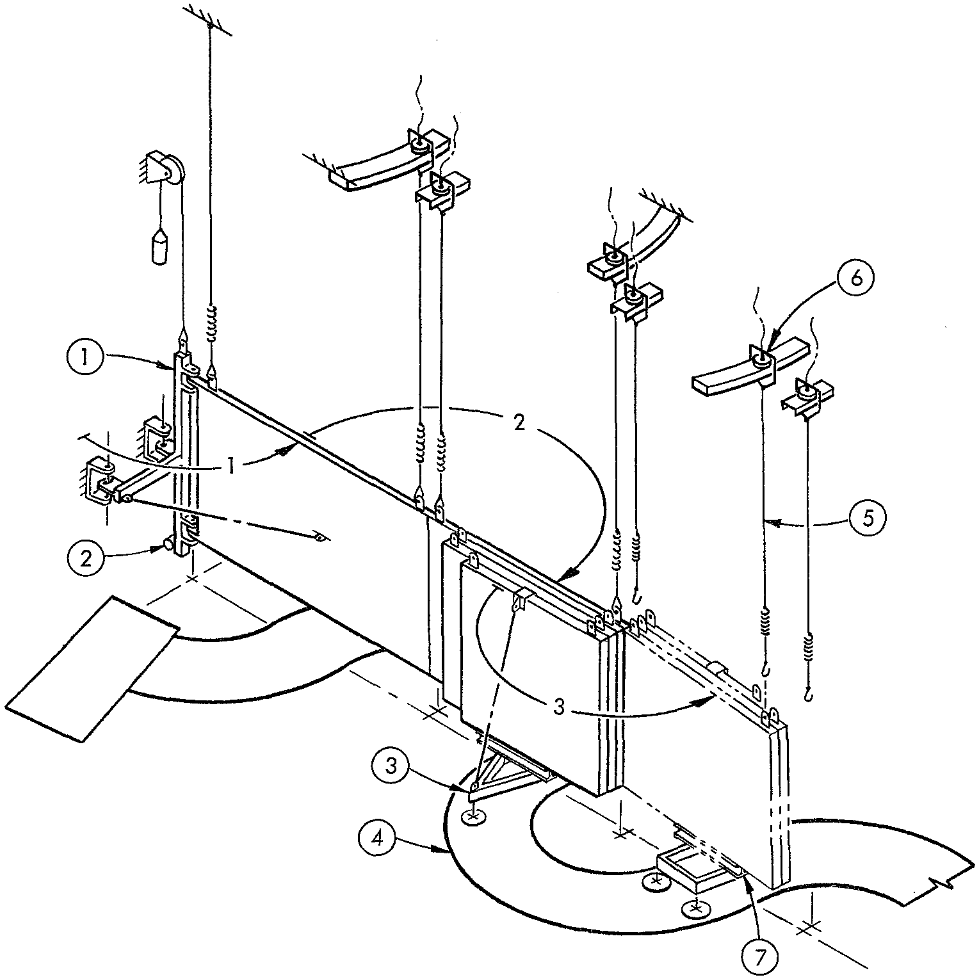

Fig. 4. Mechanical operation of deployment fixture

deployment sequence is stopped just short of closing and the trailing subpanel transferred from the air sled undercarriage to the overhead suspension lines. Various closing and opening rates of the panels can be tested by varying the restarting position for the subsequent deployment sequence.

Important design features of this fixture include the following:

(1) The air sled and air bearing track system. The lightweight air sled includes three air bearings of the configuration shown in Fig. 5. The bearings operate at about 35 psi, using shop air supply. The precision surface track is made of cast aluminum blocks, plastic faced and machined. The track levelness is critical to the operation of the fixture. A slope of 0.003 in. in 10 in. would produce a downhill coasting effect on the deploying subpanels equivalent to 1/10 the total moment available for deployment in space. Optical measurements of the track surface at the time of testing showed no average slopes this great.

(2) The overhead suspension system. The simulated spacecraft is mounted to the fixture, as shown schematically in Fig. 4, so as to allow limited free vertical translation and free rotation about two axes. It is locked against rotation in the direction of deployment. The deployed subpanels are supported by low-spring-rate, lightweight suspension lines. This suspension system is essential to compensate for vertical and torsional fluctuations of the panel assembly as it deploys. Otherwise, the inherent small hinge misalignments in any structure of this size could cause binding and hinge frictions far in excess of any that might occur in space. Steel suspension lines, as shown in Fig. 5,

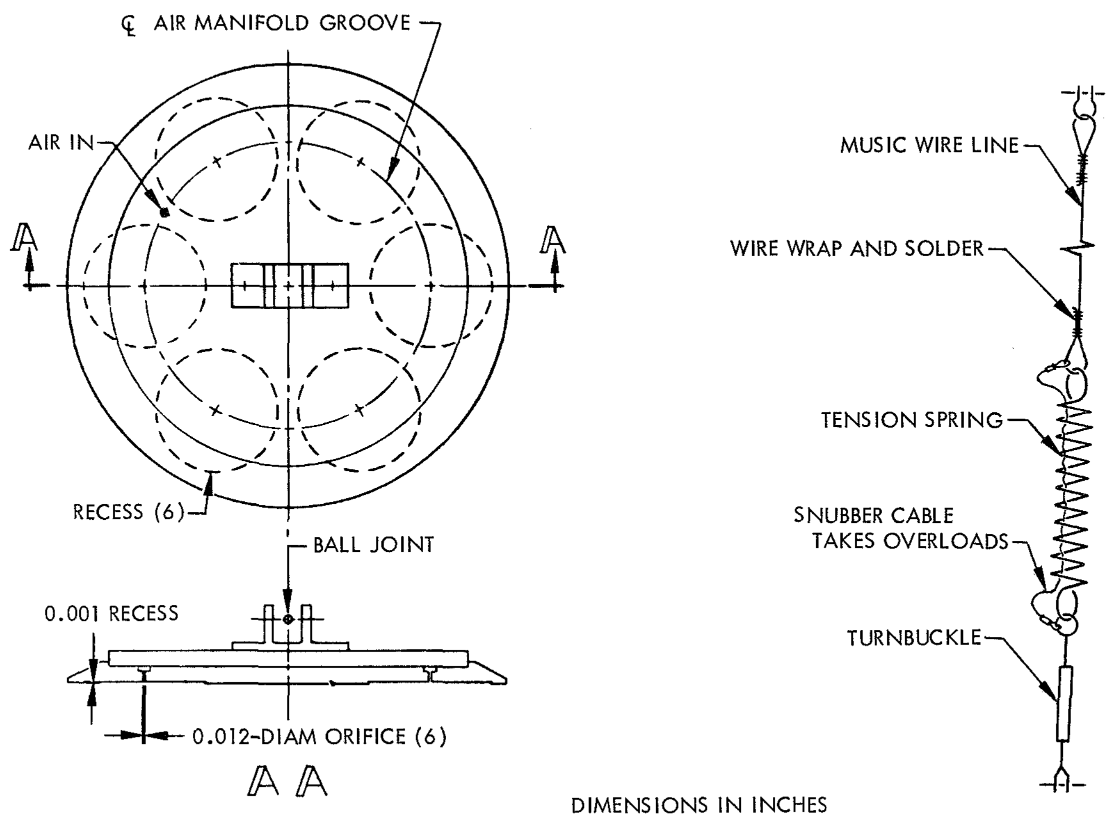

(a) AIR BEARING ASSEMBLY (b) SUSPENSION LINE ASSEMBLY

Fig. 5. Components of the testing fixture

were found to be superior to any lines using organic materials, which were prone to creep in service. These suspension lines were also used to support individual subpanels during assembly, the soft spring rates allowing careful positioning.

(3) The overhead air bearings. These bearings travel on short tracks and allow natural oscillations of the deployed subpanels. Any overhead carriages such as these must be very light. Because the carriages are not rigidly attached to the deploying subpanels (as is the air sled), the inertia as the bearings overrun the subpanels could otherwise obscure dynamic behavior.

(4) Instrumentation. Angular displacement of each deploying set of subpanels was measured by small, infinite-resolution potentiometers mounted at each hinge line. The output of these potentiometers was recorded on magnetic tape for subsequent computer usage and on an X-Y plotter for quick-look viewing. Instrumentation was also provided for deployment cable tensions and cable windup rate.

An unexpected benefit of this instrumentation and the passive, low-friction deployment system was experienced when recorded time history data indicated minor frictions due to mechanical irregularities in the panel assembly not detectable by visual examination.

V. Conclusions

The following conclusions are believed to be applicable to a variety of large, lightweight, low-powered, space-deployable structures:

(1) A passive deployment test concept provides a superior verification of ability to deploy in space. If a device will deploy itself, dragging the ground equipment along, then it will deploy in space when not so hindered.

(2) To verify deployment rates and determine stopping loads, the moments and frictions resulting from

gravity must be reduced to a minimum. Air bearings and precision surface tracks provide a feasible and not excessively costly means.

(3) In a deployable structure involving nonparallel hinge lines, deployment testing must be performed at a subassembly level that will allow hinge lines to be vertical. This is essential in any low-powered structure to obtain meaningful test data.

(4) Ground deployment equipment of the type described herein can provide an accurate simulation of time history and transient behavior for a variety of large, lightweight, space-deployable structures. The key elements of this type of equipment are the lightweight air-bearing carriages, rigidly attached to the deploying members where the deployment geometry allows, and the precisely leveled track on which the carriages travel.

Page intentionally left blank

70N21438

The Design of Aerospace Mechanisms—A Customer's Opinion*

Major James C. McSherry

Detachment 6, Office of Aerospace Research
United States Air Force
El Segundo, California

The overall design of an aerospace system is—and ought to be—highly influenced by the customer. But far too often the design of details is equally influenced by personal bias of the program manager. The biases seem to take the form of two attitudes: (1) anybody can build a mechanism, or (2) nobody can build a mechanism. It is the responsibility of mechanism designers, through efforts such as this symposium, to combat such biases.

I. Introduction

On one of the first flights of the X-7A-3 ramjet test vehicles over the White Sands Missiles Range in New Mexico, an actuator rod failed in the elevator control system. The failure caused the vehicle to nose over, go unstable, and eventually crash.

A few days after the flight, a group of engineers came into our office to show us the proposed solution. The hydraulic actuator and rod were to be replaced with an electric motor, worm gear, and rack and pinion system. This would be much stronger and give better response, etc., but would cost several dollars and delay testing about a month on a crash basis.

*The opinions expressed in this paper are those of Major McSherry himself, and do not in any way reflect the opinion of the Department of Defense, the United States Air Force, or the Office of Aerospace Research.

Since I was still quite naive in 1958, I asked them why they did not just put in a stronger actuator rod at comparably no cost, and no delay, especially since the current design had worked on two other flights, and this failure had nothing to do with the hydraulics at all, just the rod. After some uneasy squirming and a few nervous coughs the spokesman for the group said, "Well, that *was* our original proposal, but frankly, we didn't think the Air Force would buy it."

This was the first time I realized just how much the individual prejudices of the customer, be he the Project Officer, SPO, Program Manager, or whatever his title, influence the detail design of an aerospace vehicle. Some managers are often prone to arbitrary decisions based on their own bitter experiences. As a general rule, in satellites, bitter experiences with oddly behaving mechanisms are more bitter than bitter experiences with electronics.

A mechanism failure usually means mission failure: antennas that don't deploy, satellites that don't separate from their booster, etc. An electronic failure can be disastrous, but more often (and they are more often) they result in degradation, not negation, of the mission objectives. For example, two of the OV1[1] failures to achieve orbit were mechanical.

II. The Two Cases

Those managers whose programs have escaped disastrous failures of mechanisms, however, seem to feel that mechanisms are no problem since they always work. Therefore, there appear to be two basic attitudes towards mechanisms: apathetic indifference or complete distrust.

While pyrotechnics, propulsion, and electronics have often enjoyed (or suffered) top-level management attention, the lowly mechanisms have been brushed aside with the premise that since *anyone* can design a mechanism that works perfectly, there is no need to expend wasteful manhours in testing or improving these mechanisms. Following the catastrophic failure that nearly always results from such philosophy, the same high-level managers then assume that *no one* can design a working mechanism, and proceed to see how it can be replaced by a solid-state subminiaturized electronic component costing ten times as much, with many hours of testing, redesign, and qualification.

The foregoing hypothetical situation illustrates what I will call Case I and Case II thinking; that is,

Case I: Anybody can build a mechanism.

Case II: Nobody can build a mechanism.

Case I thinking is most evident in low-budget programs, where, because of the proverbial champagne tastes and beer pocketbooks, the first thing to be scratched is extensive testing of the mechanisms. This can be seen in such actions as modification of existing designs, such as stretched heat shields or adaptation of mechanisms.

Case II thinking is usually seen in high-budget programs, and as a result I don't have too much experience in this area. The examples with which I am familiar lie in the area of electronic vs electromechanical components. The trend is obviously away from anything mechanical. The solid-state commutator in telemetry systems has replaced mechanical commutators. Mechanical timers for programmers are a thing of the past. Solid-state memory circuits with literally thousands of electronic parts are replacing tape recorders for satellite data systems, and relays will someday be replaced by solid-state electronic devices. The dream of every electronic engineer is to point with pride to his satellite and proclaim "It has no moving parts." Those people who suffer from Case II thinking generally believe that "mechanical and simple" is crude, while "electronic and complex" is sophisticated. The result of this philosophy is higher cost to the customer and not necessarily higher reliability. The tape recorder in OV1-13 has now been operating for 11 months with no anomalies, and the tape recorder on OV1-15 operated until reentry.

Following are some examples of mechanism failures that may have resulted from Case I thinking.

III. SESP 68-1

In order to lower the high cost of putting satellites into orbit, one recent trend has been the increased complexities of launch vehicles as more and more satellites are launched from a single booster. This trend gives rise to complex truss, separation mechanisms, and heat shield designs.

One example of this concept was the SESP[2] 68-1 launch of an *Atlas* (SLV-3) with a *Burner II* upper stage using a *Thor/Burner* heat shield that had been stretched some 266 in. longer than its original length of 134 in. A total of 10 satellites were launched on this booster, all of which were lost because the heat shield did not separate.

IV. OV1-7

The OV1 satellite was mounted on the nose of an *Atlas* inside a "double coffin" style of heat shield. One experiment was too big to fit inside the satellite and so a small bulge was added to the heat shield. The bulge changed the aerothermal loading enough to cause the

[1]*Orbiting Vehicle*, Type 1, one of a series of basic research satellites managed by the Air Force Office of Aerospace Research. Each satellite carries a different complement of scientific experiments. OV1-17 is the seventeenth satellite in the OV1 series; OV5-4 is the fourth satellite in the OV5 series, etc.

[2]Space Experiments Support Program, managed by the Air Force Space and Missile Systems Organization.

door to temporarily hang up before opening. The delay was just enough to allow the satellite to collide with the door during the ejection sequence. Needless to say, this impact caused a rapid misorientation of the vehicle and, even though the propulsion module guidance tried to correct, the initial offset was too much. Rather than going into orbit, the satellite impacted in the Indian Ocean.

V. OV1-86

This OV1 was a basic research satellite which should have been gravity-gradient-stabilized. However, volumetric constraints dictated that the gravity-gradient system had to be mounted inside the satellite and then "unfolded" in orbit. The resulting mechanism was quite complex and failed to erect properly in space. This caused the loss of a great deal of data.

The major cause for these failures was the management decision that created the constraint. Since then, the OV1s have been mounted within an 84-in.-diameter heat shield that allows such protuberances to be mounted in the erect position. This eliminates the problem at its source.

VI. OV2-5

This satellite had many mechanisms on board to erect or deploy solar panels and experiments. The deployment sequence was very unsuccessful. Of the 12 antenna paddles and/or experiments to be unfolded or extended, only five performed without some sort of an anomaly.

The foregoing examples of what can go wrong with mechanisms are primarily examples of lack of sufficient testing in the final flight configuration, usually caused by limited funds. The program manager must decide where to limit funds, and often the mechanisms testing is the first area to be limited. Although this is a compliment to mechanism designers, the trend of more failures can cause your customers to adopt Case II philosophy and turn to the belief that anything mechanical is unreliable.

To combat this belief, it is imperative that the design engineer demand, and fight for, his share of the testing time and the development dollars. One good way to do this is to emphasize the consequences of a mechanism failure such as the examples presented here.

VII. Electrical Connectors

And while I have your attention, I would like to voice a complaint about my own pet peeve: electrical connectors that can be reversed. Mechanism designers can be of great service in preventing such failures as the following examples of Murphy's law.

During the final prelaunch test of an X-7A test vehicle the 400-cycle inverter was found to be defective. The test was halted and the faulty inverter was repaired and reinstalled. When the test was resumed, a technician noticed that the pens on his strip recorder moved the wrong way, so he quickly reversed the polarity switch. The test was finished successfully even though every gyro in the missile was running backwards.

The malfunction went undetected through launch, and *everyone* who saw the reversed polarity automatically assumed the mistake was in the test gear.

The vehicle was launched from the bomb bay of B-50 airplane, and the first disturbance came in roll a few milliseconds after release. The backward-running roll gyro sensed the error and caused the control system to move the aileron in the wrong direction, first a little bit, and then to full deflection in the wrong direction. The booster rockets ignited and the vehicle, spinning at a very high rate, proceeded directly earthward and screwed itself into the New Mexico desert, traveling about Mach 2.5 on impact. The tail of the 28-ft-long vehicle was found after digging down a little more than 10 ft.

The point here is simple. Proper design of the power connector to the inverter would have made it impossible to reverse the leads. It was a small, simple part, on which just a little bit more thought would have prevented a catastrophic failure of a million-dollar vehicle. Perhaps even more important is the fact that at least 15 people had the opportunity to catch the mistake, but no one did. The obvious fix was incorporated. The same design problem, i.e., reversing two wires at a connector, has caused catastrophic failures on other programs, such as

(1) A converted *Matador* missile, which was used at Holloman Air Force Base as a target drone for such missiles as *Nike*, *Falcon*, *Hawk*, and *Sidewinder*. The left and right controls were reversed and the drone was launched in that configuration. The flight lasted about 2 seconds and the missile

crashed a few hundred yards in front of the launch pad.

(2) The famous incident at Cape Kennedy where the Range Safety Officer's plotting board was miswired between East and West. This caused the Range Safety Officer to think that a ballistic missile heading downrange was going inland towards Orlando; whereupon, he destructed a perfectly good missile.

(3) A Q-4B target drone on which the pitch gyro was miswired, not once, but on *three* separate flights! You would think they would have learned after one.

VIII. Conclusions

The mechanisms designer, therefore, is faced with a seemingly impossible job. He must convince Case II thinkers that "mechanical" is not a dirty word, while, on the other hand, he must convince Case I thinkers that mechanisms are not so simple and trivial that development testing is unnecessary.

A Despin Assembly for the TACOMSAT Communications Satellite

C. R. Meeks
Hughes Aircraft Company
Space Systems Division
El Segundo, California

A torque-motor-driven despin bearing assembly with an integral slip ring unit was designed and tested for the Hughes Experimental Tactical Communications Satellite TACOMSAT. The dc torque motor and a magnetic shaft encoder were integrated into a position and rate feedback digital control loop. The slip ring, motor brushes, and bearings were lubricated by the Vac Kote process.

Five units were tested for performance, structural integrity, and thermal effects. One unit was life-tested in a simulated space vacuum at accelerated shaft speeds up to 175 rpm for the equivalent of 14,000 h operation at the design speed of 55 rpm. Slip ring electrical insulation breakdown due to brush wear debris buildup caused interruption of the life test; the slip ring was redesigned and life testing resumed.

I. Introduction

Spin-stabilized satellites, tracking antennas, solar panel pointing systems, and various other spacecraft subsystems require long life in drive motors and in rotating slip rings to transfer electrical power and signals. Designing for years of continuous operation requires special attention to very light preloading and alignment of ball bearings, careful control of motor and slip ring electrical power loading, and optimum selection of the materials and lubrication combinations.

The *Experimental Tactical Communications Satellite* TACOMSAT antenna system is mechanically despun from the spin-stabilized spacecraft body, through a torque-motor-driven despin bearing assembly with an integral slip ring unit. The 600-lb despun antenna and control system are supported by the despin bearing assembly, which weighs 54 lb. Two power busses in the slip ring and multiple signal channels for communications and telemetry data provide an electrical link between the antenna and the spacecraft system. Figure 1 depicts the spacecraft arrangement. Earth sensors and sun sensors on the spinning section are used for spacecraft position sensing and attitude control.

The spacecraft is designed for a multiyear life with continuous rotation of the despin bearing assembly at

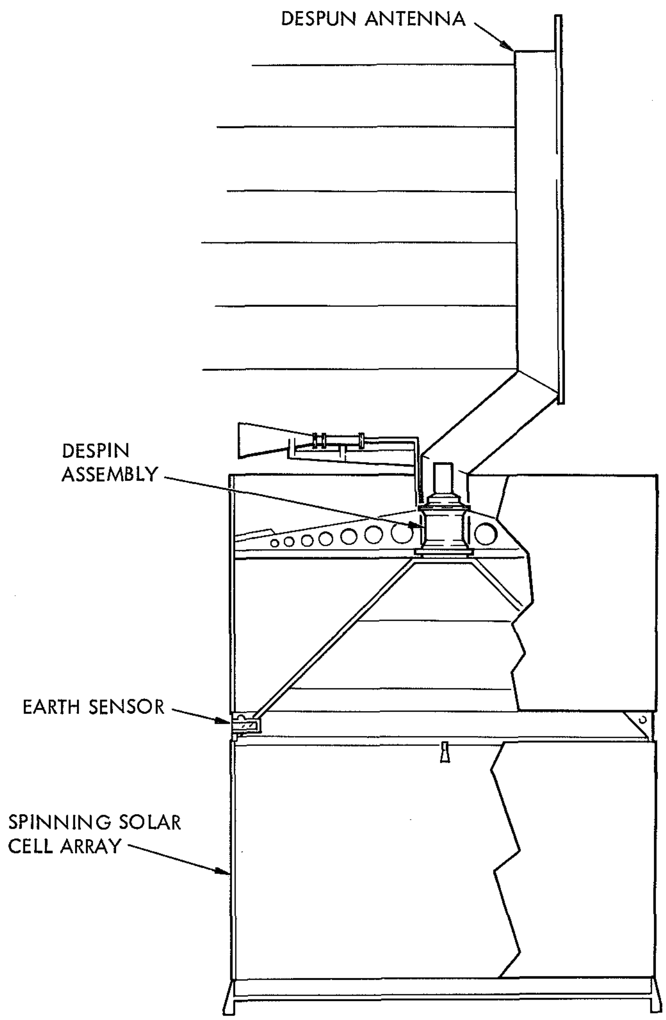

Fig. 1. TACOMSAT communications satellite configuration

55 rpm. The despin assembly was designed to achieve maximum structural stiffness of the total spacecraft and minimum antenna pointing error from bearing runout. All electrical power and signal transfer systems were designed for maximum reliability, and multiple redundancy of components was provided. The despin assembly is located in the center of the spacecraft with thermal control blankets and thermal emissivity control surfaces to keep the maximum temperature excursion in the bearings to 20 to 80°F.

II. Despin Motor Drive Assembly

The despin assembly consists of four basic elements:

(1) A structural shaft and housing joined by a pair of preloaded ball bearings.

(2) A brush-type dc torque motor.

(3) An electromagnetic pulse generator.

(4) A power and signal transfer slip ring assembly.

A cross-section view of the despin assembly is shown in Fig. 2.

A. Structural Unit

The concentric shaft and housing unit is constructed of hot-pressed, sintered beryllium block, machined and etched for maximum structural integrity. The loaded sections are stressed conservatively at 20,000 psi to avoid notch sensitivity problems due to the low ductility of beryllium. The deep-groove, Class 7, Conrad-type, 150-mm-bore ball bearings of 52100 bearing steel are press-fitted into the housing and the inside races are a slip fit on the shaft. A load ring with 12 helical compression springs provides a 40- to 60-lb preload to the bearing inner races to prevent ball skid. Oil-impregnated cotton phenolic ball retainers and porous oil reservoirs of Nylasint[1] provide the lubrication supply for long-term operation. A 0.10-in. radial gap between the shaft and the housing provides low-vacuum conductance and ensures low oil loss to the space vacuum environment.

B. Torque Motor

The despin motor is an epoxy-encapsulated, four-brush, 71-bar copper commutator of the frameless type. The permanent magnet ring and graphite/silver brush assembly rotate with the despin shaft. This arrangement permits the direct transfer of the generated power of the rotating solar cell array to the motor brushes. The despun motor winding assembly is mounted to the despun housing cover assembly. Low-vapor-pressure epoxies and fiber glass are utilized in the motor to minimize outgassing contamination of the lubrication system.

C. Pulse Generator Encoder

The pulse generator is a simple bifilar-wound E-frame coil mounted to the rotating shaft. An Alnico permanent magnet bar on the housing assembly induces a voltage in the coil with each passage. The induced voltage output is approximately a full cycle sine wave, and detection of the zero potential crossing eliminates position detection errors due to variations in magnet pass velocity.

[1]The Polymer Corporation, Reading, Pa.

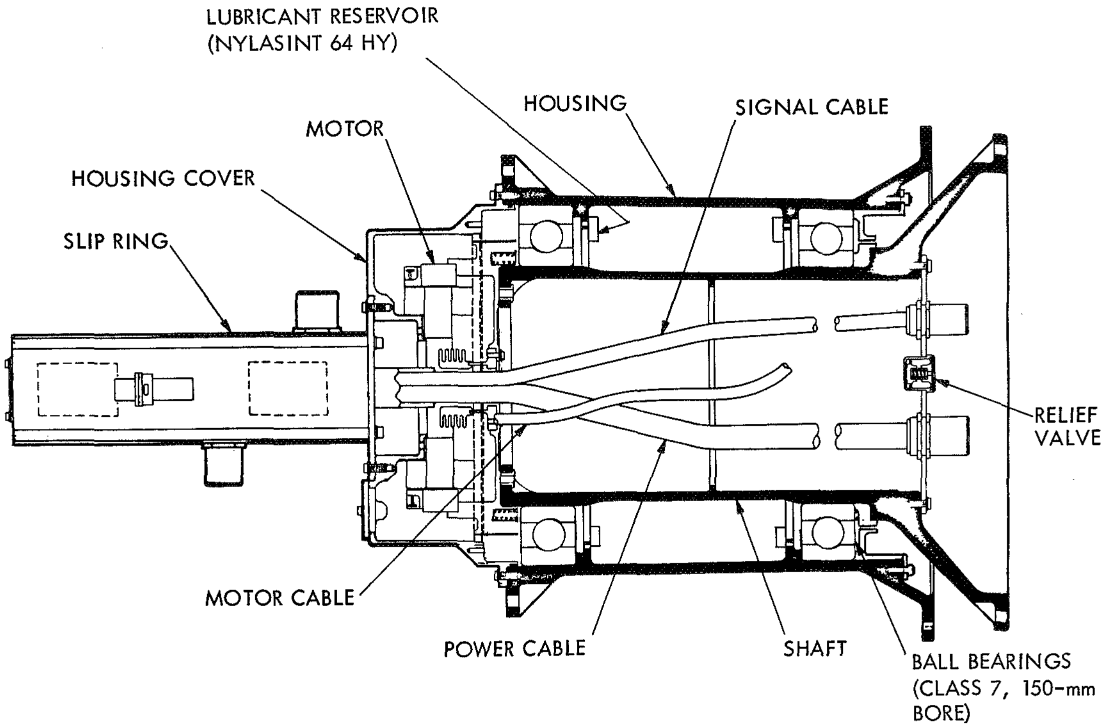

Fig. 2. Despin bearing assembly

D. Slip Ring Assembly

The slip ring assembly, shown in Fig. 3, is a separate assembly with integral shaft bearings. The housing is mounted to the despin assembly cover housing, and a bellows-type flexible coupling links the slip ring shaft to the despin assembly shaft to minimize interaction loads. The shaft has 90-10 coin silver rings with NEMA[2] Grade G-10 fiber glass epoxy insulation between rings. The shaft is epoxy-encapsulated for structural integrity and maximum heat transfer. The brushes are a composite of silver, graphite, and molybdenum disulfide and are supported by cantilevered beryllium copper springs. All housing parts are made of aluminum alloy for minimum weight. Redundancy is provided in the signal circuits by two brushes on each signal ring and in the primary and secondary power circuits by multiple brush pairs for incoming and return circuits. The slip ring, motor brushes, and bearings were lubricated by the Vac Kote process.[3]

[2]National Electrical Manufacturers Association.

[3]Ball Brothers Research Corporation, Boulder, Colo. See "Lubrication of DC Motors, Slip Rings, Bearings, and Gears for Long-Life Space Applications," by B. J. Perrin and R. W. Mayer, *Proceedings of the 3rd Aerospace Mechanisms Symposium.* Technical Memorandum 33-382, Jet Propulsion Laboratory, Pasadena, Calif., Oct. 1, 1968, pp. 65–74.

III. Test Results

Five despin assembly units were tested for structural integrity under vibration up to 19 g^2/Hz random, shock, and thermal cycling from -20 to $+110$°F. One unit was life-tested in a dry ion-pumped ultrahigh vacuum (5×10^{-8} torr) under continuous rotation at speeds from 55 to 175 rpm for 5943 h. The slip ring power and signal circuits were operated at design levels of 36 A and 100 mA respectively through the life test. The life test program included:

504 h at 55 rpm

2906 h at 110 rpm

2533 h at 175 rpm

The actual performance is compared with design requirements in Table 1.

At the end of the life test, the despin shaft bearing wear tracks were virtually undetectable. The torque motor brush average wear was $\approx$0.002 in., and the wear of the motor commutator was less than 0.0001 in. All performance was within specification limits throughout the vacuum life test, except for the slip ring assembly, which developed electrical insulation breakdown due to

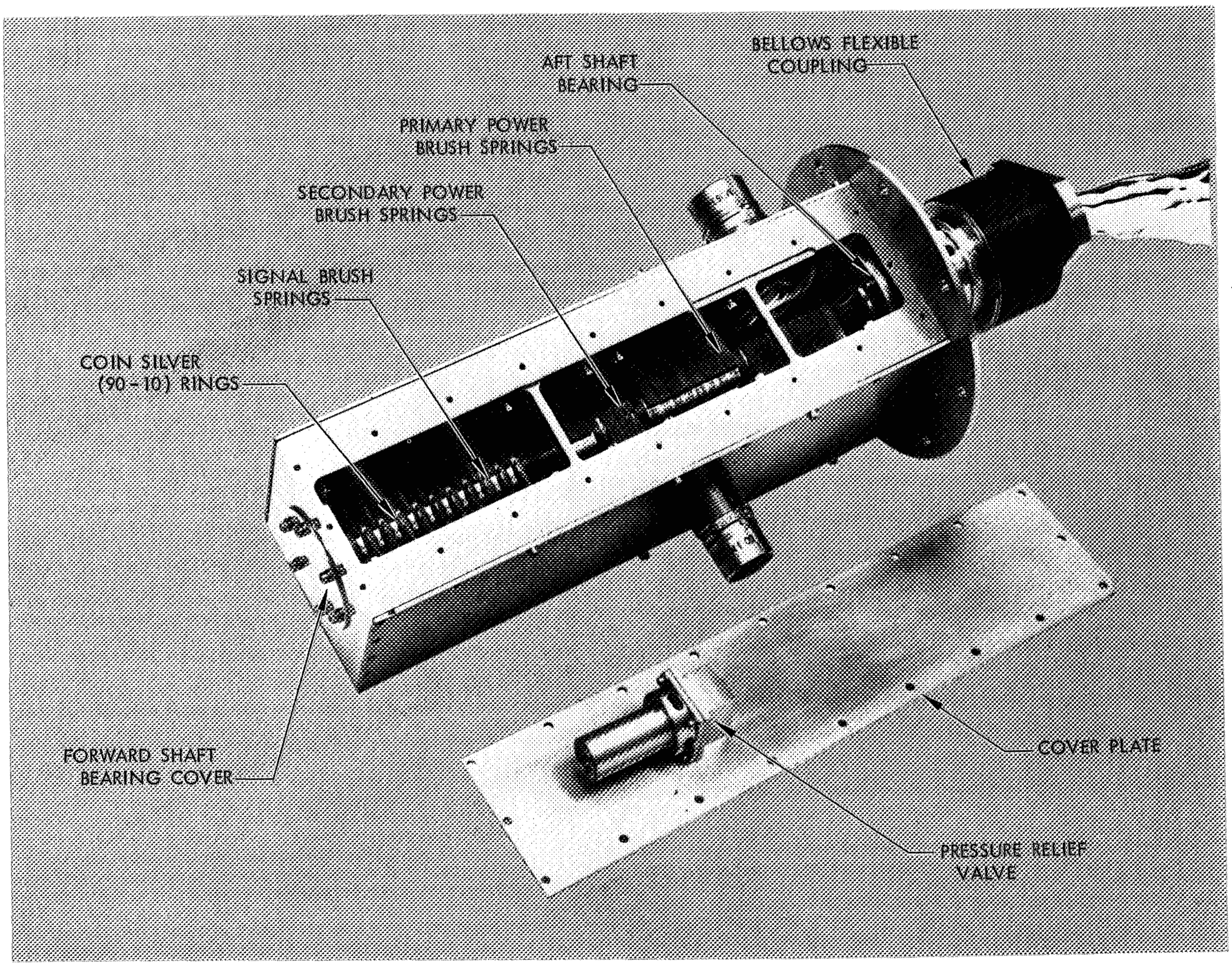

Fig. 3. Oil-lubricated brush/slip ring assembly

Table 1. Despin assembly performance results

Design parameter	Design requirement	Test result
Dynamic friction torque	<0.55 ft-lb	0.25 ft-lb
Power slip ring voltage drop	<200 mV	140–160 mV
Signal slip ring noise	<50 mV peak-to-peak	10 mV peak-to-peak

Table 2. Slip ring/brush wear summary

Brush type	Average brush wear, 10^{-3} in.	Average ring wear, 10^{-3} in.	Average brush wear rate, 10^{-14} in.^{3}/in. ring travel	Brush force, g
Primary power	5.1	3.5	124	127
Secondary power	1.1	0.5	5.3	23
Signal	3.3	0.5	15.9	23

brush and ring wear debris buildup after approximately 5900 h of operation. Figure 4 shows the condition of the slip ring when it was examined at the end of the life test. The wear of each brush and slip ring was measured, and the results are summarized in Table 2.

The higher wear rates of the primary power rings and brushes were due partially to the high force setting used to give a constant "apparent" pressure of 7.8 psi on all brushes.

The oil content of each primary power brush was determined by weighing before and after solvent washing and vacuum bakeout. The results are plotted in Fig. 5 and compared with the respective total brush and ring wear. A very clear correlation is apparent between high wear and low brush oil content at the end of life testing.

Analysis of the wear debris revealed that it consisted of fine particles (mostly 0.0005 in. and smaller) of silver, graphite, and molybdenum disulfide from the brushes and silver slivers approximately 0.0005 in. wide with lengths up to 0.75 in., which came from the rings. The silver slivers were the prime cause of electrical insulation breakdown and shorting.

IV. Slip Ring Redesign

From the failure analysis, a plan was developed to redesign and retest the slip ring assembly. The redesign had to be implemented and adequately tested within a 3-month period to maintain the spacecraft program schedule. For this reason, the redesign had to make maximum use of existing slip ring component parts and would have to be adequately retested to achieve confidence in the design within the available time.

Two redesigns were created: one maintained the same brush/ring materials and oil lubrication, and a second employed a dry-lubricated brush material. The designs were created with three basic objectives:

(1) To provide adequate electrical insulation throughout the interior to tolerate large amounts of wear debris, including silver slivers, without failure.

(2) To reduce the total wear debris, particularly in the primary power section where over 90% of the wear debris originated.

(3) To minimize the primary power *ring* wear to reduce the quantity of dangerously long silver slivers.

The redesigns (see Fig. 6) employed the original type of coin silver shaft and the original brush/spring mounting configuration. Silver/graphite/molybdenum disulfide brushes with a much higher MoS_2 content (12% MoS_2) than the original oil-lubricated design were used in the dry-lubricated design. The primary brush force was optimized empirically to 40 g in the oil-lubricated unit and to 60 grams in the dry-lubricated unit to minimize wear and to avoid high electrical noise at the predicted end of life force level.

All interior surfaces, such as brush springs, solder joints, screws, lockwire, housing, etc., were coated with electrically insulating epoxy and polymer films 0.001 to 0.003 in. thick. Insulated debris barriers were installed between the input and return rings of the power sections and between the power and signal sections. Insulating disks of 0.020-in.-thick fiber glass epoxy were placed between each signal ring and the next to increase the insulation path length.

Oil lubrication was maintained in the ball bearings of the slip ring shaft, and close-fitting, low-conductance, vacuum-type seals and low-surface-energy Teflon barrier coatings were used to avoid oil contamination of the dry-lubricated slip ring brushes.

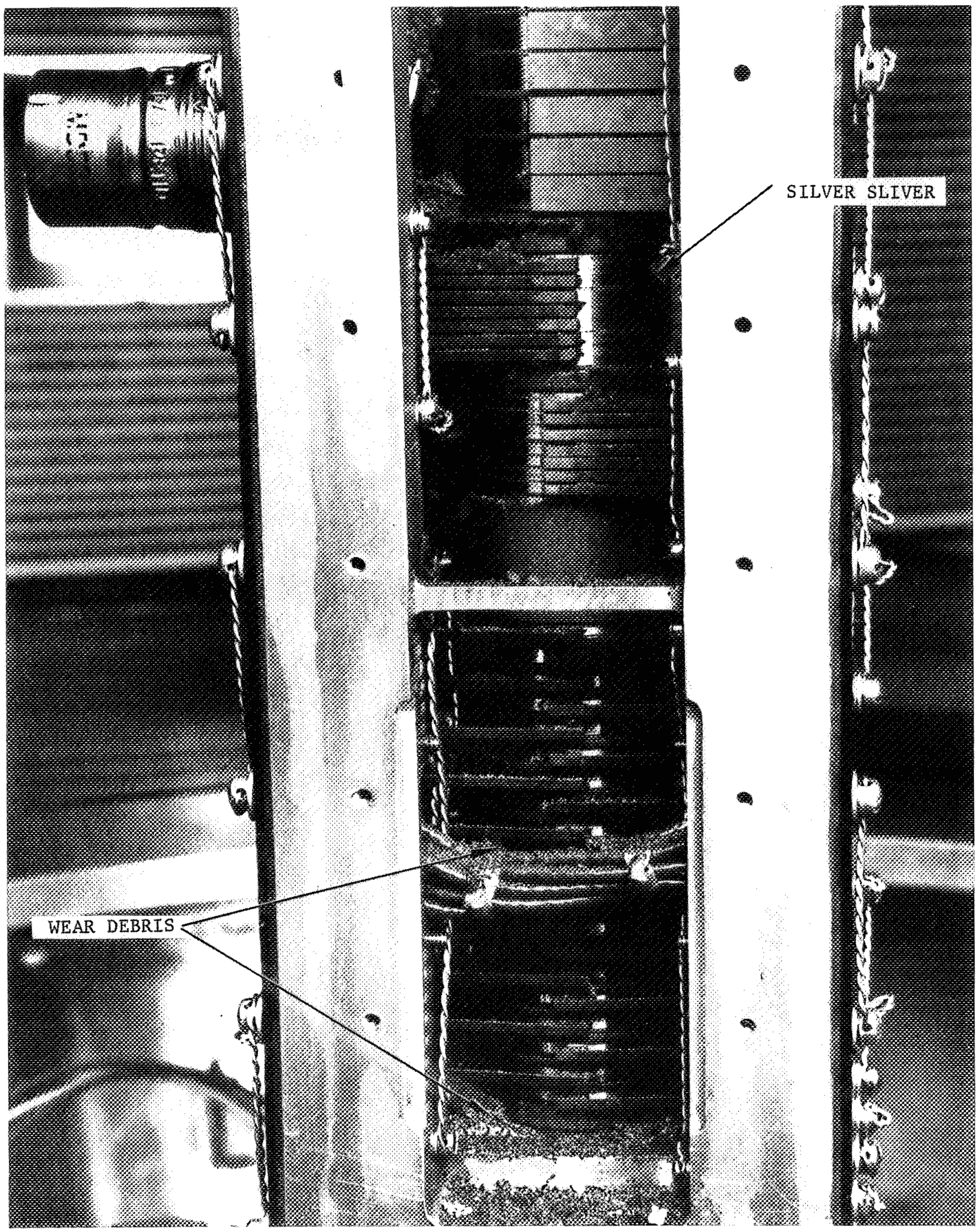

Fig. 4. Oil-lubricated slip ring assembly after 6000-h life test

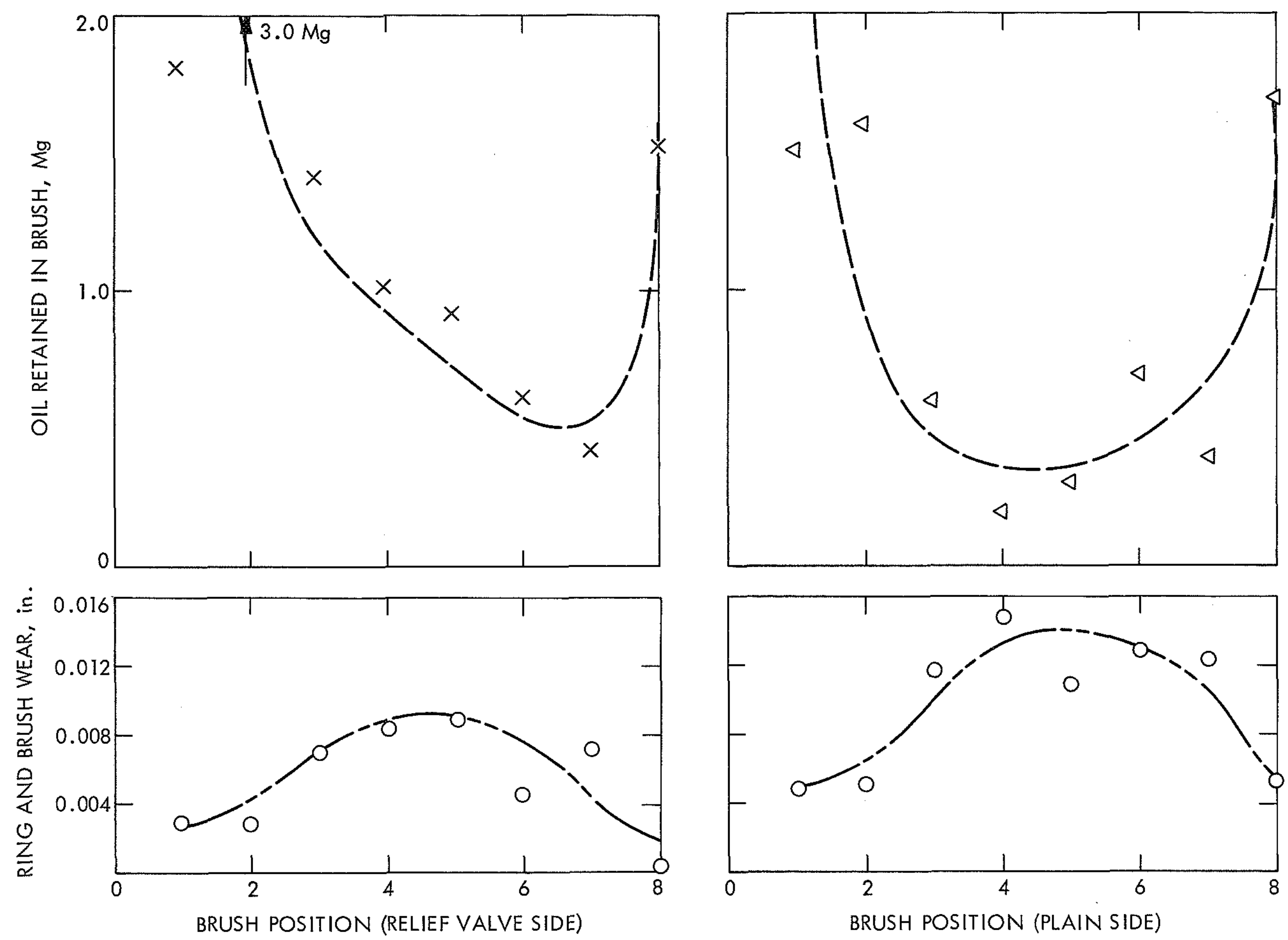

Fig. 5. Comparison of slip ring and brush wear and oil remaining in brushes after 6000-h life test. Brush positions are numbered from the aft end of the assembly

Highly accelerated testing of liquid-lubricated slip ring assemblies is limited by the buildup of a hydrodynamic film between the brushes and the slip ring. This effect degrades electrical performance because of the large dielectric gap that the current must cross, reduces the wear rates below the normal design speed wear rate because of the change from boundary to hydrodynamic film lubrication, and might cause unknown chemical or catalytic damage of the lubricating oil. Because of these testing limitations, the oil-lubricated design was retested only at 55 rpm. The dry-lubricated unit was tested at speeds up to 1000 rpm. The life test summary to date is:

Oil-lubricated unit	*Dry-lubricated unit*
1500 h at 55 rpm	1272 h at 55 rpm
	144 h at 500 rpm
	169 h at 1000 rpm

The total of shaft revolutions of the dry-lubricated design is equivalent to 5644 h of 55-rpm operation.

The primary power brush wear rates of both the oil-lubricated and dry-lubricated designs were less than 40×10^{-14} in.^{3}/in. of ring travel, which significantly reduced the total wear debris generated. The dry-lubricated unit slip ring wear was less than 0.0002 in. The oil-lubricated slip ring wear has not been measured. Extrapolation of the measured wear rates yields a prediction of multiple years of life in either of the redesigned slip ring assemblies. The measured electrical performance was within design limits, and no wear debris shorting was observed.

The choice of which slip ring to fly on the spacecraft had to be made on the basis of the available test times as listed above. Because of the greater *equivalent* test

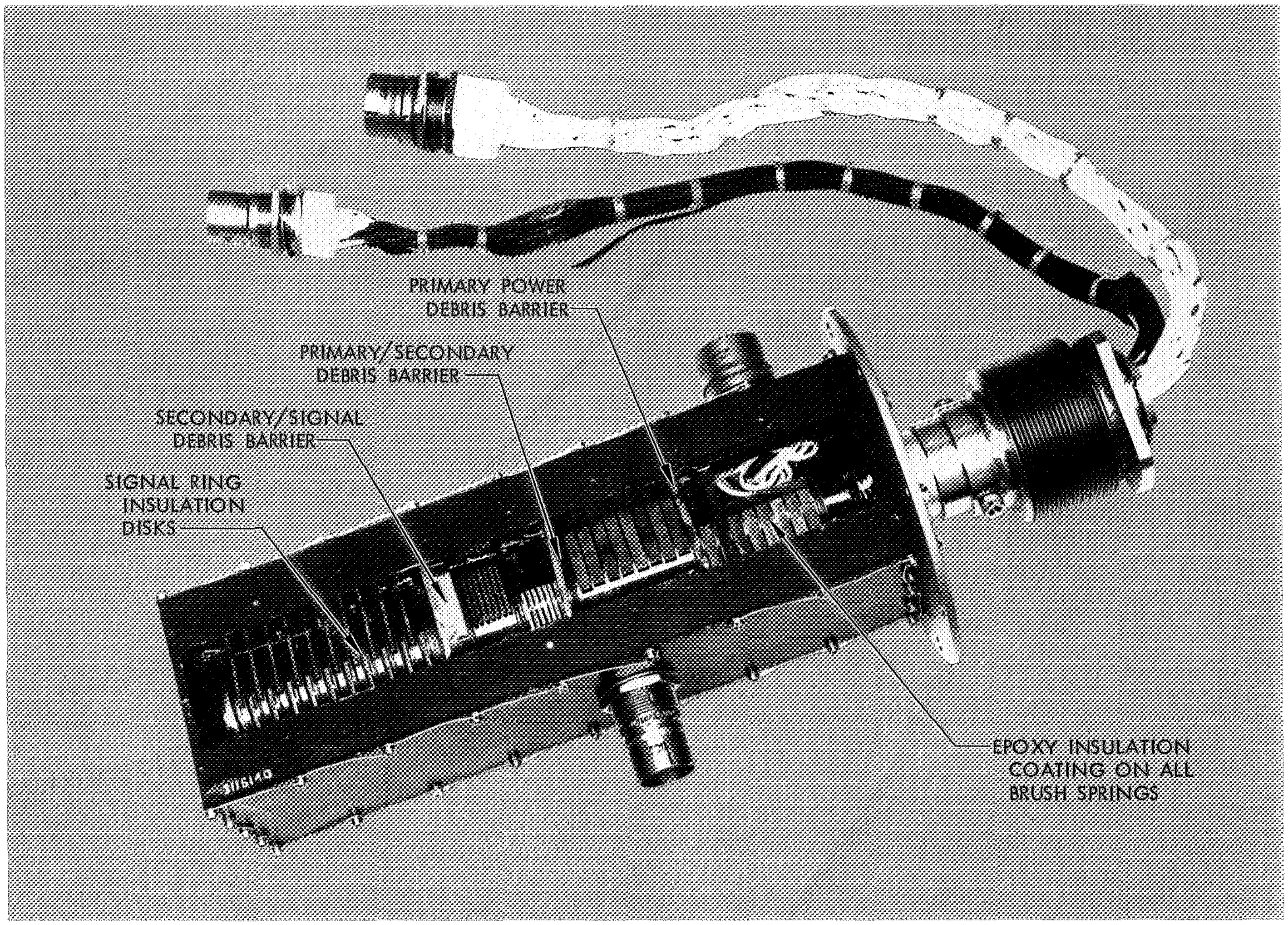

Fig. 6. Redesigned slip ring assembly

time on the dry-lubricated unit on the final decision date, that unit was used on the spacecraft. Life testing of both units has continued since the launch.

V. Conclusions

The TACOMSAT communications satellite despin motor and slip ring assembly design has demonstrated the capability to survive launch vibration up to 19 g^2/Hz, shock loading of 10 g, and temperatures from -20 to $+110°F$, and sustained operation in hard vacuum for 6,000 h and shaft revolutions equivalent to 14,000 h. Extrapolation of the wear and lubrication performance in the despin bearings and torque motor and slip ring brushes indicates the feasibility of multi-year continuous operation.

The slip ring life test results and redesign efforts established the following:

(1) For long-life slip ring applications using composite brush materials, special attention should be given to controlling the wear debris generated.

(2) All surfaces that can collect debris should be protected by electrical insulation.

70N21440

The *Mariner Mars 1969* Scan Actuator*

Gerald S. Perkins
Jet Propulsion Laboratory
Pasadena, California

The actuator that will drive the scan platform on the Mariner Mars 1969 spacecraft is described. The scan platform is a two-axis device for carrying and pointing the science packages on the spacecraft. Motion for each of the two axes (clock and cone) is provided by an identical and interchangeable actuator. The scan actuator is a geared servomechanism, and particular emphasis is given in the paper to the gear arrangement and the dynamic characteristic of the gear train. Design experience is described, and test results are presented.

I. Introduction

The *Mariner Mars 1969* scan platform is a two-axis device similar to an elevation azimuth mount. The axes are clock and cone; the clock axis is through the center of the spacecraft, and the cone axis supporting the platform is carried by the clock axis and is perpendicular to the clock. The function of the scan platform is to carry the science instruments for the *Mariner Mars 1969* mission.[1]

Two scan actuators are required, one for each axis. The functional requirements for the actuators for each axis are identical. Therefore, it was possible to design one actuator that could be used interchangeably on either the clock or cone axis.

The actuator was designed at the Jet Propulsion Laboratory in collaboration with J. W. Harrison of Honeywell Inc., Aerospace Division. Ten actuators were manufactured, and four of them are now enroute to Mars on the two *Mariner* spacecraft. In operating tests, the actuators performed within predicted limits.

The actuator was designed to meet the following performance requirements:

(1) Starting voltage. The actuator shall start and run smoothly with no more than 1.5 V rms applied to the motor.

(2) Slewing speed. The slewing speed under full voltage with no load shall be not less than 1.3 deg/s. The actuator is intended to drive the scan platform at a rate no slower than 1 deg/s.

*This paper presents the results of one phase of research carried out at the Jet Propulsion Laboratory, California Institute of Technology, under Contract No. NAS 7-100, sponsored by the National Aeronautics and Space Administration.

[1]*Mariner VI* was launched on Feb. 25, 1969, and is expected to reach Mars on July 31, 1969. *Mariner VII* was launched on Mar. 27, 1969, and is expected to reach Mars on Aug. 5, 1969. Both are flyby missions.

(3) Clutch slip torque. The overload protection clutch shall be adjusted to slip between the torque settings of 200 and 550 lb in., while either being driven by the motor or being backdriven mechanically.

(4) Backlash. The drive train backlash measured at the output shaft shall be less than ½ deg.

(5) Mechanical stiffness. The torsional compliance of the actuator should be between 20,000 and 30,000 lb ft/rad.

II. Description

The scan drive actuators provide the controlled rotary motion of the scan platform structures, which mount the science instruments. The actuator consists of a size 11, two-phase servo motor, reduction gearing including a worm gear stage to prevent back-driving, and a slip clutch to provide overload protection during ground handling and testing (see Fig. 1). Control signal is provided by an output position feedback potentiometer. Two additional potentiometers provide coarse and fine output shaft position angle telemetry data. These elements are contained within a sealed, pressurized enclosure of polished aluminum (see Figs. 2 and 3). The gas used for pressurization is a mixture of 90% nitrogen and 10% helium. The helium trace makes it possible to measure the actuator housing leak rate with a mass spectrometer leak detector. A resistance heater is mounted in the actuator to prevent damage due to low temperature during the cruise portion of the flight. A box mounting,

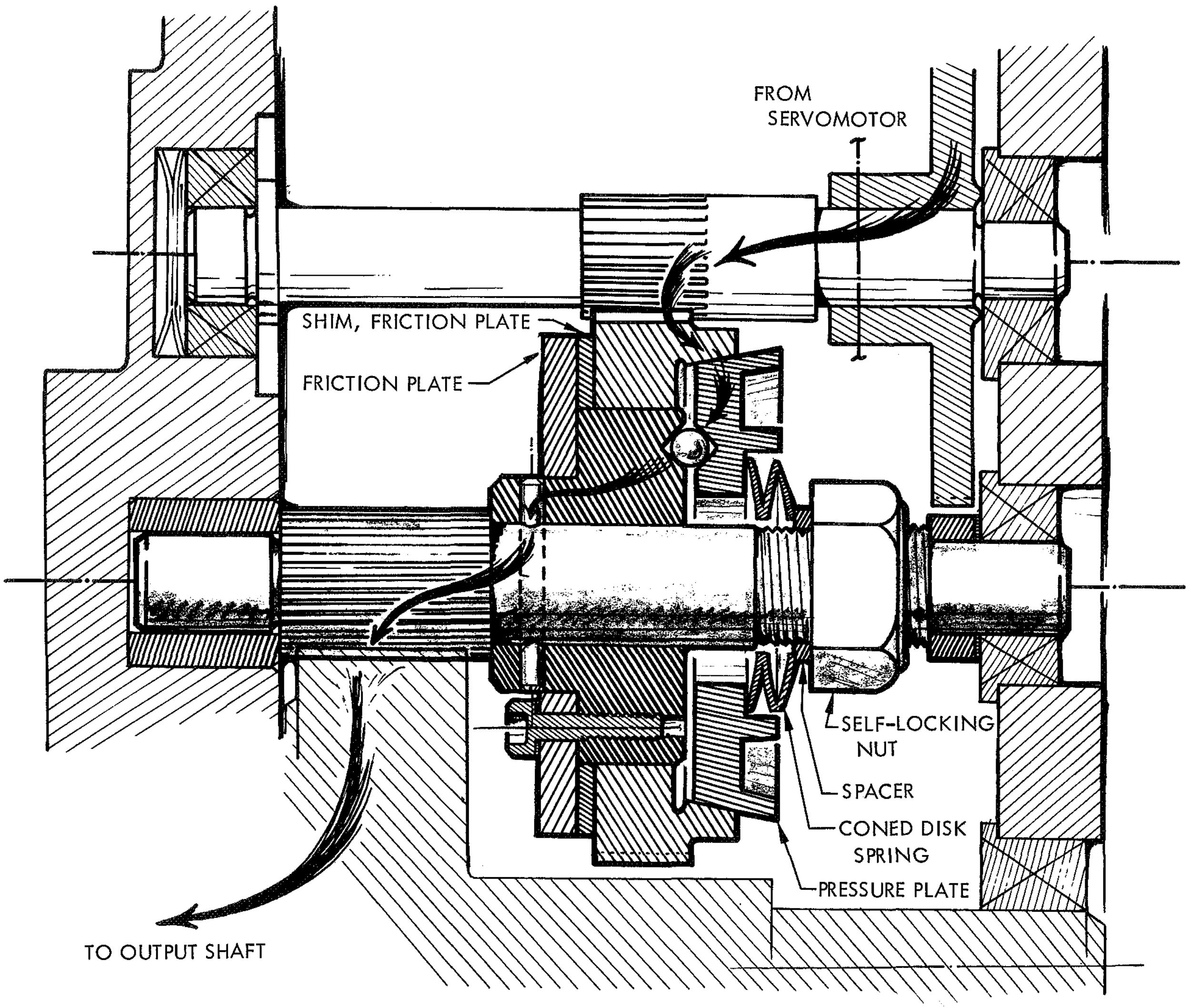

Fig. 1. Clutch assembly

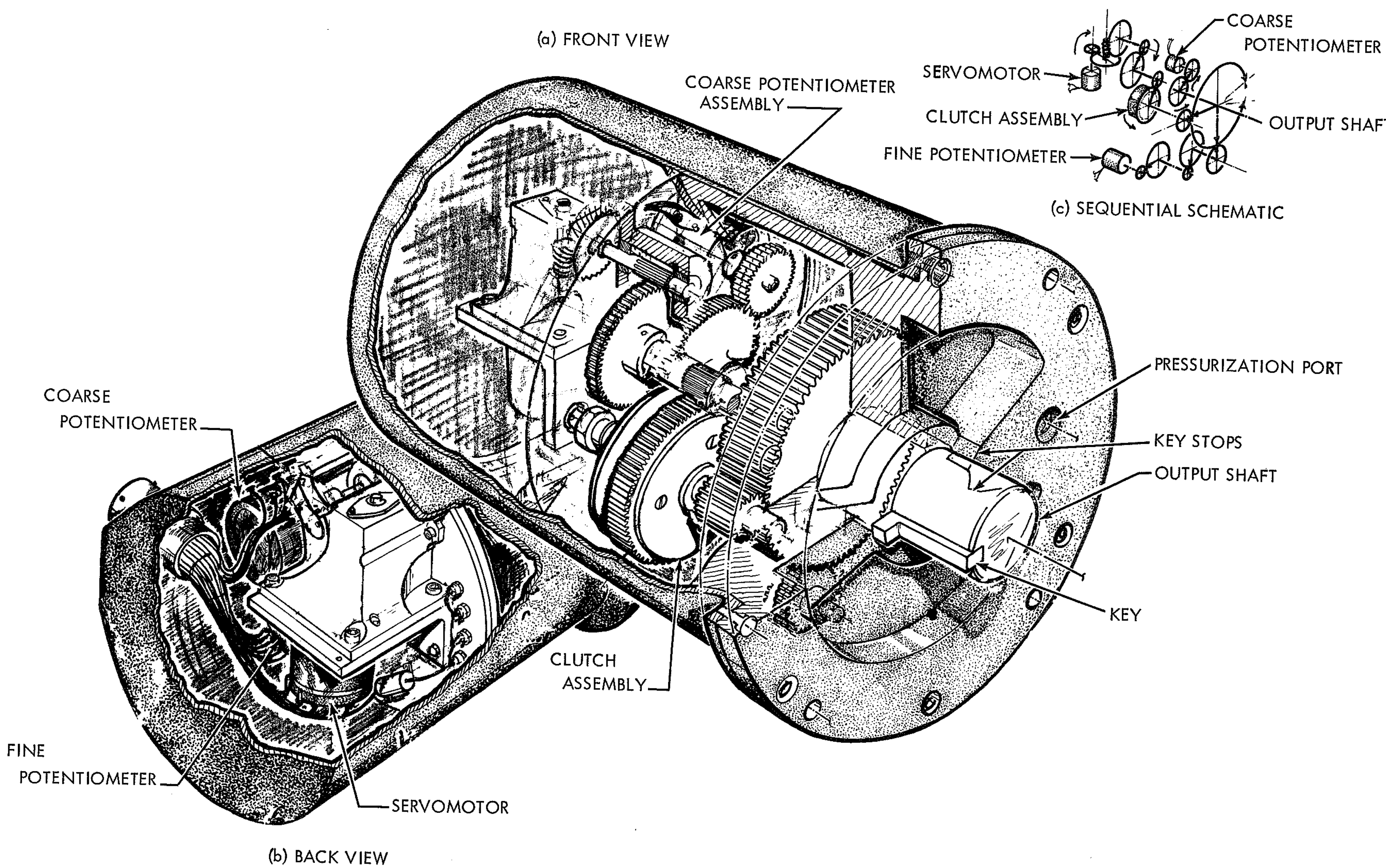

Fig. 2. Schematic drawing of scan actuator

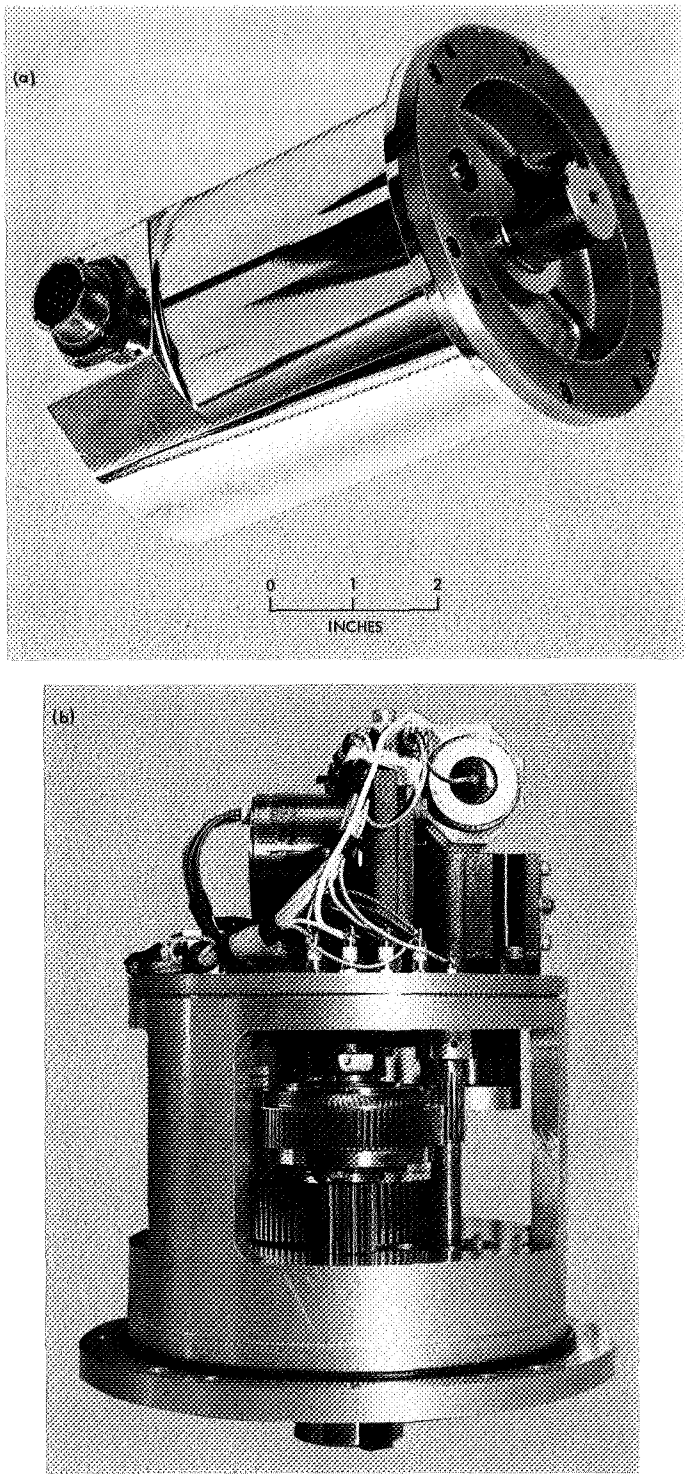

Fig. 3. Scan actuator: (a) complete, (b) cutaway showing gears

hermetically sealed electrical connector mounted on the side of the actuator enclosure provides for electrical inputs and outputs. The actuator's rotary motion is coupled to the scan platform through a crank arm that is keyed and clamped to the actuator output shaft. The arms engage forks in the platform shafts. The crank arm is not considered as a part of the actuator.

The actuators are fitted with mechanical stops that limit the output shaft rotation to approximately 300 deg. The function of the stop is to preserve the potentiometer phasing, which would be lost if the actuator made more than one full turn. This is true because of nonintegral gear ratios in the potentiometer drive gearing. The actuator weighs 3.91 lb and is 6 in. long and 4 in. in diameter.

III. The Gear Train

A. General Requirements

A gear train specifically designed for use in an instrument servomechanism such as the scan actuator is necessarily unique. The gear train must perform its purpose—the transfer and transformation of power from a servo motor to the output shaft—with a minimum of friction and inertia and with backlash held between defined limits. The upper limit of backlash is defined by the control system to ensure stable performance; the lower limit is established by clearances required to ensure smooth operation and avoid binding up.

Two important phases in the design of an optimum gear train for a servo actuator are as follows:

(1) The function of the gear train must be assured by selection and arrangement of the gears.

(2) The optimum gear ratio must be selected in order to fit the motor to the actuator and to provide the desired slewing speed.

Neglect of either phase would result in inferior system performance.

B. Selection of Gears

In the scan actuator, a precision gear train is desired. Spur gears are the easiest to make precise because they are the least sophisticated. The simple straight spur gear is the best for precision application, unless other requirements rule out its use. The spur gear mesh does not produce shaft axial thrust, and it is more efficient than helical, bevel, or worm gear meshes. Spur gears may be spring-loaded in order to virtually eliminate backlash. This technique is used in the scan actuator gear train for coupling the readout devices.

The scan actuator requires a self-locking, no-back-driving gear train. This self-locking feature is provided by a worm–helical gear stage in the gear train. The worm gear mesh used in the actuator gear train was provided by mating a high-precision worm to a standard helical gear rather than to a worm gear. The helical gear can be produced and inspected to a much higher quality than a worm gear. The use of a worm driving helical gear does result in a point contact. However, the worm–helical gear action remains conjugate even if the center distance changes.

The advantages discussed above are dependent on proper lubrication in order to prevent wear at the point of contact, with resultant loss of the involute profile. The worm–helical drive required in the gear train, in order to be self-locking, represents the use of low-quality gears in a precision gear train. In order to minimize this potential error effect, the worm–helical gear stage is put next to the motor, as far from the output shaft as it can reasonably be placed. The effect of its errors on the gear train output are thus reciprocally reduced.

For maximum precision in the spur gear train, 20-deg pressure angle gears have been selected. Minimum-pitch-size gears are used within the constraints required by load, in order to maximize the contact ratio. (Contact ratio may be described as the number of teeth simultaneously in contact in a pair of mating gears.) The advantage of the high contact ratio is that it produces greater tooth-to-tooth error averaging, which results in smoother tooth action and decreased tooth-to-tooth variable backlash and less position error. For these reasons, contact ratio in precision meshes should be maintained higher than those in commercial-quality gears. A ratio of 1.4 or higher is desirable; the contact ratio of the spur gears used in the scan actuator gear train is 1.681.

In selecting the best functional gear train for the actuator, the gear ratio n is defined as the input angle divided by the output angle. Its performance parameters are described as follows:

(1) The torque available at the output shaft, neglecting friction, is equal to the torque at the input multiplied by n.

(2) The speed at the output shaft is equal to the speed at the input divided by n.

(3) The angular acceleration at the output shaft, which is a direct function of speed variation, is equal to the input acceleration divided by n.

(4) The moment of inertia, as reflected at the output shaft, is a direct function of torque and an inverse function of acceleration. Therefore, it is equal to the input moment of inertia multiplied by n^2.

An important consideration when dealing with servos where rapid response is required is the maximum load acceleration α_L. This is given, neglecting friction, by

$$\alpha_L = \frac{nT}{J_m n^2 + J_L} \tag{1}$$

where

$1/n$ = gear reduction from motor to output

T = motor torque

J_m = motor inertia, including gears on motor shaft

J_L = load inertia measured at load

Differentiating Eq. (1) for α_L with respect to n and setting it equal to zero, that is,

$$\frac{d\alpha_L}{dn} = 0 \tag{2}$$

results in

$$J_m = \frac{J_L}{n^2} \tag{3}$$

This tells us that, for maximum acceleration of the load, the inertia of the load as seen by the motor shaft J_L/n^2 should be matched to the motor inertia. This is also the condition for maximum power transfer to the load. There is an interesting analogy here. The gear train is a mechanical transformer, where the product of speed and torque are not affected by gear ratio any more than the product of voltage and current are affected by transformer turns ratio. Furthermore, the moment of inertia at the gear train output is matched to the moment of inertia at the source, similar to impedance matching in a transformer.

By substituting Eq. (3) into Eq. (1) and solving for α_L, we obtain the maximum acceleration measured at the load,

$$\alpha_L = \frac{T}{2\,(J_m J_L)^{1/2}} \tag{4}$$

For maximum acceleration in the presence of load friction or load torque, the gear ratio n should be increased somewhat. In the typical servo actuator, n^2 is so large that the inertial load at the motor is essentially that of the motor armature and the first few gears. This condition is true in the scan actuator gear train. Equation (3) as it applies to the scan actuator gear train may be rewritten as follows:

$$J_m \geq \frac{J_L}{n^2} \tag{5}$$

C. Selection of Gear Ratio and Motor

An important consideration in the design of the scan drive system is the balancing of factors affecting the choice of gear ratio used in the scan actuator. It is desirable from the standpoint of smoothness and stability to have a large reduction between the motor and the load. From the standpoint of speed of response, maximum speed, and maximum power transfer to the load, relatively low gear ratios are desirable.

The lowest speed at which the motor will run smoothly, divided by the desired minimum output speed, sets a lower limit on n, where $1/n$ is the gear reduction. The highest speed at which the motor may be run with a reserve of torque for acceleration, divided by the desired maximum running speed of the output, sets an upper limit on n. In order to slew the actuator, the top speed of the motor, the actuator output slewing speed and the torque demand on the actuator will set a new and, usually, lower upper limit on n.

The scan actuator slewing speed requirement under full voltage, with no load, is desired to be greater than 1.3 deg/s. In order to be self-locking and resist back-driving, the gear train must be less than 50% efficient.

Using this information, the motor desired for the scan actuator can now be selected. A given requirement is that the motor will be a two-phase, alternating current, 400-Hz servo motor. The motor no-load slewing speed is 6500 rev/min. The estimated torque required of the scan actuator in order to drive the scan platform in the 1-g field is 75 lb in. This value is based on an evaluation of the scan platform design. In the 0-g field, while the spacecraft is in flight, it is expected that this torque will drop to 20 lb in. This information is an extrapolation based on an evaluation of telemetry data returned from the performance of the scan platform on *Mariner IV*.[2]

[2]The *Mariner IV* spacecraft carried out a flyby mission to Mars in 1965.

The parameters for selecting the actuator motor are listed as follows:

(1) Gear train efficiency $\leq$50%.

(2) Actuator slewing speed $\geq$1.3 deg/s.

(3) T_{L_1} (actuator load torque at 1 g) = 75 lb in.

(4) T_{L_0} (actuator load torque at 0 g) = 20 lb in.

(5) Power = 10 W (maximum).

The first iteration for a gear ratio value for use in the motor selection will be

$$\frac{1}{n} = \frac{1.3 \text{ deg/s} \times 60 \text{ s/min}}{6500 \text{ rev/min} \times 360 \text{ deg/rev}} = \frac{1}{30000} \tag{6}$$

From this iteration, the final value of the actuator gear ratio is expected to be slightly less than 30,000 to 1. In order to size the motor, the motor torque demand in both the 1-g and 0-g conditions will be evaluated. With friction losses considered, the motor torque T_{m_1} and T_{m_0} will be as follows:

(1) At 1-g condition (ground test),

$$T_{m_1} = \frac{75 \text{ lb in.} \times 16 \text{ oz/lb}}{30{,}000 \times 0.5} = 0.08 \text{ oz in.} \tag{7}$$

(2) At 0-g condition (space flight),

$$T_{m_0} = \frac{20 \text{ lb in.}}{75 \text{ lb in.}} \times 0.08 \text{ oz in.} = 0.0223 \text{ oz in.} \tag{8}$$

The slewing speed torque demand on the motor, ranging from 0.02 to 0.08 oz in., occurs at the high-speed, low-torque portion of the motor characteristic performance curve. For satisfactory performance of the actuator, the stall torque of the motor should be on the order of eight times greater than the slewing torque demand on the motor. There are now sufficient data for selecting the actuator motor. These data are as follows:

(1) Motor speed, 6500 rev/min (minimum).

(2) Stall torque, 0.16–0.64 oz in. (minimum).

(3) Power, 10 W (maximum total).

The motor selected for the scan actuator is a Kearfott size 11, two-phase, 400-Hz alternating current servo motor.[3] Mechanical and electrical characteristics of the motor are shown in Tables 1 and 2. From these tables, it may be seen that the 0.5-oz in. stall torque of the motor falls within the desired range. The stall power demand of 3.9 W/phase or a total of 7.8 W is within the power allotment of 10 W.

Table 1. Motor characteristics (mechanical)

Parameter	Value
Stall torque, oz/in.	0.5 (min)
No-load speed, rev/min	6500 (min)
Rotor inertia, g-cm^2	0.76 (ref)
Theoretical acceleration (stall), rad/s^2	61,200 (ref)
Weight, oz	3.0 (ref)

Table 2. Motor characteristics (electrical)

Parameter	Fixed phase	Control phase	
		Series	Parallel
Voltage (400 Hz), V	26 ±3%	20 ±3%	10 ±3%
Current (stall), A	0.235 ±10%	0.305 ±10%	0.610 ±10%
Power input (stall), W	3.9 (max)	3.9 (max)	3.9 (max)
Power factor (stall)	0.575 (ref)	0.575 (ref)	0.575 (ref)
R (stall), ohms	64 ±15%	37.8 ±15%	9.45 ±15%
X (stall), ohms	91 ±15%	53.7 ±15%	13.4 ±15%
Z (stall), ohms	111 ±15%	65.7 ±15%	16.4 ±15%
Effective R (stall), ohms	194 (ref)	115 (ref)	28.8 (ref)
DC resistance, ohms	22.4 ±15%	15.0 ±15%	3.7 ±15%
Starting voltage, V		0.68 (max)	

In order to select the nominal value for the gear ratio n, we must consider the motor characteristic, the actuator load, and slewing speed. The motor characteristic is approximated by

$$T_m = T_s - \frac{T_s}{\dot{\theta}_m} N \tag{9}$$

where

$\dot{\theta}_m$ = motor speed = 6500 rev/min

T_s = motor stall torque = 0.5 oz in.

[3]General Precision Systems Inc., Kearfott Products Division, Little Falls, N.J.

The torque demand on the motor while slewing the actuator load is

$$T_m = \frac{75 \text{ lb in.} \times 16 \text{ oz/lb}}{n} \tag{10}$$

and N, the motor speed while slewing the actuator load, is

$$N = \frac{1.3 \text{ deg/s} \times 60 \text{ s/min}}{360 \text{ deg/rev}} \times n \tag{11}$$

By substituting the values for $\dot{\theta}_m$ and T_s and Eqs. (10) and (11) into Eq. (9) and solving for n, the nominal value for the actuator gear ratio, we obtain

$$n^2 - 29{,}900n + 71{,}800{,}000 = 0 \tag{12}$$

and

$$n = 27{,}100 \tag{13}$$

It is shown that the actuator gear ratio should be on the order of 27,000:1. The indicated nominal value of 27,100 to 1 may vary 1 or 2% with negligible effect on the actuator performance. The value of n selected for convenience in laying out the gear train during the design of the actuator was 27,039:1. This is less than ¼% (actually, 0.225%) lower than the nominal value of 27,100:1.

The slewing performance of the actuator can be evaluated by writing an expression for power conservation and substituting into it the actuator gear train speed reduction and the idealized torque speed curve for the motor. The power put into the load by the actuator must be equal to the power put into the actuator by the motor. Considering friction losses, this is

$$T_L \dot{\theta}_L = T_m \dot{\theta}_m \eta \tag{14}$$

where

T_L = actuator load torque

$\dot{\theta}_L$ = actuator slewing speed

T_m = motor torque

$\dot{\theta}_m$ = motor slewing speed

η = actuator gear train efficiency

The equation for gear train speed reduction is

$$\dot{\theta}_L = \frac{\dot{\theta}_m}{n} \tag{15}$$

The resulting equation for the actuator slewing speed performance is

$$\dot{\theta}_L = \frac{6\dot{\theta}_m}{n}\left(1 - \frac{T_L}{T_s n \eta}\right) \tag{16}$$

Parametric plots of this equation showing the actuator slewing rates for loads of 20 lb in., 75 lb in., and 125 lb in. are shown in Fig. 4.

Figure 1, an isometric schematic diagram of the gear train, shows the drive train from motor to output shaft to be a series of four spur gear meshes and one worm helical gear mesh. Each spur gear mesh will be approximately 96% efficient, considering its condition of mounting and lubrication. The static efficiency η of the actuator gear train can thus be expressed as

$$\eta = 0.96^4 \times 0.49 \times 100 = 41.4\% \tag{17}$$

Since this efficiency determination is at best an estimate, it is expected the actuator gear train efficiency will be between 35 and 45%.

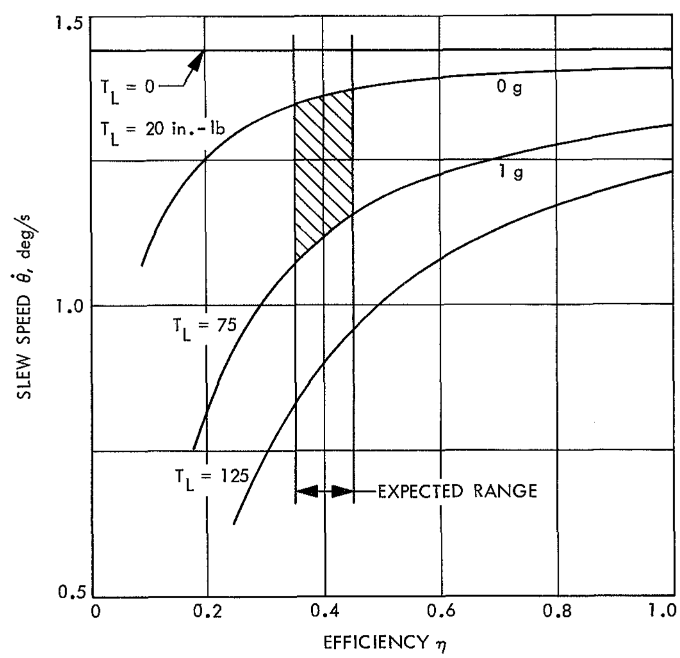

Fig. 4. Actuator slewing performance

IV. Summary of Performance

Ten scan actuators were manufactured. Average performance measurements of the 10 actuators, along with predicted performance levels, are presented in Table 3. Four of the actuators, two each on each spacecraft, are on their way to Mars, on board *Mariner VI* and *Mariner VII*.

Table 3. Scan actuator performance parameters

Parameter	Value		
	Specified	Predicted from design analysis	Test results
Starting voltage, V rms (max)	1.5	<1.0	0.3
No-load slewing speed, deg/s	>1.3	1.4	1.4
Clutch slip torque, lb in.	200–550	200–550	300
Gear train backlash, arc min	<30	13.7	15
Mechanical stiffness, ft lb/rad	20,000–30,000	30,000	20,000
Static efficiency, %	<50	41.4	41.2

Selected Bibliography

Analysis of Stresses and Deflections in Ball Bearings, Vols. 1 and 2. General Motors Corporation, New Departure Division, Bristol, Conn., 1946.

Buckingham, E., and Ryffel, H. H., *Design of Worm and Spiral Gears.* The Industrial Press, New York, 1960.

Buckingham, E., *Manual of Gear Design*, Sec. 1, "Mathematical Tables"; Sec. 2, "Spur and Internal Gears"; and Sec. 3, "Helical and Spiral Gears." The Industrial Press, New York, 1935.

Dudley, D. W., *Gear Handbook*, First Edition. McGraw-Hill Book Co., Inc., New York, 1962.

Greenwood, I. A., Holdam, J. V., and MacRae, D., *Electronic Instruments*, MIT Radiation Laboratory Series, Vol. 21. McGraw-Hill Book Co., Inc., New York, 1948.

Michalec, G. W., "Precision Gear Trains," *Machine Des.*, Feb. 3, 1966.

Perkins, G. S., "Analysis of Servomechanisms for Instrument and Power Drives," *Prod. Eng.*, Vol. 17, No. 4, p. 332, Apr. 1946.

Page intentionally left blank

Session IV

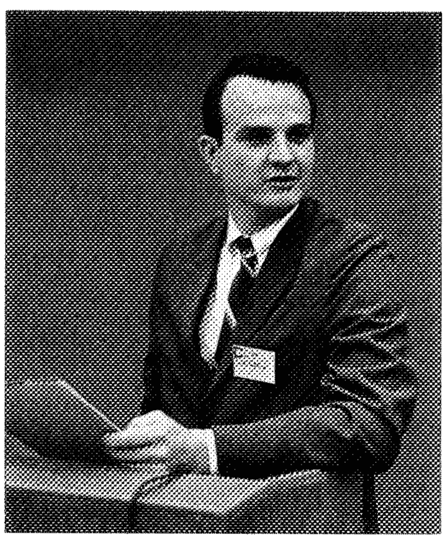

OVERLEAF: *Fred Forbes, United States Air Force Aero Propulsion Laboratory (left), Session Chairman; and Alfred Rinaldo, Lockheed Missiles & Space Company (right), Session Co-chairman*

70N21441

A Flow-Control Valve Without Moving Parts

W. L. Owens, Jr.
Lockheed Missiles & Space Company
Sunnyvale, California

The design and operation of a "valveless" flow-control device that has been flown on Application Technology Satellites A and D are described. A considerable increase in reliability over a mechanical valve is possible in applications where response times on the order of minutes are acceptable at thrust levels below 10^{-2} lbf. Theoretical performance curves for flow termination time and mass loss rate are presented for several candidate subliming materials. Good agreement between calculated and experimental values of flow termination time and mass loss rates is demonstrated.

I. Introduction

Valve reliability is a major consideration in the design of low-thrust systems. This is especially true for long-life missions where successful operation of from 1 to 3 yr is required. This paper describes a flow-control device which, in certain cases, allows one to eliminate mechanical valves from the system. The resulting "valveless design" has the advantage of high reliability, low leakage rate, and the feature of being fail-safe. The primary disadvantages are response times that are on the order of minutes, larger power requirements than those of the equivalent mechanical valve, and a general limitation to systems of less than approximately 10^{-2} lbf thrust. In many low-thrust space applications such as drag makeup, station keeping, orbit adjustment, and satellite inversion where very small thrusts are used for extended periods of time, thrust start-up and termination times on the order of minutes are acceptable.

The principle involved utilizes the phenomenon of solid-vapor phase change associated with subliming substances. In this respect, the valveless design is limited to applications suitable for subliming solid thrusters, which are discussed in Ref. 1. Flow control for the valveless design is effected by placing a condensing element at some point in the propellant delivery line. The condensing element can be a screen or porous plug upon which the propellant condenses to terminate flow. Flow is terminated by allowing the screen temperature to fall below the equilibrium value; as a result, the propellant is condensed on the screen and eventually blocks the flow through the pores. Resumption of flow is effected by reversing the process and heating the screen to a temperature above the equilibrium value, thus causing the condensed propellant to vaporize and reopening the pores to flow. Thermal control of the condensing element is maintained by an electrical heater used in conjunction with a heat-rejection device such as an optical solar reflector.

II. Design

The porous plug or evaporating-condensing valve assembly is composed of the exit tube, a condensing element that contains the screen or porous plug, a heat-rejection device, and one or two heaters. Figure 1 shows the construction of the porous plug assembly used in the *Application Technology Satellite* (ATS) program. The design is predicated primarily on the thermal response and steady-state operating temperatures necessary to provide the required start-up and termination times and to provide a minimum propellant loss. In general, the faster the porous plug is cooled to a value sufficiently below the propellant equilibrium temperature, the sooner flow termination will occur. Also, the colder the screen is maintained in the *off* condition, the smaller the propellant mass loss. To accomplish these two objectives requires a design that minimizes porous plug thermal capacitance and thermal conductance with the rest of the system. The principal conductances are the exit and delivery lines along with the heater leads. The tube wall thickness will generally be determined by the expected vibration loading, while the heater lead wire size and length can be chosen to minimize conduction and electrical losses. The condensing element and heat sink combination should have the minimum possible thermal capacitance while providing a high-conductance heat path between the mirror and the screen.

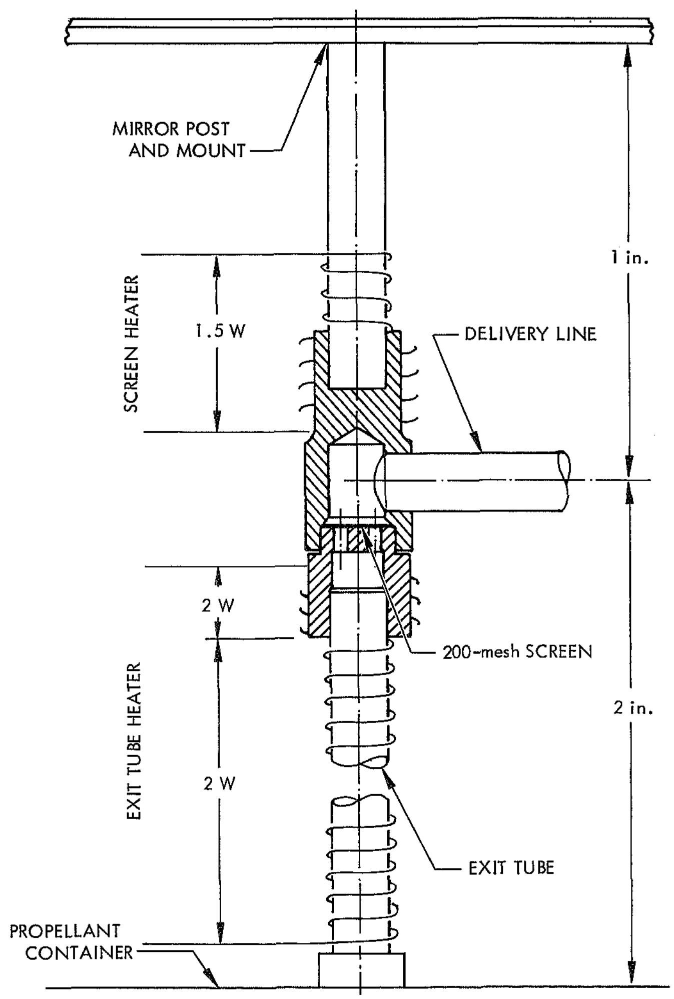

Fig. 1. Evaporating–condensing valve

The mirrors were of a type known as optical solar reflectors, designed to have a high thermal emittance and a low solar absorptance. The mirrors used in the present application are described in Ref. 2, where measured values of α_s and ϵ of 0.048 and 0.80 respectively were reported. Bonding of the mirrors to a copper mounting plate was accomplished with RTV 615 adhesive. The 3-in.^{2} mirror area represents a trade-off between (1) the required cool-down rate and minimum equilibrium temperature for flow termination and (2) the power necessary to maintain the porous plug at the required operating temperature during thrusting.

In the *no-flow* condition the screen and exit tube are colder than the propellant container, which results in a migration of propellant to the exit tube. If the unit is inactive for a considerable length of time, the exit tube can fill completely with propellant; this necessitates its being heated along with the porous plug section during start-up. Having to heat the exit tube during start-up generally requires that the condensing section be placed as close to the propellant container as possible to minimize propellant plug length and conserve power. The limit on how short the exit tube can be made is imposed by the exit tube thermal resistance necessary to provide the desired minimum porous plug temperature in the *off* condition. The second heater mounted on the condensing section is used to maintain the assembly at the desired operating temperature after the exit tube heater is turned off.

A potential failure mode is the failure of the heaters; however, the heaters can generally be made to be very reliable. This type of failure mode is fail-safe since cutting off the power to the heaters terminates the flow. A second possible failure mode would be a change in the optical properties of the mirrors, but these properties have been found to be very stable in a space environment. Two principal failure modes exist for this type of flow control device. The primary mode is heater failure, which is fail-safe since cutting off the power to the heaters terminates the flow. A second failure would be a change in the optical properties of the mirrors, which have been found to be very stable in a space environment. The overall reliability of the porous plug assembly is judged to be superior to that of the comparable mechanical valve.

III. Operation

The operation of the porous plug valve can best be visualized from test results shown in Fig. 2, where thrust, chamber pressure, and total system power have been shown versus time. The 2.4-W power requirement at time zero represents heat loss to the environment to maintain the propellant at 155°F, plus nozzle heater and electronics power. The command to thrust was given at 100 s with the application of power to the exit tube and porous plug. The gradual increase in thrust accompanied by the two spikes is the result of vaporization of the plug of propellant. (Not all startups exhibited random spikes.) The actual opening of the screen and tube to flow is accompanied by a decrease in chamber pressure and an increase in propellant heater power. A proportional controller is used to regulate power to a 10-W heater to maintain the chamber pressure at the prescribed value. Ten minutes after the command to thrust, the exit tube power is cut off and the porous plug is maintained at its operating temperature by the 1.5-W heater. Thrust is terminated by turning off the porous plug heater; this results in the eventual decay in thrust to a zero value approximately 10 min after the command is given. The first 400-s period does not produce any change in thrust. This represents the time required for the porous plug to fall below the equilibrium temperature, plus the time required to restrict the screen flow area to the point where it begins to produce a measurable pressure drop. Once this point is reached, the actual termination of flow requires approximately 3 min.

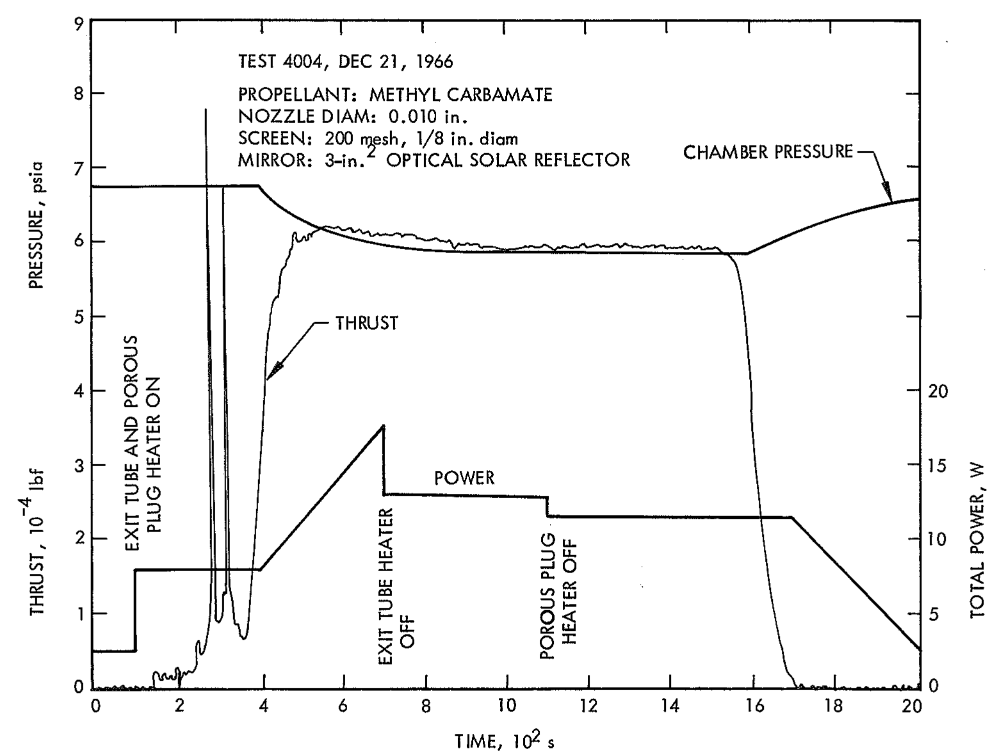

Fig. 2. Thrust start-up and termination for the valveless ATS subliming solid reaction control system

Telemetry data from ATS A and D for chamber pressure and temperatures indicate that these units are operating normally despite the fact that the intended synchronous orbits were not attained.

IV. Theoretical Performance

An analytical solution for flow-termination time developed in Ref. 1 is[1]

$$\frac{\rho_p}{\alpha}\left(\frac{\pi R T_m}{2 g_c}\right)^{1/2}(L - D_w) = \int_0^{t_0} [P_c - P'(T_s)]\, dt \tag{1}$$

If one assumes that the variation in the square root of the absolute mean temperature is small, then the left

[1]Symbols are defined in the Nomenclature.

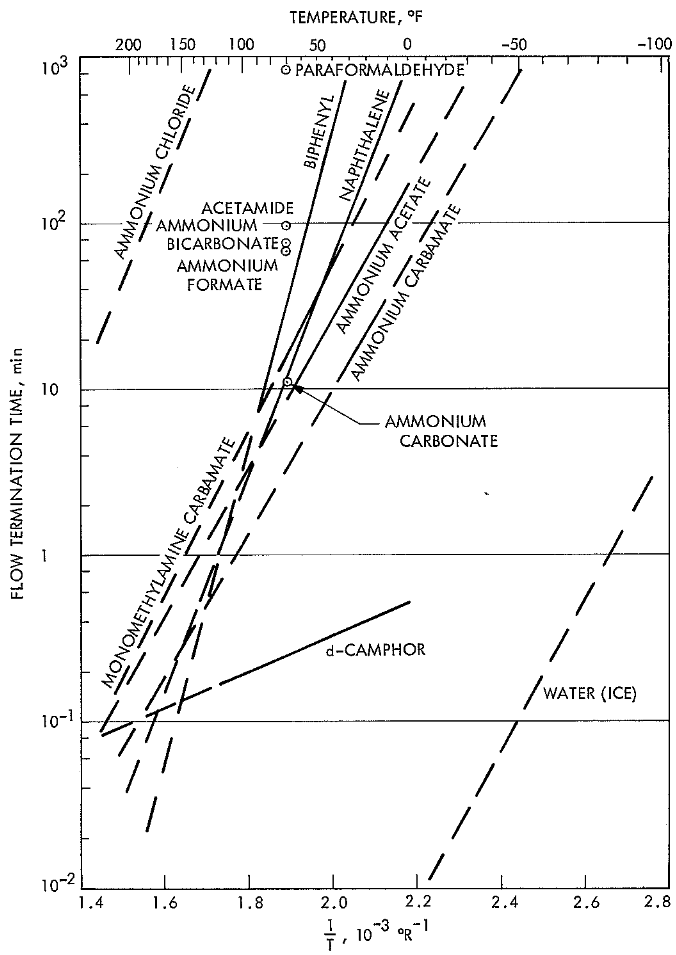

Fig. 3. Minimum theoretical flow termination time vs. temperature for a 200-mesh screen

hand side of Eq. (1) is a constant dependent on the physical properties of the propellant, the mean operating temperature, and the mesh opening. For a fixed chamber pressure P_c and screen cool-down transient, which determines $P'(T_s)$, the flow-termination time will be minimized by making the left side of Eq. (1) as small as possible. The minimum theoretical flow-termination time will be given for the case where the screen temperature drops instantaneously to a value providing $P_c >> P'(T_s)$. For a constant chamber pressure, the minimum flow-termination time will be given by

$$t_0 = \frac{\rho_p}{\alpha P_c}\left(\frac{\pi R T_m}{2 g_c}\right)^{1/2}(L - D_w) \tag{2}$$

From Eq. (2), it may be seen that flow-termination time is proportional to the mesh opening and inversely proportional to chamber pressure and the condensation coefficient. Equation (2) has been plotted as a function of temperature in Fig. 3 for several subliming materials. A mesh opening of 0.0029 in., corresponding to a 200-mesh screen, was used along with a propellant specific gravity that is generally characteristic of these substances. It will be seen that fairly rapid flow-termination times are theoretically possible for most of the substances as long as the operating temperature is high enough. The solid portion of the curves represents the temperature range for which experimental values of the evaporation coefficient are available. It was assumed that the evaporation coefficient could be used for the condensation coefficient.

In order to achieve short flow-termination times, it is necessary to provide a porous plug design that will have a fast thermal response along with a suitable operating temperature. The ability of Eq. (1) to predict flow-termination times is demonstrated in Fig. 4. Measured values of chamber pressure and porous plug temperature were used to evaluate the integral of Eq. (1), yielding fairly good agreement with the experimentally obtained values of flow-termination time. Test conditions are given in Table 1.

The amount of propellant leakage can be estimated from an expression derived in Ref. 1, which yields

$$\frac{\dot{m}}{A_t} = \frac{C_W P'(T_s)}{\dfrac{1}{C_D} + \dfrac{1.26\, A_t}{\alpha\, A_p}} \tag{3}$$

Table 1. Test conditions for Fig. 4

Symbol	Propellant	Thrust, lbf	Throat diameter, in.	Evaporation coefficient	Screen size	
					Mesh	Diam, in.
○	Methyl carbamate	~3×10^{-4}	0.020	1.8×10^{-5}	40	¼
△	Methyl carbamate	~3×10^{-4}	0.020	1.8×10^{-5}	40	¼
□	Methyl carbamate	~2×10^{-5}	0.010	1.8×10^{-5}	40	¼
◇	Ammonium formate	~4×10^{-4}	0.020	2.8×10^{-3}	100	⅛

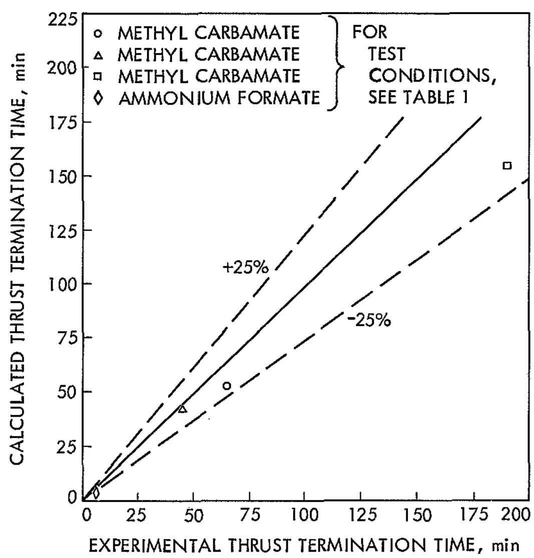

Fig. 4. Calculated vs. experimental thrust termination time (Ref. 1)

The term A_p represents the exposed propellant surface area on the downstream side of the screen, and $P'(T_s)$ is its equilibrium vapor pressure. For many cases the second term in the denominator of Eq. (3) is much larger than the first, with the result that the loss mass rate may be estimated from the following simplified relationship:

$$\dot{m} = \alpha C_W A_p P'(T_s) \tag{4}$$

Comparison of Eqs. (2) and (4) indicates that the propellant characteristics providing the shortest flow termination time also produce the greatest mass loss. The mass loss can be kept small by maintaining the porous plug at a sufficiently low temperature during the thruster *off* time. Equation (3) is shown plotted in Fig. 5, where the solid portions, once again, represent the range for which values of the evaporation coefficient are available. The points represent substances for which the evaporation coefficient was available only at 70°F. Their

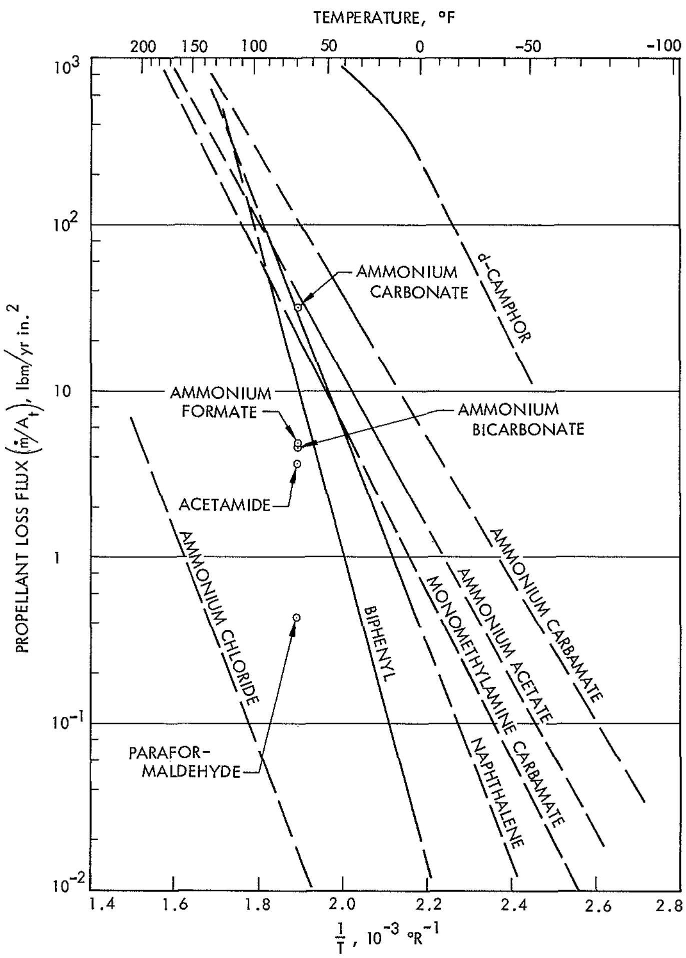

Fig. 5. Porous plug propellant loss vs. temperature for $A_p/A_t = 10$

variation with temperature, at least for the ammonium salts, should be similar to the ones that are shown. The actual yearly mass loss for an area ratio of 10 is obtained by multiplying the values shown on the figure by the nozzle throat area.

The values of pressure and evaporation coefficient used in Figs. 3 and 5 were taken from Ref. 1, in which the various data sources are identified. Experimental determination of the propellant loss from the porous plug assembly shown in Fig. 1 produced values that decreased with time after flow termination. This variation was assumed to be due to the propellant initially condensing in the delivery line during flow termination, providing a diminishing vaporization area with time as it re-evaporated. The measured mass loss rates were from 3 to 5 times the theoretical values. This difference probably represents the uncertainty in the actual vaporization surface area.

V. Conclusions

The evaporating–condensing valve described in this paper has been flight-qualified for a 3-yr life, and telemetry data from *Application Technology Satellites* A and D have indicated normal operation in space. The following conclusions can be drawn regarding the valve:

(1) Where operating conditions allow response times on the order of minutes and thrust levels less than 10^{-2} lbf, the evaporating–condensing valve or porous plug valve may be used with a significant increase in reliability over a mechanical valve.

(2) Response times of from 1 to 10 min are possible, depending on the propellant, operating conditions, and thermal response of the porous plug.

(3) Very low propellant leakage rates are possible with most of the candidate subliming materials when the porous plug is maintained at a suitable temperature.

(4) Estimation of flow termination times and propellant leakage rates is possible using the expressions presented in the paper.

Nomenclature

A area

C_D nozzle discharge coefficient

C_W theoretical nozzle mass flow coefficient

D diameter

g_c conversion factor in Newton's law of motion

L screen mesh length

$\dot{m}$ mass rate

P_c chamber pressure

$P'(T_s)$ propellant equilibrium vapor pressure at the screen

R gas constant

t time

T temperature

α evaporation or condensation coefficient

ρ density

Subscripts

m mean

o flow termination

p propellant

t throat

w wire

References

1. Owens, W. L., Jr., "Design Aspects of Subliming Solid Reaction Control Systems," Paper 68-516, presented at the ICRPG/AIAA 3rd Solid Propulsion Conference, Atlantic City, N.J., June 4–6, 1968. To be published in *J. Spacecraft Rockets*.

2. Marshall, K. N., and Breuch, R. A., "Optical Solar Reflector: A Highly Stable, Low α_s/ϵ Spacecraft Thermal Control Surface," *J. Spacecraft Rockets*, Vol. 5, No. 9, pp. 1051–1056, Sept. 1968.

70N21442

Three Simple Mechanisms To Solve Unique Aerospace Problems

E. Groskopfs
Spar Aerospace Products, Ltd.
Malton, Ontario, Canada

Three simple, reliable, inexpensive mechanisms are described. The first mechanism is a swinging-gear drive that permits two or more electric gearhead motors to be coupled together to a common load. If one motor fails, it is automatically disconnected from the common load, thus permitting the remaining motor to operate without the burden of the failed one. The second mechanism, a breather cartridge, is a two-way air valve that provides a low-resistance air passage but closes immediately when a contact with water is made. This device does not require electrical power and is almost foolproof. The third mechanism, a hypocycloid timer, provides an actuating pulse from a rotating shaft. A large number of revolutions per pulse are obtained without the use of gear reduction passes.

All three mechanisms have been qualified for space use and flown on manned or unmanned missions.

I. Introduction

Today, when interplanetary travel is a reality and when the equipment to achieve this becomes more and more complicated, the need for simple and reliable mechanisms is more apparent than ever before. Almost daily in the aerospace industry, requirements arise that can best be met by finding or rediscovering a simple device to perform a complex function. Generally, if parts can be eliminated from a mechanism without a loss in performance, the mechanism will be simpler and more reliable, and it will weigh and cost less. It is also true that things that are not used do not cause failures. Therefore, this paper presents three mechanisms that are simple, reliable, and inexpensive. All three mechanisms have been qualified for space use and have been flown on manned or unmanned space missions.

The basic mechanisms presented in this paper—a swinging-gear drive, a breather cartridge, and a hypocycloid timer—are not necessarily new inventions but, rather, embody familiar principles that have been adapted to solve specific design problems.

II. The Swinging-Gear Drive

A. General

It is a mechanism designer's nightmare when, for reliability reasons, two or more electric gear motors are required to drive a common load. Usual design approaches require the use of differentials, clutches, or other means to couple and decouple the redundant motors. Even under these conditions, a failure of one motor can still cause that motor to be a burden to the remaining one, and, in most cases, unless the failed motor is decoupled, it will render the total mechanism inoperative.

Generally, driving a common load by more than one electric gear motor is not practical because the advantages that a multidrive system offers are overshadowed by an increase in complexity, and, consequently, the hoped-for increase in reliability is not achieved.

The swinging-gear drive (Fig. 1) overcomes most of these conventional problems. It is adaptable to any kind of prime mover and can also be used when the motor is to be assisted by manual operation. This mechanism permits a drive to a common load through two or more worm reducers without the use of any clutches. Its operation is fully automatic—if one of the drives is stopped, the remaining drive(s) will carry on and automatically reject the nonoperating drive.

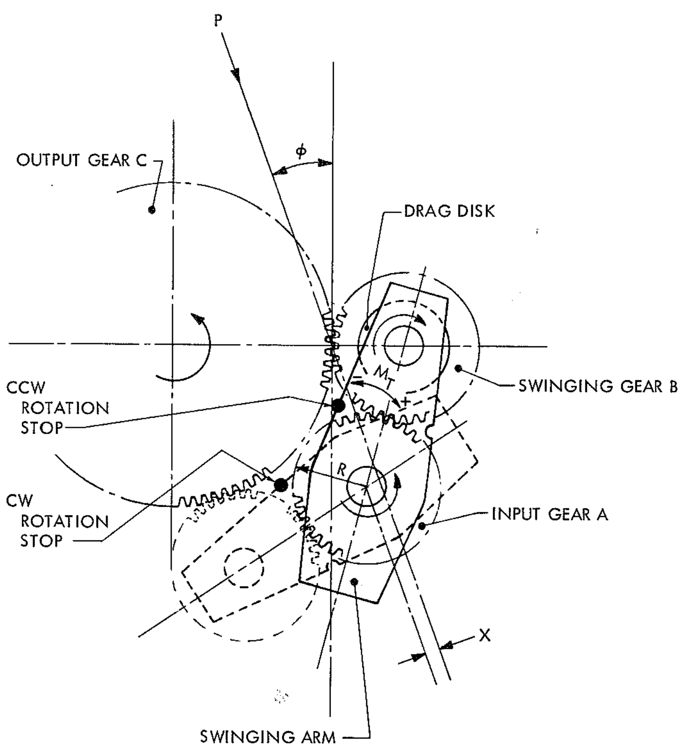

Fig. 1. Basic swinging-gear mechanism

B. Principle of Operation

The basis for this mechanism is a swinging gear called a flip-flop. For simplicity, this discussion will be limited to an application in which two electric gear motors drive a common load. However, since each motor drive is completely independent, the number of drives is limited only by practical considerations such as space and weight. Figure 1 shows a basic flip-flop mechanism; for a multidrive operation, similar flip-flop mechanisms are added to the same output gear.

The input gear A is mounted directly on the motor shaft or on a shaft that is geared to the motor. On the same shaft, a swinging arm is also mounted in such a way that gear B is always in contact with the input gear A. Thus, by applying rotation to the input gear, the swinging gear is also rotating. The swinging arm has a natural tendency to rotate in the same direction as the input gear. This tendency is increased by adding a slight drag between the swinging arm and gear B. Thus, by turning the input gear in a counterclockwise direction, the swinging arm also moves in a counterclockwise direction, until the swinging gear B contacts the output gear C. To limit this motion and to provide proper gear mesh, a counterclockwise stop is added. As long as rotational motion is maintained on the input gear, full input power is transmitted from the input to the output gear.

If rotation of the input gear is reversed to the clockwise direction, the swinging arm will move until the clockwise stop is reached. At this instant, the swinging gear B will be in the proper contact with the output gear C and will deliver the full input power to the output gear in the clockwise direction.

When two flip-flop mechanisms are arranged so that both can engage the same output gear, either or both mechanisms can drive the output gear. Should one of the two motors stop, the output gear would automatically push the swinging arm gear of the stopped motor out of mesh. Figure 2 illustrates schematically various modes of operation of two flip-flop mechanisms.

As shown in Fig. 1, there is a friction disk that exerts a torque M_T (negative) between gear A and the swinging arm; this torque keeps gears B and C in mesh during the

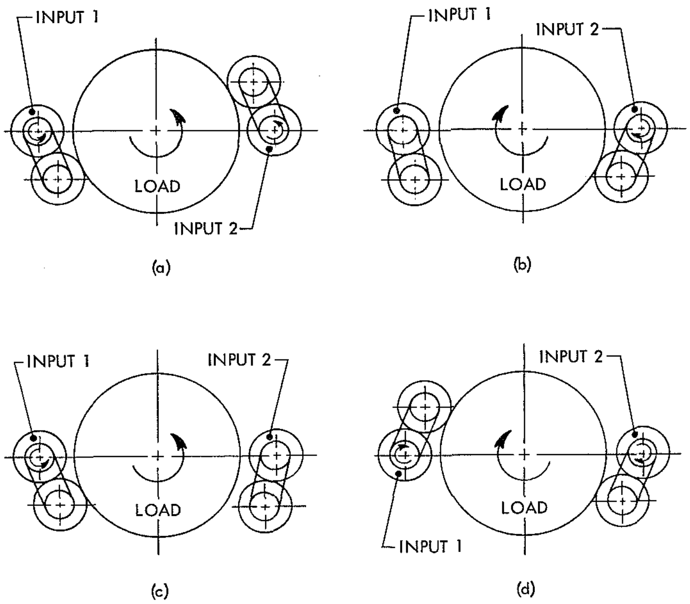

Fig. 2. Operation of swinging-gear drive: (a) both inputs 1 and 2 driving common load counterclockwise, (b) input 2 only driving load in clockwise direction, (c) input 2 only driving load in counterclockwise direction, (d) both inputs 1 and 2 driving common load clockwise

counterclockwise rotation of the input gear A. During the clockwise rotation of the input gear A, the torque M_T (positive) tends to reengage the swinging arm gear B with gear C in the dotted position shown.

The following relationship exists for the swinging arm to swing:

$$M_T + PX > PR \cos \phi$$

and this criterion governs the relative positions of gears A, B, and C.

Note that the torque exerted by M_T in either direction is swinging the arm only; this torque is not required to maintain mesh between the swinging gear and the common load. Both gears B and C have a "pull-in" tendency while any torque is being transmitted through the gear train.

When two motors are simultaneously driving the output gear, both motors must have similar speed-torque characteristics and output speeds—otherwise, the faster-driving motor will bounce in and out from the common gear C.

III. The Breather Cartridge

A. General

During the initial phases of development of the high-frequency recovery antenna for the *Gemini* spacecraft, a requirement was established for a breather cartridge—a two-way air valve that would instantaneously close when contact with water was made. The purpose of this valve was to vent an equipment container to ambient pressure during spacecraft ascent and descent, but not to admit water when landing at sea.

Many design approaches were investigated, including an electrical system consisting of a solenoid valve, water sensor, and associated electronics. All such systems required considerable development and were complicated and expensive. Since the valve had to work only once, a "single shot" cartridge valve was developed that would pass air in either direction, but would clog automatically when submersed in water.

A long list of porous materials was tested until one substance that would meet all requirements was found. This material is called Serutan ("Nature's," spelled backwards).[1] It is a commonly known laxative and can be purchased in any drug store. A specially designed capsule filled with this material was developed, was fully qualified to spacecraft specifications, and was flown successfully on all *Gemini* missions.

B. Design

The breather cartridge is a cylinder 2.3 in. long and 0.5 in. in diameter, divided into two compartments. Located at both ends and in the middle of the body are three stainless steel wire screens. The two volumes, which are separated by the centre screen, are filled with granular Serutan particles and are shown in Fig. 3.

The two compartments' grain sizes, cross-sectional area, and length were carefully selected to meet equipment requirements. Typical air flow values measured on a breather cartridge as used on this program are between 2.9 and 4.4 litres/min with a 2-psi pressure differential. When the cartridge was subjected to an instantaneous water pressure of 3 psi, moisture penetration in the fine-grain compartment was only about 0.75 in. The water-blocking mechanism (if the term mechanism may be

[1]Manufactured by the J. B. Williams Co., Inc., Pharmaceutical Division, Cranford, N. J.

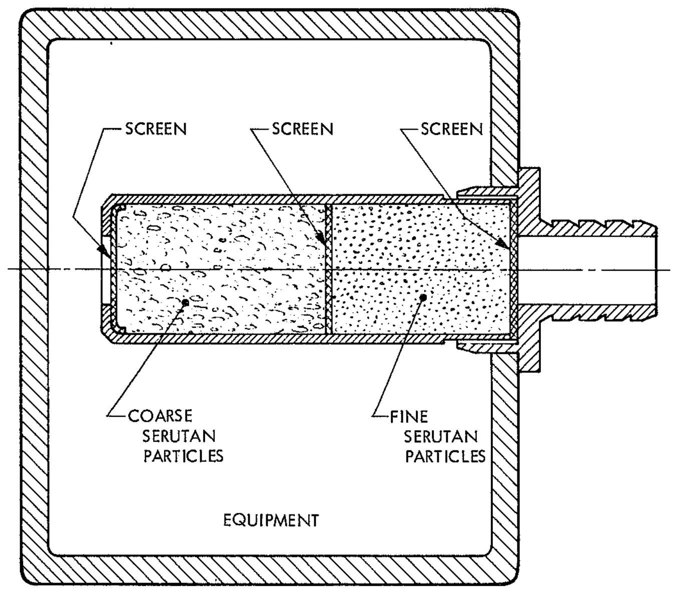

Fig. 3. Typical breather cartridge

applied in this case) is very simple—the granular particles that permit air to pass through in either direction dissolve partially in water, forming a gum-like mass that plugs the breather valve.

The Serutan granule sizes were carefully selected so that almost instantaneous clogging action would occur. A compromise between "fast acting" fine particles and coarse low-air-resistance particles was carefully established to meet mission requirements. Although the fine-grain chamber was adequate to stop water penetration, the coarse-grain chamber was added for increased reliability.

The following is a brief summary of advantages offered by this mechanism:

(1) Operation is fully automatic.

(2) There are no moving parts.

(3) No electrical or mechanical input is necessary for operation.

(4) The mechanism is light, inexpensive, and extremely reliable.

IV. Hypocycloid Timer

A. General

The hypocycloid timer was developed for use on a deployable spacecraft antenna. The antenna operation required an electrical actuating pulse at a precise preset number of spool turns. Many conventional approaches, such as a rotating cam, traveling lead screw, etc., were investigated and were found to be either inaccurate or too complicated and expensive. Since in this application the actuating pulse had to be obtained from a rotating shaft, a simple hypocycloid mechanism was developed, tested, and qualified. The mechanism is shown in Fig. 4. A noteworthy feature of this mechanism is an extremely accurate pulse repeatability that is obtained from the rotating shaft.

Figure 4 illustrates the physical configuration in which an eccentric pinion carrier is fixed to the rotating shaft. The pinion, which rotates on the carrier, has one tooth of greater face width than the remaining teeth and is in continual mesh with a stationary internal gear. A spring-loaded push pin is located in the internal gear and is actuated periodically whenever the wide tooth of the pinion coincides with its position. Figure 4 also illustrates graphically the locus of the wide tooth and the points at which it meshes with the ring gear. A specific number of turns is required before there is again a coincidence at the actuating pin.

B. Design

The following simple relation exists between the internal gear, pinion gear, and number of shaft turns per pulse:[2]

$$L = N$$

$$M = N + 12 \text{ teeth (minimum)}$$

where

L = shaft revolutions per pulse

N = number of pinion teeth

M = number of ring gear teeth (prime number only)

Example: It is desired to provide a pulse every 28th revolution.

Solution: From the relationship above, the number of pinion teeth $N = 28$. The number of ring gear teeth $M = N + 12$ minimum (prime number only). Therefore,

$$M = 41 \text{ or } 43, 47, 53, 59, \text{etc.}$$

[2]For 20-deg tooth pressure angle.

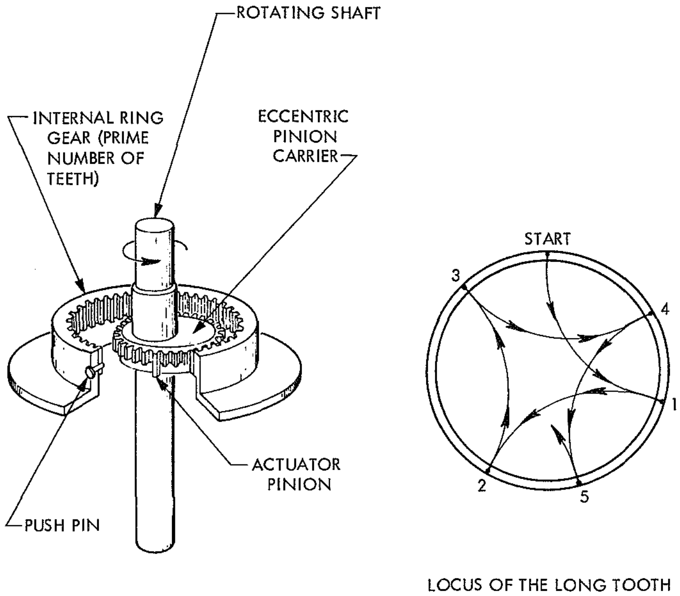

Fig. 4. Hypocycloid timer mechanism

Note that shaft revolutions per pulse are not affected by the ring gear number of teeth if M is a prime number. Two pinions with different numbers of teeth may be operated against a common ring gear, and, by properly arranging actuator pins, a very large number of turns per pulse may be obtained.

The main advantages of this mechanism over more conventional techniques are:

(1) This timer provides a precise switching point regardless of the number of turns.

(2) It does not require multipass gear reductions when a high number of revolutions per pulse is required.

(3) It is inexpensive, light, and reliable.

(4) Only low torque is required to drive this mechanism.

V. Conclusions

It is true that "first cut" designs of mechanisms are usually more complicated than the final product. It is also probably true that the simplest mechanism is not the easiest to design—because, in the design labyrinth, to find the simplest and shortest solution usually is most difficult. In addition to this, almost any mechanism design involves some degree of compromise.

Therefore, this paper has presented three simple mechanisms which can take their place alongside complex units requiring long and costly development. All three have been tested and qualified and successfully used. It is also the intention of this paper to show that there is always "a simpler way of doing it."

Acknowledgment

The author wishes to thank Spar Aerospace Products, Ltd., for permission to publish this paper and particularly to acknowledge the contributions of J. A. Fry and H. J. Taylor, who developed the mechanisms discussed above.

Page intentionally left blank

70N 21443

Thermal Heliotrope: A Passive Sun-Tracker*

R. C. Byxbee and D. R. Lott
Lockheed Missiles & Space Company
Sunnyvale, California

Because of the high cost and mechanical problems associated with large fixed solar arrays, sun tracking is of special interest to aerospace engineers. Moreover, since conventional electromechanical tracking systems have proved to be complicated and expensive, a passive approach is desirable. By utilizing solar energy to activate a bimetal helix, a passive Thermal Heliotrope is possible. This concept has been used successfully for louvers and thermal switches in thermal control. Initial model tests have proved the heliotrope concept, and development work is being performed to establish feasibility. Three types of Thermal Heliotrope are discussed: a reset tracker, an incremental tracker, and a seasonal adjuster.

I. Introduction

Power levels and mission durations continue to increase, adding to the emphasis on reliable solar array sun-tracking devices. Considerable weight and cost savings are available with tracking solar arrays. A non-oriented array in a tri-form configuration, for example, must be on the order of 3.7 times the area of a tracking array. This suggests penalties of 270 ft^2 of array area and well over half a million dollars for a 1-kW array. Solar array tracking mechanisms of the electromechanical type, which require electrical power for their operation, have been developed. The complexity of such electromechanical systems, however, may cause reliability problems. Table 1 shows some of the tracking systems currently available or under development.

The use of bimetallic elements has been flight-proved in thermal switches and louvers (see, for example, Ref. 5). This straightforward approach has been adapted to a sun-tracking device. This paper discusses several devices entitled Thermal Heliotropes (system F, Table 1), which use bimetals actuated by solar energy. These heliotropes evolved as an outgrowth of an earlier tracker that used electrically energized bimetallic spiral units (system A, Table 1). The Thermal Heliotropes have been successfully subjected to simulated orbit environments and have led to the study and development of a family of related sun-tracking systems. Unlike a previously reported passive system that used both bimetallic and expandable fluid systems (Ref. 6), the Thermal Heliotropes use only bimetallic elements for motive force.

*The work reported here was performed for the NASA Goddard Space Flight Center under Contract NAS 5-11637, Technical Officer, J. Fairbanks.

Table 1. Solar array tracking mechanisms

System	Description	Application	Type	Reference
A	Bidirectional single-axis heat motor	Led to patent disclosure in 1962 of system F thermal heliotrope	Semipassive (radiative reset)	LMSC[a]
B	Single-axis tracking and reset with secondary axis adjust (27 lb/300 oz-in.)	Qualified and flown	Electromechanical	Ref. 1, Part 1, p. 36
C	Single-axis tracking and reset (16 lb/700 oz-in.)	Qualified and flown	Electromechanical	Ref. 1, Part 1, p. 71
D	Two-axis continuous tracking (11 lb/60 oz-in.)	Qualified	Electromechanical	Ref. 2
E	Single-axis continuous tracking (20 lb/182 oz-in.)	Qualified and flown	Electromechanical	LMSC
F	Thermal Heliotrope	Under development and study	Passive	LMSC, Contract NAS 5-11637
G	Single-axis continuous tracking (11 lb)	Used for *Nimbus* solar paddles	Electromechanical	Ref. 3
H	Double-axis continuous tracking	Under development	Electromechanical	Ref. 4

[a]Lockheed Missiles & Space Company.

II. Theory of Bimetallic Thermostats

Bonding two or more dissimilar metals together in a strip sandwich produces a metal thermostat. The use of bimetallic thermostat devices is not new; the first patent for a brass–iron couple was awarded in 1831, and the principle had been known long before. Since then, many bi- and tri-metal systems have been developed. A temperature increase in the metal will cause one component to expand more than the other, creating a compressive stress in the high-expansion material and a tensile stress in the low-expansion material. Both stresses are created at the bond line, and since the stresses are uniform over the strip, it will deflect into an arc. Deflection formulas for specific elements such as helical coils are developed to yield thermal rotation and torque as a function of flexivity, modulus of elasticity, temperature, and coil geometry (Refs. 7 and 8).

Bimetals may be optimized for maximum work by making the component with the lower modulus of elasticity thicker than that with the higher modulus. The thicknesses should be inversely proportional to the square roots of the moduli. Also, for a given application, a minimum-volume device is obtained by applying half of the thermal action to produce force and half for deflection. Physically, a helical coil will produce more work per unit weight than a simple cantilevered element. A bimetal helix produces its work in the form of rotational motion, and restraining this motion to any degree produces torque. Unlike the action of a simple cantilevered strip, nearly all the curvature change in the helix is confined perpendicularly to the unwound length axis, thus producing some 50% more work (Ref. 9). The application of bimetallic helix theory to sun-seeking devices is a reliable passive method of solar array orientation.

III. Principles of Bimetallic Trackers

A bimetallic tracking device consists of two main components: (1) a heliotrope element, or helical bimetallic coil and (2) control mechanisms. The bimetallic coil, which produces torque and angular displacement with temperature change, acts as the motor element of the device. The control mechanism is generally a pair of shades, one to control the tracking rate and another to provide reset by cooling the coil.

A. Bimetallic Coil

A heliotrope tracker is shown schematically in Fig. 1. The coil is hard-mounted to the vehicle at one end and

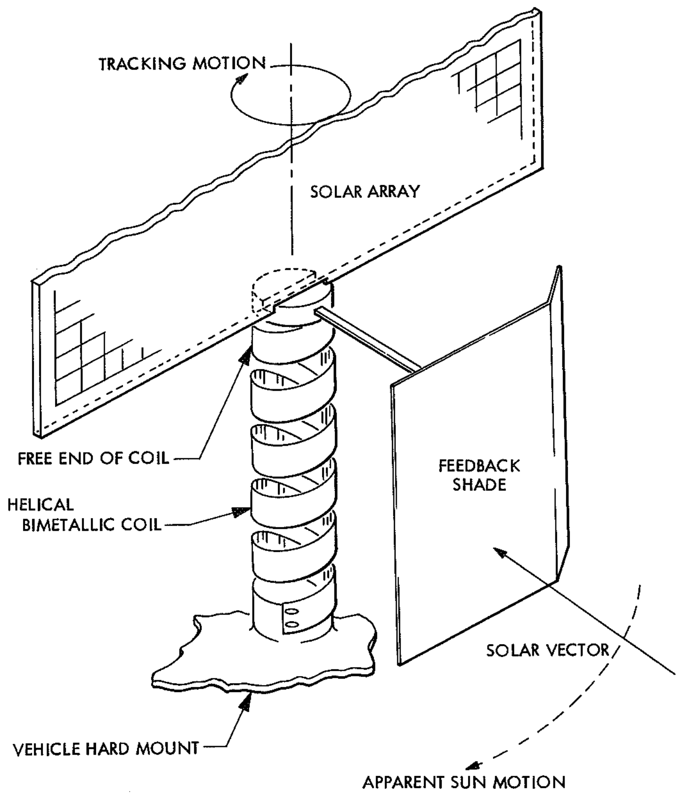

Fig. 1. Reset tracker

is free to rotate at the other. The free end of the coil is attached to the solar array. Misorientation of the array allows solar energy to reach the coil, causing a temperature rise and resultant rotation.

The main critical design parameter is coil sizing. For maximum available torque, it is desirable to have a relatively wide coil, since torque is directly proportional to width and the square of thickness. However, an important tradeoff is required here, since transient heating and cooling rates are inversely proportional to thickness. The design approach is to size the coil thickness to provide the necessary thermal response and to maximize the width within the limits of the physical size and winding diameter.

Other design considerations include the type of thermal coatings applied to the coil. It is desirable to have a high solar absorptance and relatively low emittance in order to have a high operating temperature. Even with fairly low emittance values, the thermal response in cooling is improved as a result of higher operating temperatures (approximately 200°F).

The coil must be given a stabilizing heat treatment after winding. This redistributes stresses induced by manufacturing processes and winding. Because the redistribution of stresses causes a permanent deformation in the coil, allowances must be made at the time of winding. After heat treatment, the bimetallic coil is thermally stable within the temperature limit of the treatment.

B. Control Mechanisms

The control mechanism in the Thermal Heliotrope usually consists of two shade systems: (1) the feedback shade and (2) the reset shade. For some configurations, however, one shade provides both feedback and reset functions.

1. Feedback shade. The function of the feedback shade is to provide tracking rate control. It is attached to the array and the free end of the coil. The heliotrope element is sized to provide rotation at a greater rate than that of the vehicle around the orbit. So, to prevent overtracking, a feedback shade is used. As shown in Fig. 1, for example, when the array is sun-oriented, the feedback shade prevents full exposure of the coil to incident solar energy. The coil operates at a quasi-steady-state temperature. Misorientation of the array allows the coil to become illuminated, thus causing a temperature rise. The array and shade will then track clockwise into the sun until the coil is again partially shaded.

2. Reset shade. For each angular degree of windup, the heliotrope element must reset an equal amount. This is accomplished by cooling the coil. Shading the coil from solar illumination will cause radiative cooling and hence a reset action. The shading may be provided by earth eclipse or by mechanical means.

For most low earth orbits, the vehicle is shaded by the earth's shadow for a portion of every orbit. On a three-axis-stabilized vehicle, for example, tracking takes place during the illuminated portion of the orbit, winding up the coil some 200 or more degrees. When the vehicle enters the earth's shadow, the coil cools, and the solar panel resets to a stop, ready for normal exposure upon reentry into the illuminated portion of orbit (see Fig. 2). This cycle occurs once per orbit.

The reset approach to high-orbit applications such as synchronous orbit (where a daily eclipse does not always occur) does not depend on earth shadow for reset cooling. Instead, the reset shade time is provided with a mechanically actuated shade. One method of providing

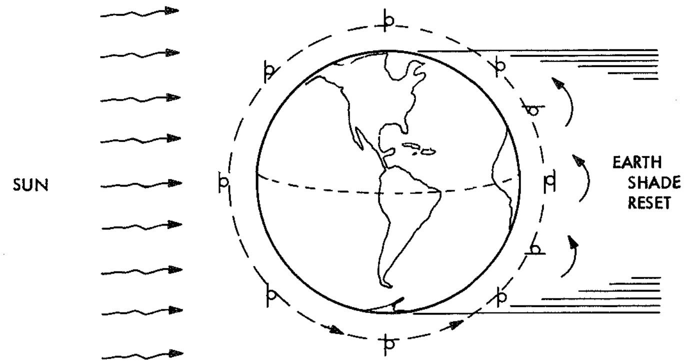

Fig. 2. Reset heliotrope using earth shade

this shade time utilizes a fixed shade on the vehicle proper. Once per orbit, the entire coil assembly is shaded for a given period depending on physical shade size and distance from the coil. Another method of providing reset shading is by using a flip shade, which shades the coil for a period once per orbit. The flip shade may be actuated by a mechanical trip governed by array position or by a small secondary bimetallic element that functions when tracking capacity is lost at the end of an orbit. The flip shade stops solar illumination of the coil until the array has reset.

IV. Thermal Heliotrope Devices

Three types of Thermal Heliotrope devices have been fabricated and tested. Reset trackers reset once per day and therefore do not require a slip ring interface between the solar array and the vehicle. On the other hand, continuous trackers are unidirectional, and slip rings are required. Seasonal adjusters track only plus and minus a given angle and do not require slip rings. The specific purposes and principles of these trackers are given below.

A. Reset Tracker

The first type of Thermal Heliotrope is very similar to that shown in Fig. 1 and is referred to as a reset tracker. One end of a bimetallic coil is fixed to the vehicle and the other to the solar array. Pitch axis tracking is provided with rate control by a feedback shade. Either earth shade or a reset shade may be used to effect full reset of the coil.

B. Continuous Incremental Tracker

The second and most versatile type of Thermal Heliotrope is a continuous incremental tracker. That is, tracking occurs in small-angle increments instead of smooth motion. This device may be used for pitch axis tracking at any altitude. Since only 5% incident energy is lost by solar panel misorientation of ± 18 deg, tracking increments need not be minute. By the provision of 20 increments of tracking per revolution, illumination loss is reduced to 1.23%. Figure 3 schematically illustrates the action of an incremental tracking device. In operation, misorientation of the panel allows solar energy to illuminate the helix. Rotation of the helix is restrained by a spring-loaded detent. When the panel is disoriented enough to expose nearly all of the helix, enough torque is produced to snap the wheel to the next detent. In the new position, the coil is shaded by the combination feedback–reset shade. The coil element then cools and resets through a ratchet until illuminated again at a later orbit position. The snap action work is stored in a small spring, and the damped output of the spring orients the solar panel in a few seconds. Variations of the incremental trackers include a device that will orient itself from any degree of initial misorientation.

C. Seasonal Adjuster

The third type of Thermal Heliotrope (seasonal adjuster) is used for making seasonal adjustments to the array about the roll axis of the vehicle (Fig. 4). On some vehicles, seasonal adjustment is not necessary. For instance, the *Nimbus 1* and *2* vehicles had an inclination-altitude orbit such that a uniform daily retrogression occurred, resulting in a constant low orbit–sun angle, minimizing benefits obtainable from seasonal adjustments (Ref. 3). For a vehicle having an orbit–sun angle of nearly 90 deg, such as SERT II (an ion propulsion experiment), the array will be continuously in the sun and will have a very high effectivity (integrated projected area per revolution). Also, a zero-angle vehicle is not affected by seasonal changes. Except for the specific cases mentioned above, nearly all vehicles can benefit from seasonal adjustments. Many low-altitude, earth-orbiting vehicles are flown where it is not feasible to use a continuously tracking array because of propulsion weight penalties associated with drag make-up. In these cases, the arrays are deployed in the pitch-roll plane in such a way that the array leading edges present a minimum frontal profile to the line of flight. Small incremental changes in the array position about the roll axis of the vehicle (seasonal alpha angle adjustments) can dramatically improve the efficiency of the solar arrays by increasing their effectivity. Figure 5 illustrates the results of a study to determine the necessity of seasonal adjustments. Note how array effectivity improves with

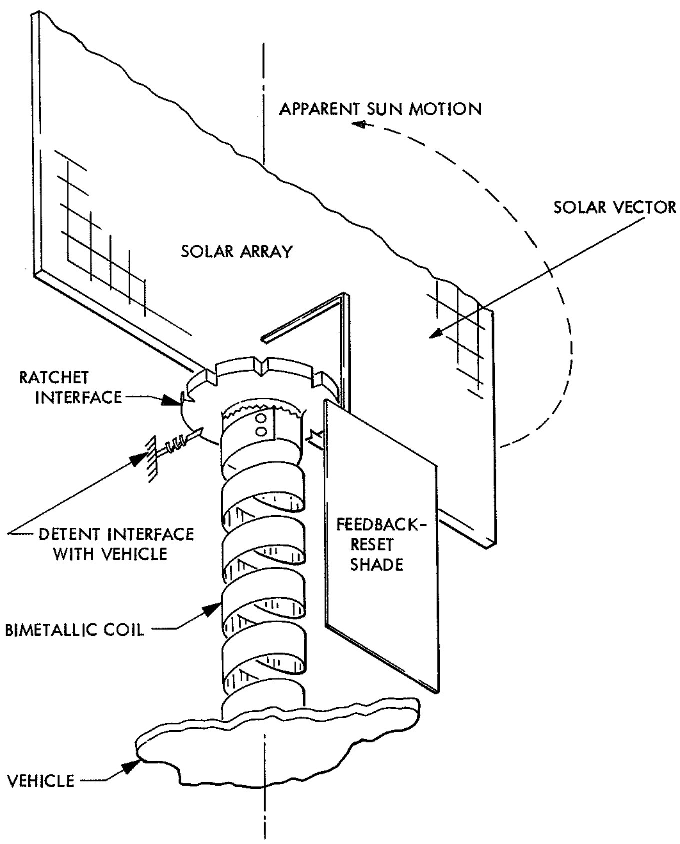

Fig. 3. Continuous incremental tracker

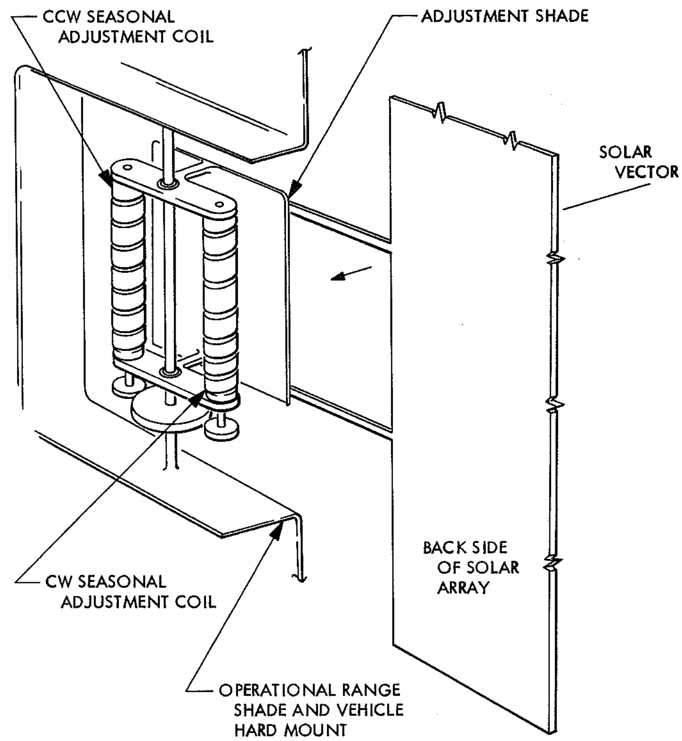

Fig. 4. Seasonal adjuster

simple 5-deg seasonal adjustments for various orbit–sun angles up to ± 60 deg.

The seasonal adjuster depicted schematically in Fig. 4 consists of two oppositely wound coils. The plus helix effects clockwise rotational adjustments about the vehicle roll axis, and the minus helix effects counterclockwise adjustments. When either coil is illuminated, it engages the solar array and rotates it to a normal sun position. The adjustment shade prevents rotation when the array is oriented. The optimum orbit position for effecting array seasonal adjustments is as the vehicle passes through the orbit point nearest the sun. Therefore, this type of heliotrope is positioned in such a way that it is shaded except in this region. Shading in the latter region is provided by the operational range shade.

V. Conclusions

The feasibility of Thermal Heliotropes has been demonstrated via fabrication and testing of such devices in simulated orbit conditions. Reliability is greatly enhanced because of the relative simplicity, the lack of dependence on supplementary electric power, and the major parts count reduction. A developed Thermal Heliotrope had six parts and replaced an existing electromechanical device that had over 100 parts. Design parameters of bimetal width and thickness have been found to be most important. Other factors influencing design are bimetal couple choice, coil active length, thermal coatings, and shade configuration. Major area, weight, and cost savings can be realized with the use of tracking arrays, and the development of passive sun-tracking devices can add to space power system growth and versatility, thus expanding the operational range and duration of many solar photovoltaic powered spacecraft.

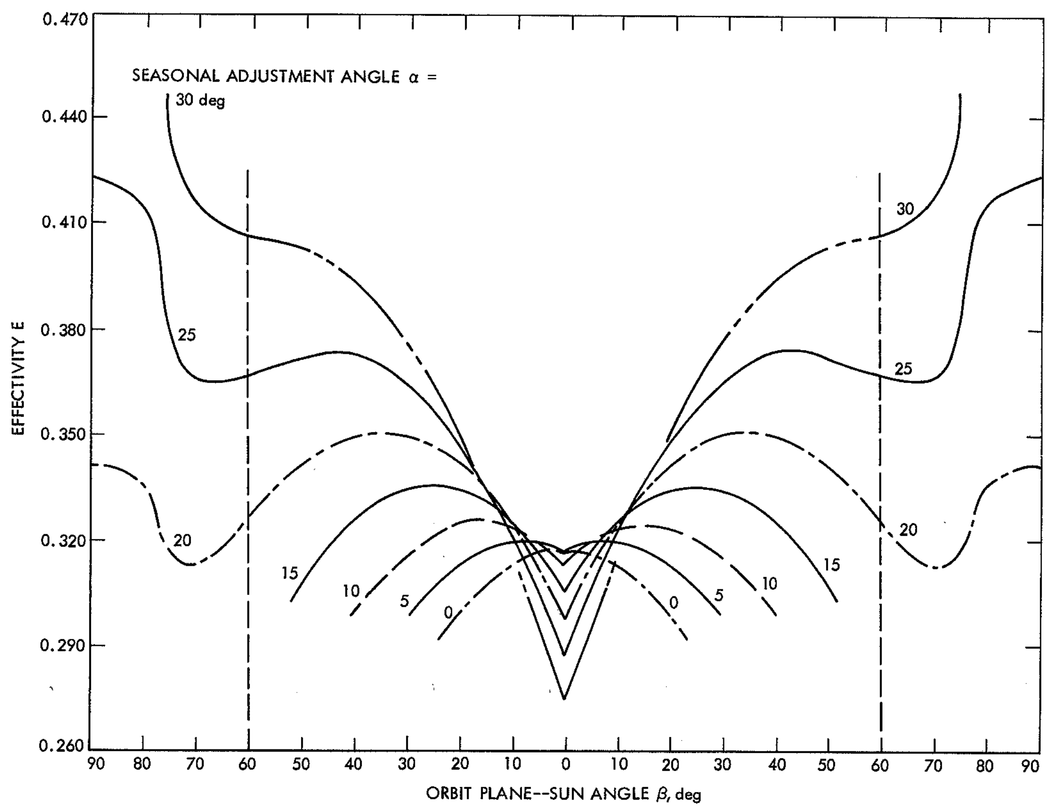

Fig. 5. Improvement in array effectivity as a function of seasonal adjustments vs orbit plane angle. The most useful range for seasonal adjustment lies between the vertical dotted lines

References

1. Lott, D. R., *Pictorial Review of Lockheed Capability in Solar Photovoltaic and Battery Electrical Power Systems*, LMSC A-834772. Lockheed Missiles & Space Company, Sunnyvale, Calif., Apr. 1967.

2. Savage, P. G., *Analysis of the Zombie Two-Axis Solar Array Servo System*, LMSC A-376457. Lockheed Missiles & Space Company, Sunnyvale, Calif., July 1963.

3. Merten, K. F., Hanson, K. L., and Schlotter, W. J., *Nimbus 2: Photovoltaic Power Systems on Flight Spacecraft*, 68SD4222. General Electric Company, Missile & Space Division, Philadelphia, Pa., Feb. 23, 1968.

4. Turner, W. N., and Olson, M. C., *Orientation Linkage for a Solar Cell Array: OLSCA*, Final Report, SSD-80221R. Hughes Aircraft Company, Space Systems Division, El Segundo, Calif., July 1968.

5. Deal, T. E., "The Surveyor Thermal Switch," in *Proceedings of the 2nd Aerospace Mechanisms Symposium*, Technical Memorandum 33-355. Jet Propulsion Laboratory, Pasadena, Calif., Aug. 15, 1967.

6. Samuels, R. L., "A Passive Solar Panel Orientation Servomechanism," in *Proceedings of the 3rd Aerospace Mechanisms Symposium*, Technical Memorandum 33-382. Jet Propulsion Laboratory, Pasadena, Calif., Oct. 1, 1968.

7. Timoshenko, "Analysis of Bimetal Thermostats," *J. Opt. Soc. Am.*, Vol. 11, No. 3, pp. 233–255, Sept. 1925.

8. *Truflex Thermostat Metals*, Catalog TRU-1B. Texas Instruments Inc., Dallas, Tex., 1966.

9. Alban, C. F., "Maximum-Work Bimetals," *Machine Des.*, p. 143, Apr. 16, 1959.

Page intentionally left blank

70N21444

A Nutation Damper for a Spinning Satellite

N. I. Totah and R. Rollins
Philco-Ford Corporation
Space and Re-entry Systems Division
Palo Alto, California

This paper discusses the design, testing, and fabrication of a nutation damper for a small spinning satellite. The factors influencing selection of the damping technique are discussed, along with some of the parametric studies to determine damper parameters. The damper discussed is a ball-in-tube type that employs a gas as the damping fluid. An analogy is drawn between the performance of the damper on the satellite and on a pendulum test fixture, enabling the use of test data for predicting flight performance. Finally, manufacturing techniques necessary for achieving the low stiction[1] level are discussed.

I. Introduction

Spin-stabilized satellites frequently require a means of damping the spacecraft nutation induced by the attitude control system or by an orbit maintenance system (Ref. 1). Given enough time, structural damping will remove the cross-axis energy, but waiting may not be acceptable since system performance is degraded during this time. Such is the case of a Philco-Ford satellite for which it is desired to minimize the time after maneuvers that system performance is degraded. To achieve a shorter time-constant, a passive nutation damper of the ball-in-tube type has been designed. The damper is to provide a nutation angle decay time-constant of less than 6 min and to reduce residual satellite nutation to less than 0.2 deg.

The ball-in-tube damper (Ref. 2) is similar to other fluid/bob dampers in that it depends on the relative motion of the ball within the tube to produce energy dissipation. The tube is curved to provide a centrifugal spring, and it is mounted in such a way that the plane of the curve contains the spin axis.

The design problem amounted to selecting a mounting location and damper parameters to meet the requirements discussed above. Those parameters are the ball mass, the length and radius of curvature of the tube, the tube–ball gap size and the damping fluid. After these parameters had been determined, it was necessary to test performance in a 1-g field.

The paper starts with a comparison of some of the passive damping techniques available and a discussion of some of the criteria influencing damper selection, followed by a description of the analytical model used and the parametric studies done. Finally, testing and manufacturing techniques are discussed.

[1]Static friction.

II. Selection of Damper Configuration

Several passive techniques are available for providing the required energy dissipation to damp nutation of spinning satellites (Refs. 2–4). Such techniques include impact dampers, magnetic hysteresis dampers, magnetic eddy current dampers (all used by Philco) and fluid-filled containers with or without moving bobs (used on OSO-1,[2] *Pioneer I*, and *Telstar*). The ball-in-tube damper is a specific example of the latter.

A typical impact damper could be a pendulum with the hinge axis normal to the satellite spin axis. Lossy stops would dissipate energy when the pendulum mass impacts them. A potential problem arises, however, if damping at small nutation angles is required. The minimum damping angle may be reduced by decreasing the distance between the stops, but this is done at the sacrifice of efficient large-angle damping. This disadvantage makes an impact damper impractical for meeting the damping requirements of this application.

Magnetic hysteresis dampers also rely on relative motion inside the spacecraft for energy dissipation. A typical configuration could be a magnet on a pendulum. The relative motion of the pendulum would move the air gap of the magnet over a material with high hysteresis losses, thereby dissipating energy by causing the material to traverse a hysteresis loop. An alternative would be to fix the magnet(s) and let the hysteresis material undergo relative motion. Difficulties that may be encountered using this technique are excessive magnet weight, difficulty in meeting vibration specifications, uncertainty in characteristics of the hysteresis material, maintaining gap tolerances, etc. Because of high magnet weights and close tolerances, it may be necessary to cage the moving part to ensure undamaged survival of the launch phase, and this adds complexity to the damper. The prime advantage of the magnetic hysteresis damper is that it need not be sealed; i.e., it can remain open to hard vacuum.

Magnetic eddy current dampers use the eddy currents generated in a conductor by a changing magnetic field. Generally, the changing magnetic field is obtained either by moving a permanent magnet near a conductor or by moving a conductor through the working gap of a permanent magnet. Thus, a pendulum type of configuration is again convenient for obtaining the relative motion required. Because of the similarity of this configuration to the magnetic hysteresis damper, it suffers from many of the same disadvantages and difficulties. It does have an advantage over the hysteresis damper from an analytical point of view: the damping torque is a linear function of the relative velocity, making performance prediction more certain. Again, no sealing is required.

Many dampers for spinning satellites use a mass moving in a fluid. One common technique is to use a pendulum moving in a viscous fluid. Another is to use a ball rolling or sliding in a viscous fluid in a straight or curved tube. Variations of both these techniques have provided successful dampers for spacecraft in the past. Using a liquid for the damping medium can present a potential weight problem if the required travel distance of the bob is very great, since the liquid must fill a large volume. Use of a gas as the damping medium largely eliminates this potential problem, but obtaining the required damping coefficient will then usually entail using closer tolerances than would be required in a liquid system.

The Philco-Ford satellite is a dual-spin system with an antenna that is despun to point always toward the earth's center. However, the moment of inertia of the despun section is so small with respect to the rest of the satellite that the analysis assumes a single-spin system.[3,4] In a single-spin system, selecting a required energy dissipation rate is a function of the desired time constant and expected cross-axis energy levels. Thus, a satellite with a very large cross-axis inertia would require a higher energy dissipation rate to achieve a given time constant than one having a small cross-axis inertia.

For dual-spin systems with an appreciable despun section, the damper requirements are essentially the same as for a single-spin system; if the spinning section is spinning about its axis of least inertia, then the requirement for spin axis stability is that the energy dissipation rate on the despun section be greater than on the spinning section. On the spinning portion, the primary sources for energy dissipation will be fuel slosh and structural damping. Since both of these are difficult to predict with any accuracy, the damper must be capable of dissipating more than enough energy to make up for the uncertainty. Because of the potentially high damping requirements and the different environment (e.g., no centrifugal force and different excitation frequencies), the damper configuration will often be different than for single-spin systems.

[2]*Orbiting Solar Observatory.*

[3]The significant parameters are $I_3 = 22.8$ slug-ft^2, $I_1 = I_2 = 17.6$ slug-ft^2, $\Omega = 90$ rev/min, $I_{despun\ section} = 0.17$ slug-ft^2.

[4]Mathematical symbols are defined in the Nomenclature section and in Fig. 4.

The technique utilized for this application is a ball that rolls in a curved, gas-filled tube. The damping coefficient is controlled by controlling the viscous drag of the gas on the ball as the ball rolls back and forth in the tube. The desired spring constant is obtained by curving the tube and placing it at an appropriate distance from the spacecraft spin axis. The disadvantage of the ball-in-tube damper is that, like all fluid dampers, it must be sealed. However, it is extremely simple, and its life is limited only by the length of time that the internal gas can be contained. The very light weight and simplicity were the reasons for choosing this technique for this application.

III. Analytical Model

The equations of motion of the system shown in Fig. 1 may be derived by using the Lagrangian approach with a Rayleigh dissipation function or by employing the Newtonian method for two rigid, hinged bodies. Using either method, and upon linearizing, one obtains a set of differential equations (Ref. 2).

Through the use of the "energy sink" method (Refs. 3 and 5), an approximate solution may be obtained in the form of expressions for nutation decay rates τ_s and residual nutation angle η_{res}. An exact solution can be obtained, of course, by determining the roots of the characteristic equation.

IV. Selection of Damper Parameters

In order to select the desired set of damper parameters, a series of parametric studies was performed, varying c, m, h, R, and Ω and solving for τ_s using a digital computer root-finding program. By varying these parameters, it is possible to "tune" the damper to provide optimum performance in terms of damping time constant. However, it is not desirable to tune the damper too sharply, as manufacturing tolerances, spin rate changes, and temperature variations would then give rise to too large a variation in damping time constant.

Vehicle spin rate Ω is not a variable that can be chosen to enhance performance but is, instead, a part of the environment over which the damper must operate satisfactorily. Nominally, the spin rate is not expected to go outside the range of 76 to 105 rev/min. For the nominal values of the other parameters chosen, the damping time constant τ_s varied from 157 to 197 s over this spin rate range. This is well within the desired performance.

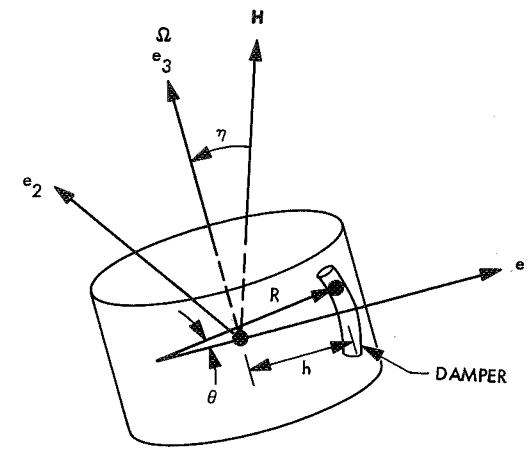

Fig. 1. Model of satellite and damper

Selection of the mass of the ball is an iterative process, with the initial guess correlated with previous experience. More detailed analysis shows whether the mass initially selected is more or less than that required. A mass of 0.0029 slug was chosen for this design by this process.

In implementing a desired spring constant, both R and h have to be considered. At a given mounting location h, there will exist an optimum radius of curvature R, and vice versa. The maximum mounting radius was limited by the radius of the spacecraft. For a given R, increasing h is equivalent to increasing the spring restraint on the ball. Likewise, for a given mounting location, decreasing R is the same as increasing the spring restraint. Figure 2 shows the damping time-constant as a function of the damping coefficient c for various values of R. The time constant reaches a minimum for $R = 15.5$ ft at a mounting location 1.92 ft from the spin axis. Performance for $R = 10$ is better than for $R = 7$, but sensitivity to changes in c are greater for $R = 10$. Also, tube misalignment on the satellite causes the ball to seek a new equilibrium off the center of the tube. The equilibrium shift is given by

$$\Delta_e = R\phi_M$$

where

Δ_e = equilibrium shift

ϕ_M = misalignment tolerance

The alignment sensitivity consideration indicates that the large radius of curvature should be reduced. A compromise of $R = 7$ ft was selected for the final design.

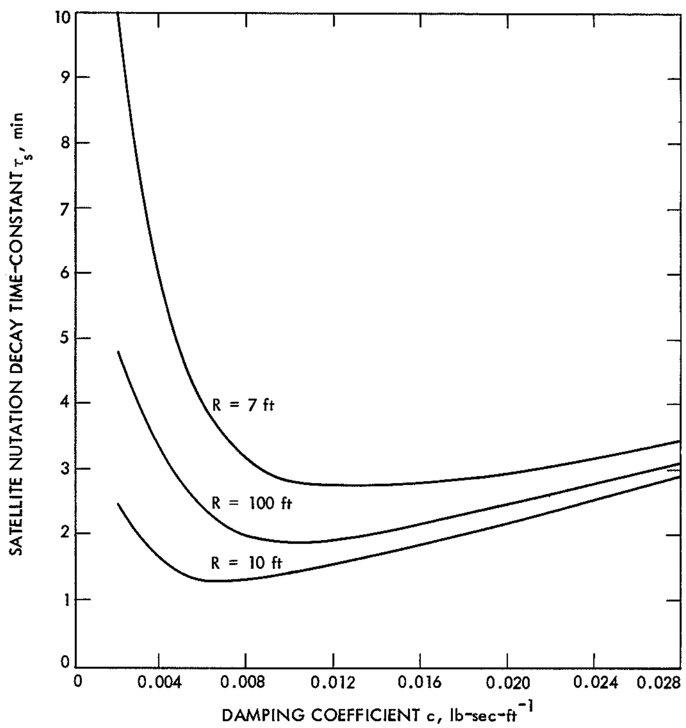

Fig. 2. Satellite nutation time-constant vs damper damping coefficient

The damper drag coefficient was finally specified to be 0.008 to 0.030 lb-s/ft, giving a variation in damping time constant of 164 to 220 s.

After the selection of c, m, h, and R, the length of the tube is selected by finding the amplification factor (i.e., the ratio of ball angular motion to satellite angular motion) and determining the maximum nutation angle for which damping is required. For this application, a tube length of 12 in. was selected.

V. Experimental Evaluation of Damper

A. Design of Pendulum Test Fixture

Because of the complexities inherent in any efforts to evaluate the damper on a simulated satellite, the method employed here is based on simply evaluating the damper's key characteristics[5] (i.e., the damping coefficient c and the sphere's stiction threshold θ_{res}) and using these data in the spacecraft equations of motion to determine system performance. Unfortunately, the ball-in-tube configuration does not lend itself to direct laboratory evaluations of this sort unless sophisticated X-ray equipment is readily available. For this reason, a pendulous device (a metronome) was designed and used to assess the damper's performance, as shown diagrammatically in Fig. 3.

The pendulum itself is shown in Fig. 4. It consists of a ¾-in. aluminum rod, at the ends of which are attached two equal masses. The position of the pivot point is arbitrary as long as it is not coincident with the pendulum's center of mass. The critical parameters of the pendulum are its weight and the location of the damper and the system's center of mass from the pivot. The total length and the location of the tip masses are entirely arbitrary.

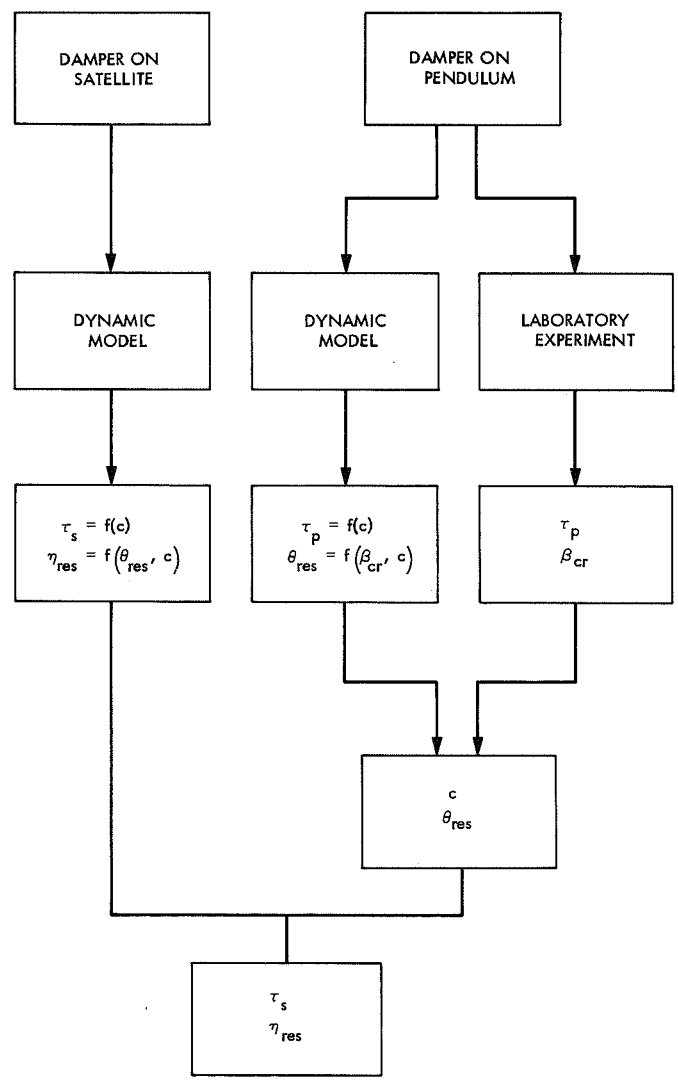

Fig. 3. Diagram of steps taken in inferring orbital behavior from laboratory tests

[5]These are the only parameters not readily obtainable physically.

B. Pendulum Equations

In deriving the damper-pendulum equations of motion, it was considered that ambient air damping is negligible, that the sphere rolls without slipping, and that $R \pm r = R$.

The equations were derived using the Lagrangian method with a Rayleigh dissipation function.

A solution of these equations (i.e., the degree of stability) was obtained using an approximate method (for initial parametric studies) (Ref. 6) and, eventually, for actual damper evaluation, by using a computerized root-finding program. The results of the former approach, in closed form, are

$$\tau_p = -\frac{a_1 a_2 a_3 - a_0 a_3^2 - a_1^2 a_4}{2a_3(a_1 a_3 + a_2^2 - 4a_0 a_4)} \tag{1}$$

where

$$a_0 = (mgR)(MgD - mgD)$$

$$a_1 = (cR^2)(mgR + Mgd - mgD)$$

$$a_2 = (mgR)\left[M(d^2 + k^2) + mD^2 + \frac{2}{5}mR^2 + \frac{7}{5}MRd - \frac{7}{5}mRD\right]$$

$$a_3 = (cR^2)\left[M(d^2 + k^2) + mD^2 + mR^2 - 2mDR\right]$$

$$a_4 = (m^2R^2)\left[\frac{7M}{5m}(d^2 + k^2) + \frac{2}{5}D^2 + \frac{2}{5}R^2 - \frac{4}{5}DR\right]$$

and

$$\theta_{\text{res}} = \left(\left\{\left(\frac{\lambda^2 b_4^2}{b_1^2}\right)\left[\frac{\left(\frac{b_3}{b_4}\right)^2 + \lambda^2}{\left(\frac{b_2}{b_1} - \lambda^2\right)^2 + \left(\frac{b_3}{b_1}\right)^2 \lambda^2}\right]\right\} - 1\right)\beta_{\text{cr}} \tag{2}$$

where

$$\lambda^2 = \frac{Mgd - mgD}{M(d^2 + k^2) + mD^2 + \frac{2}{5}mR^2}$$

$$b_1 = \frac{7}{5}mR^2; \qquad b_2 = mgR$$

$$b_3 = cR^2; \qquad b_4 = mDR + \frac{2}{5}mR^2$$

and where

β_{cr} = pendulum amplitude when the damper ceases operating due to its stiction level.

C. Experimental Procedure

The equations relate τ_p to c and θ_{res} to β_{cr}. In order to determine τ_p and β_{cr}, the pendulum amplitude is plotted vs elapsed time yielding a graph as shown in Fig. 5. From this experimental plot, τ_p is determined by simply observing the time for $\beta_{\max}$ to diminish to a value of $1/e\ \beta_{\max}$. Since τ_p is a constant as long as the damper is operating, a plot of $\beta = \beta_0 \exp(-t/\tau_p)$ superimposed on the experimental plot will allow determination of β_{cr}, which will be the value of $\beta_{\max}$ when the two plots begin to diverge.

The values of τ_p and β_{cr}, obtained in this way, are now used in Eqs. (1) and (2) to determine c and θ_{res}. These values, in turn, are used in the satellite-damper equations to determine τ_s and η_{res}.

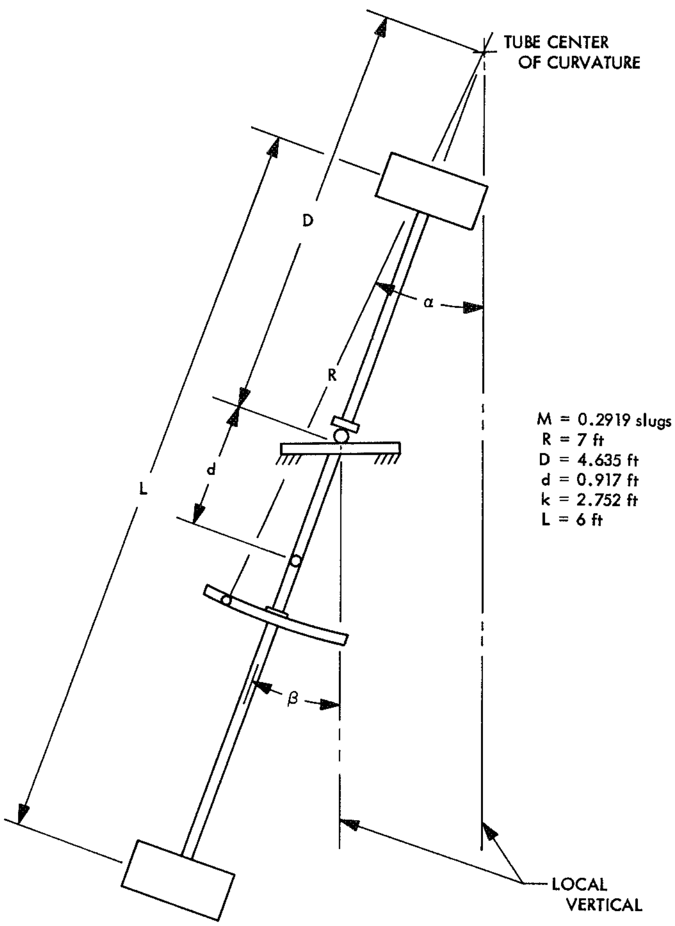

Fig. 4. Pendulum

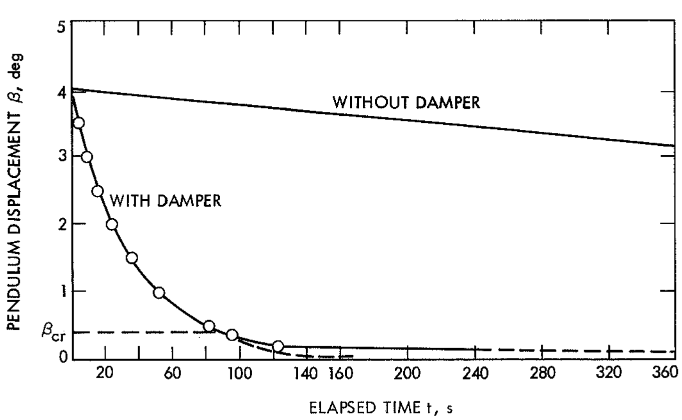

Fig. 5. Pendulum oscillation decay (experimental)

Testing of the completed damper yielded values of c and θ_{res} of 0.018 lb-s/ft and 0.02 deg respectively. In terms of satellite performance, these represent a nutation angle decay time constant of $\tau_s = 180$ s and a residual nutation of $\eta_{res} = 0.025$ deg.

VI. Damper Design and Manufacture

A. Materials

The damper tube (Fig. 6) is made of 6061-T6 aluminum, chosen because of its availability, strength, and workability. The sphere is tungsten-carbide; this material was chosen for its high density. In selecting a gaseous damping fluid, consideration was given mainly to viscosity, inertness, and viscosity variation due to temperature changes, with emphasis on the latter. The gas chosen is nitrogen at 1 atm, mixed in a 9:1 ratio with helium for leak detection. The design requirements specified a tube ID finish of <16 μin. rms, a bend radius of 7 $\pm$0.5 ft, a length of 12 in. and a tube–ball gap[6] (tube ID minus sphere diameter) of 0.007 $\pm$0.001 in.

B. Manufacture

The damper tube was acquired from tube stock of ¾ in. OD. In order to obtain the finish and the required gap (sphere size is 0.6875 in.), the tube was internally honed to an ID of 0.6935 to 0.6955 in. (a Sheffield air gauge was used to measure the ID). The tube was then bent on a template to obtain the 7-ft radius. To maintain circularity, a mandrel was inserted in the tube. Sealing the tube ends was accomplished by arc welding the two end caps while the entire assembly was in a controlled-environment chamber containing 90% nitrogen and 10% helium at 1 atm pressure. Because of the long-life requirements (>5 yr) the weld is required to have a leakage rate not in excess of 10^{-9} cm^3/s under a vacuum of 10^{-4} torr.

Those seemingly simple manufacturing operations proved to be the major problem area of the entire damper development. First, the honing operation resulted in the scrapping of 70% of the tubes. Second, three tubes were required in order to discover that to obtain a 7-ft bend-radius, a 5-ft radius template is required, because of the tube's elasticity. Lastly, the welding operation became a hit-and-miss proposition. High leakage rates necessitated rewelding a number of the units.

In assessing the reasons for these early problems, it was concluded that most of the failures are attributable to: (1) normal operator learning curve, and (2) initial reluctance of manufacturing personnel to place sufficient importance on such an insignificant-looking device.

[6]This value of the gap was based on an earlier study of damping coefficient vs gap (Ref. 7).

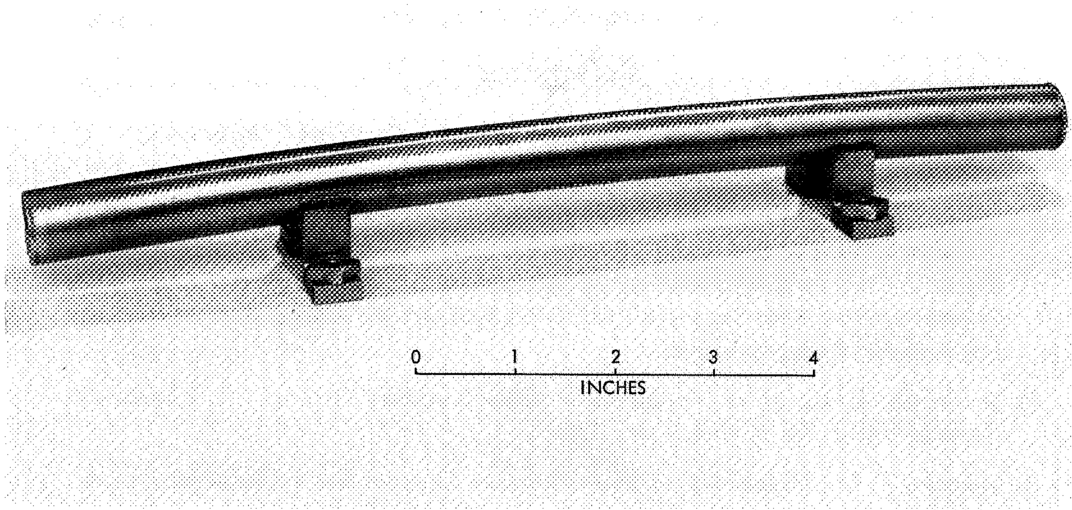

Fig. 6. Nutation damper assembly

VII. Conclusions

The feasibility of using a gas as the damping fluid in a ball-in-tube damper is established. This approach provides one of the simplest and lightest devices used in passive nutation damping. While this damper's decay-time capability is not especially outstanding, its threshold level is. Laboratory tests reveal a capability of reducing satellite nutation angles to 1.5 arc-minutes. Other features include the damper performance's relative insensitivity to temperature and the damper's ruggedness in withstanding launch loads.

Nomenclature

c	damping coefficient
e_1,e_2,e_3	body-fixed principal axes
I_1,I_2,I_3	spacecraft moments of inertia
g	gravitational constant
h	location of damper relative to satellite's center of mass
$\mathbf{H}$	angular momentum
k	pendulum radius of gyration relative to pendulum's center of mass
m	damper sphere mass
M	pendulum mass
r	damper sphere radius
R	damper tube radius of curvature
t	elapsed time
β	pendulum amplitude
η	nutation angle
θ	angular displacement of sphere relative to tube $(\alpha - \beta)$
τ_p	pendulum decay time-constant
τ_s	spacecraft nutation angle decay time-constant
Ω	vehicle spin rate

Subscripts

cr	critical
max	maximum
res	residual

References

1. Reiter, G., "Theory and Design of Nutation Dampers," *Proceedings of Symposium on Attitude Stabilization and Control of Dual-Spin Spacecraft*, TR-0158(3307-01)-16. Aerospace Corporation, Los Angeles, Calif., Nov. 1967.

2. Auelmann, R. R., and Lane, P. T., "Design and Analysis of Ball-in-Tube Nutation Dampers," *Proceedings of Symposium on Attitude Stabilization and Control of Dual-Spin Spacecraft*, TR-0158(3307-01)-16. Aerospace Corporation, Los Angeles, Calif., Nov. 1967.

3. Wadleigh, K. H., et al., "Spinning Vehicle Nutation Damper," *J. Spacecraft Rockets*, Vol. 1, No. 6, Nov.–Dec. 1964.

4. Spencer, T. M., "Cantilevered-Mass Nutation Damper for a Dual-Spin Spacecraft," *Proceedings of the Symposium on Attitude Stabilization and Control of Dual-Spin Spacecraft*, TR-0158(3307-01)-16. Aerospace Corporation, Los Angeles, Calif., Nov. 1967.

5. Thomson, W. T., and Reiter, G. S., "Attitude Drift of Space Vehicles," *J. Astronautical Sci.*, Vol. VII, Nov. 2, 1960.

6. Fuller, A. T., and MacMillan, R. H., "Expressions for the Damping and Natural Frequency of Linear Systems," *Quart. J. Mech. Appl. Math.*, Vol. IX, Part 3, 1956.

7. Bauer, A. B., and Du Puis, R. A., "Fluid Drag on a Sphere Rolling in a Tube," *J. Appl. Mech.*, Preprint 67-APM-18, 1967.

70N21445

30-ft-Diam Antenna for the ATS F and G Synchronous Satellite*

R. R. Carman and E. Rottmayer
Goodyear Aerospace Corporation
Akron, Ohio

One of the main elements in the ATS (Applications Technology Satellite) F and G synchronous satellite is the 30-ft-diam antenna that will be used in space communications experiments. A full-scale model of the antenna has been designed, fabricated, and tested by Goodyear Aerospace Corporation. The design employed in the antenna is referred to as a curved hinge-line concept and offers structural continuity, close surface tolerances, and high reliability for successful erection. This paper describes the basic concept and its particular application to the ATS F and G antenna.

I. Introduction

To meet the stringent volume and reliability restrictions on space-deployable structures, a design was conceived and patented for a large, one-piece, compound-curvature surface that can be packaged in a relatively small volume and automatically deployed in space.[1] This concept, providing a structurally efficient arrangement in the packaged configuration and using conventional materials in the construction of the design, was applied later to the 30-ft-diam ATS F and G antenna that was designed to operate in the X band after the satellite is in synchronous orbit. The curved hinge-line concept has many potential applications for space. For example, it can be used to reflect solar energy or radio frequency energy, to mount solar cells, or to serve as a sun shield.

II. Curved Hinge-Line Concept

The curved hinge-line concept is a design that permits a surface with compound curvature, such as a paraboloid of revolution, to be cut straight along radial or nearly radial lines to make a number of segments or petals. These petals are connected by hinges to provide structural continuity in the deployed configuration. Proper design permits the petals to be straightened out along the hinge line, and the two adjacent petals are folded with respect to one another. In this manner, the paraboloid is transferred into a conical shape, and the original curved hinge lines become straight-line elements of the

*The application of the curved hinge-line concept to the ATS F and G antenna was performed by Goodyear Aerospace Corporation, Akron, Ohio, under Contract NAS 5-10318 from the NASA Goddard Space Flight Center. The report number assigned to this paper by Goodyear Aerospace Corporation is GER-14254.

[1]Carman, R. R., and Pipitone, S. J., *Collapsible Dish Reflector*, U. S. Patent 3,397,399 (assigned to the Goodyear Aerospace Corporation, Akron, Ohio). U.S. Department of Commerce, Washington, Aug. 13, 1968.

cone. Considerable design latitude is permissible in the final packaged shape, and each particular application must be studied to determine the best design. Deployment is achieved by controlling the motion of a point near the midspan of the petal intersections and can be accomplished in a number of ways.

When the petals first unfold, they act as parts in a linkage with virtually no force required. As the surface approaches its final shape, there is a position where unfolding will not progress as a simple linkage. The circumferential members have an excess length, and a small force is required to push the petals through this near-final position. After the attachment point is brought to rest at the proper position, the petals are then at their original fabricated position and in a zero-strain condition.

III. ATS F and G Application

Figure 1 shows the completed antenna in packaged, partially deployed, and fully deployed positions. The antenna consists of (1) the deployable reflector (30-ft diam, (focal length)/diameter = [illegible]4), (2) the deployment system, (3) the feed support, and (4) two equipment modules that were simulated structures for this model. One equipment module is at the focal plane and the other is at the reflector apex; they are referred to as the earth-viewing module and the aft module, respectively. The packaged (or launch) configuration has been designed to the constraints of an *Atlas/Centaur* launch vehicle.

The significant results obtained to date by analysis and/or test are as follows:

(1) The antenna gain varies from 50.8 to 53.7 dB at 8 GHz, depending upon the orbital position (50 dB required).

(2) The unit weight of the reflector and the deployment system is 0.22 lb/ft^2 (0.30 lb/ft^2 required). The unit weight of the reflector alone is 0.06 lb/ft^2.

(3) The natural frequency of the reflector in the deployed configuration is 4 Hz (2.5 Hz required).

(4) Four unqualified successful deployments, made under 1 g without aids, demonstrated good repeatability of the contour.

(5) Fabrication accuracy of the reflector contour was within ±0.015 in.

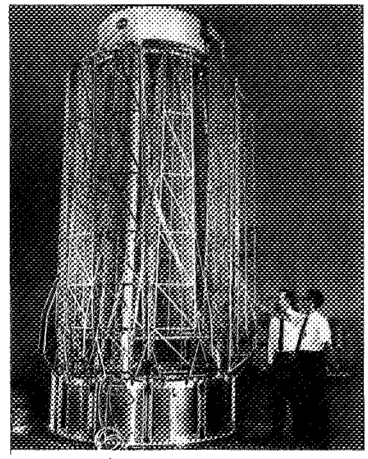

(a) PACKAGED CONFIGURATION

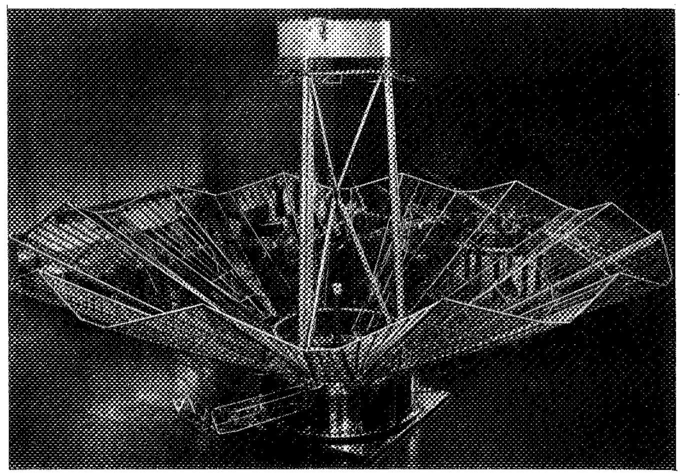

(b) NEAR-FINAL CONFIGURATION

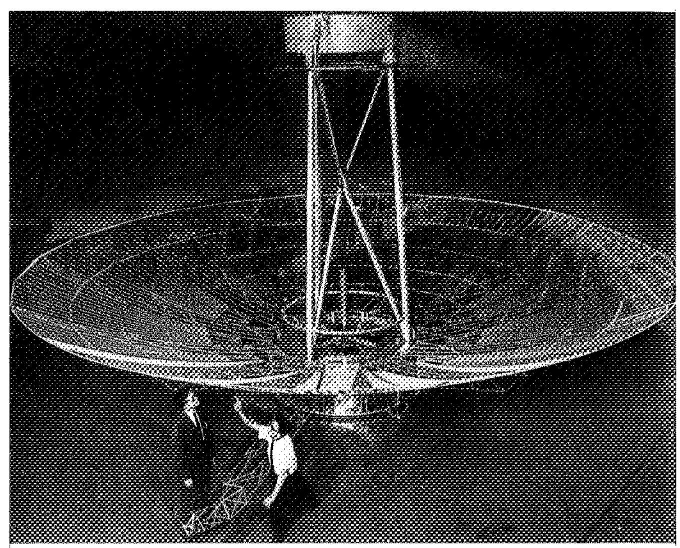

(c) FINAL ZERO-STRAIN CONFIGURATION

Fig. 1. Deployment sequence

The deployable reflector and the deployment system are each significant mechanisms. The reflector implements the curved hinge-line concept, and the deployment system fully controls deployment and moves the deployed reflector into a precise final position.

IV. Deployable Reflector

The sequence in Fig. 1 shows the general arrangement of the reflector. The reflector consists of 36 petals; 24 are triangular and 12 are trapezoidal. There are six hinges along each of the 36 hinge lines. These hinges are located in line with each of the six circumferential members to provide structural continuity in the deployed condition. In addition, there are two hinges at the root of each of the 12 trapezoidal petals to provide attachment to the support hub. Twelve reflector support trusses attach to the reflector at a radius of 101.5 in. and provide the controlled motion of these points during deployment.

The triangular-to-triangular petal hinges are on the outside surface of the reflector and the triangular-to-trapezoidal hinges are on the inside surface. This permits the triangular petals to be folded inward. When completely packaged, the triangular petals are in a nearly radial plane, and the trapezoidal petals are approximately vertical and evenly spaced around the circumference.

The petals consist of an open framework covered by a screen to provide the reflecting surface. The primary structural members are ¾ in. wide. There are also ⅜-in.-wide secondary members that are spaced about 4.5 in. apart on the average to reduce the screen deviations from the theoretical parabolic contour for good microwave performance. These primary and secondary members are constructed of Bondolite[2] and consist of 0.3-in.-thick aluminum honeycomb; 2.5-mil titanium face-sheets are bonded with Bloomingdale FM-1000 adhesive. Each petal is laid up and cured in a single operation to the desired parabolic contour.

The petals are positioned on an assembly fixture, and the hinges are located and attached with blind rivets. This procedure permits the contour of the reflector to be assembled in a virtually unstrained condition and to be nearly as accurate as the assembly fixture itself.

[2]Trademark of the Goodyear Aerospace Corporation for bonded sandwich structures.

One difficulty encountered so far has been to provide moment continuity at the petal-to-petal hinges. The eccentricity caused by the hinges being on alternate sides of the hoop members rotates the circumferential members when they are axially loaded. This rotation changes the hoop length, which then causes a deflection of the reflector surface, and this deflection is undesirable.

Two mechanisms to solve this problem are under consideration (Fig. 2). The first is a torsion spring and stop combination (Fig. 2a) that is considered satisfactory for the ultimate space application where the hoop load due to thermal gradients is small. (For checking the reflector contour in the presence of the earth's gravitational field, however, the hoop loads are relatively high, and springs designed to function satisfactorily for this particular condition are not compatible with the overall requirements. One proposed solution is to design the springs for the space requirements and mechanically keep the stops closed for the reflector contour check.) The second mechanism being investigated is the self-locking hinge (Fig. 2b). This hinge has two slotted tongs into which the self-loaded pin will drop when the two slots are aligned to within about 5 deg of one another.

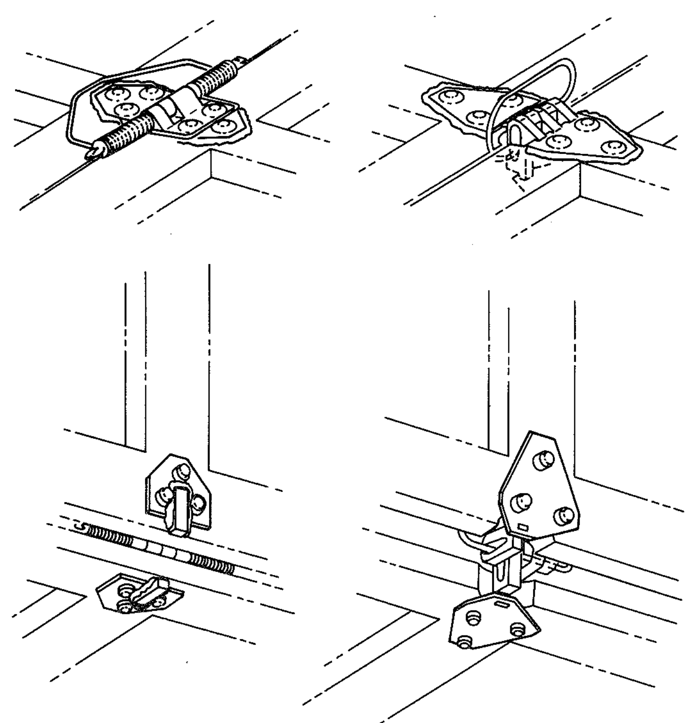

(a) SPRING-STOP HINGE (b) SELF-LOCKING HINGE

Fig. 2. Moment continuity mechanisms

V. Reflector Deployment System

The reflector deployment system is required to move the packaged reflector from the packaged (or launch) configuration to the fully deployed configuration. The ground rules applicable to the development of the deployment system were as follows:

(1) Back (reflector support) trusses are required as part of the reflector structure system after deployment.

(2) Controlled and sequential release of the stored energy in the petals is required throughout the complete deployment cycle.

(3) The system must be designed to function without aids but with gravity-aiding and gravity-retarding deployment.

The reflector surface is deployed by positive drive rotation of each of the 12 reflector support trusses about their fixed pivots to the fully open position. Each truss/reflector surface interaction may be considered as a 4-bar linkage, as typically illustrated in Fig. 3. The deployment mechanism consists of (1) 12 actuation linkages (one in the plane of each support truss), (2) a drive chain interconnecting each of the actuators, and (3) a drive motor.

As shown in Fig. 3, each actuation linkage consists of an actuator link that connects the reflector/support truss to the ball nut of a ball bearing screw actuator. Thus, the linear travel of the ball nut, resulting from rotation of the screw, causes the controlled rotation of the reflector support truss. A yoke on the actuation link connects the link to the ball nut, and therefore the reacting force is on the axial centerline of the screw.

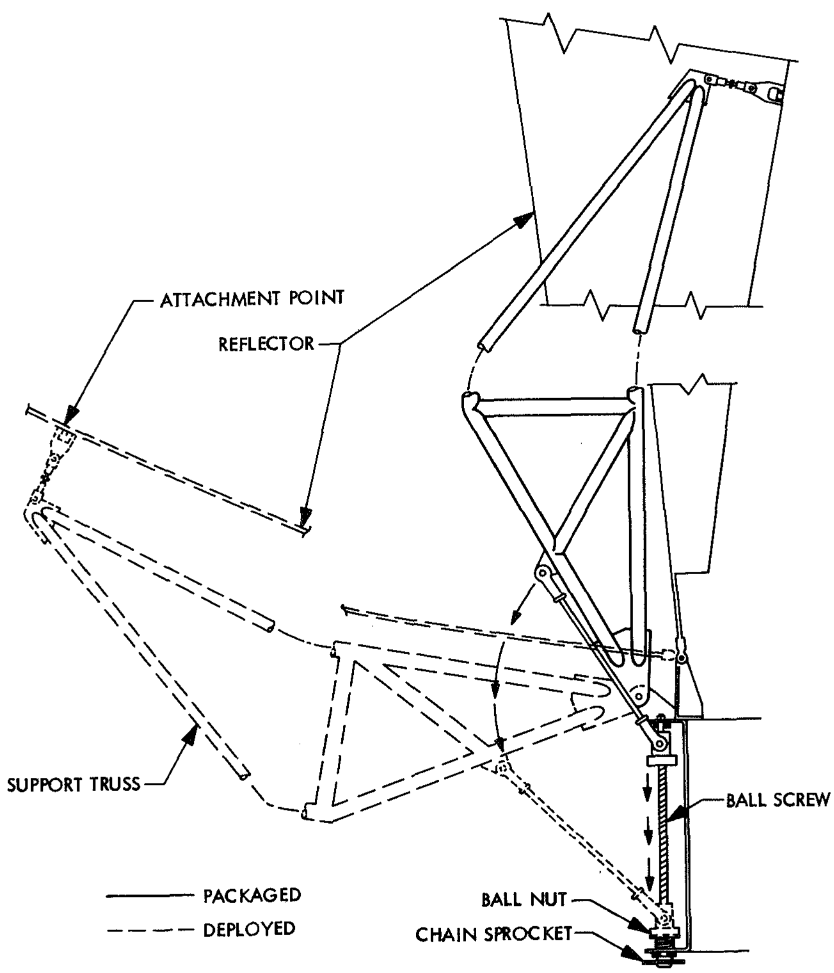

Fig. 3. Linkage between truss and petal

With the 12 screws being driven in unison by the single drive chain, the requirement for sequential deployment of the petals is satisfied by varying the drive sprocket diameter on the individual screws. In this particular arrangement, two sprocket sizes are used so that alternate trusses deploy 2.9 s (approximately 5 deg) ahead of the remaining trusses. This sequential deployment then imposes a requirement on the design for the torque driving force to "freewheel" on some screws and still transmit torque to others until they have completed their excursion.

The freewheeling feature is accomplished by the arrangement shown in Fig. 4. The driving torque for the screw is transmitted by the drive chain to the screw sprocket, through the bearing retainer, and to a keyed, toothed female clutchplate. The female clutchplate is free to slide axially and is spring loaded into a male clutchplate that is an integral part of the screwshaft. The flanged end of the ball bearing nut disengages the clutch faces at the end of travel. This disengagement interrupts the torque that is transmitted between the drive sprocket and screwshaft and then the drive sprocket continues to turn without further linear travel of the ball nut.

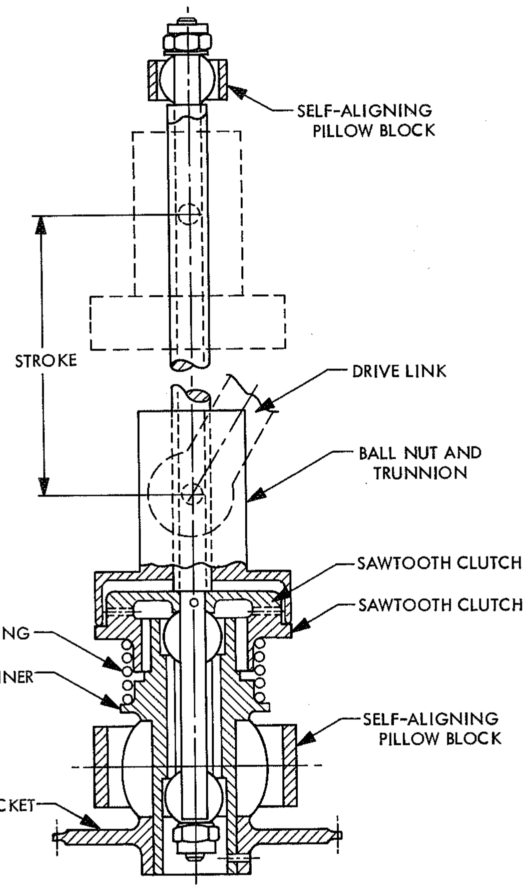

Fig. 4. Arrangement of clutchplates for freewheeling

VI. Conclusions

A basic design approach to the problem of packaging a large compound-curvature shell for launch and deploying it in orbit has been described. The feasibility of the design has been demonstrated by applying it to a full-scale engineering model of the ATS F and G 30-ft-diam antenna. There is sufficient design flexibility in the selection of petal arrangements, deployment systems, and materials to satisfy many specific applications where large size, light weight, and close-tolerance surfaces are required in orbit with a high degree of reliability.

Page intentionally left blank

70N21446

Dragline Sample-Acquisition Mechanism*

H. M. Alexander
Jet Propulsion Laboratory
Pasadena, California

A dragline sample-acquisition mechanism for sampling planetary surface soils collected 85 g from a 50-μm silica flour test bed when dragged 45 ft at 7 ft/s. On Pisgah Crater's dry desert playa hardpan, the sampler collected 6 g of soil when dragged a distance of 145 ft. A torpedo-shaped device with 96-cm³ capacity, the sampler is designed to be mortar-launched from a planetary lander and returned to it by an attached dragline. Blades located immediately aft of the bullet-shaped nose deflect surface particles through radial slots and into the sample case. When triggered by a fluted odometer, a unique device closes the slots and prevents sample contamination.

I. Introduction

In the near future, unmanned exploration spacecraft will land on other planets to carry experimental apparatus for measuring chemical, physical, and other properties of surface soils. Several experiments on these landers will conduct life-detection analysis on samples of these soils. To ensure validity of results, the soil samples used in these experiments must be free from spacecraft-borne contamination.

This paper discusses a soil sample-acquisition mechanism (sampler) that was developed for the *Voyager* project, now canceled, to collect samples of Martian soil for analysis by the *Voyager* surface laboratory.[1] Each experiment required sample volumes varying from 1 to 10 cm^3 with particles generally less than 1000 μm (Ref. 1). Preliminary analysis[2] indicated that a zone of 100-ft radius surrounding the spacecraft should be considered to be contaminated by rocket exhaust products; thus an acceptable sample would have to be obtained from the surface outside this zone and then returned to the spacecraft while avoiding sample contamination. For design purposes, an outer zone of 500-ft radius was selected.

Of the several methods considered for conveying and retrieving the sampler, the simplest was to use a mortar

*This paper presents the results of one phase of research carried out at the Jet Propulsion Laboratory, California Institute of Technology, under Contract No. NAS 7-100, sponsored by the National Aeronautics and Space Administration.

[1]The surface laboratory is a planetary lander from which experiments are performed. Data from these experiments are stored for transmission to earth during subsequent communication periods.

[2]*Voyager Project* internal report, Jet Propulsion Laboratory, Nov. 15, 1967.

to launch the sampler and then to employ an attached line to retrieve it. During the retrieval process, a sample would be acquired. A unique mechanism would be used to close the sampler before it entered the contaminated zone around the lander.

It should be noted that the selected procedure generated some critical design problems. These problems were carefully considered, although they will not be detailed at length in this paper. For example: (1) To survive possible impact with a hard object, the sampler's impact energy would have to be dissipated; (2) To ensure that the sampler remains on the surface of any soft, yielding terrain, penetration-prevention attachments would have to be provided.

The plan for developing a dragline sample-acquisition mechanism to meet the above requirements was as follows:

(1) Design, calibrate, and field-test a feasibility model of the sampler.

(2) Based on the results of (1), modify and test a second-generation sampler.

II. Sampler Development

A 10-cm^3 feasibility test sampler and a 96-cm^3 dragline sample-acquisition mechanism were designed to acquire a surface sample with an annular, slotted device that contained an odometer-triggered sampler closure mechanism. From the original configuration, the 96-cm^3 design was evolved as described below.

A. Feasibility Model

The 10-cm^3 brass feasibility sampler (Fig. 1a) contains three major subassemblies: the conical nose by which the sampler is pulled with its dragline; the sample-holding case, whose leading edges are three slot-forming, equally spaced, sawtooth blades; and the shaft-mounted music wire odometer, which was formed on a die having helical grooves machined into its cylindrical midsection and its truncated-cone ends. Three roll prevention wires are mounted 120 deg apart at the fore and aft ends of the case. Through the center of its conical nose, the sampler receives its motion from dragline force. As the sampler moves, its blades shear the surface material and deflect the particles radially through the nose slots and into the case. The wire odometer was incorporated to determine whether this configuration might be used to trigger a spring-actuated closure device after a predetermined number of rotations. It was assumed that if case rotation were prevented and the odometer were free to turn relative to the case, sampling could be limited to uncontaminated areas since the number of odometer rotations would be directly proportional to the distance traveled by the sampler. Test results later invalidated some of the design assumptions.

Because the wire drag area was too small, negligible odometer rotation occurred during the 10-cm^3 sampler drag testing on newly excavated soil. Also, some of the odometer's wire joints failed. When tested on 30-deg hillsides, the roll stabilizer wires were too flexible under lateral loading. Thus, the sampler rotated with the odometer. On the other hand, the stabilizer wires did permit sampler passage through constricted spaces, and the sharp annular blades did acquire small surface samples with their scraping motion. In effect, the prototype sampler served its purpose by pointing the way to further design improvements.

B. Sampler Design

On the basis of the test results, certain features of the feasibility sampler were modified and applied to the 96-cm^3 sampler (Fig. 1b). All components except the odometer were made of aluminum. The new odometer was formed by fluting a brass hollow cylinder, giving the odometer a cascade of blades and increased weight. Stiffer stabilizers made of music wire, with increased radial span, were provided. To allow a larger rate of sample flow, the three blade heights were increased. The sampler length and diameter were also increased. The conical nose was replaced by a hemispherical nose after drag tests on various solid bodies, conducted by the Space and Re-entry System Division of Philco-Ford Corporation, showed that a cylinder with a hemispherical nose performed best.[3] To facilitate sample removal, the nose cylinder was knurled on the surface adjacent to the hemisphere.

The sampler closure mechanism (see Fig. 1b) permitted the sampler to be returned to the surface laboratory with an uncontaminated sample. The mechanism operates as follows: The sampler is dragged, making the odometer blades cut into the soil and forcing the odometer to rotate away from its position next to the bulkhead.

[3]The tests were performed for the Jet Propulsion Laboratory under Contract 951935 and sponsored by the National Aeronautics and Space Administration under Contract No. NAS 7-100.

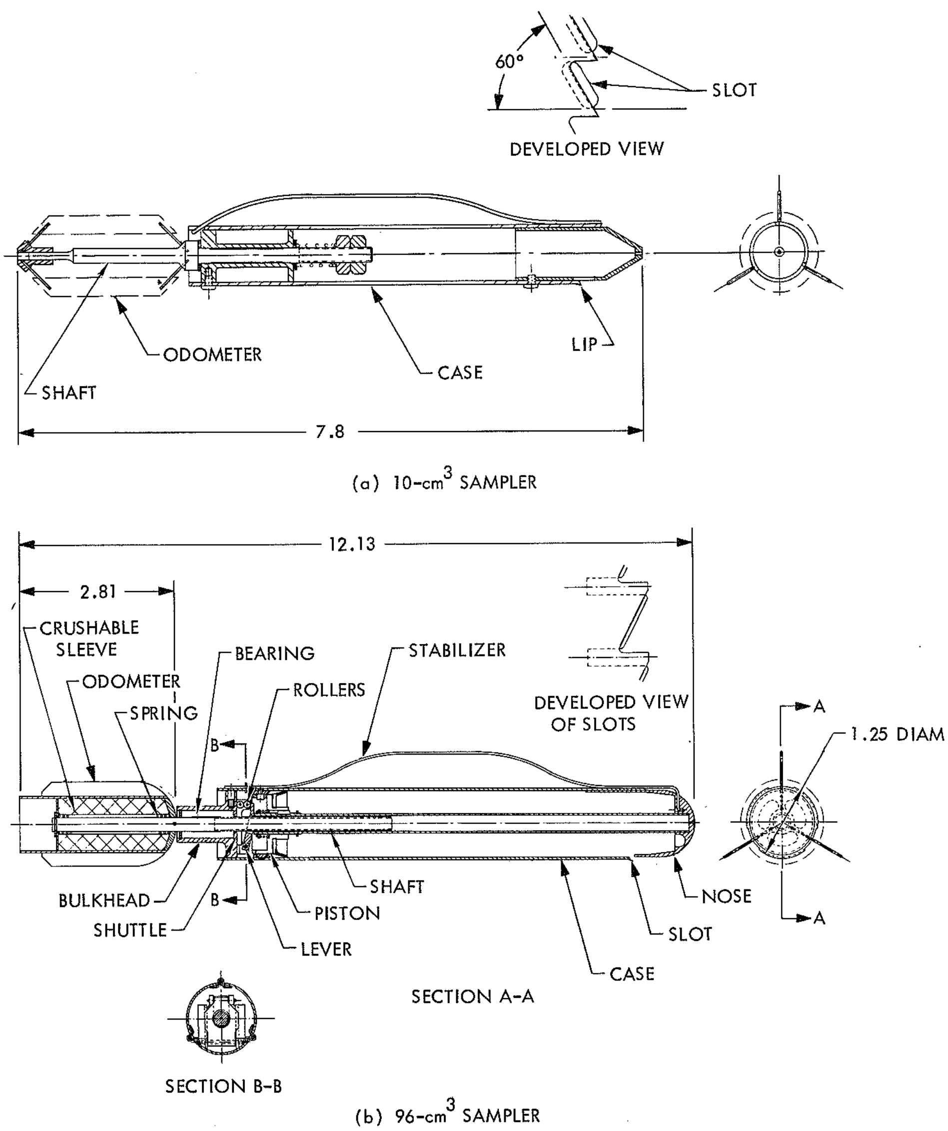

Fig. 1. Dragline samplers

When the odometer shaft end passes the shuttle, the spring-loaded lever which bears on the shuttle rollers forces the rollers upward. The shuttle's vertical movement releases the spring that closes the nose assembly. Thus, sample contamination is precluded.

To remove the sample from the case, the case is held to prevent rotation. Then the nose assembly is grasped by its knurled surface, turned counter-clockwise, and pulled forward. This force is transmitted through the shaft to the sample removal piston. As the piston moves forward, the nylon lip of the cup-shaped piston scrapes the sample from the inner walls of the case and unloads the sampler.

C. Sampler Calibration Testing

Since life detection is the assumed primary goal for some of the experiments, the sampler's optimum speed for the probable soil terrain in which life is most likely to occur had to be estimated. Based on preferred sample sizes in the 50- to 300-μm range (Ref. 1), the speed was estimated in a test medium of 50-μm silica flour. On the basis of the sampler speed, system power requirements could be calculated. Equally essential for successful sample retrieval was a dragline tension-measuring capability. (If it is inadequately sized, a dragline might be snapped during sampler impact with a hard object.)

To empirically determine an optimum retrieval speed, a retrieval system (Fig. 2) was designed and built. The system includes three bearing-mounted pulleys, a tether spool mounted on a ¼-in. drill shaft, and a 20-lb-test monofilament nylon dragline that is fed through the pulley system as the line is payed out or rewound. The system also includes an auto-transformer for drill speed control. The spring-loaded idler is constrained to move vertically by a scribed vertical post. The scribe marks indicate the tension acting on the spring or in the dragline. When the sampler collides with an obstacle during retrieval, the spring deflects and absorbs the shock load; thus, system load surges are indicated. A similar shock absorption mechanism would be part of the surface laboratory retrieval system. From these data, dragline stresses can be estimated.

Before the sampler retrieval runs were made, the retrieval system was calibrated; then the sampler was prepared for retrieval runs. In the 50-μm silica flour test bed, the sampler performed best at an average velocity of 7 ft/s; 85 g of sample were collected. At velocities above or below 7 ft/s, the sample weight varied erratically. As shown in Fig. 3a, silica flour particles were sprayed forward at high velocities (e.g., 20 ft/s). Figure 3b shows the sampler skimming the test bed surface at 7 ft/s without spraying silica particles.

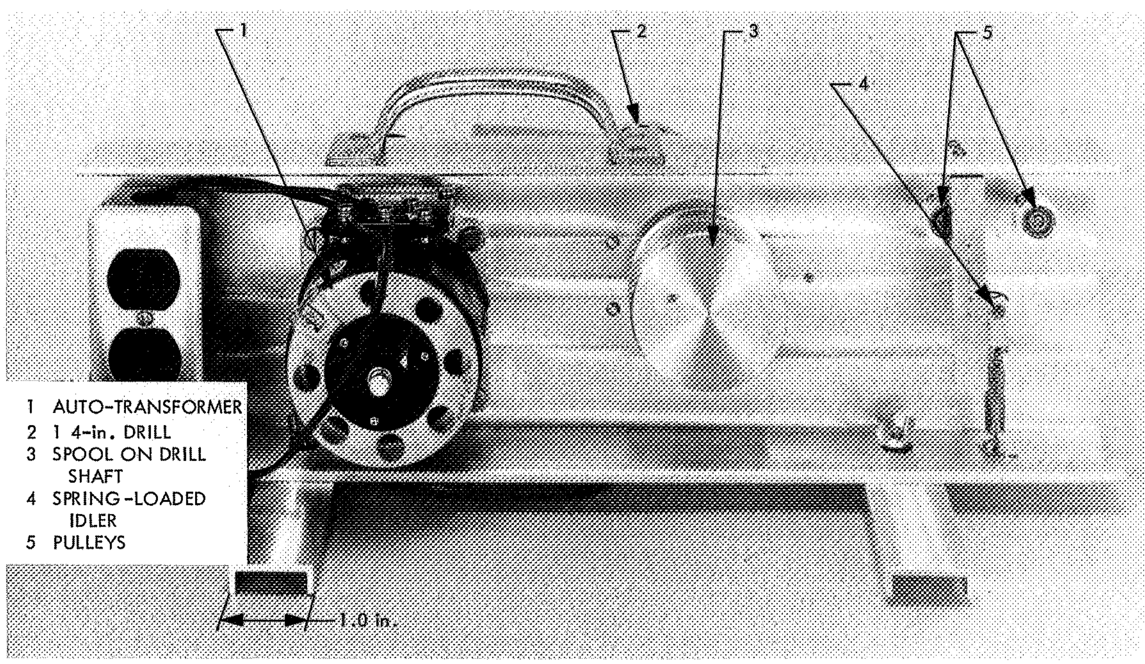

Fig. 2. Sampler retrieval system

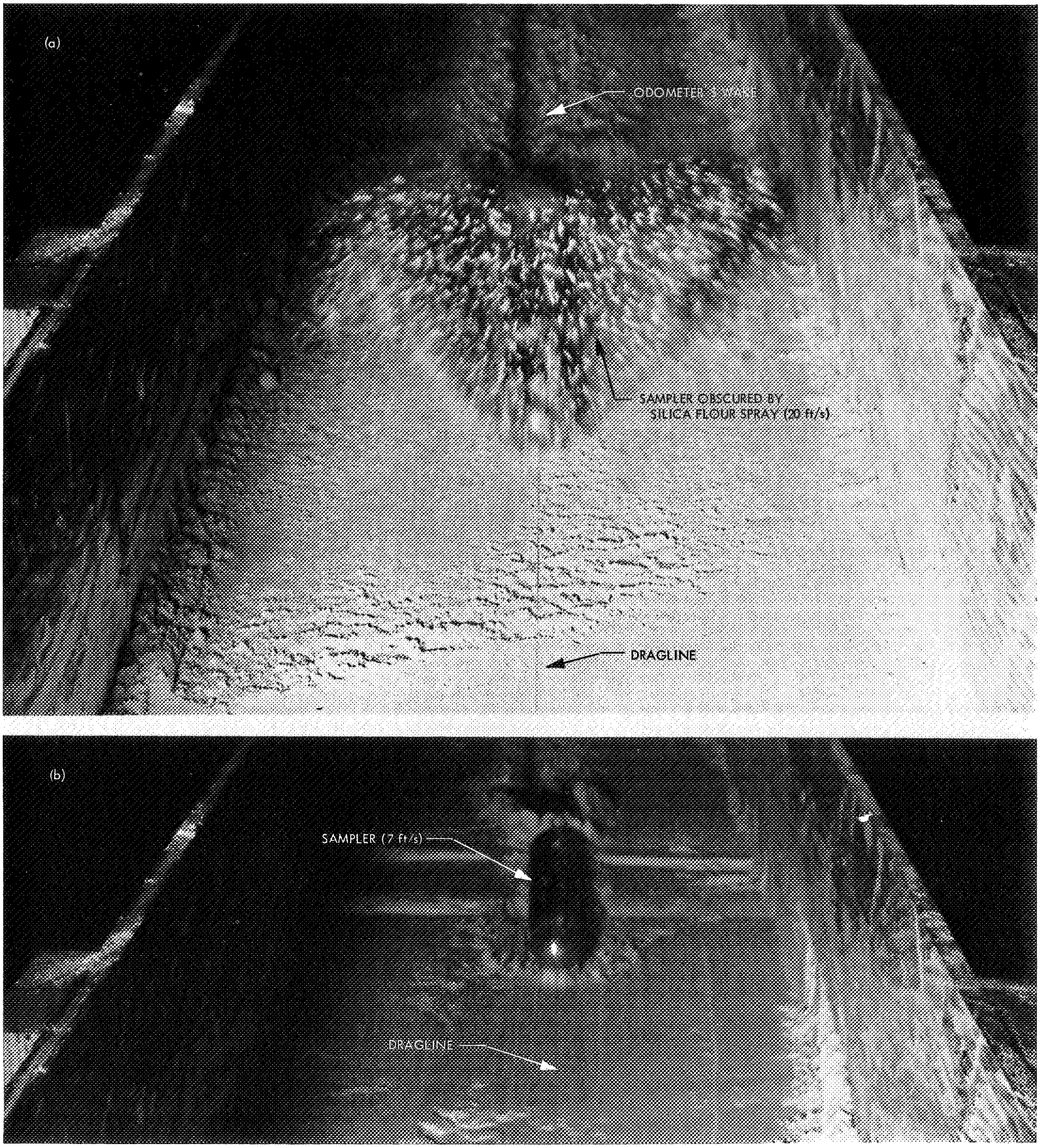

Fig. 3. Dragline sampler performance in silica flour test bed: (a) at 20 ft/s, (b) at 7 ft/s

The average odometer wake depth in the test bed was ½ in., while the odometer's average displacement from the bulkhead was 1 in. for drag distances up to 45 ft. This indicates that the odometer would probably produce closure after a sampler travel of 200 ft. For soils similar to the silica flour, closure at some shorter distance could be achieved by shortening the odometer shaft. At low velocities, the sampler was observed to drift. When the sampler was dragged at the same velocity without the odometer, no sampler veering occurred, and the sample weight was smaller.

As part of the test procedure, random bearing pressures were taken with a Proctor penetrometer[4]; however, with only a 4-in. thickness of silica flour in the test bed, bottoming effects could not be totally eliminated. The average bearing pressure was 5 psi. This kind of information serves to define the nature of test soil acquired, and, to some extent, exhibits a correlation with the amount of sample gathered.

Testing the dragline sampler in the laboratory provided such advantages as controlled test conditions, an opportunity to observe the performance of the sampler under these ideal circumstances, and no exposure to natural elements like rocks and sand. Under these favorable conditions, the sampler retrieval system performed well, but there was no assurance that it would do as well in a natural desert environment.

D. Sampler Remote Site Testing

To observe sampler performance under varied conditions, the system was taken to Pisgah Crater in California's Mojave Desert. At Pisgah Crater there were five geological types of soil and rock surfaces; lava flow; wind-blown sand superimposed on lava; cinders; playa composed of fine-grained silt, clay and duricrust material; and desert pavement composed of fractured basalt superimposed on sand.[5]

Although there were five geological rock and soil types, there were only two types of terrain on the basis of static bearing pressure: one type with an average static bearing capacity of 20 psi, and the other with an average pressure of 156 psi. The lower pressure was obtained from loose materials, whereas the higher pressure indicated hard-packed soils. Particle sizes for the materials averaged 74 and 44 μm, respectively. Table 1 presents some of the Pisgah Crater data. On the soft, sandy soil, the 1-in.-diam disk of the Proctor penetrometer easily penetrated to a depth of 3 in. No penetration was possible for the hard-packed playa; the indicator went off the scale.

Table 1. Pisgah Crater test data

Test factor	Sandy area	Desert pavement	Playa
Particle size, diameter		Similar to sandy area	44 μm
Average, mm	0.5		
Maximum, mm	2.0		
Minimum, mm	0.02		
Sample mass, g	12	12	6.5
Sampler travel, ft	70	70	140
Static bearing pressure			
Average, psi	22.8	20.0	156
Maximum, psi	28.0	23.2	178
Minimum, psi	9.0	16.0	147

From a desert pavement terrain covered with basalt pebbles as large as a centimeter in diameter, the sampler collected a sample by plowing down through the pebbles to the 2.38-mm sand particles below. Thus, the sampler exhibited the capability to "discriminate" between particles on this kind of terrain. On dry playa hardpan, 6 g of sample were obtained over a drag distance of 145 ft. An equivalent weight of sample was obtained when the sampler was dragged 260 ft on wet playa. The odometer displacement was 0.5 and 1.5 in., respectively, for these tests. These results demonstrated the sampler performance with soils of varied consistency.

III. Conclusion

For soils similar to 50-μm silica flour, the dragline sampler will collect approximately 85 g of uncontaminated sample when dragged approximately 200 ft. For solids with characteristics like those of Pisgah Crater, California, 6 g may be acquired. If these acquisition levels represent the best and worst performance of the sampler, and if the planet's soil characteristics are between those of the 50-μm silica flour and those of Pisgah Crater, then the soil sample-acquisition mechanism's performance is adequate for fulfilling experiment sample requirements when retrieved at 7 ft/s.

[4]The Proctor penetrometer or plasticity needle is a rod with an enlarged tip which is forced into the soil at a given rate. The tip is exchangeable, and tips of different sizes from 0.01 to 1 in.^{2}, giving readings in pounds per square inch, are used, according to the degree of soil softness (Ref. 2).

[5]Dr. Roy G. Brereton, staff scientist, Advanced Studies Office, Jet Propulsion Laboratory, personal communication.

Acknowledgments

The 96-cm^3 and 10-cm^3 dragline samplers developed in this program were designed by Allen G. Ford of the Jet Propulsion Laboratory. Many of the ideas for development tests came from discussions with Dwain F. Spencer and William J. Carley of the Jet Propulsion Laboratory.

References

1. Nash, D. B., *Sampling of Planetary Surface Solids for Unmanned In Situ Geological and Biological Analysis: Strategy, Principles, and Instrument Requirements*, Technical Report 32-1225. Jet Propulsion Laboratory, Pasadena, Calif., Nov. 15, 1967.
2. Krynine, D., *Soil Mechanics*, First Edition. McGraw-Hill Book Co., Inc., New York, 1941.

Page intentionally left blank

70N21447

The *Apollo* Command Module Side Access Hatch System

L. J. Walkover, R. J. Hart, and E. W. Zosky
Space Division, North American Rockwell Corporation
Downey, California

The Apollo command module side access hatch system was redesigned on an expedited basis. This paper discusses the development of the redesign criteria and rationale and the redesign of the side access hatch system. A definition of the mechanisms and a description of the development testing required to qualify the system are included. This work was done under contract to NASA's Manned Spacecraft Center, Houston, Texas.

I. Introduction

After the accident with *Apollo* Spacecraft 012 at Kennedy Space Center, the command module side access hatch system was redesigned. Management at the Space Division of North American Rockwell Corporation realized the difficulty of designing and building a new hatch system in the time required by the revised *Apollo* Command Service Module Program schedule. A task force, staffed with management and design personnel from the engineering and manufacturing functions involved, worked seven days a week. NASA participated in the definition of criteria and the selection of the final redesign, which was turned over to the functional design groups for detailed design, analysis, and drawing release. North American Rockwell and NASA requested information from McDonnell Douglas Corporation on the definition of their mechanism and seals for the *Gemini* hatch; this information was immediately received.

A short description of the spacecraft is required to understand the design problems involved. The command module, which houses the astronauts, consists of three structures:

(1) An aluminum honeycomb inner structure, which serves as the pressurized crew compartment.

(2) A stainless steel heat shield covered with an ablative material. The heat shield is permanently attached to the inner structure by special fittings that allow relative motions between the structures due to thermal expansion and pressure variation.

(3) A lightweight boost protective cover, which covers and protects the heat shield during launch. The boost protective cover is attached to and jettisoned with the launch escape tower after second-stage booster ignition.

Spacecraft 012 had three hatches located in and latched to the three command module structures:

(1) The inner structure hatch was an inward-opening, completely removable, lightweight structure designed to react the applied loads with interlocking edge members on three sides and latches on the fourth. Cabin pressure was used to aid in sealing; the pressure differential had to be balanced before the hatch could be removed and stowed.

(2) The heat shield hatch was an outward-opening, removable structure with interlocking edge members and latches on four sides.

(3) The boost protective cover hatch was a removable lightweight structure of fiber glass and cork, which opened outward. Its latches could be opened from within the command module by manually striking a plunger which penetrated the heat shield hatch and contacted the boost protective cover latch mechanism. It could also be opened from the outside by the use of a special tool.

The basic procedure for egress was to:

(1) Equalize pressure across the inner structure hatch.

(2) Unlatch and remove the inner structure hatch and stow inside the command module.

(3) Strike the plunger to open the boost protective cover hatch latches.

(4) Unlatch the heat shield latches.

(5) Push the heat shield hatch and boost protective hatch outboard.

(6) Egress.

This hatch system was deemed acceptable for early *Apollo* spacecraft (designated Block I) because there was no firm requirement for extravehicular activity, and a 90-s egress time for the three astronauts was thought to be sufficient. Previous consideration for using a large explosive blowout panel for simultaneous exit for three astronauts was eliminated because of the danger of pyrotechnics inside the crew compartment.

The series of spacecraft designated Block II was designed for lunar orbit rendezvous and had an improved side access hatch system for extravehicular activity. The main difference between Block I and Block II was the heat shield hatch, which hinged outward for Block II and had latches with greater reach and pull-down capacity.

II. New Hatch Design Requirements

Because many of the Block II structures had been fabricated, systems installed, and heat shields assembled to the inner structures when the hatch redesign was started, management decided that:

(1) Major changes would be confined to the hatches, and rework to the inner structure and heat shield would be limited.

(2) The heat shield would not be removed for rework.

(3) No welding would be used for heat shield rework.

(4) Only readily available materials and machinery would be used.

(5) Excess strength margins would be used in structures, mechanisms and fasteners.

The normal engineering practice of designing for minimum weight was sacrificed for expediency and ruggedness. Furthermore, there was to be no planned future change point, which implied that the excess weight might never be eliminated.

The prime functional requirement was that the hatch would operate satisfactorily for normal usage, and the requirements for rapid emergency egress during manned command module checkout and prelaunch activities were changed drastically. Time allowed for opening the side hatch system was cut to 3 s and time for egress of three pressure-suited astronauts was reduced to 30 s.

A secondary functional requirement was for improved extravehicular activities characteristics including:

(1) Up to 20 min for the hatch to remain open for the most severe command module solar orientation.

(2) One-handed operation of mechanisms from either inside or outside.

(3) Inside operating handle motion: push open, pull closed.

(4) Outside operation: tool interface within interconnect to a lock pin.

(5) Emergency ingress for an unaided astronaut.

(6) An emergency (backup) method of hatch latching.

(7) A rapid pressure dump valve.

(8) No reduction in size of hatch opening; increased angle of hatch swing.

(9) Provision for replacing the hatch window with the Block I air lock to be used for scientific experiments on later flights.

(10) An operating force of 20 lb nominal.

Additional criteria were specified as the design progressed:

(1) One-hour opening of the hatch for extravehicular activity but not necessarily in worst solar orientation.

(2) Capability for the hatch to be left ajar for long-duration extravehicular activity.

(3) One hundred operating cycles without degradation to confirm repeat usage.

(4) Hatch damage acceptable in emergency use during test or prelaunch, under increased internal pressure, but damage to the command module structure not acceptable.

(5) No increase in the hatch leak rate.

III. Design Proposals

Some of the designs which were proposed but discarded are listed below to indicate the scope of redesigns attempted.

(1) A blowout panel design which was large enough for three astronauts to exit simultaneously was proposed. This was discarded because too much existing hardware would be changed, extravehicular activity would not be improved, and pyrotechnics inside the cabin would be dangerous.

(2) It was proposed to retain existing hatches, but incorporate small blowout panels. This was discarded for much the same reasons as above.

(3) It was proposed that the inner structure hatch and the boost protective cover hatch be mounted to, and supported by, the outward opening hinged heat shield hatch. When closed, the hatches would be individually latched to their respective structures. This proposal was discarded because of mechanical complexity and alignment problems.

(4) The inner structure hatch and heat shield hatch were proposed to be each hinged outward and latched independently. This was discarded because of mechanical complexity.

(5) Retention of the existing three-hatch system was proposed, with the addition to a power actuator for opening the heat shield hatch and an outward-opening door built within the confines of the inner structure hatch and operated by a quick-acting device. This was considered attractive because it did not change existing structure, but it had the disadvantages of extra mechanisms and reduced hatch opening. Moreover, the difficulty of handling and stowing the hatch by a pressure-suited astronaut counted heavily against this proposal.

IV. The Unified Hatch Concept

The concept proposed by North American Rockwell and approved by NASA is known as the unified hatch (Fig. 1). The design combines the functions of the heat shield hatch and the inner structure hatch into a single outward-opening hinged hatch with one set of mechanisms. The boost protective cover hatch was retained, but modified to be compatible with the unified hatch. The unified hatch provides the primary structure for pressure loads and the seal for the inner structure and supports the ablative material for thermal protection.

Two adapter frames are used, one attached to the inner structure and one attached to the heat shield, to provide structural continuity and transmit primary structure loads around the hatch. The frames reduced the hatch opening; however, NASA provided a new opening criterion. The reduction in the hatch egress path opening was offset by the minimum rework required to the existing structures.

The unified hatch is hinged and latched to the inner structure adapter frame; the heat shield and its adapter frame float relative to the hatch. The resulting gap between the hatch periphery and the heat shield adapter frame is blocked by a rubber thermal seal to prevent entry of thermal flow. This passive thermal design technology of thermal flow blockage was being proven at that time.

Although studies were made to eliminate the boost protective cover hatch, the decision was made to retain it with minor modification. Because the boost protective cover hatch represented another set of mechanisms, its elimination would have required drastic changes to the command module ablative material which were not possible because of schedule commitments.

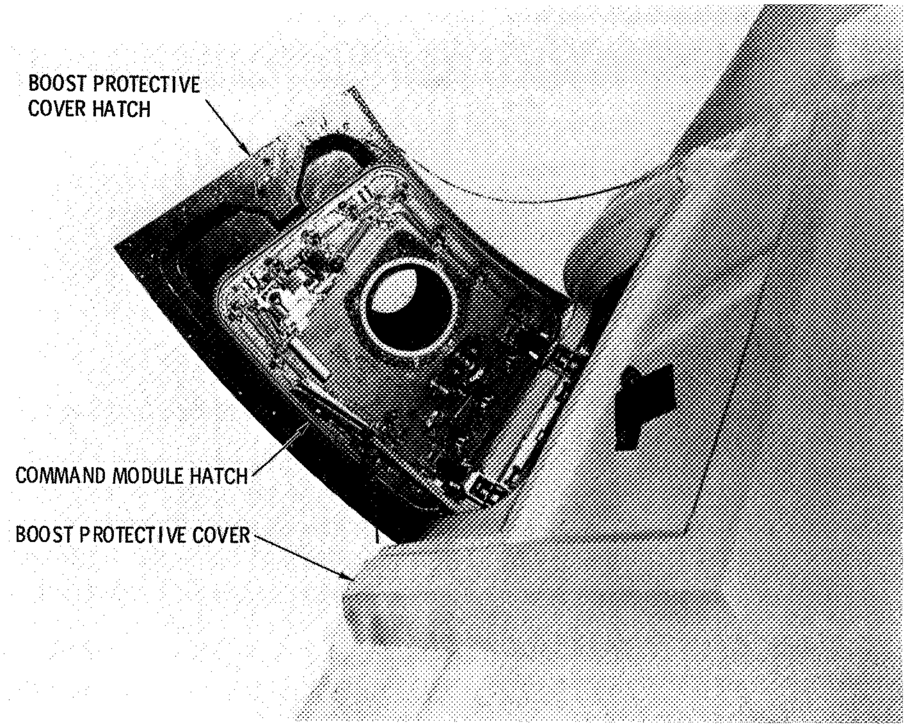

Fig. 1. Unified hatch in open position

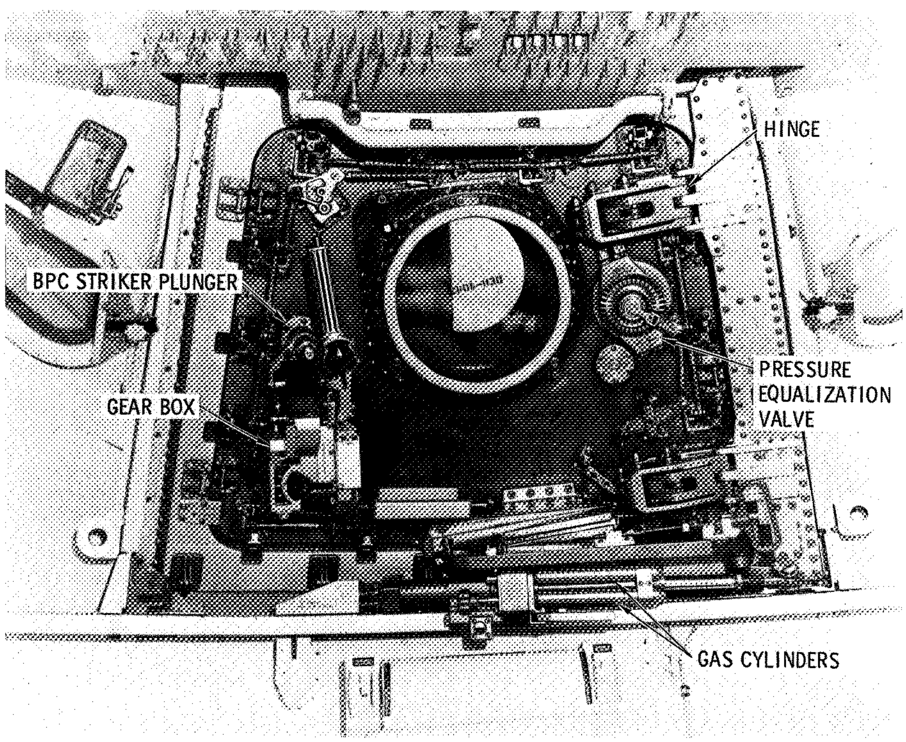

Fig. 2. Unified hatch from inside command module

V. Boost Protective Cover Mechanisms

The boost protective cover (BPC) hatch is slightly larger than the command module (CM) hatch and has a piano hinge along one vertical edge so that the two hatches swing open in the same direction. The other three edges are secured to the boost protective cover structure by latches which are linked to a central operating lever and are normally opened and closed by the ground crew outside the command module with a removable tool. For emergency egress, the boost protective cover hatch latches are released by the astronauts from inside the command module by means of a plunger (the boost protective cover striker plunger) that is automatically actuated when the astronaut performs the unlatching function for the unified hatch by operating the gear box handle. The boost protective cover hatch then remains resting against the command module hatch. An alternative emergency procedure is for the ground crew to pull on an external lanyard to open the boost protective cover latches and hatch.

VI. Unified Hatch Mechanisms

The command module unified hatch contains the following mechanical components (Fig. 2):

(1) Latches to retain the hatch in the closed position.

(2) Linkage to transmit motion to the latches.

(3) A manually operated gearbox to drive the linkage.

(4) A plunger mechanism to open the boost protective cover hatch latches (the boost protective cover striker plunger).

(5) A gas-powered piston/bell crank to push the hatch open and attenuate the travel (the counterbalance).

(6) A manually operated valve to equalize pressure across the hatch.

(7) A screwjack attachment for emergency hatch closure and retention.

A. Latches

The requirements of the command module hatch latches are:

(1) To hold the command module hatch closed and maintain the hatch pressure seal.

(2) To pull the hatch down when the hatch is within ½ in. of the mating surface. This allows hatch closure if the hatch is warped due to temperature differentials across the hatch structure.

(3) To cam the hatch open approximately ⅜ in. when the latches move to the open position.

These requirements are met by the use of the cone latch which has several features that make it advantageous to our hatch application (Fig. 3).

(1) It translates motion through 90 deg, thus permitting its drive linkage to be placed close to the hatch surface.

(2) Its mechanical advantage changes throughout its stroke so that the output force increases as the latch moves toward the latched position.

(3) Near the end of its closing stroke, the output lever passes over center, and cabin pressure then assists in holding the latches in the closed position.

(4) Cabin pressure forces do not feed back through the latch to the driving linkage, which can, therefore, be safetied with a comparatively light locking pin.

There are 15 latches spaced at approximately 5½-in. intervals around the periphery of the hatch. Each latch consists of a driving lever, a connecting lever, and a driven lever assembled in a housing secured to the inner surface of the hatch. Shims under the housings enable them to be rigged for equal distribution of seal squeeze load, and a gauging surface machined into each housing simplifies adjustment for correct amount of overcenter travel of the latch driving lever. The driven lever is shaped to form the pull-down dog and has an effective travel of ¾ in., which is more than sufficient to compensate for calculated hatch thermal warpage.

The latch driving linkage is a simple push–pull rod system with threaded adjustments for each latch.

B. Gearbox

The function of the gearbox is to open and close the command module hatch latches and to provide a drive for emergency opening of the boost protective cover hatch latches. It has two inputs and two outputs (Fig. 4).

(1) One manual input from the hatch exterior.

(2) One manual input from the hatch interior.

(3) One output to open and close the command module hatch latches via the driving linkage.

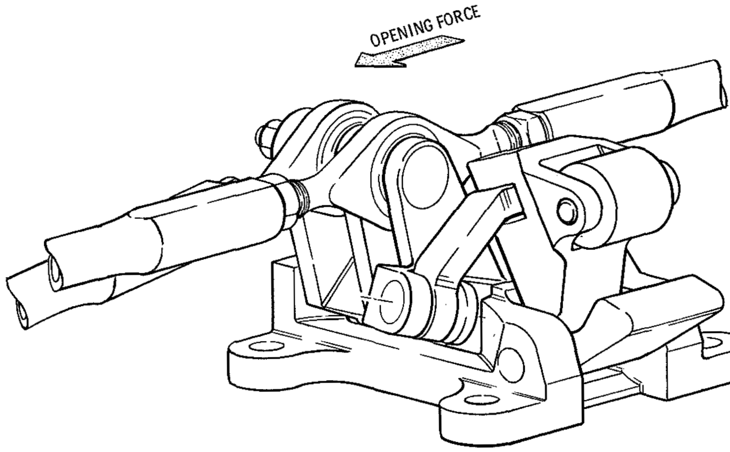

UNLATCHED

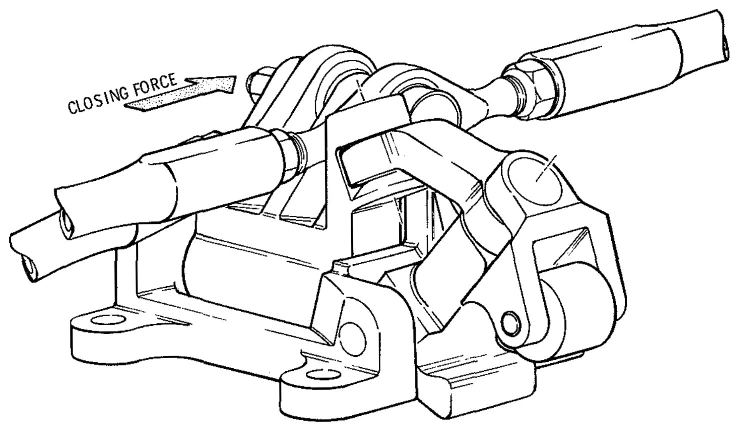

LATCHED

Fig. 3. Unified hatch latches

(4) The output to drive the boost protective cover hatch striker plunger to unlatch the boost protective cover hatch.

The exterior input is a socket in a recessed shaft, which penetrates the command module hatch and is rotated by a removable hand tool. It is used for ground operations, for checkout and test, for extravehicular activities, and for postlanding rescue. Because it is exposed to and must survive reentry heating, it is protected by a beryllium copper heat sink and is thermally insulated from the cabin interior by glass fabric spacers.

The interior input is a push–pull handle which moves normal to the command module hatch plane and is used by the astronauts during extravehicular activities and postlanding and emergency egress. The handle drives through pawls to a ratchet wheel splined to a gear train, which in turn drives the two gearbox outputs. Five oscillations of the handle are required to either open or close the command module latches. The motion of the ratchet wheel and output gear train relative to that of the push–pull handle is selected by two control knobs which engage and disengage the pawls.

One control knob is mounted on the handle and engages either one of two pawls which control the direction of advancing the ratchet wheel. The other selector knob is mounted on the gearbox housing and similarly engages pawls which prevent the ratchet wheel from backing off during the idling stroke of the push–pull handle. The arrangement of pawls is such that the handle push stroke is the working stroke for opening the latches and the pull stroke for closing them. A secondary set of pawls is staggered at half ratchet tooth spacing to reduce backlash between the handle and ratchet wheel

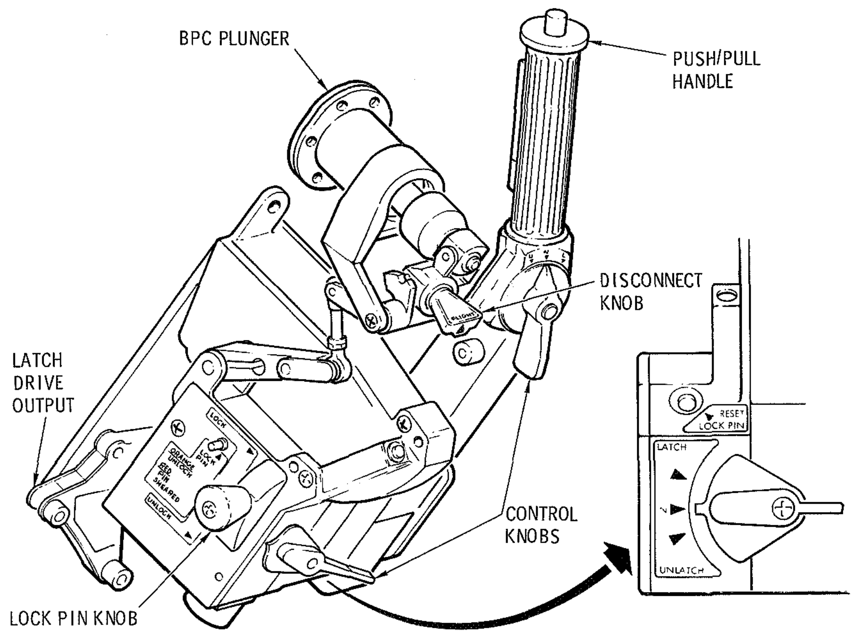

Fig. 4. Unified hatch gear box

and to provide a redundant safety feature. Immediately after the astronauts are locked inside the command module, the two selector knobs are set to the "open latches" position in readiness for an emergency egress.

The gearbox output for opening and closing the command module latches is a bellcrank driven by the gear train, the last gear of which is a 120-deg segment. The bellcrank has two quick-disconnect clevis joints, each driving half of the command module latch system, and an overcenter spring to retain it in either extreme of travel. The other gearbox output is a lever for operating the boost protective cover hatch latch release (the boost protective cover striker plunger). It is driven by a cam slot machined in the side of the 120-deg segment gear and is sequenced to open the boost protective cover hatch latches before the command module hatch latches have moved a significant amount (i.e., they are still in the overcenter locked position).

A safety locking pin is spring-loaded to lock into a matching hole in the segment gear at the end of the command module latch closing cycle and thus prevent accidental opening of the hatch because of vibration or human error. For normal (i.e., nonemergency) hatch opening, the locking pin is manually disengaged before the gearbox handle is operated. When the exterior input is used, this is accomplished by rotating the shaft 15 deg clockwise before rotating counterclockwise to unlatch the hatch. The locking pin is sized so that it will shear when a force greater than normal (35 versus 20) is applied to the push–pull handle, as, for example, in emergency egress.

C. Boost Protective Cover Mechanism

Because the boost protective cover is a separate structure and is jettisoned during boost, its hatch mechanism presents special problems. Before launch, it must be operable from outside the boost protective cover and from inside the command module for emergency egress; but after jettison, the command module hatch must present a smooth ablative surface. Also, for egress, it is required that the boost protective cover hatch latches open before the command module hatch latches so the two hatches can swing open together. These problems are solved by the boost protective cover striker plunger (Fig. 5), which is driven by the gearbox second output. The plunger penetrates the command module hatch and is capped by an ablative end piece which is flush with the hatch exterior surface. When activated by the gearbox, it moves outboard toward the latch mechanism of the boost protective cover hatch. Because the boost protective cover is a comparatively nonrigid structure and offers little resistance to a steady push, the plunger must apply its force very quickly. To accomplish this, the plunger contains a stack of Belleville spring washers

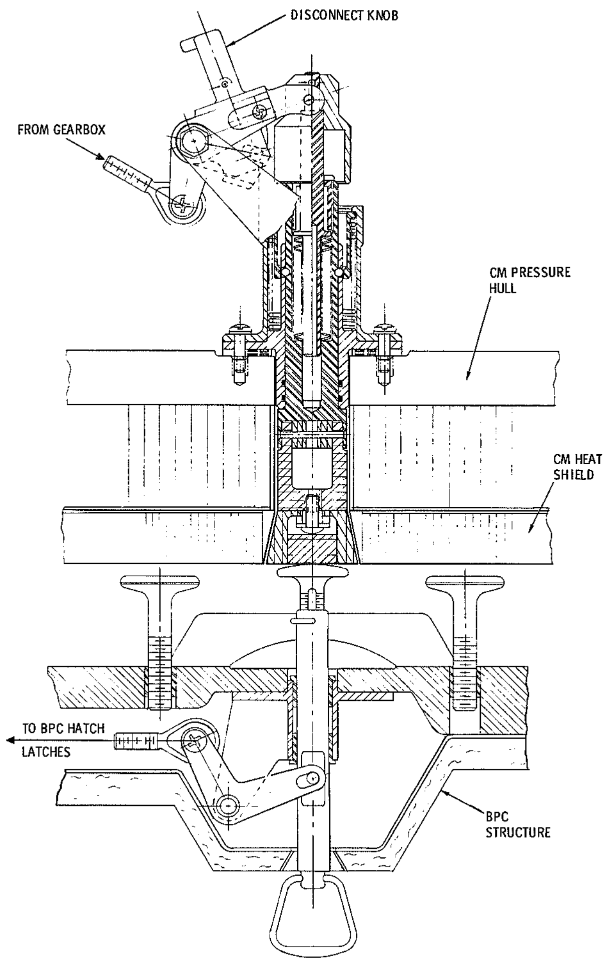

Fig. 5. Boost protective cover striker plunger

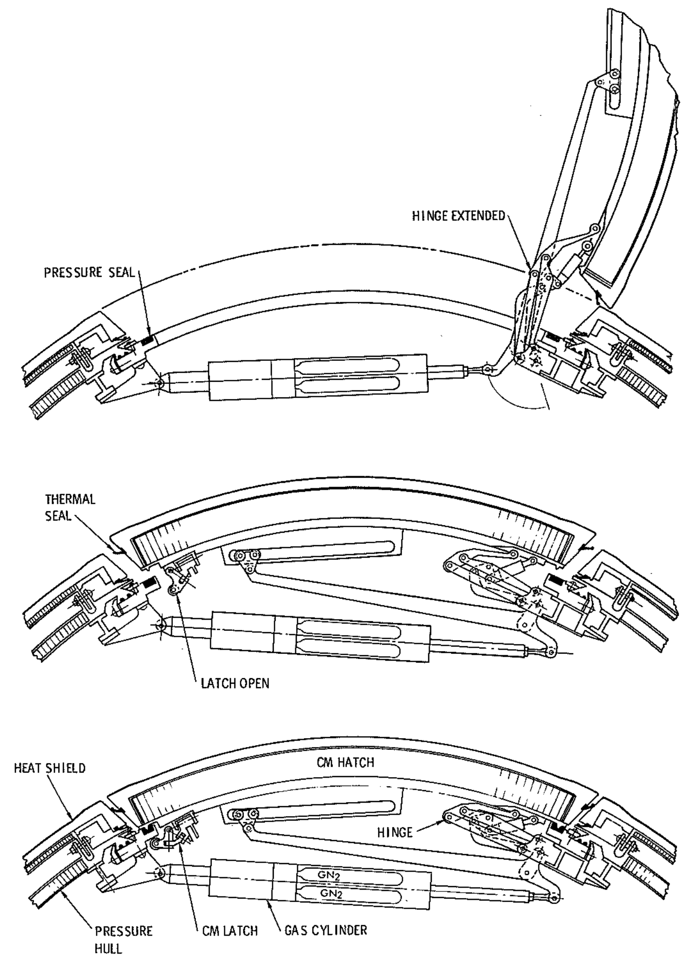

Fig. 6. Command module unified hatch

which are compressed at the beginning of the stroke and then released, the resulting hammer blow opening the boost protective cover hatch latches before the structure can deform. This action takes place during the first working stroke on the gearbox handle. During the remainder of the unlatching cycle, the command module hatch latches are opened and the boost protective cover striker plunger returns to its original position. Since it can serve no useful purpose after launch, the plunger is deactivated during orbit by turning a knob which disconnects it from the gearbox second output.

D. Hinges

The main problem associated with the command module hatch hinges is one that has plagued many mechanism designers. It is to hinge a thick, flush, closely fitting door, which, because of thermal and structural considerations, does not permit a hinge point to be located within its thickness. It is also desirable to design for minimum space usage in the cabin interior. The solution is a pair of collapsible linkage hinges mounted to the inner surface of the hatch (Fig. 6). The linkage unfolds and moves the hatch directly outboard before rotating, as the hinge point constantly changes. A spring-loaded bungee is incorporated to centralize the hatch in its opening when thermal warpage occurs.

E. Counterbalance

The function of the counterbalance (Fig. 7) is to push open the command module and boost protective cover hatches for emergency egress immediately after they are unlatched. Because the combined hatches weigh 350 lb, it is difficult, although not impossible, to open them without this assistance. The cylinder is powered by GN_2 contained in two sealed bottles at 5000 psi, one of which is punctured prior to launch, while the other is reserved for use during extravehicular and postlanding activities.

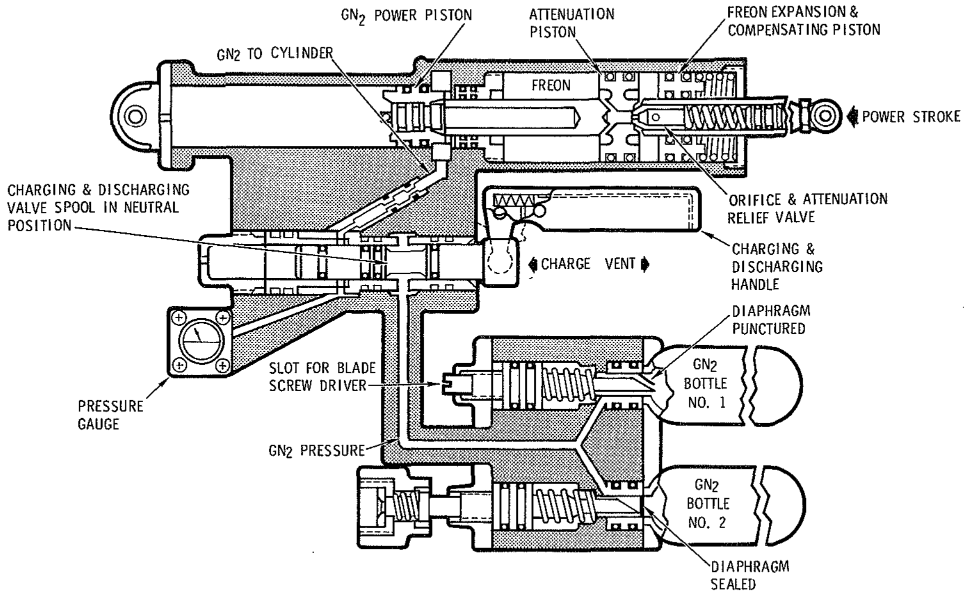

Fig. 7. GN_2 counterbalance schematic

A manually operated spool valve controls the GN_2 flow from the bottles to a power cylinder and piston. A control cylinder is mounted axially in line with the power cylinder and houses a piston and orifice to regulate the flow of Freon which controls the hatch opening velocity. The control cylinder also attenuates shock at the end of the hatch opening stroke. The counterbalance rotates a bellcrank which moves the hatch and engages a safety lock to hold it in the fully open position. The sequence of hatch operations at launch is:

(1) Pressurize the cylinder (ground crew).

(2) Board the spacecraft (flight crew).

(3) Force command module hatch closed against the cylinder pressure (ground crew).

(4) Close the command module hatch latches (flight crew).

(5) Set the gearbox control knobs to the "open latches" position (flight crew).

(6) Close and latch the boost protective cover hatch (ground crew).

The hatch system is then configured for emergency egress. The flight crew has only to operate the gearbox push–pull handle to:

(1) Shear the safety locking pin.

(2) Load and release the spring-loaded boost protective cover striker plunger to open the boost protective cover hatch latches.

(3) Release the command module hatch latches and allow the counterbalance to swing both hatches open approximately 100 deg.

(4) Lock the command module hatch in the open position.

The emergency egress procedure is for the right hand crewman to operate the gearbox (approximately 3 s) and to egress last.

Backup or redundant features were added to assure the safe return of the command module and crew even if primary mechanisms fail. The only mandatory requirement is to be able to hold the command module hatch closed during reentry, although other factors such as oxygen retention and flotation must be considered. To achieve redundancy, the command module latches are divided into four groups and are separable from each other and from the gearbox by quick-disconnect clevis pins so that latch failures can be localized. If the gearbox is inoperable, the disconnected latches can be manipulated by a hand wrench. Another difficulty which may arise is that during extravehicular activity the command module hatch thermally warps more than the latches can accommodate. To overcome this, a set of three small screwjacks is provided to attach to the hatch and force it closed to provide structural integrity for reentry.

VII. Test Program

The test program was planned to support the accelerated design effort and to develop confidence in the hatch system using a step-by-step approach starting with simple ground tests and ending with a lunar-landing mission. A large amount of ground testing had to be performed to prove that the hatch system satisfied the design requirements (Table 1) before a flight could be attempted.

An existing wooden mockup of the command module was revised to include the new hatch design. Although the mechanisms were not functional, they enabled engineering to control the configuration and to evaluate handle and controls placement. Astronauts assisted with preliminary egress tests to verify hatch size opening and determine crew limitations in spacesuits. At the same time a component test program was started to develop and verify the performance of the hatch pressure seal, individual latches, a hinge, and the counterbalance.

To satisfy the requirements for a formal ground qualification test, five vehicles were used, designated 004B, 2TV-1, 2S2, 105, and 007A. Vehicle 004B is a Block I flight vehicle refurbished with a production unified

Table 1. General design requirements

Subject	Unmanned tests	Manned checkouts and prelaunch	Orbital, midcourse or extravehicular activity	Reentry or abort	Postlanding activity
Cabin pressure[a] (at hatch closing)	0–0.01 psi	0–0.01 psi	0–0.01 psi		0–0.01 psi
Hatch closing initiated from	Outside	Inside or outside	Inside		Inside or outside
Hatch closing energy supplied by	Ground crew	Ground crew or flight crew	Flight crew		Recovery crew or flight crew
Hatch closing time	5 min maximum	5 min maximum	5 min maximum normal[b]		5 min maximum[b]
Cabin pressure[a] (while hatch closed)	−1.75–6.2 psi[c]	−1.75–6.2 psi emergency 0–3.0 psi normal[c]	0–0.01 psi emergency 6.2 psi normal	−1.75–0.01 psi 8.3 psi normal	0.10–8.0 psi emergency[d] 0–8.0 psi normal (hydrostatic)
Cabin pressure[a] (at hatch opening)	0–0.10 psi	−1.75–6.2 psi emergency 0–0.10 psi normal[c]	0–0.01 psi		0–0.10 psi[e]
Hatch opening initiated from	Outside	Inside emergency Outside normal	Inside or outside[f]		Inside emergency Outside normal
Hatch opening energy supplied by	Ground crew	Ground crew Flight crew Counterbalance	Flight crew		Recovery crew Flight crew Counterbalance
Hatch opening time	2 min maximum	2 min maximum 3 s maximum emergency[g]	2 min maximum		2 min maximum 3 s maximum emergency[g]
Hatch maximum opened time	Indefinite	Indefinite	20 min (worst orientation)		Indefinite
Crewmen egress		5 min maximum 30 s maximum emergency[h]	5 min maximum		5 min maximum 30 s maximum emergency[h]

[a]Cabin pressures given are psi above external pressure.
[b]Heat shield thermal integrity only, effectively water-tight for limited flotation capability.
[c]Ground support equipment may be utilized at pressures above 3 psi.
[d]Hydrostatic water loads are ultimate; all other pressures are limit values.
[e]Command module in stable No. 1 position or No. 2 position apex down.
[f]Extravehicular activities operations—unaided outside crewman.
[g]Time required for crewmen to unlock hatch latches.
[h]Include crewmen disconnect, hatch opening, and egress for three active, unaided crewmen.

hatch and a portion of the boost protective cover including a complete boost protective cover hatch. This vehicle was used mainly to check out mechanism functions and was subjected to the following tests:

(1) Functional cycling of all mechanisms at room (ambient) temperatures between each of the environmental tests.

(2) Pressure seal leakage.

(3) Pressure and temperature differential: 9.75 psig, $+180°F$ interior, $-175°F$ exterior.

(4) Thermal reentry; $+500°F$ for 10 min.

(5) Emergency opening of command module and boost protective cover hatches at maximum and minimum command module pressures.

(6) Simulated water landing: 10-psi water pressure pulse and maximum 11-g force in hatch opening direction.

(7) Hatch mechanism operational life cycles.

(8) Corrosive environment simulating command module cabin during flight: salt solution, oxygen, humidity, and temperature cycling.

(9) Ultimate load tests on gearbox, latches, linkage, and counterbalance fittings.

(10) Shock test to 70 g.

Vehicle 2TV-1 is a Block II command module assigned for use by NASA in its large thermal vacuum chamber at Houston. Many manned and unmanned test runs were performed to check various phases of a mission. The tests simulating solar heating of the open hatch during extravehicular activities demonstrated a greater change in shape and size than was anticipated, and consequently the rigging procedure was revised to obtain greater clearances in critical areas. Vehicles 2S2 and 105 are Block II command modules assigned for structural and vibration tests. Vehicle 007A is a command module used for postlanding flotation tests. The unified hatch was not tested separately but in conjunction with the remainder of the command module.

Two Block I vehicles were available for unmanned test flights. *Apollo 4* was flown in earth orbit but simulated a lunar mission reentry. The spacecraft had an old Block I hatch with simulated unified hatch thermal seal and gap in place of a window. *Apollo 6* was another simulated lunar mission but with a complete unified hatch. Successful completion of these two flights led to a manned earth orbit mission, *Apollo 7*, followed by *Apollo 8*, the first manned lunar orbit mission. During both of these flights, the unified hatch, and indeed the whole spacecraft, performed flawlessly.

At the time of writing, the spacecraft and its unified hatch are being readied for another flight, that of *Apollo 9*, which will demonstrate performance in extravehicular activity and crew transfer. This flight is a major milestone. It says "GO" for a lunar landing in this decade.

List of Attendees

ADAMS, JAMES L.
Stanford University
AGUILERA, E. P.
General Dynamics
Convair Division
ALEXANDER, HOSEA M.
Jet Propulsion Laboratory
ALEXANDER, PAUL, JR.
Jet Propulsion Laboratory
ANDERSON, A. L.
Philco-Ford Corporation
ASHLEY, A. B.
Lockheed Missiles & Space Company
AVERY, HUGH M.
Lockheed Missiles & Space Company

BACHLE, WILFRED H.
Philco-Ford Corporation
Space & Re-entry Systems Division
BAKKE, A.
NASA Ames Research Center
BALL, JIM
Lockheed Missiles & Space Company
BEAL, ROBERT
United States Naval Research Laboratory
BEESTON, FRANK
Dalmo Victor Company
BERRY, THOMAS G.
Fairchild Hiller Corporation
BERRY, WILLIAM E.
NASA Ames Research Center
BINZ, ERNEST
North American Rockwell Corporation
BLAISE, HERMAN T.
NASA Marshall Space Flight Center
BLOCKINGER, R. A.
Lockheed Missiles & Space Company
BOHLING, RAYMOND F.
NASA Headquarters
BOLENDER, JOHN W.
The Boeing Company
BOMKE, PAUL W.
Jet Propulsion Laboratory
BRACCINI, A. A.
Dalmo Victor Company
BROWN, JERRY C.
Lockheed Missiles & Space Company
BROWN, T. M.
NASA Ames Research Center
BROWN, W. J.
Lockheed Missiles & Space Company
BUCKLEY, K. W., JR.
Lockheed Missiles & Space Company
BUEHLER, MARY FRAN
Jet Propulsion Laboratory
BUERGER, EDGAR J.
General Electric Company
BUNSON, G. A.
Santa Barbara Research Center

BYRNE, JOHN P.
Lockheed Missiles & Space Company
BYXBEE, R. CRAWFORD
Lockheed Missiles & Space Company

CAMPBELL, B. E.
Radiation Incorporated
CAMPBELL, G. K. C.
Lockheed Missiles & Space Company
CARMAN, ROBERT R.
Goodyear Aerospace Corporation
CHAMNESS, O. V.
Singer–General Precision, Inc.
CHASE, CHARLES P.
Beckman Instruments, Inc.
CHRONES, C. J.
TRW Systems Group
CLARK, T. S.
United Technology Center
CLEVETT, M. L.
Martin Marietta Corporation
CLINE, GEORGE B.
Lockheed Missiles & Space Company
CONN, ROBERT G.
Philco-Ford Corporation
CONNER, GARY
United Technology Center
CRANE, W. F.
Lockheed Missiles & Space Company
CUTTS, J. A.
Jet Propulsion Laboratory

DATSKO, JOSEPH
The University of Michigan
DOIGUCHI, S.
NASA Ames Research Center
DWYRE, DOUGLAS
Philco-Ford Corporation

EASTMAN, D. E.
Lockheed Missiles & Space Company
EDSTROM, ANDREW H.
Quantic Industries, Inc.
EGLINGTON, R. E.
NASA Ames Research Center
ENGELBERT, D. F.
NASA Ames Research Center
ENGSTROM, JOHN G.
The Bendix Corporation
EVANS, D. E.
McDonnell Douglas Astronautics Company

FERRIS, F. DONALD
University of Santa Clara
FILLERBROWN, W. C.
McDonnell Douglas Astronautics Company
FIRTH, ROBERT
Singer–General Precision, Inc.
FISHELL, ROBERT E.
The Johns Hopkins University
Applied Physics Laboratory
FISHER, E. J.
University of Santa Clara
FITZGIBBONS, JAMES W.
Sylvania Electric Products, Inc.
FLEMING, ALAN W.
Stanford University
FORBES, FRED W.
United States Air Force
Aero Propulsion Laboratory
Wright-Patterson Air Force Base
FORD, A. G.
Jet Propulsion Laboratory
FORSTER, A. S.
Aerospace Corporation
FRANKEL, HENRY
NASA Goddard Space Flight Center
FRANKENY, J. A.
International Business Machines Corporation
FRISCH, H. P.
NASA Goddard Space Flight Center

GIBBENS, JOHN S.
The Boeing Company
GIBBONS, GLEN D.
Lockheed Missiles & Space Company
GIVEN, R.
Lockheed Missiles & Space Company
GLASSOW, FRANK A.
Hughes Aircraft Company
Space Systems Division
GLOVER, PERRY
Lockheed Missiles & Space Company
GOODWIN, FRANK A.
Jet Propulsion Laboratory
GRABBI, R.
TRW Systems Group
GRADISAR, ALBIN A.
Philco-Ford Corporation
GRAHAM, JOHN D.
Spar Aerospace Products, Ltd.
GRAM, M. B.
Jet Propulsion Laboratory
GREBENSTEIN, EDWARD G.
Fairchild Hiller Corporation
GRIFFITH, JOHN S.
Jet Propulsion Laboratory
GROSKOPFS, E.
Spar Aerospace Products, Ltd.
GUDIKUNST, JAMES B.
General Electric Company
GUERSTER, RENE
Ametek, Inc.
Hunter Spring Division
GUSTAFSON, HELEN E.
Quantic Industries, Inc.

List of Attendees (contd)

GALBRAITH, DON
Lockheed Missiles & Space Company
GRIFFITH, WAYLAND C.
Lockheed Missiles & Space Company
GROSKOPFS, E.
Spar Aerospace Products, Ltd.

HACKER, RUSSELL
California State College at San Jose
HARTHAN, L. J.
TRW Systems Group
HAYES, DUDLEY W.
Lockheed Missiles & Space Company
HAYES, G. T.
Philco-Ford Corporation
Space & Re-entry Systems Division
HEALY, TIMOTHY J.
University of Santa Clara
HERZL, GEORGE G.
Lockheed Missiles & Space Company
HESPRICH, GLEN
Lockheed Missiles & Space Company
HEYDON, DOUGLAS A.
TRW Systems Group
HICKS, PHILLIP
Ametek, Inc.
Hunter Spring Division
HOEKSTRA, PHILIP, JR.
Amerace Esna Corporation
Stimsonite Division
HOLMES, R. E.
NASA Ames Research Center
HOPPER, KENNETH
Martin Marietta Corporation
HOWEY, CHARLES K.
Aerospace Corporation
HUANG, FRANCIS F.
California State College at San Jose

IMUS, ROBERT E.
Jet Propulsion Laboratory

JOHNSON, MANLY E.
Philco-Ford Corporation
JONES, CALVIN L.
ESSA-NESC

KAEHLER, ALFRED E.
Lockheed Missiles & Space Company
KAMACHAITIS, WILLIAM
Fairchild Hiller Corporation
KAMPINSKY, A.
NASA Goddard Space Flight Center
KANE, THOMAS R.
Stanford University
KANNING, GERD
NASA Ames Research Center

KINDRED, ROBERT
Dalmo Victor Company
KIRK, RUSSELL F.
Sylvania Electric Products, Inc.
KODA, RICHARD
Lockheed Missiles & Space Company
KOONTZ, O. L.
NASA Ames Research Center
KRAMER, NATHAN R.
General Electric Company
KUHN, J. G.
Santa Barbara Research Center
KURLAND, RICHARD
TRW Systems Group

LACKEY, JAMES A.
The Boeing Company
LEWIS, G. R.
McDonnell Douglas Corporation
LIKINS, PETER W.
University of California at Los Angeles
LINDBERG, D.
Lockheed Missiles & Space Company
LINLOR, WM. L.
NASA Ames Research Center
LOCATELL, FRANK
Jet Propulsion Laboratory
LOMAS, W. E.
Lockheed Missiles & Space Company
LOTT, D. R.
Lockheed Missiles & Space Company
LUCKEY, GEORGE R.
TRW Systems Group
LUNDBERG, R. E.
Aerotherm Corporation
LYMAN, PETER T.
Jet Propulsion Laboratory

MACLAREN, ARTHUR P.
British Embassy, Washington, D.C.
MACLEAN, CHARLES F.
Lockheed Missiles & Space Company
MACNAUGHTON, J. D.
Spar Aerospace Products, Ltd.
MAJORS, HARRY, JR.
Seattle University
MARX, M. H.
TRW Systems Group
MATHEWS, RICHARD G.
Ball Brothers Research Company
MATSUHIRO, DENNIS
NASA Ames Research Center
MATTEO, DONALD N.
General Electric Company
MAYER, R. W.
Ball Brothers Research Corporation
MCSHERRY, JAMES C.
United States Air Force
Office of Aerospace Research

MEEKS, C. R.
Hughes Aircraft Company
Space Systems Division
MENTZELL, JOHN
Westinghouse Electric Corporation
MERONEK, DENNIS
Aerospace Corporation
MERRICK, VERNON K.
NASA Ames Research Center
MIATECH, GERALD J.
NASA Ames Research Center
MIKSCH, RUSSELL S.
Lockheed Missiles & Space Company
MOBLEY, FRED
Johns Hopkins University
MULHOLLAND, DON
NASA Ames Research Center
MURPHY, JAMES B.
Spar Aerospace Products, Ltd.

NELMS, W. L.
Philco-Ford Corporation
Space & Re-entry Systems Division
NELSON, P. T.
TRW Systems Group
NOURSE, M. S.
NASA Ames Research Center
NOVICK, M. W.
TRW Systems Group

OCKERT, CARL E.
General Electric Company
Missile & Space Division
OLSON, MERLYN C.
Hughes Aircraft Company
O'NEILL, JAMES P.
TRW Systems Group
OWENS, W. L., JR.
Lockheed Missiles & Space Company

PACKER, ROBERT
RCA, Astro-Electronics Division
PALMER, W. B.
TRW Systems Group
PARDON, ROBERT
University of Santa Clara
PEFLEY, RICHARD K.
University of Santa Clara
PERKINS, G. S.
Jet Propulsion Laboratory
PERRIN, B. J.
Ball Brothers Research Corporation
PETERSON, RODNEY J.
General Dynamics Corporation
PISTOLE, GORDON S.
Philco-Ford Corporation
PRATER, CHARLES R.
Lockheed Missiles & Space Company

List of Attendees (contd)

PRIAN, V. D.
California State College at San Jose

QUEENER, FRANK
North American Rockwell Corporation
Atomics International Division

RADOVCICH, NICK A.
Lockheed-California Company
RAMOS, DANIEL O.
General Electric Company
REITER, G. F.
Hughes Aircraft Company
Space Systems Division
RENNIE, BRUCE B.
The Boeing Company
REYNARD, DUNCAN L.
Philco-Ford Corporation
Space & Re-entry Systems Division
REYNOLDS, M. M.
Physics Research & Development, Inc.
RINALDO, ALFRED
Lockheed Missiles & Space Company
ROBILLARD, G.
Jet Propulsion Laboratory
ROBINSON, R. L.
Philco-Ford Corporation
Space & Re-entry Systems Division
ROSENBERG, HAROLD H.
Jet Propulsion Laboratory
ROSENBERG, LARRY
ITT Aerospace–Optical Division
ROTH, WILLIAM S.
Aeroflex Labs, Inc.
ROLLINS, ROGER
Philco-Ford Corporation
WDL Division
ROTTMAYER, E.
Goodyear Aerospace Corporation
ROUSSEAU, R. J.
Lockheed Missiles & Space Company
RUSSELL, WM. J.
Aerospace Corporation
RUSTAD, LEON
Westinghouse Electric Corporation
RYDER, E. R.
Aerospace Corporation

SARDELLA, CARL
Grumman Aircraft Engineering Corporation
SCHICK, WILLIAM F.
Sylvania Electronic Systems
SCHER, MARK
Stanford University
SCHWARTZ, S. A.
Aerojet General Corporation
SCOTT, STAN G.
NASA Ames Research Center
SELLENS, MIKE
Altair
SELLS, JOHN C.
Hughes Aircraft Company
SELENE, L.
Philco-Ford Corporation
Space & Re-entry Systems Division
SHARPLESS, ERIC
Ametek, Inc.
Hunter Spring Division
SHOLLENBERGER, JAMES M.
North American Rockwell Corporation
SILVER, J. M.
NASA Ames Research Center
SIPOS, RAYMOND
Jet Propulsion Laboratory
SKOLNIK, SOL
Aerospace Corporation
SMALLEN, HAROLD
Aerospace Corporation
SMITH, WILLIAM G.
Aerospace Corporation
SONNICHSEN, DEKE
Menlo Oaks Balloon Field
Menlo Park, California
STARKEY, DONALD
Jet Propulsion Laboratory
STAUGAITIS, CHARLES
NASA Goddard Space Flight Center
STEPHENS, J. B.
Jet Propulsion Laboratory
STOCKWELL, DONNELL W.
Jet Propulsion Laboratory
STRAIN, J. D.
ESL, Inc.

TALCOTT, JAMES M.
Fairchild Hiller Corporation
TERRY, THE VERY REV. THOMAS D.
University of Santa Clara
THOMSON, G. S.
Hughes Aircraft Company
THOMPSON, JAMES G.
Aerotherm Corporation
THOMPSON, R. J.
Lockheed Missiles & Space Company
TIMM, JULIAN
Quantic Industries, Inc.
TINLING, BRUCE E.
NASA Ames Research Center
TOTAH, NABBEH I.
Philco-Ford Corporation
WDL Division
TULT, G. E.
North American Rockwell Corporation

UPTON, D. T.
Santa Barbara Research Center
URMAN, WALLY
United States Naval Research Laboratory

VEILLETTE, L.
NASA Goddard Space Flight Center

WALKOVER, LOUIS J.
North American Rockwell Corporation
WANG, T. C.
Applied Research Laboratories
WARD, H. CONNELL
Sylvania Electric Products, Inc.
WATTENBARGER, R. L.
TRW Systems Group
WEISSENBERGER, STEIN
University of Santa Clara
WEST, HARRY W.
Lockheed Missiles & Space Company
WHEATON, ELMER P.
Lockheed Missiles & Space Company
WHEELER, BRYCE A.
Hughes Aircraft Company
WHIPPLE, VIRGINIA P.
Lockheed Missiles & Space Company
WIEDMAN, R. A.
Philco-Ford Corporation
Space & Re-entry Systems Division
WOOD, LORIN A.
Douglas Aircraft Company
WORTISKA, GEORGE J.
Lockheed Missiles & Space Company
WRENCH, E. H.
General Dynamics Corporation
Convair Division

YOUNG, J. W.
Philco-Ford Corporation
Space & Re-entry Systems Division

ZENGER, JERRY H.
University of California at Berkeley
ZOSZAK, JOHN
Lockheed Missiles & Space Company

NASA — JPL — Coml., L.A., Calif.